UNIVERSIDAD COMPLUTENSE DE MADRID

FACULTAD DE CIENCIAS FÍSICAS

TESIS DOCTORAL

Studying the chromospheric activity of the M-type stars of CARMENES using iSTARMOD for implementing the spectral subtraction technique

Estudio de la actividad cromosférica de las estrellas tipo-M de CARMENES usando iSTARMOD para implementar la técnica de sustracción espectral

MEMORIA PARA OPTAR AL GRADO DE DOCTOR

PRESENTADA POR

Fernando Labarga Ávalos

DIRIGIDA POR

David Montes Gutiérrez

Universidad Complutense de Madrid

Facultad de Ciencias Físicas

Tesis doctoral

Studying the chromospheric activity of the M-type stars of CARMENES using `iSTARMOD` *for implementing the spectral subtraction technique*

Estudio de la actividad cromosférica de las estrellas tipo-M de CARMENES usando `iSTARMOD` *para implementar la técnica de sustracción espectral*

Programa D9AE - DOCTORADO EN ASTROFÍSICA
Memoria para optar al grado de Doctor

presentada por

Fernando Labarga Ávalos

Director

David Montes Gutiérrez

UNIVERSIDAD COMPLUTENSE MADRID

DECLARACIÓN DE AUTORÍA Y ORIGINALIDAD DE LA TESIS PRESENTADA PARA OBTENER EL TÍTULO DE DOCTOR

D./Dña. Fernando Labarga Ávalos,
estudiante en el Programa de Doctorado D9AE - DOCTORADO EN ASTROFÍSICA,
de la Facultad de Ciencias Físicas de la Universidad Complutense de Madrid, como autor/a de la tesis presentada para la obtención del título de Doctor y titulada:

Studying the chromospheric activity of the M-type stars of CARMENES using iSTARMOD for implementing Spectral Subtraction Technique

Estudio de la actividad chromosfèrica de las estrellas tipo-M de CARMENES usando iSTARMOD para implementar la Técnica de Sustracción Espectral

y dirigida por: David Montes Gutiérrez

DECLARO QUE:

La tesis es una obra original que no infringe los derechos de propiedad intelectual ni los derechos de propiedad industrial u otros, de acuerdo con el ordenamiento jurídico vigente, en particular, la Ley de Propiedad Intelectual (R.D. legislativo 1/1996, de 12 de abril, por el que se aprueba el texto refundido de la Ley de Propiedad Intelectual, modificado por la Ley 2/2019, de 1 de marzo, regularizando, aclarando y armonizando las disposiciones legales vigentes sobre la materia), en particular, las disposiciones referidas al derecho de cita.

Del mismo modo, asumo frente a la Universidad cualquier responsabilidad que pudiera derivarse de la autoría o falta de originalidad del contenido de la tesis presentada de conformidad con el ordenamiento jurídico vigente.

En Madrid, a 14 de noviembre de 2025

Firmado digitalmente por Fernando Labarga Ávalos
Fecha: 2025.11.14 20:11:49 +01'00'

Fdo.: _____

Esta DECLARACIÓN DE AUTORÍA Y ORIGINALIDAD debe ser insertada en la primera página de la tesis presentada para la obtención del título de Doctor.

f

When you start on your way to Ithaca,
pray that the journey be long,
rich in adventure, rich in discovery.
[...]
Always keep Ithaca fixed in your mind.
Arrival there is your destination.
Yet do not hurry the journey at all;
better that it lasts for many years
and you arrive an old man on the island,
rich from all that you have gained on the way,
not counting on Ithaca for riches.

For Ithaca gave you the splendid voyage
without her you would never have embarked
She has nothing more to give you now

"Ithaca" by C.P. Cavafy, cited in S. Fry (2024)

"...these relationships cannot be invented,
they have been there since the creation of the world."
Werner Heisenberg

A man who works beyond the surface of things, though he may be wrong himself, yet he cleans the way for others, and may chance to make even his errors subservient to the cause of truth.

A Philosophical Enquiry into the Origin of Our Ideas of the Sublime and Beautiful
by Edmund Burke (1757) taken from E. Burke (2015)

Summary

The most numerous population of stars in the Universe, the M-type dwarfs, remains among the least visible and most difficult to characterize. They pose observational challenges due to their intrinsic faintness and profusion of activity, despite their ubiquity and importance in exoplanetary research, and require the development of own methods and tools.

This PhD thesis entitled **Studying the chromospheric activity of the M-type stars of CARMENES using `iSTARMOD` for implementing the Spectral Subtraction Technique**, focuses on the development of a modernized and extended version of the classic `STARMOD` code–originally written in FORTRAN 77–into a Python 3 implementation, named `iSTARMOD`. The aim is to provide a modular, efficient, and user-friendly software tool for the analysis of large stellar spectral datasets, fully integrated with current astrophysical workflows. The modernization ensures compatibility with contemporary scientific libraries such as `Astropy`, `NumPy`, and `SciPy`, as well as adaptability to high-resolution echelle spectra from instruments like the CARMENES spectrograph.

The main objectives include: (i) migration and restructuring of the legacy code to Python; (ii) adaptation of spectral reading and preprocessing routines to FITS data formats; (iii) validation of the spectral subtraction technique algorithms through iterative least-squares fitting for radial velocity alignment and rotational broadening; (iv) implementation of automatic equivalent width (EW) and uncertainty measurements; (v) extension to single and spectroscopic binary (SB1 and SB2) systems via weighted spectral synthesis; (vi) preliminary design of a graphical user interface (GUI) to enhance usability and visualization; (vii) automation of large-scale batch processing for surveys like CARMENES; (viii) highlight the scientific relevance of `iSTARMOD` applying the tool to the study and characterisation of M-dwarfs; and (viii) dissemination of results through scientific publications and conferences.

The `iSTARMOD` software applies the spectral subtraction technique to measure chromospheric activity in late-type stars through multiple activity indicators, including the Hα, other Balmer lines, He I D_3, Na I D_1, D_2, Ca II H & K, and Ca II infrared triplet lines in the visible, as well as the Paschen series and He I λ10830 Å in the near-infrared. The code is distributed with a suite of examples and calibration functions (the χ-functions) to convert excess emission equivalent widths into absolute surface fluxes, enabling automatic characterization of chromospheric activity across large samples of stars. This methodology also helps mitigate stellar activity effects on radial velocity measurements in exoplanet searches.

Within the context of the CARMENES project–an ultra-stable, dual-channel spectrograph operating at the 3.5 m Calar Alto telescope–this research aims to extract and analyze chromospheric activity and its variability (rotational modulation, flares, etc.) across approximately 300 M-type dwarfs. The spectral subtraction analyses focus on the key indicators above mentioned, spanning from the visible–in the VIS channel of CARMENES–to the near-infrared–in the NIR channel. Using `iSTARMOD` in conjunction with the χ-factor method allows the study of fluxflux relationships between lines formed at different chromospheric depths.

Following the development of `iSTARMOD`, it was employed in this thesis to study chromospheric activity through the spectral subtraction of 3428 spectra in ten chromosperic activity indicators, corresponding to 101 M-type stars from the CARMENES sample. The study derived the excess fluxes in Hα, Ca II IRT, He I D_3, Na I D_2, Paβ and Paδ lines, converting them into fractional luminosities normalized to the bolometric luminosity via the χ-factor method.

An analysis of flux-flux relationships, primarily characterized through the $L_{\mathrm{H}\alpha}/L_{\mathrm{Bol}}$ versus $L_{\mathrm{Ca\,II\,IRT\text{-}a}}/L_{\mathrm{Bol}}$ relationship, revealed the existence of three distinct emitter populations.

- **Branch I:** Highly active, fast-rotating M3.5-M7.0 stars located beyond the fully convective boundary. These stars exhibit enhanced Hα emission, high variability, strong magnetic fields, and occupy the saturated regime of the Hα-Rossby relation. They are likely young objects with intense dynamo action.

- **Branch II:** Intermediate stars, also beyond the fully convective limit but typically older and less magnetically intense, showing moderate emission levels and significant variability. Their properties suggest an evolutionary link between Branch I and less active stars.

- **Branch III:** Earlier-type M0-M5 dwarfs with comparatively lower activity, slower rotation, and weaker magnetic fields. They fall in the non-saturated regime, corresponding to more evolved and magnetically quieter stars.

The derived least-squares fits for these three groups display distinct slopes, underscoring systematic differences in their chromospheric energy dissipation mechanisms. These results provide robust evidence that stellar internal structure–particularly the transition from partially to fully convective interiors–plays a central role in shaping chromospheric activity patterns.

The results of the research confirm the bimodality of chromospheric excess emission–likely linked to differences in magnetic field configurations–and reveal a transitional population of very late-type stars occupying the region

corresponding to the supposed VaughanPreston gap. These findings contribute to a deeper understanding of magnetic activity and its evolution in cool, late-type stars.

Resumen

La población más numerosa de estrellas en el Universo, las enanas de tipo M, sigue siendo una de las menos visibles y más difíciles de caracterizar. Plantean importantes desafíos observacionales debido a su intrínseca debilidad y a su profusión de actividad, a pesar de su ubicuidad e importancia en la investigación exoplanetaria, y requieren el desarrollo de métodos y herramientas propios.

Esta tesis doctoral titulada **Estudio de la actividad cromosférica de las estrellas de tipo M de CARMENES utilizando `iSTARMOD` para la implementación de la Técnica de Sustracción Espectral** se centra en el desarrollo de una versión modernizada y ampliada del código clásico `STARMOD` originalmente escrito en `FORTRAN 77` hacia una implementación en `Python 3` denominada `iSTARMOD`. El objetivo es proporcionar una herramienta de software modular, eficiente y fácil de usar para el análisis de grandes conjuntos de espectros estelares, totalmente integrada en los flujos de trabajo astrofísicos contemporáneos. La modernización garantiza la compatibilidad con bibliotecas científicas actuales como `Astropy`, `NumPy` y `SciPy`, así como la adaptabilidad a espectros echelle de alta resolución provenientes de instrumentos como el espectrógrafo CARMENES.

Los objetivos principales incluyen: (i) migración y reestructuración del código heredado a Python; (ii) adaptación de las rutinas de lectura y preprocesado espectral a formatos de datos FITS; (iii) validación de los algoritmos de la Técnica de Sustracción Espectral mediante ajustes iterativos de mínimos cuadrados para la alineación en velocidad radial y el ensanchamiento rotacional; (iv) implementación de medidas automáticas de anchura equivalente (EW) y sus incertidumbres; (v) extensión a binarias espectroscópicas de líneas aisladas o dobles SB1 o SB2, mediante síntesis espectral ponderada; (vi) diseño preliminar de una interfaz gráfica de usuario (GUI) para mejorar la usabilidad y la visualización; (vii) automatización del procesado masivo de datos para estudios como CARMENES; (viii) destacar la relevancia científica de `iSTARMOD` aplicando la herramienta al estudio y caracterización de enanas M; y (ix) difusión de los resultados mediante publicaciones científicas y congresos.

El software `iSTARMOD` aplica la técnica de sustracción espectral para medir la actividad cromosférica en estrellas de tipo tardío a través de múltiples indicadores, incluyendo Hα, otras líneas de Balmer, He I D_3, Na I D_1, D_2, Ca II H & K y las líneas del triplete infrarrojo de Ca II en el visible, así como la serie de Paschen y la línea He I λ10830 Å en el infrarrojo cercano. El código se distribuye con un conjunto de ejemplos y funciones de calibración (las funciones χ) para convertir las anchuras equivalentes de los excesos de emisión cromosférica en flujos absolutos superficiales, permitiendo la caracterización automática de la actividad cromosférica en grandes muestras de estrellas. Esta metodología también ayuda a mitigar los efectos de la actividad estelar en la determinación de velocidades radiales en búsquedas de exoplanetas.

En el contexto del proyecto CARMENES –un espectrógrafo de doble canal, ultraestable, instalado en el telescopio de 3.5 m de Calar Alto– esta investigación tiene como objetivo extraer y analizar la actividad cromosférica y su variabilidad (modulación rotacional, fulguraciones, etc.) en aproximadamente 300 enanas de tipo M. Los análisis basados en sustracción espectral se centran en indicadores clave que abarcan desde el visible (p.,ej., Na I D_1, D_2, He I D_3, Hα) hasta el infrarrojo cercano (p.,ej., Ca II IRT, He I λ10830, y líneas de la serie de Paschen). El uso de `iSTARMOD` junto con el método del factor χ permite estudiar relaciones flujo-flujo entre líneas formadas a diferentes alturas de la cromosfera.

Una vez desarrollado `iSTARMOD`, este fue empleado en la tesis para estudiar la actividad cromosférica mediante la sustracción espectral de 3428 espectros en doce indicadores de actividad, correspondientes a 101 estrellas de tipo M de la muestra de CARMENES. El estudio determinó los excesos de flujo en Hα, Ca,II,IRT, He,I,D_3, Na,I,D_2 y las líneas de Paschen, convirtiéndolos en luminosidades fraccionarias normalizadas a la luminosidad bolométrica mediante el método del factor χ.

El análisis de las relaciones flujo-flujo, principalmente caracterizado mediante la relación $L_{\mathrm{H}\alpha}/L_{\mathrm{Bol}}$ frente a $L_{\mathrm{Ca,II,IRT\text{-}a}}/L_{\mathrm{Bol}}$, reveló la existencia de tres poblaciones emisoras distintas:

- **Rama I:** Estrellas M3.5-M7.0 altamente activas y de rotación rápida situadas más allá del límite de completamente convectivo. Presentan una emisión Hα intensificada, alta variabilidad, fuertes campos magnéticos y se localizan en el régimen saturado de la relación Hα-Rossby. Probablemente son objetos jóvenes con una acción dinamo muy intensa.

- **Rama II:** Estrellas intermedias, también más allá del límite completamente convectivo pero típicamente más viejas y menos intensamente magnéticas, que muestran niveles moderados de emisión y variabilidad significativa. Sus propiedades sugieren un vínculo evolutivo entre la Rama I y estrellas menos activas.

- **Rama III:** Enanas M0-M5 de tipo más temprano, con actividad comparativamente menor, rotación más lenta y campos magnéticos más débiles. Se sitúan en el régimen no saturado, correspondiente a estrellas más evolucionadas y magnéticamente más tranquilas.

Los ajustes de mínimos cuadrados obtenidos para estos tres grupos muestran pendientes claramente diferenciadas, lo que subraya diferencias sistemáticas en sus mecanismos de disipación de energía en la cromosféra. Estos resultados aportan evidencia sólida de que la estructura interna estelar, particularmente la transición entre interiores parcial y totalmente convectivos, desempeña un papel central en la configuración de los patrones de actividad cromosférica.

Los resultados de la investigación confirman la bimodalidad de los excesos de emisión cromosférica –probablemente vinculada a diferencias en las configuraciones del campo magnético– y revelan una población transicional de estrellas de tipo muy tardío que ocupa la región correspondiente al supuesto gap de Vaughan-Preston. Estos hallazgos contribuyen a una comprensión más profunda de la actividad magnética y su evolución en estrellas frías de tipo tardío.

Acknowledgements

I would like to express my deepest gratitude to all those who have accompanied me along the long path that led to this thesis.

To my grandfather, Antonio Ávalos Rebollo (1915-1995), a humble and devoted schoolteacher, who not only taught me to read but also showed me how to look up and wonder. It was he who first pointed out the stars to me, planting the seed of curiosity that has guided my life ever since.

To the memory of my father, Fernando Labarga Castillo (1938-2024) and my mother, Antonia Ávalos Martín (1942-1987), for their constant support, patience, and unconditional love – the solid ground beneath every step I took while they wandered onto this planet. Their example of perseverance, kindness and love for knowledge has been my greatest lesson.

To my former wife, María José, whose companionship and shared dreams during part of this journey also shaped who I am today. Without her I would not be here. And to my daughters Aurora and Miriam, for their patience and love. We will make up for the lost time.

I am also sincerely grateful to the Departamento de Física de la Tierra y Astrofísica of Facultad. C.C. Físicas, and the Doctoral Program in Astrophysics of the Universidad Complutense de Madrid (UCM) for providing the academic environment and resources that made this research possible. My thanks extend as well to my colleagues and fellow PhD candidates, whose discussions, encouragement, and friendship have enriched both my work and my life during these years.

And finally to my thesis advisor, Prof. David Montes Gutiérrez, who patiently endured endless discussions without agreeing with me – thank you for putting up with me this far.

Contents

CHAPTER 1

Introduction

1.1 The Character of M dwarfs and its chromospheric activity

The most numerous population of stars in the Universe is barely visible, less measurable by us humans. Even Teegarden's Star, in spite of being among the nearest to Earth (3.8 pc), one of the seven stars with greatest proper motion and host of three planets, was largely overlooked until 2003, and its planets not detected until 2019 (M. Zechmeister et al., 2019).

The reason for this can be found in the Hertzsprung-Russel (HR) diagram . They are located in the lower right side of the Main Sequence in this diagram. That is to say: they are still hydrogen-burning stars, but with very low-mass ($0.075 - 0.61\ M_{\odot}$) and therefore very low-luminosity ($0.0001 - 0.06\ L_{\odot}$). As a consequence of their low mass and the strong mass dependency of the p-p H-burning nuclear reaction, they have very long lifespans (≥ 100 Ga) and very slow evolution rate, so as none of them have evolved off the Main Sequence (G. Laughlin et al., 1997).

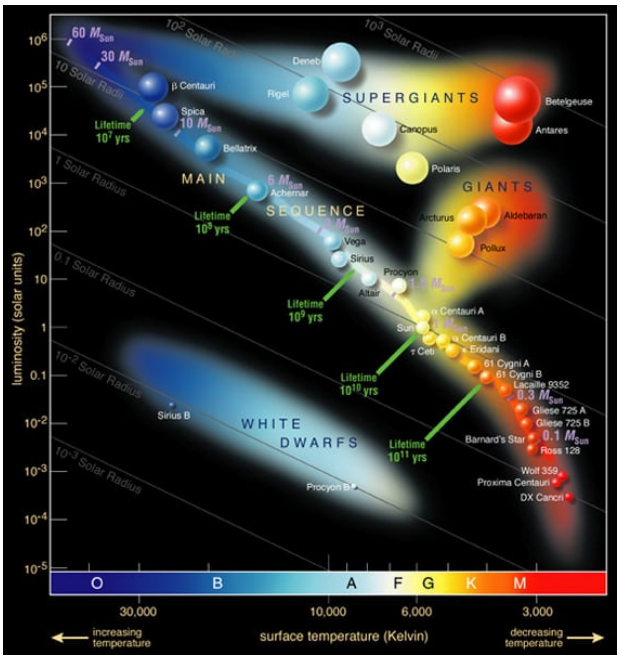

Figure 1.1. The Hertzsprung-Russel Diagram. As mentioned in the text, M-dwarfs are located in the lower right end of the Main Sequence. Many stars studied in this thesis are even further down the MS of the examples depicted in the this figure. Credit: ESO (used under CC BY 4.0). Adapted from standard HR diagram representations in astronomy literature and educational resources like CESAR (Cooperation through Education in Science and Astronomy Research) of the European Space Agency.

Being the most numerous stars, they dominate the stellar population of the Milky Way, representing approximately 75% of all stars in it and forming, for the most part, the unresolved, diffuse starlight background of our Galaxy.

These stars tend to be single more often than higher-mass stars, with only about 27% existing in multiple systems. Their orbital characteristics often include short-period binaries that have undergone tidal circularization. However it should be noted that this figure on binarity proportion could be revised, given the intrinsic faintness of red dwarfs, and the difficulty of its detection. This fact points out to future lines of research to elucidate the actual binarity proportion of M-dwarfs with profound implications on our models of stellar formation and its rates.

So, M-dwarfs stars are important to our understanding of stellar populations, magnetic activity in stars, and given their number and features, the search for habitable exoplanets. They require the application of own methods for analyzing their emission properties and studying their activity and evolution, given that, despite their ubiquity, their intrinsic faintness challenges the performance of our instruments.

This thesis will study the character of M-dwarfs from the point of view of chromospheric emission and to the effects of the internal structure on the M-dwarfs observables **M-dwarfs observables**. The internal structure of M-dwarfs has a strong influence on their observable properties, especially **magnetic activity, rotation, and lifespan**, or the evolution of these observables. We found that there are meaningful differences in the outer layers of fully convective versus partially convective M-dwarfs, although these are subtle compared to the internal differences.

1.1.1 Physical and Structural Characteristics of M Dwarfs

M dwarfs span a relatively broad range of temperatures (2100 – 3900 K) and masses, in their range of spectral types (M0V to M9.0V), and correspondingly displaying a wide range of radii, luminosities, and photometric properties. But the key structural distinction within M dwarfs is the existence of a transition between partially and fully convective interiors, which occurs near 0.35 - 0.5 $M_{\odot}$ for main-sequence stars G. Chabrier & I. Baraffe (1997); A. Reiners & G. Basri (2009); K. G. Stassun et al. (2011); D. Shulyak et al. (2014, 2019). It is the only stellar spectral type population that possess this structural transition.

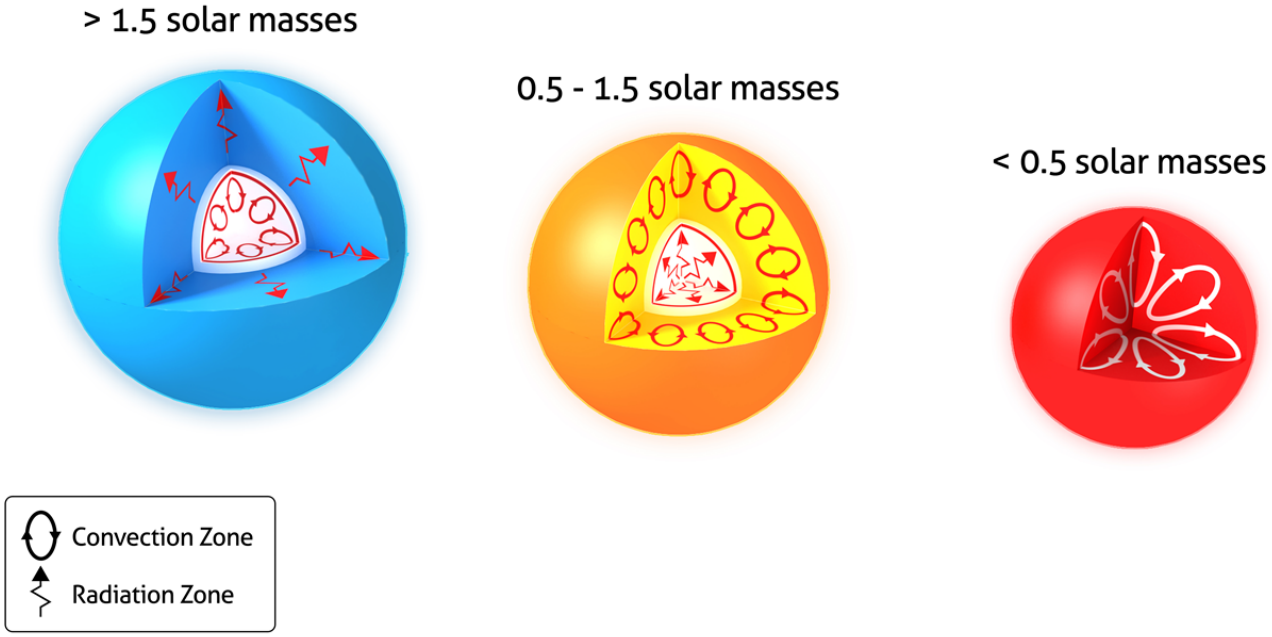

Figure 1.2. Diagram illustrating the internal structure of stars depending on their masses: *Right*: A fully convective star (mass 0.3-0.4 $M_{\odot}$) where convection extends from core to surface. *Center*: A partially convective star (0.5 to 1.5 $M_{\odot}$, like the Sun) with a radiative core and an outer convective envelope. *Left*: A highermass star ($\gtrsim 1.5M_{\odot}$), then NOT a M-dwarf, exhibiting a convective core and a radiative envelope. (Adapted from a Stellar Structure diagram originally shared on Physics Forums, illustrating energy transport zones across stellar masses.)

From one side, intermediate-mass M-dwarfs (M$\epsilon[0.35, 0.6]$ in $M_{\odot}$) are partially convective. In a convective envelope, the outer layers transport energy via convection, while in the radiative core, in the inner region, energy transport is dominated by radiation. This structure starts to resemble the Sun's and other cool stars. The transition region exhibits complex behavior, such as convective kissing instabilities-temporary mixing of radiative and convective zones–likely influencing rotational and magnetic evolution.

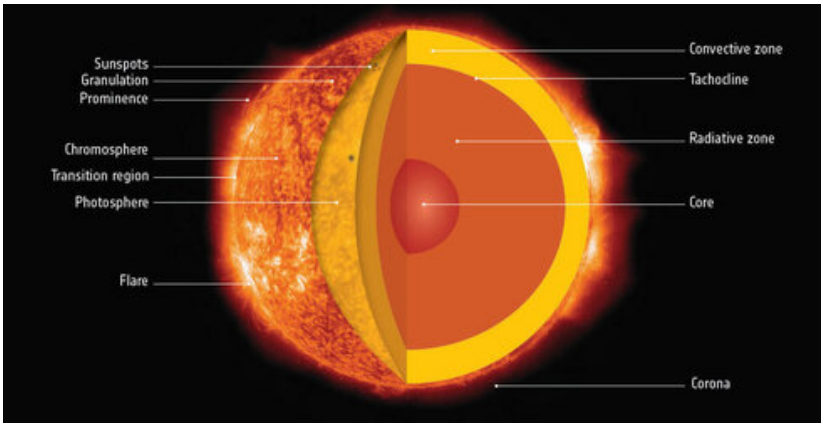

Figure 1.3. *Anatomy*, or Internal Stucture of the Sun, as a model for the rest of Partially Convective Stars. Although marked, there is no difference between Core and Radiative Zone, as the Core is also radiative. For late type stars, the relative depth of convective zone is greater, until covering all the way down in fully convective M-dwarfs. Credit: ESA-S.Poletti under License CC BY-SA 3.0 IGO

On the other hand, low-mass M-dwarfs ($\leq 0.35M_{\odot}$) are fully convective, that is, within the entire interior, energy is transported throughout by convection. This has the implication that hydrogen is mixed thoroughly, allowing efficient

fuel usage, but prevents helium buildup in the core and enables a near-uniform composition through the star. This leads to slow, steady hydrogen fusion via the proton-proton chain (pp-chain), and the in turn they possessing very long lifetimes (up to trillions of years). Moreover, there is no solar-type dynamo: magnetic fields likely generated by a turbulent dynamo process instead. So there are strong magnetic fields and stellar flares due to convective turbulence.

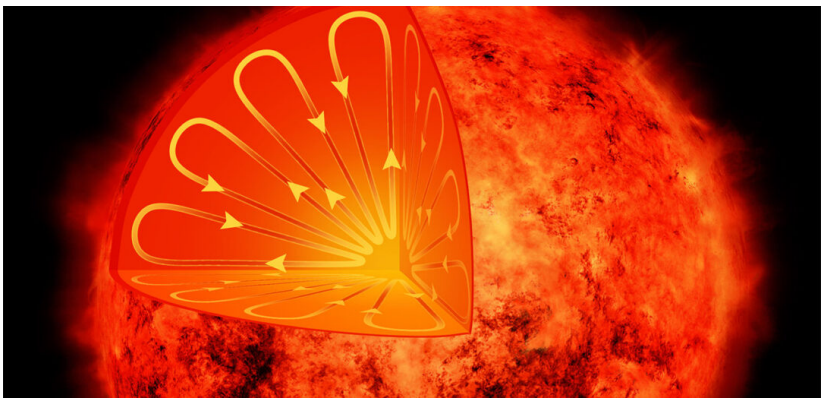

Figure 1.4. Illustration of the interior of a fully convective star. Nevertheless the differences in structure with the partially convective stars, the outer layers could be similar. Credit: [NASA/CXC/M.Weiss and AAS Nova]

The difference in these internal structures, lead to posing different dynamo processes: solar-type $\alpha\Omega$ dynamo for partially convective stars, and turbulent α^2 dynamo for fully convective stars. It is reasonable to think that this difference in dynamo processes should have effect on the characteristics of their activity and its related cycles (V. See et al., 2016). But as mentioned in K. G. Stassun et al. (2011), this transition from partially to fully convective regime lacks of an observationally sharp or discrete evidence. The transition between both structures is marked by a "main sequence gap" (really a slight discontinuity) in observational Gaia DR2 Hertzsprung-Russell diagrams (W.-C. Jao et al., 2018; J. MacDonald & J. Gizis, 2018; I. Baraffe & G. Chabrier, 2018) for nearby M-dwarf stars. This thesis will provide, by means of the study of flux-flux relationships, additional arguments favoring this hypothesis, not as a an explanation of the dip in the luminosity function, but as an observational evidence of such transition.

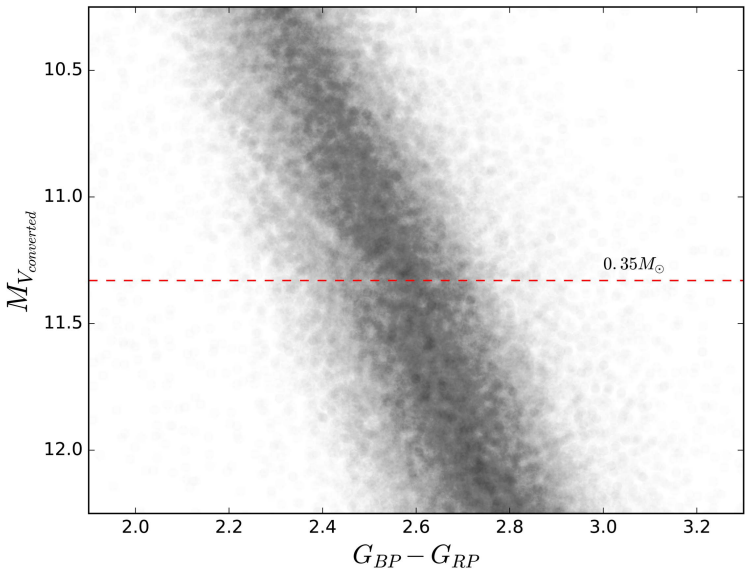

Figure 1.5. The Jao gap. A low density region, or slight discontinuity of star counts in an observational Hertzsprung-Russel diagram (HRD), marking the transition from partially convective to complete convective stars. It has been drawn the red line, corresponding to $M \sim 0.35 M_{\odot}$, where the upper side of the gap intersects the middle of the HRD. Taken from W.-C. Jao et al. (2018)

1.1.2 Binarity

The binarity of M-type stars is notably lower than that of earlier-type stars, with a binary fraction estimated at approximately 25-30% (e.g., J. G. Winters et al. 2019; C. Cifuentes et al. 2025). This contrasts sharply with the 50-60% binarity observed among G-type stars and even higher rates among massive O- and B-type stars. The declining multiplicity trend with stellar mass presents a significant constraint for star formation theories, suggesting reduced fragmentation efficiency or enhanced dynamical disruption in the low-mass regime. Observationally, M dwarfs

pose challenges due to their intrinsic faintness and tight binary separations, leading to underestimation in surveys, particularly for close or low-mass-ratio systems. Recent astrometric data from Gaia have begun to uncover new binaries and tighten multiplicity constraints. Understanding M-dwarf binarity is crucial not only for star formation models but also for interpreting exoplanet demographics and refining initial mass function estimates, especially in the low-mass domain.

1.1.3 Chromospheres in Cool Stars

The presence of convection in the outer layers of the star has dramatic consequences for the stellar atmosphere structure, giving rise to the appearance of the chromosphere and corona, as well as the presence of surface features such as starspots, flares, prominences, and granulations. Convection, combined with differential rotation, implies the emergence of dynamo mechanisms and non-thermal heating, which we will describe bellow. We can define chromosphere as:

Chromosphere

Definition:. The chromosphere is the layer of a stellar atmosphere above the photosphere where temperature increases with altitude due to non-radiative heating (J. L. Linsky, 2017).
This layer is prominent in stars from spectral type F to M. Their surface manifestations include:

- *Starspots*, cooler and magnetically active regions on the photosphere, analogous to sunspots;
- *Plages* and *faculae*, bright magnetic regions observed in the chromosphere and photosphere;
- *Flares*, resulting from rapid magnetic reconnection events that release energy across the electromagnetic spectrum;
- *Prominences* and *coronal mass ejections*, indicative of large-scale magnetic structures and instabilities.

It is important to consider the nature and manifestation of the different sources of the non-thermal heating, that lead to the presence of a series of emission line in the spectra of active cool stars in general and M-dwarfs in particular. Chromospheric emission in cool stars arises from a combination of complex heating processes that elevate

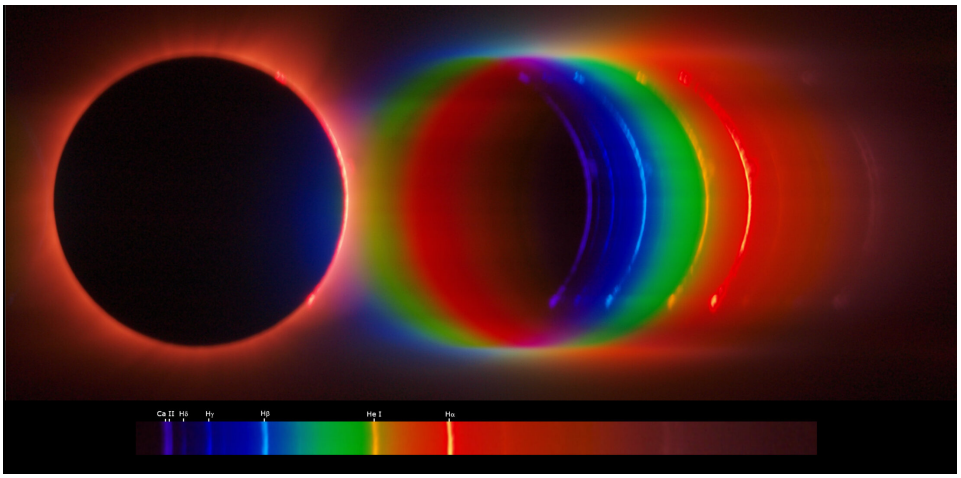

Figure 1.6. *Chromosphere flash spectrum* captured during the total solar eclipse that occurred over the United States on 21 August 2017. It was taken by ESAs expedition team who monitored the eclipse from Casper, Wyoming, showing the principal diagnostic lines. It can be seen Ca II H&K in the blue end, continuing with Balmer series, and He I D3 in the yellow part and H_α, in the red end of the spectrum. The Chromosphere is clearly visible as the coloured ring around the eclipsing Moon. A similar structure is supposed to form in M-dwarfs. Credit: European Space Agency (ESA).

the temperature of the stellar atmosphere above that predicted by radiative equilibrium, a characteristic exacerbated in the corona. The key mechanisms include magnetic heating and acoustic wave dissipation.

1.1.3.1 Magnetic Heating

Magnetic fields play a dominant role in heating the chromospheres of cool stars, particularly those exhibiting significant levels of magnetic activity. Magnetic reconnection events and the dissipation of magnetic energy in the form of Alfvén waves and magnetohydrodynamic (MHD) turbulence can heat plasma to temperatures sufficient to produce the observed emission in lines such as CaII H & K and H_α. These processes are especially efficient in stars with convective envelopes and rapid rotation, where stellar dynamos are more effective.

Magnetic Surface Features: Plages and Starspots Analogous to solar features, plages (bright chromospheric regions) and starspots (cool, magnetically active surface regions) contribute to spatial and temporal variability in chromospheric

emission. Plages are especially important in the enhancement of CaII line cores, while starspot coverage is often correlated with activity cycles and flaring behavior. Plages are also the main responsible for the emission in the Ca II IRT, because the flux ratio between the two members of the triplet is typically in the range 1.5-3, indicating optically thick emission (e.g. (J. C. Hall & L. W. Ramsey, 1992a)). The presence and distribution of such features provide insight into the underlying stellar magnetic field geometry.

Flares and Transient Events Occasionally, cool stars –particularly M dwarfs– experience sudden, intense flaring events due to magnetic reconnection, which can cause a temporary but dramatic increase in chromospheric emission across multiple spectral lines. These transient events are critical to understanding stellar magnetism and have important implications for the atmospheres of orbiting exoplanets. *Prominences* This ejection of material due to large-scale magnetic instabilities produce an increase of the ratio of the excess emission between Ca II IRT-λ8542 and Ca II IRT-λ8498. Empirically, it has been established that this ratio increases up to 9 (J. C. Hall & L. W. Ramsey, 1992a).

1.1.3.2 Acoustic Heating of the Chromosphere in Cool Stars

In stars with low magnetic activity –such as older solar-type stars– the chromospheric heating may be dominated by acoustic (pressure) waves generated in the turbulent convection zones. These waves propagate upward, steepen into shocks, and dissipate their energy in the chromosphere. Although this mechanism is generally less efficient than magnetic heating, it sets a "basal flux" level of chromospheric emission that represents the minimum observable emission in quiet stars.

The details of the chromospheric heating problem along the complete sequence of M-type to L stars remains as a challenge in stellar astrophysics. While magnetic mechanisms are often invoked to explain the high chromospheric temperatures observed in late-type stars, non-magnetic processes, particularly those involving acoustic waves, may also play a significant role, especially in the least active or magnetically quiet stars.

Acoustic heating arises from the dissipation of mechanical energy carried by pressure (sound) waves generated by turbulent convective motions in the stellar photosphere. The vigorous convection present in late-type stars continuously excites a broad spectrum of acoustic oscillations through stochastic processes associated with granulation and convective overshoot. These waves propagate upward into the less dense chromospheric layers, where their amplitudes grow due to decreasing density, eventually steepening into shocks. The dissipation of these shocks converts mechanical energy into thermal energy, contributing to the heating of the chromosphere (P. Ulmschneider, 1970; Z. E. Musielak et al., 1994).

The total acoustic flux $F_{\rm ac}$ generated by convection can be approximated by scaling relations of the form

$$F_{\rm ac} \propto \rho v_{\rm c}^3, \tag{1.1}$$

where ρ is the photospheric density and $v_{\rm c}$ the convective velocity. More detailed models include dependencies on the Mach number and the efficiency of mode conversion from turbulent motions to acoustic waves (Z. E. Musielak, 2004).

However, both theoretical and observational studies indicate that pure acoustic heating is insufficient to account for the observed levels of chromospheric emission in most active late-type stars (S. Mohanty et al., 2002), especially in the later types. Instead, it appears to provide a basal component of emission, below which no chromospheric flux is observed. This “basal flux” represents the minimum level of non-magnetic heating present in all cool stars, and its correlation with stellar effective temperature supports the idea of a common acoustic origin (C. J. Schrijver, 1987).

In summary, acoustic heating constitutes a universal, non-magnetic baseline mechanism operating in the chromospheres of cool stars. It likely dominates in the most quiescent, weakly magnetized stars, whereas magnetic heating (via waves, reconnection, or dissipation of magnetic stresses) becomes dominant in magnetically active stars. The interplay between acoustic and magnetic heating remains a central topic in the study of stellar atmospheres.

1.1.4 Relevance of M-dwarfs for stellar activity and exoplanets studies

All M dwarfs exhibit some level of stellar activity, which can be observed through chromospheric emission lines (e.g., Hα), photometric variability, and X-ray/EUV emissions. Activity levels are strongly tied to rotation, with fast rotators generally being more magnetically active. A transition from saturated to solar-like (unsaturated) activity occurs as stars age and spin down. This profusion of activity lies mainly in the chromosphere.

M dwarfs are fertile grounds for exoplanet detection due to their small radii and masses, which enhance the detectability of planetary transits and radial velocity signals. Most planets discovered around M dwarfs are terrestrial or neptunian in size; jovian planets are rare (S. Sabotta et al., 2021; A. Kaminski et al., 2025), with the conspicuous exception of the planet discovered by the CARMENES group (J. C. Morales et al., 2019, 2025).

The study of stellar activity is also central to the evaluation of habitability of exoplanets orbiting them. High levels of stellar activity, particularly in the form of flares and coronal mass ejections, drivers of powerful stellar winds, can erode planetary atmospheres, affecting then surface conditions on these exoplanets M. M. Katsova (2020) Three main families of mechanisms contribute to atmospheric loss in exoplanets: photoevaporation, thermal escape and even the proper stellar winds on exoplanets lacking intrinsic magnetic fields, as has been recently explored in A. Canet et al. (2024); A. Canet & A. I. Gómez de Castro (2021). Most M-dwarfs, being active stars, pose unique challenges for the habitability of orbiting exoplanets. A. Segura et al. (2010) examined the effects of stellar activity on exoplanetary

atmospheric chemistry, using data from AD Leo –a particularly active star included in the present study. These mechanisms, driven by stellar activity play, as has just been mentioned, a role in the atmospheric erosion of close-in exoplanets (J. E. Owen & S. Mohanty, 2016; M. Salz et al., 2018), particularly those orbiting young, fast-rotating M-type stars. So the magnetic activity not only influences the settle of conditions for habitability, but also the exoplanet formation and evolution. Recent observations have provided empirical support for models of atmospheric escape in close-in exoplanets (L. Nortmann et al., 2018; F. J. Alonso-Floriano et al., 2019a), reinforcing the role of stellar magnetic activity in shaping planetary atmospheres.

These evolution features of late-type stars have been found to be critical in regards to the ability of hosted exoplanets to sustain life (see e.g. the white paper L. Corrales et al. (2023)), which is closely related with the aims of CARMENES survey focused in search for Earth-like rocky exoplanets orbiting in the habitable zones of their host M-dwarf stars.

M dwarfs are long-lived, stable laboratories for studying stellar structure and exoplanetary environments. The evolution of solar-type stars, traced through rotation and magnetic activity, offers insights into both stellar physics and the habitability of surrounding planets.

The intersection of these two research areas highlights the importance of M dwarfs not only as dominant stellar constituents but also as key hosts in the ongoing search for life beyond Earth, as is the case of CARMENES scientific program.

1.2 Stellar Activity and Magnetism

As seen in section 1.1 cool stars, typically of spectral types F, G, K, and M, possess outer convective envelopes that play a central role in generating magnetic fields through dynamo processes. The interplay between convection and differential rotation within these stars sustains magnetic fields that emerge at the surface in various manifestations of stellar activity (E. N. Parker 1955,P. Charbonneau 2020 and the recent review of S. Bellotti & J. Morin 2025).

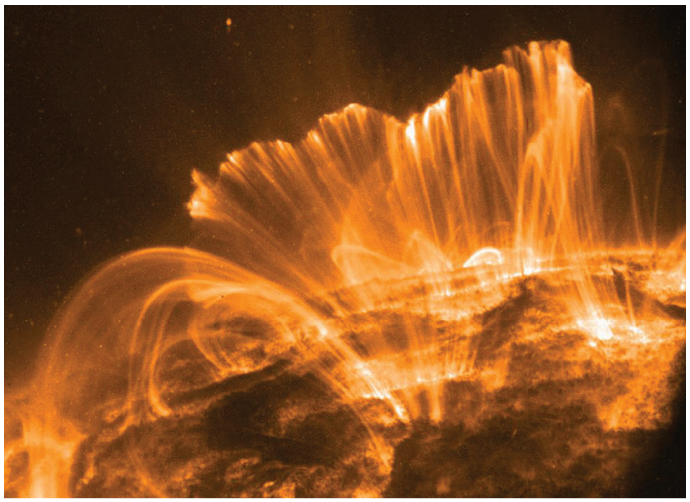

Figure 1.7. Coronal loops over a solar active region. Glowing brightly in extreme ultraviolet light, the hot plasma entrained above the Sun along arching magnetic fields is cooling and raining back down on the solar surface. Taken from N. A. of Sciences Engineering & Medicine" (2025)

1.2.1 Magnetic Field generation

The magnetic activity of cool stars originates in the stellar dynamo, which converts kinetic energy of convective motions and rotation into magnetic energy. Following E. N. Parker (1955), the magnetic field $\mathbf{B}$ is generated due to the velocity field of the moving plasma particles $\mathbf{v}$ due to convection, obeying:

$$\frac{\partial \mathbf{B}}{\partial t} = \nabla \times (\mathbf{v} \times \mathbf{B}) + \frac{1}{\mu\sigma}\nabla^2\mathbf{B} \tag{1.2}$$

where σ is the conductivity and μ is the magnetic permittivity of free space.

Magnetic fields modulate the structure and emission of stellar atmospheres. The magnetic field originated in the tachocline or in the photosphere and propagating through it reaches the chromosphere where manifests as a series of surface features as the ones mentioned in 1.1.3.

Magnetic heating gives rise to non-thermal emission in the chromosphere, transition region, and corona. Chromospheric lines such as Ca II H & K, Hα, and Mg II h & k serve as sensitive indicators of magnetic activity (J. L. Linsky & E. H. Avrett, 1970; A. Skumanich et al., 1975; D. Montes et al., 1995a, 1996a,b, 2000). Coronal emission observed in X-rays is closely correlated with chromospheric emission, both tracing the efficiency of magnetic heating (G. S. Vaiana et al., 1981; J. H. M. M. Schmitt, 1997).

1.2.2 Activity–Rotation–Age Relationship

Cool stars exhibit a well-established activity–rotation–age relation: young, rapidly rotating stars are highly active, with strong chromospheric and coronal emission. Over time, magnetic braking via stellar winds leads to rotational spin-down, which reduces dynamo efficiency and, consequently, magnetic activity (R. P. Kraft, 1967; A. Skumanich, 1972). This allows activity indicators to serve as stellar age diagnostics (*gyrochronology*).

1.2.3 Magnetic Cycles

Like the Sun's 11-year cycle, many cool stars show cyclic variations in magnetic activity, detected through long-term monitoring of the Ca II H & K emission (e.g., the Mount Wilson survey). These activity cycles provide insight into the operation and variability of stellar dynamos across different spectral types (S. L. Baliunas & A. H. Vaughan, 1985; S. H. Saar & A. Brandenburg, 1999; S. Saar & A. Brandenburg, 2001; T. S. Metcalfe et al., 2013; R. V. Ibañez Bustos et al., 2025).

M. M. Katsova (2020) review further explores the solar analogs of varying ages, noting that the young Sun likely rotated 10-20 times faster than it does today and had an intense magnetic field. During this early period (0.2-0.6 Gyr), the Sun underwent a shift from saturated activity to a solar-type regime with regular spot cycles forming. This transition is marked by rotation periods of $\tilde{1}.1$ days for G-type stars and $\tilde{3}.3$ days for K-types.

Magnetic field strength and configuration also evolve with age, with younger stars hosting stronger and more complex magnetic topologies. Both Zeeman Doppler Imaging (ZDI) and Zeeman broadening studies indicate that stars younger than ∼120 Myr typically exhibit mean surface magnetic fields of ∼1.3–2.0 kG (J.-F. Donati & J. D. Landstreet, 2009; C. P. Folsom et al., 2016), while older stars show significantly weaker fields, declining to ∼0.2–0.8 kG (A. Reiners et al., 2009; A. A. Vidotto et al., 2014).

1.2.4 Dynamo Mechanisms in Cool Stars

Cool stars, typically those of spectral types F, G, K, and M, exhibit magnetic activity generated by internal dynamo mechanisms, which convert kinetic energy from convective motions and differential rotation into magnetic energy. The type of dynamo operating in a star depends strongly on its internal structure and rotation rate.

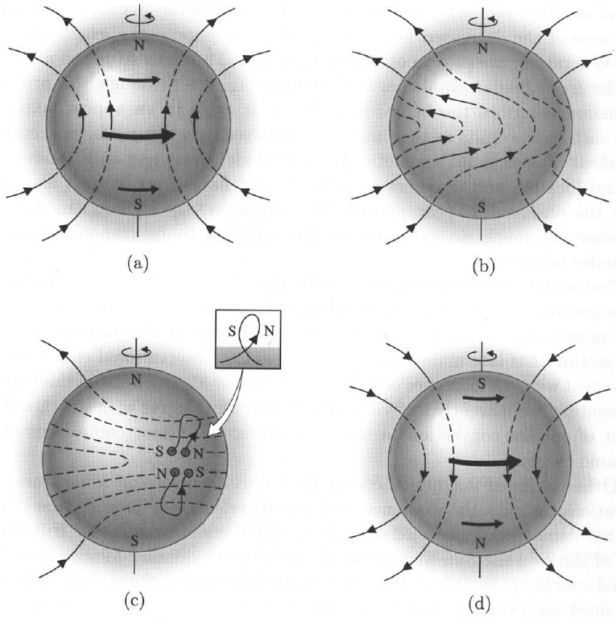

Figure 1.8. The $\alpha - \Omega$ dynamo along a complete cycle. Schematic illustration of large-scale magnetic field generation and evolution in a rotating, conducting sphere ($\alpha - \Omega$ dynamo). Adapted from W. Cao, Phys 320 Lecture 18: Solar Magnetism – Dynamo, New Jersey Institute of Technology W. Cao (2015).

1.2.4.1 Solar-like $alpha$–Ω Dynamo (Interface Dynamo)

Solar-like α–Ω Dynamo (Interface Dynamo) operates in stars possessing a radiative core and a convective envelope, such as the Sun and early K-type stars. The Ω-effect arises from differential rotation, which stretches poloidal magnetic fields into toroidal ones, while the α-effect, caused by helical convective turbulence, regenerates poloidal fields from toroidal fields. These processes interact most effectively in the *tachocline*, the shear layer between the radiative interior and the convective envelope. This dynamo typically produces large-scale, cyclic magnetic fields, as in the solar 11-year activity cycle, with efficiency increasing with rotation rate until reaching magnetic saturation.

1.2.4.2 Turbulent α^2 Dynamo

Fully convective stars, such as late M dwarfs below $\sim 0.35\,M_{\odot}$, lack a tachocline and therefore cannot sustain an α–Ω interface dynamo. In these objects, magnetic fields are generated by a purely turbulent α^2 dynamo, in which the α-effect alone maintains both poloidal and toroidal components through convective and rotationally induced helicity. The resulting fields are often strong, stable, and non-axisymmetric, with predominantly dipolar or multipolar topologies, consistent with observations of persistent magnetism in slowly rotating, fully convective stars.

1.2.4.3 Distributed or $\alpha^2 - \Omega$ Dynamo

In partially convective stars, both turbulent convection and differential rotation contribute to magnetic field generation throughout the entire convection zone, without a sharply defined tachocline. This regime, intermediate between the solar-like and fully convective cases, produces both large-scale organized and small-scale turbulent magnetic components, often leading to irregular or quasi-cyclic variability.

1.2.4.4 Small-scale or Local Dynamos

Local turbulent dynamos may operate in any convective layer, amplifying magnetic fields on small spatial scales independently of large-scale rotation or shear. They generate mixed-polarity fields that contribute to the basal level of chromospheric emission observed even in magnetically "inactive" stars.

1.2.4.5 Rotational Dependence and Transition

The efficiency of stellar dynamos is governed by the *Rossby number*,

$$Ro = \frac{P_{\rm rot}}{\tau_c}, \tag{1.3}$$

where $P_{\rm rot}$ is the rotation period and τ_c is the convective turnover time. Low Rossby numbers (rapid rotation) correspond to efficient, saturated dynamos, while high values (slow rotation) produce weak magnetic activity (R. W. Noyes et al., 1984). This situation is clearly pictured in Figure 1.9, taken from E. R. Newton et al. (2017). The rotation period can be measured directly, but while stellar convective turnover times can be calculated theoretically, it is also possible to estimate them empirically based on the assumption of a universal rotation-activity relationship for active stars (N. J. Wright et al., 2018). The transition from α–Ω to α^2-type behavior across the fully convective boundary explains the observed changes in magnetic topology and the activity–rotation relationship among cool stars (E. R. Newton et al., 2017; N. J. Wright et al., 2018). This shift naturally should produce the differences seen in the saturation levels of $L_{\rm x}/L_{\rm Bol}$ as a function of Rossby number.

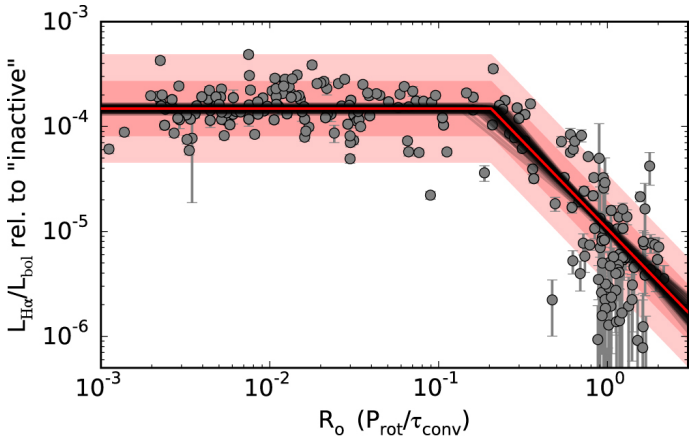

Figure 1.9. *Left*: $L_{H\alpha}/L_{Bol}$ vs Rossby Number (R_0), taken from E. R. Newton et al. (2017). Shows clearly the constancy of Hα excess emission at low values of Rossby Number

1.3 Observables for the Study of Chromospheric Activity in M-dwarfs

The study of chromospheric activity in M-dwarf stars relies on a range of observational diagnostics that trace the non-thermal emission produced by magnetic heating in the chromosphere. These observables can be broadly divided into *spectroscopic*, *photometric*, and *magnetic* indicators.

1.3.1 Chromospheric Activity Indicators

Spectroscopic diagnostics are the most direct means of probing chromospheric activity. They are based on emission or filling-in of specific spectral lines formed in different layers of the stellar atmosphere. The chromospheric activity

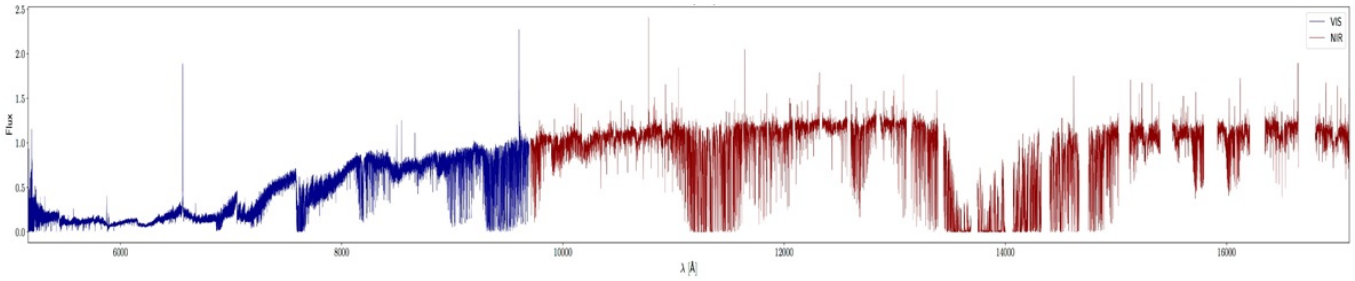

Figure 1.10. Example of Spectrum of a highly active M-dwarf star: YZ CMi, with spectral type M4.5V. The blue side of the spectrum correspond to the VIS channel of CARMENES instrument, while the red side to NIR channel. The profusion of *quiescent* absorption lines are clearly visible, and are more abundant in the red side of the spectrum, a feature common to all cool stars, as their $T_{\rm eff}$ lowers. These absorption lines are seen along with a series of emission lines, many of them used as *chromospheric activity indicators*. The highest levels of excess emission in the blue side of the spectrum are apparent and reached at the wavelengths of H_α and Ca II IRT lines

of late-type stars manifests itself through a variety of emission features in optical and near-infrared spectra, arising from non-radiative heating processes associated with stellar magnetic fields (J. L. Linsky, 1980; J. C. Hall, 2008). This remarkable feature, common to all chromospherically active stars, is apparent in the spectrum shown in Figure 1.10, where this activity can be detected through a limited series of lines. The *activity indicators*, can be seen in emission, in an otherwise quiescent (most of the times) i.e. absorption spectrum. Each of them probing different layers and physical conditions of the chromosphere.

1.3.1.1 Ca II H & K Lines

The classical tracers of chromospheric activity are the resonance lines of singly ionized calcium, Ca II H and K, centered at 3968.5 Å and 3933.7 Å, respectively (R. W. Noyes et al., 1984; V. Perdelwitz et al., 2021). The $R'_{\rm HK}$ index, widely used in solar-type stars, can still provide useful comparisons. These lines form in the upper chromosphere and often exhibit core emission reversals in active stars, though in late-type M-dwarfs they become increasingly difficult to observe due to low fluxes in the blue region.

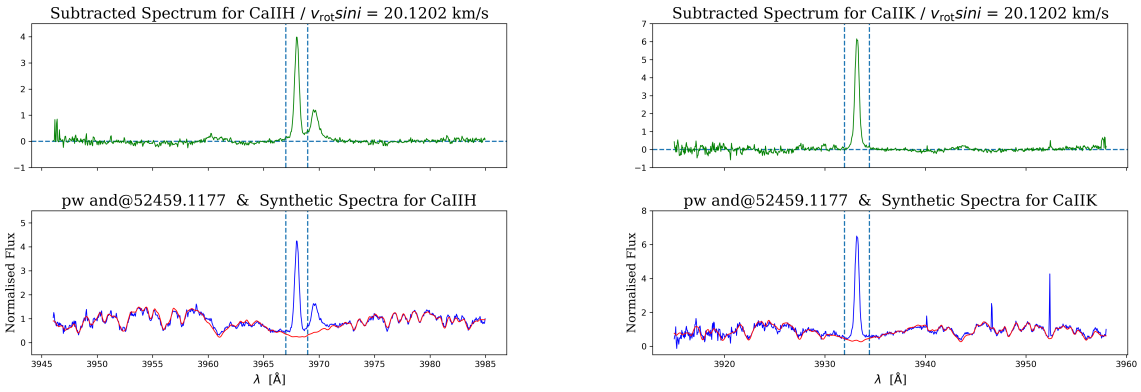

Figure 1.11. Spectral Subtraction Example from PW And, a K2V star. The different spectra shows chromospheric indicators in Ca II H & K (*upper figures*), using FOCES spectra For each figure: *Lower panel*: observed target spectrum (blue) and synthetic spectrum (red), obtained from a reference star spectrum. *Upper panel*: subtracted spectrum (green). In both panels: the vertical blue dashed lines mark the integration limits for the chromosoheric excess emission *EW* determination. From F. Labarga & D. Montes (2026). See chapter 2

The strength of these lines is commonly quantified using the *S-index*, originally defined by the Mount Wilson survey (A. H. Vaughan et al., 1978). A photospheric-corrected version, $\log R'_{\rm HK}$, provides a more intrinsic measure of activity, normalized to the stellar bolometric luminosity (R. W. Noyes et al., 1984).

1.3.1.2 Hα line (6564.6 Å):

It is the most widely used chromospheric activity indicator in M-dwarfs (A. A. West et al., 2004; S. Mohanty et al., 2002; E. R. Newton et al., 2017). The Hα line, formed in the mid-to-upper chromosphere has a complex behaviour:

in inactive stars, Hα appears in absorption; in active stars, it becomes partially filled or fully in emission due to chromospheric heating. It is particularly sensitive to plages, prominences, and flares (D. Montes et al., 1995a; L. E. Cram & M. S. Giampapa, 1987). The equivalent width (EW) or the ratio $L_{\mathrm{H}\alpha}/L_{\mathrm{bol}}$ are commonly used as quantitative measures (L. M. Walkowicz et al., 2004; L. M. Walkowicz & S. L. Hawley, 2009; A. Reiners & G. Basri, 2008)

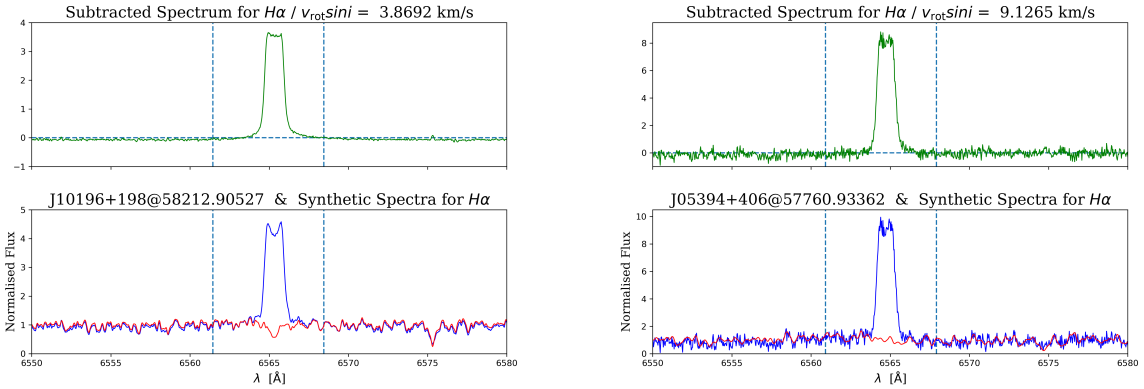

Figure 1.12. Spectral subtraction example from the CARMENES survey I. Ribas et al. (2023), showing Hα line as chromospheric activity indicator. (*Left*) AD Leo (J10196+198), a especially active M3.0V star. The reference star is HO Lib, showing clearly Hα in absorption. (*Right*) J05394+406, a M8.0V star, while its reference star is Teegarden's Star an M7.0V one. Note the profusion of lines of this spectrum, as opposed to the spectrum of AD Leo. The colour code is the same as fig. 1.11

1.3.1.3 Ca II Infrared Triplet (IRT)

The Ca II IRT lines at 8498, 8542, and 8662 Å are useful chromospheric diagnostics in cool stars, especially when the blue-violet region is inaccessible in redder M-dwarfs (J. Martin et al., 2017). These lines are less affected by interstellar absorption and provide good diagnostics of the lower chromosphere (D. Montes et al., 2000; R. Martínez-Arnáiz et al., 2011). The Ca II Infrared Triplet (IRT) is the equivalent in the IR of Ca II H & K lines as one of the primary indicators of stellar activity (D. Hintz et al., 2019; J. Martin et al., 2017) thus making it especially suitable for the analyses made from the CARMENES data. A. Quirrenbach et al. (2020). Considering, after B. R. Durney et al. (1981) that the Ca II emission closely follows the changes in stellar magnetic fields, and its emission strength in the IRT correlates with that of Hα, can be used to probe chromospheric heating depth.

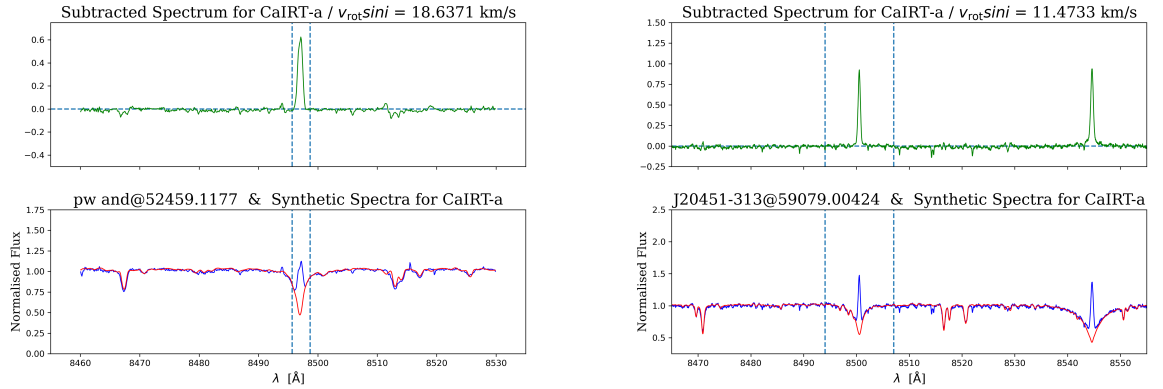

Figure 1.13. *Left* Spectral Subtraction Example from PW And, a K2V star. The FOCES provided spectrum shows chromospheric indicators in Ca II IRT-λ8498 line (referred to in the graphic titles as Ca II IRT-a). *Right* Spectral subtraction example from (J20451-313) AU Mic a specially young and active M0.5V star. The CARMENES I. Ribas et al. (2023) provided spectra shows chromospheric activity in Ca II IRT-λ8498 and Ca II IRT-λ 8542lines. Colour codes as in fig. 1.11

1.3.1.4 Helium Lines

The He I D_3 line at 5876 Å and the near-IR He I line at 10830 Å trace the upper chromosphere and transition region. They are useful for diagnosing flare activity and magnetic topology (B. Fuhrmeister et al., 2018; S. J. Schmidt et al., 2012). The lines He I D_3 accompanied by Na I D_1, D_2 are clear chromospheric activity indicators. He I D_3 in emission is widely known to be present when radiative cooling of non-radiative heating processes (D. A. Landman, 1981) occurs, given that photospheric temperatures are not enough ($T_{\mathrm{He\ I}\ D_3} \in [8,000, 40,000]$) to excite this atomic species to generate the line (S. H. Saar et al., 1997).

Regarding the He I IR triplet at 10830 Å, it is an important activity indicators in this spectral range for two reasons: first, is a line very sensitive to the level of activity (B. Fuhrmeister et al., 2020) and, on the other hand, is an excellent probe of the atmospheres of close-in transiting planets, either they be extended or also evaporating (L. Nortmann et al., 2018; M. Salz et al., 2018; F. J. Alonso-Floriano et al., 2019a)), detected by transmission spectroscopy in the star. Thus, subtracting the activity of the star, apparent in He I λ10830, is important in evaluating the extent of phenomena, as e.g. mass loss, happen to occur in the atmosphere of those planets, as well as the determination of their evolutionary stages.

1.3.1.5 Other Indicators

Additional lines include the Na I D doublet (5890 and 5896 Å), as mentioned in the previous sections, and higher-order Balmer lines such as Hβ and Hγ. These are particularly relevant for flare studies, though they often suffer from photospheric contamination. These indicators are widely used in stellar astrophysics to infer magnetic activity levels, study stellar cycles, constrain stellar ages, and assess the impact of high-energy radiation on exoplanetary atmospheres.

The Sodium doublet line is especially useful because it is produced at different depths of the chromosphere than Hα. The emission of He I D_3 and Na I $D_{1,2}$ lines are closely related with the plages around star-spots and flares. The sodium doublet lines, which often mirrors the behaviour of Hα, reflects the condition of middle-to-lower chromosphere, in contrast with the Hα line, that reflects the condition of middle-to-higher chromosphere (M. Kumar & R. Fares, 2023).

Balmer series (Hβ, Hγ, Hδ, ...) are used during flares or in highly active stars to trace temperature stratification in the chromosphere (see e.g. S. L. Hawley et al. 2003; A. García Soto et al. 2025 or D. Montes et al. 2000; M. C. Gálvez et al. 2002a for active binaries).

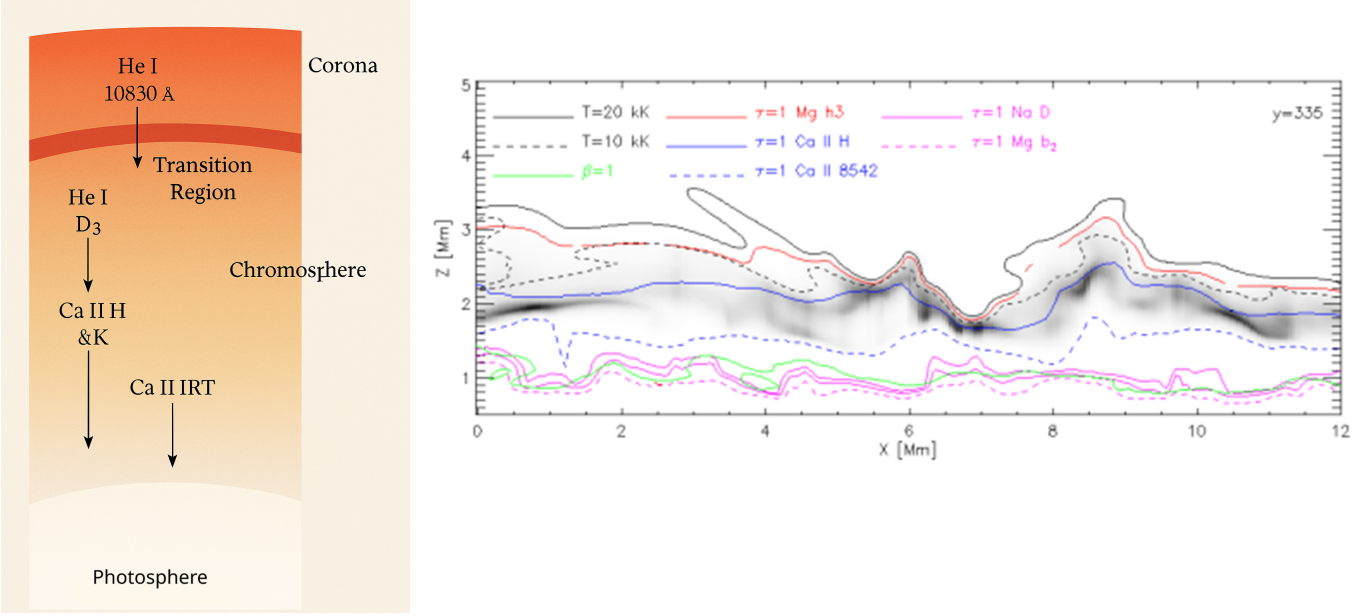

Figure 1.14. *(Left)* Schematic representation of the atmospheric layers of a late-type star, highlighting the approximate formation regions of common chromospheric activity indicators. The Ca II H & K lines originate in the upper chromosphere, while the Hα line forms in the mid-to-upper chromosphere. The Ca II infrared triplet (IRT) lines are typically formed in the lower chromosphere. The He I D_3 and 10830 Å lines trace the upper chromosphere and transition region, and are especially sensitive to high-activity phenomena such as flares and prominences. The photospheric continuum is shown for reference, with overlying layers progressively more rarefied and hotter. *(Right)* Formation heights of various chromospheric spectral lines computed from the self-consistent chromospheric modeling code Bifrost (Gudiksen et al. 2011). The snapshot from a time series shows the iso-temperature surfaces (black lines), the plasma-$\beta = 1$ layer (green) and the optical depth $\tau = 1$ layers for the spectral lines as labeled in the figure. The layer of absorption in the Hei 1083 nm triplet is indicated by the gray-shaded area. Taken from Carlsson et al. (2015). (Figure taken from A. Lagg et al. 2017)

Just as Balmer lines are widely used as diagnostics of chromospheric activity, the infrared Paschen series–particularly the Pβ, Paγ, and Paδ emission lines–provides valuable insight into the physical processes occurring in active stellar regions, such as flares and coronal mass ejections. The Paschen β (Pβ) line in emission is generally associated with flare events rather than with quiescent chromospheric conditions. In most M dwarfs, the quiescent chromosphere does not attain temperatures and electron densities sufficient to significantly populate the upper hydrogen levels involved in the $n = 5 \rightarrow 3$ transition. Under these conditions, the level populations remain close to their low-temperature equilibrium values, and the line source function does not exceed the local continuum intensity, preventing the appearance of Pβ in emission.

During magnetic reconnection events (flares), the chromospheric plasma is rapidly heated to $T \gtrsim 10^4$ K and reaches enhanced electron densities. The resulting increase in collisional excitation and recombination rates drives departures

from quiescent level populations and enhances the line emissivity, allowing the source function to exceed the continuum and the Pβ line to emerge in emission.

Since M-type stars emit most of their flux at longer wavelengths, Paschen lines–especially Paβ, located in the near-infrared at $\lambda = 12\,821.59$ Å–are particularly advantageous for observations in regimes where interstellar absorption is minimal, although with the set off of a higher telluric contamination P. Schöfer et al. (2019). Moreover, the near-infrared continuum of M dwarfs is substantially stronger than in the optical, so a comparatively large line emissivity is required for the emission to rise above the photospheric background. Consequently, Pβ is typically detectable only during sufficiently energetic events. In agreement with this interpretation, B. Fuhrmeister et al. (2023a) report that Pβ emission is characteristic of flares, although a subset of ultra-active M dwarfs ("very active emitters") can exhibit Paschen lines in emission even in pseudo-quiescent states. They also find a tight correlation between Pβ and Hα, with Pβ becoming detectable only above an activity threshold of $L_{\mathrm{H}\alpha}/L_{\mathrm{bol}} \sim 10^{-4}$.

These phenomena can have significant implications for the habitability of planets orbiting active stars, and Paschen-line studies therefore complement diagnostics obtained at other wavelength ranges (A. Segura et al., 2010). Additionally, the Paβ-to-Hα flux ratio, which often reveals a strong correlation, is a powerful diagnostic of the physical conditions in accretion flows, both in accreting young stars and in protoplanetary discs (Y. Aoyama et al., 2021; G. D. Marleau et al., 2022).

Although Paschen lines are generally less sensitive to typical levels of stellar activity–as we will see in chapter 3–, they remain excellent tracers of flares thanks to their purely chromospheric origin (B. Fuhrmeister et al., 2023a). Their study, however, is still relatively limited because only a few high-resolution spectrographs cover this region of the spectrum. Calibrations in these infrared ranges are challenging for late-type M dwarfs, for which the continuum level is often difficult to define. This makes the Paschen series particularly suitable for analysis through the spectral subtraction technique implemented in `iSTARMOD`, which enables a more reliable characterization of these lines.

1.3.2 Photometric Indicators

Magnetic activity in M-dwarfs induces brightness modulations due to starspots and flares, which are detectable through photometric monitoring. This modulation can be **rotational** as periodic variability in light curves arisen from long-lived starspots. The rotation period provides an indirect measurement of stellar angular momentum and is correlated with activity level (E. R. Newton et al., 2017; C. Cifuentes et al., 2020; Y. Shan et al., 2024). In the case of **flare emission**, a rapid and transient increases in brightness (typically in the UV, blue, or white-light bands) trace impulsive magnetic reconnection events. Flare frequency and energy distributions serve as indicators of magnetic energy release rates (J. R. A. Davenport, 2016). The photometric indicators due to **UV and X-ray fluxes** are measured by space-based observatories (e.g., *GALEX*, *XMM-Newton*) provide ultraviolet and X-ray fluxes tracing chromospheric and coronal heating, respectively (J. Robrade & J. H. M. M. Schmitt, 2009).

1.3.3 Magnetic and Rotational Diagnostics

Magnetic fields are the ultimate driver of chromospheric activity, and several indirect and direct methods can be used to infer their properties. In **Zeeman broadening and splitting**, measurements of line broadening in magnetically sensitive lines (e.g., Fe I lines) allow estimation of mean surface magnetic field strengths (A. Reiners, 2012; D. Shulyak et al., 2019). **Zeeman-Doppler Imaging (ZDI)** provides maps of large-scale magnetic field topologies from circular polarization measurements in spectral lines (see J. Morin et al. 2008 or J.-F. Donati et al. 2008, where abrupt change in the large-scale magnetic topologies of M dwarfs, occurring at spectral type M3). Using **Rotation-activity relations**, has been found observational correlations between $L_{\mathrm{H}\alpha}/L_{\mathrm{bol}}$ and rotation period (or Rossby number) describe the magnetic braking and saturation regimes characteristic of M-dwarfs (A. Reiners et al., 2014; E. R. Newton et al., 2017; N. J. Wright et al., 2018). The quoted field strengths of Table 1.1, summarizing 1.2.3, reflect both large-scale magnetic fields derived from ZDI and total unsigned fields measured via Zeeman broadening, with the former systematically underestimating the total magnetic flux (J.-F. Donati & J. D. Landstreet, 2009; D. Shulyak et al., 2014, 2017, 2019). Especially in D. Shulyak et al. (2017), where it is explicitly demonstrated that

$$\langle B \rangle_{\mathrm{ZDI}} \ll \langle B \rangle_{\mathrm{Zeeman}} \tag{1.4}$$

Table 1.1. Typical surface magnetic field strengths as a function of stellar age.

Age range	Field strength	Key references
$\lesssim$120 Myr	1.3–2.0 kG	J.-F. Donati & J. D. Landstreet (2009); C. P. Folsom et al. (2016)
>120 Myr	0.2–0.8 kG	(A. Reiners et al., 2009; A. A. Vidotto et al., 2014)

1.3.4 Derived Quantities

From the observables above, several derived parameters quantify the level of chromospheric activity:

- $R'_{\rm HK}$: the photosphere-corrected Ca II H&K flux ratio (R. W. Noyes et al., 1984). The combined EW of the lines Ca II H and Ca II K allows to define one the most widely used activity indicator: $R^{'}_{HK}$ (J. L. Linsky & T. R. Ayres (1978)). To integrate data from other instruments that complement the data from CARMENES, as in V. Perdelwitz et al. (2021), the calibration for the Ca II HK doublet has been included in what follows.

  The fluxes obtained from the calibration shown in Fig. 1 and Table 1 are equivalent to $R'_{\rm HK}$, given the sum of Ca II H or Ca II K EWs. So denoting R'_{HK} as the ratio between Ca II H&K emission and the stellar bolometric flux, as defined in J. L. Linsky et al. (1979):

$$R^{'}_{HK} = \frac{\mathcal{F}'_H + \mathcal{F}'_K}{\sigma T^4_{\rm eff}} \tag{1.5}$$

  Where the primes raise from subtracting the photospheric contribution:

$$\mathcal{F}'_{\rm line} = \mathcal{F}_{\rm line} - \mathcal{F}_{\rm line,phot} \tag{1.6}$$

- $L_{\rm H\alpha}/L_{\rm bol}$: normalized H$\alpha$ luminosity, a widely used metric for M-dwarfs (L. M. Walkowicz et al., 2004; L. M. Walkowicz & S. L. Hawley, 2009; A. Reiners & G. Basri, 2008; S. J. Schmidt et al., 2014).
- *Activity indices* such as $S_{\rm HK}$, IRT indices, or equivalent-width ratios (J. C. Hall & L. W. Ramsey, 1992a).
- *Flux-flux relationships*. that will be treated *in extenso* in chapter 3
- *Flare frequency distributions (FFDs)* derived from long-term photometric monitoring (J. R. A. Davenport, 2016).

These observables, when combined with stellar parameters (e.g., $T_{\rm eff}$, age, rotation period), provide a comprehensive picture of magnetic and chromospheric behavior across the M-dwarf sequence.

1.4 Methods and Tools

Accurate characterization of chromospheric emission requires a combination of observational and analytical techniques designed to isolate, quantify, and interpret the chromospheric contribution in stellar spectra.

- *High-Resolution Spectroscopy*. The most direct method involves obtaining high-resolution optical spectra capable of resolving narrow chromospheric line cores. Observations of the CaII H & K doublet and Hα line are commonly employed. Spectral resolution $R \geq 30,000$ is typically required to distinguish chromospheric emission from photospheric absorption, especially in slowly rotating or weakly active stars.
- *Spectral Subtraction Technique* To isolate chromospheric excess emission, the spectral subtraction method is often applied. This technique involves subtracting a template spectrum of an inactive star of the same spectral type and luminosity class from the target stars spectrum. The resulting residuals reveal net chromospheric emission in lines such as CaII H & K, H, and the CaII infrared triplet (IRT). The method is sensitive and effective, especially when small levels of activity are present.
- *Activity Indices* Several indices have been developed to quantify chromospheric activity:

  S-index (Mount Wilson scale): Measures the relative strength of emission in the cores of the CaII H & K lines compared to nearby continuum bands.

  $R'_{\rm HK}$: A refined index that corrects the S-index for the basal photospheric contribution and normalizes it to the stellar bolometric luminosity, allowing for comparisons across different spectral types defined as in 1.5

  Flux Ratios: Fluxes from various chromospheric lines (e.g., Hα vs. CaII K or vs. the more suitable for studying M-dwarfs Ca II IRT) are used to study the relative contributions of different emission processes and to investigate correlations among activity diagnostics.
- *Time-Domain Monitoring* Long-term monitoring of chromospheric lines (or activity indices like S-index R. V. Ibañez Bustos et al. 2025) enables the study of stellar activity cycles, analogous to the solar 11-year cycle. Variability in chromospheric indices can be linked to magnetic cycles, rotational modulation due to active region coverage, and transient flaring events. Time-series data are essential for characterizing the temporal evolution of stellar activity and distinguishing between rotational and intrinsic variability.
- *Ultraviolet and Space-Based Observations* For hotter chromospheric lines such as Mg II h & k–2800 Å– (A. P. Buccino & P. J. D. Mauas, 2008), observations must be carried out from space (e.g., with the Hubble Space Telescope or previously with the IUE). These lines serve as complementary diagnostics for more active or young stars, especially where chromospheric emission extends significantly into the UV regime J. L. Linsky et al. (2020).

1.4.1 Broadening of Spectral lines

To analyze the chromospheric emission, the subtraction of the photospheric contribution must be performed, according to (1.6). This has the implication that phenomena producing broadening of the spectral lines must be taken into account. Considering purely the radiative transfer, and following V. A. Sheminova (2017); L. Crivellari et al. (2019), an observed normalized line flux profile $\mathcal{F}(\lambda)$ can be represented as the convolution of the intrinsic line profile F^0_λ with the broadening functions describing stellar rotation, macroturbulence, and instrumental response:

$$\mathcal{F}(\lambda) = G(\lambda) * \Theta(\lambda) * I(\lambda) * F^0_\lambda, \tag{1.7}$$

where the symbol $*$ denotes convolution.

In the Fourier domain, Eq. (1.7) becomes a simple product:

$$f(\sigma) = g(\sigma)\,\theta(\sigma)\,i(\sigma)\,f^0_\lambda(\sigma), \tag{1.8}$$

where lowercase letters indicate Fourier transforms of the corresponding functions, and σ is the Fourier frequency (in cycles per nanometer or per $\mathrm{km\,s^{-1}}$).

1.4.1.1 Rotational Broadening

Rotational broadening comes from the different Doppler shift of each strip of the apparent disk of a rotating star

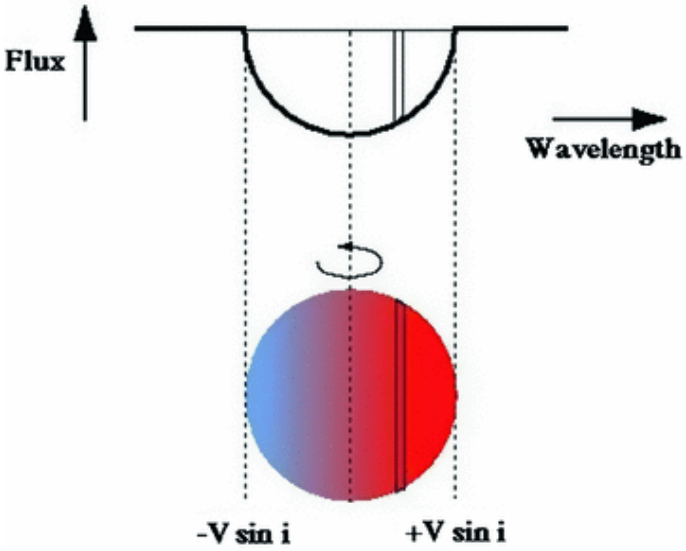

Figure 1.15. Origin of the rotational broadening of spectral lines. Here limb darkening is not taken into account, so in the Gray profile $\epsilon = 0$. (Figure taken from G. Catanzaro 2014)

As can be seen in Figure 1.15, the side of star that due to rotation is moving away from the observer will suffer its emission red-shifted. Conversely, the side approaching will suffer a blue-shift. Assuming solid-body rotation and linear limb darkening, the rotational profile $G(\lambda)$ is given by

$$G(x) = c_1(1-x^2)^{1/2} + c_2(1-x^2), \tag{1.9}$$

with coefficients

$$c_1 = 2(1-\epsilon), \qquad c_2 = \frac{\pi\epsilon}{2}, \tag{1.10}$$

and

$$x = \frac{\Delta\lambda}{\lambda}\,\frac{c}{v\sin i} \qquad |x| \leq 1. \tag{1.11}$$

The limb-darkening coefficient ϵ follows the law

$$I_c(\theta) = I_c(0)\,[1 - \epsilon + \epsilon\cos\theta]. \tag{1.12}$$

And take into account that the star is a tridimensional object projected onto a 2D surface. For late type stars, the limb darkening coefficient is fixed to $\epsilon = 0.6$. The study of the limb darkening parameter is an active field of research, mainly in the study of planet transits, and have bee empirically measured in eclipsing binaries (A. Frasca et al., 2023) and transiting planetary systems (P. F. L. Maxted 2022 for stars in the $T_{\rm eff}$ range $[5000, 7000]$), often using multi-parameter laws. Other studies use theoretical limb darkening model grids covering also cool stars and then interpolate or convert the values obtained from these models. However, direct constraints on linear limb-darkening coefficients for M-dwarfs stars relevant to this work remain limited. For this reason, the above mentioned solar linear limb-darkening coefficient was adopted as a practical approximation.

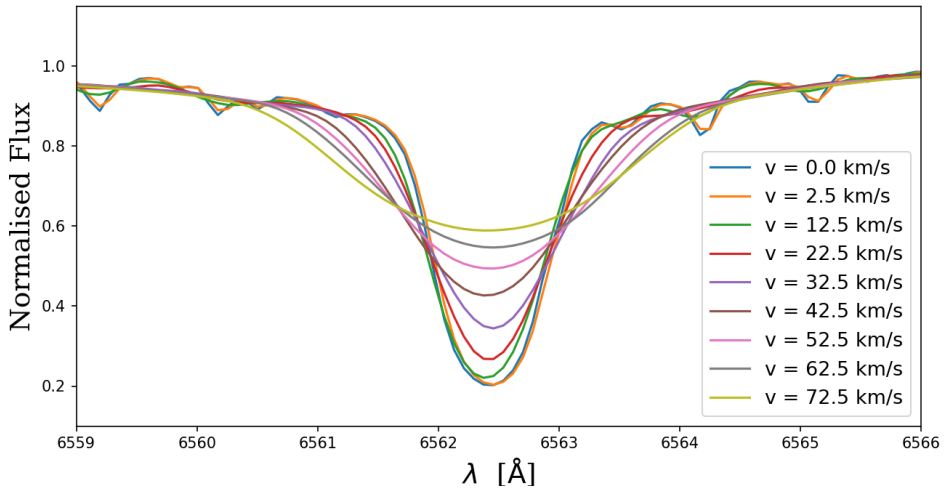

Figure 1.16. Different rotationally broadened profiles obtained by the convolution of an Hα profile of a K2V star with a Gray profile including the solar limb darkening coefficient $\epsilon = 0.6$ applied to different values of $vsini$

1.4.1.2 Macroturbulent Broadening

Macroturbulence represents large-scale, nonthermal motions in the photosphere. It refers to large–scale velocity fields, a scale much larger than the wavelength of the photons contributing to the line profile, in the stellar atmosphere. They broaden absorption line profiles beyond the contributions of instrumental, thermal, and rotational broadening. In contrast to microturbulence, which alters the equivalent width of spectral lines through its effect on line opacity, macroturbulence modifies only the *shape* of the line profile, redistributing absorption over a wider velocity interval without changing the integrated line strength. It can be described either by an isotropic Gaussian function,

$$\Theta(\xi) = \frac{1}{\xi_{\rm mac}\sqrt{\pi}} \exp\left[-\left(\frac{\xi}{\xi_{\rm mac}}\right)^2\right], \tag{1.13}$$

More elaborate radial–tangential models (e.g. D. F. Gray, 2022) can also be used:

$$\Theta(\xi) = (\pi\xi)^{1/2}\left(\frac{\lambda}{\xi}\right)\int_0^{\xi/\lambda} \exp\left(-1/u^2\right) \mathrm{d}u, \tag{1.14}$$

where the integral is evaluated separately for radial (ξ_R) and tangential (ξ_T) components, often assuming equal areas ($S_R = S_T = 0.5$) and velocities ($\xi_R = \xi_T = \xi_{\rm RT}$).

1.4.1.3 Instrumental Broadening

Finite spectral resolution introduces an instrumental profile $I(\lambda)$, often represented by a Gaussian of full width at half maximum (FWHM):

$$I(\lambda) = \frac{1}{\beta\sqrt{\pi}} \exp\left[-\left(\frac{\Delta\lambda}{\beta}\right)^2\right], \qquad \beta = \frac{\lambda V}{c}, \quad V = \frac{\mathrm{FWHM}}{2\sqrt{\ln 2}}. \tag{1.15}$$

For a spectrograph with resolving power R, the FWHM is $\mathrm{FWHM} = c/R$.

1.4.1.4 Residual Transform and Parameter Determination

By dividing Eq. (1.8) by the transforms of the instrumental and intrinsic profiles, the residual transform is obtained:

$$m(\sigma) = \frac{d(\sigma)}{i(\sigma)\, f_\lambda^0(\sigma)}. \tag{1.16}$$

The best fit of the residual transform to the product of theoretical rotation and macroturbulent transforms yields the parameters $\xi_{\rm mac}$ and $v \sin i$. The microturbulent velocity $\xi_{\rm mic}$ is determined iteratively by matching the side-lobe structure or the amplitude of the main lobe in $d(\sigma)/i(\sigma)$.

1.4.2 Use of the Cross-Correlation Function (CCF) in the Spectral Analysis of Cool Stars

The *Cross-Correlation Function* (CCF) is widely employed in stellar spectroscopy to extract information about the *radial velocity* (RV) and *line profile variations* of cool stars. It provides an efficient means to combine the signal from

numerous spectral lines, enhancing the signal-to-noise ratio (S/N) and enabling precise velocity measurements even in spectra with moderate quality.

The CCF is computed by correlating the observed stellar spectrum $S(\lambda)$ with a **template spectrum** or numerical mask $T(\lambda)$:

$$\mathrm{CCF}(v) = \int S(\lambda)\, T(\lambda_v)\, d\lambda, \tag{1.17}$$

where $\lambda_v = \lambda(1 + v/c)$ is the Doppler-shifted wavelength corresponding to a velocity v. The velocity at which the CCF reaches its maximum (or minimum) corresponds to the radial velocity of the star.

1.4.2.1 Radial Velocity Determination

For late-type (cool) stars, which exhibit dense absorption-line spectra, the CCF efficiently averages the Doppler information across many lines, reducing random noise (M. Zechmeister et al., 2018). The radial velocity is derived by fitting a Gaussian profile to the extremum of the cross-correlation function (CCF). The nature of this extremum (minimum or maximum) depends on the adopted template and sign convention. When a binary mask composed of positive delta functions at the positions of absorption lines is used, the CCF displays a minimum (A. Baranne et al., 1996), whereas when a real or synthetic spectrum is adopted as a template, the CCF exhibits a maximum. When the latter approach is used, and the radial velocity is obtained by fitting a Gaussian profile to the CCF maximum, the projected rotational velocity $v \sin i$ from the CCF width (FWHM) and the line contrast (or depth) as a proxy for stellar activity or line filling.

1.4.2.2 Diagnostics of Stellar Activity

Cool stars often exhibit line asymmetries caused by spots, plages, or convective motions. These induce distortions in the CCF profile that can mimic or mask RV shifts (M. Lafarga et al., 2021). Quantitative diagnostics include:

- *Bisector Inverse Slope (BIS):* measures the asymmetry of the CCF profile to detect activity-induced RV variations;
- *CCF FWHM and contrast:* variations correlate with chromospheric activity, magnetic field evolution, or pulsations.

Different masks (G2, K5, M2, etc.) are used to match the spectral type of the target star. For M dwarfs, where molecular bands dominate, the use of synthetic templates or *Least-Squares Deconvolution* (LSD) is often preferred to optimize the cross-correlation efficiency (M. Lafarga et al., 2020). The CCF approach is conceptually similar to template-matching methods and LSD profiles, but with simplified computational treatment. It remains the cornerstone of radial velocity pipelines in high-resolution spectrographs such as *CARMENES*, *HARPS*, *SOPHIE*, and *ESPRESSO*.

1.4.3 Spectral Subtraction Technique

The spectral subtraction technique is one of the most effective methods for quantifying the chromospheric contribution to the radiative outflow in active late-type stars across several activity indicators. This contribution is typically measured as excess emission relative to a quiescent reference in equivalent width (EW) units for specific optical and near-infrared spectral lines, which are well-established indicators of chromospheric activity in FGKM-type stars ((C. J. Marvin et al., 2023) and references therein). Some codes have been developed in the past for applying this tecniche e.g. STARMOD (S. C. Barden, 1985; D. Montes et al., 1995a,b, 2000) and ROTFIT (A. Frasca & S. Catalano, 1994; A. Frasca et al., 2003, 2006).

The excess emission need to be measured against the photospheric contribution to the radiative outflow:

$$\mathcal{F}'_{\mathrm{line}} = \mathcal{F}_{\mathrm{line}} - \mathcal{F}_{\mathrm{line,phot}} \tag{1.18}$$

where $\mathcal{F}'_{\mathrm{line}}$ is the chromospheric excess emission line flux, $\mathcal{F}_{\mathrm{line}}$ is the total flux emitted along this line, and $\mathcal{F}_{\mathrm{line,phot}}$ is the photospheric contribution to the outflow along this line. All activity indices refers to equation 1.18 in one way or another, as happen with the S-index or R'_{HK}. They subtract the contribution of the photosphere applying low-band filters to positions of the continuum near and at both sides of the considered line. The spectral subtraction technique requires recovering the continuum through synthesizing a quiescent version of the spectrum from a reference star, and with the same spectral type, radial velocity and rotational state. Finally, the EW measurement obtained through this method is converted to line flux or, equivalently, line luminosity normalized to bolometric.

1.4.4 iSTARMOD

This thesis describes methods and tools, among which we can find `iSTARMOD`, an updated and extended version of the original `STARMOD` code, to analyze the above mentioned features with chromospheric activity indicators, as the extensively studied Hα along with the rest of Balmer lines in the visible, together with He I D_3 and Na I $D_{1,2}$, Ca II

H&K and the less studied Ca II IRT lines in the near infrared (see D. Montes et al. (2000)). Further in the spectral range can be analyzed Paschen series (Paschen δ, γ and β), along with He I λ10830 P. Schöfer et al. (2019).

1.4.5 Activity and Flux-Flux relationships

The study of flux-flux relationships is a powerful tool for characterizing M dwarfs. These correlations allow astronomers to probe stellar activity and derive key stellar properties, thereby gaining insight into the physical processes that govern these stars (D. Montes, 1995; D. Montes et al., 1996a; J. López Santiago, 2005). Deviations from the typical log-linear trends–often caused by flares, starspots, or other chromospheric phenomena–also provide valuable diagnostic information (R. V. Ibañez Bustos et al., 2023), including clues about the nature and distribution of the underlying emitter populations.

A comprehensive analysis of this type on the emitter populations was performed by R. Martínez-Arnáiz et al. (2011), to which parts of the the present work constitutes, in part, a natural extension. In that study, the presence of (at least) two distinct chromospheric emitter populations among M dwarfs was clearly identified.

In this context, the CARMENES project offers a unique opportunity: it delivers high-resolution spectra across the entire M-dwarf sequence, reaching the latest and faintest subtypes, well beyond the fully convective boundary. This unprecedented spectral coverage enables a more detailed and homogeneous exploration of flux-flux relationships in these stars.

1.5 M-dwarfs activity and radial velocities determination. CARMENES program

Recent advances in studying chromospheric activity in cold stars stem from the need to detect the shift, or jitter, in spectral lines caused by exoplanets orbiting those stars and to understand its impact on the formation, evolution, and habitability of these exoplanets. The radial velocity (RV) modulation must be distinguished from shifts induced by stellar activity. As it is known (L. Tal-Or et al., 2018; S. V. Jeffers et al., 2022; L. Lindegren & D. Dravins, 2003; I. Boisse et al., 2013; X. Dumusque, 2018; J. C. Costes et al., 2021), activity produces line profile deformation that limits the precision of the determination of RVs. So stellar rotation, stellar activity cycles, starspots and surface inhomogeneities, convective features, flare events (A. Reiners, 2009; E. N. Johnson et al., 2021) and even Zeeman broadening (A. Reiners et al., 2013) caused by intense magnetic fields in the starspots can mimic the RV modulation of the host star produced by exoplanets. Considering these effects, made it possible, at least partially (D. Kossakowski et al., 2022), to confirm or rule out potential planets around stars. The analyses account for the fact that the radial velocity method yields better results for Earth-like rocky planets orbiting late-type (less massive) stars, as their RV modulations fall within the instrumental precision required for detection. Moreover, chromospheric activity is more pronounced in M-type stars than in earlier type stars. Therefore, in exoplanet search surveys targeting M-type stars, accurately characterizing stellar activity is paramount to succeed (A. Quirrenbach et al., 2020, 2024).

As discussed in detail in Section 1.1.4, stellar magnetic activity in M dwarfs plays a central role not only in the detectability of exoplanets but also in their atmospheric evolution and potential habitability. High levels of chromospheric and coronal activity, including flares, coronal mass ejections, and associated stellar winds, can drive atmospheric erosion processes such as photoevaporation and thermal escape (e.g. A. Segura et al., 2010; J. E. Owen & S. Mohanty, 2016; M. Salz et al., 2018; A. Canet et al., 2024; A. Canet & A. I. Gómez de Castro, 2021).

In the context of radial-velocity surveys such as CARMENES, these same activity phenomena are particularly relevant because, as mentioned, they introduce RV signals that can mimic or obscure planetary-induced Doppler shifts, reinforcing the need for a precise characterization of stellar activity indicators in M-type stars. In addition to affecting planetary atmospheres, chromospheric activity can also bias observational diagnostics such as transmission spectroscopy, altering the inferred atmospheric properties of transiting exoplanets (V. Perdelwitz et al., 2025).

In spite of these observational challenges, M-dwarfs stars (or red dwarfs) are increasingly targeted in the search for exoplanets due to their abundance and favorable planet-star contrast ratios, a fact that has been mentioned in 1.1.1. The analysis of detectability of exoplanets orbiting M-type stars, using RV observational techniques (J. T. Wright & B. S. Gaudi, 2013), is based on the amplitude of RV variations, given by the equation:

$$K = \left(\frac{2\pi G}{P}\right)^{1/3} \frac{M_p \sin i}{(M_* + M_p)^{2/3}} \frac{1}{\sqrt{1-e^2}} \tag{1.19}$$

Where K is the radial velocity semi-amplitude, measured in $ms^{-}1$, G is the gravitational constant, P is the orbital period measured in seconds, M_p is the mass of the planet, $M_\star$ is the mass of the star, i is the inclination of the orbit, and e is the orbital eccentricity. For earth-sized exoplanets, where $M_\mathrm{p} \ll M_\star$, the following approximation, for our discussion purposes, applies:

$$K \approx \left(\frac{2\pi G}{P}\right)^{1/3} \frac{M_p \sin i}{M_*^{2/3}} \frac{1}{\sqrt{1-e^2}}$$

The analysis considers stellar activity, brightness, and habitable zone constraints, comparing detection efficiency across different stellar subtypes and instrument sensitivities. Results indicate that despite observational challenges such as increased stellar activity and lower luminosity, M-type stars offer excellent opportunities for detecting terrestrial, potentially habitable exoplanets.

1.5.1 CARMENES Instrument Overview

CARMENES[1] (*Calar Alto high-Resolution search for M dwarfs with Exoearths with Near-infrared and optical Échelle Spectrographs*) is a dual-channel, high-resolution spectrograph mounted on the 3.5-meter telescope at the Calar Alto Observatory (CAHA) in Spain. Designed by a German-Spanish consortium, it enables precise radial velocity (RV) measurements to detect exoplanets around M-type dwarf stars. This dual-channel spectrograph has a visible (VIS) and a near-infrared (NIR) arm. The VIS one has a spectral coverage of 0.52–0.96 μm with spectral resolution of $R \approx 94{,}600$, operating at 284 K, while the NIR channel has spectral coverage 0.96–1.71 μm with spectral resolution $R \approx 80{,}400$.

Its design consists of White-pupil, fiber-fed, cross-dispersed échelle spectrographs housed in vacuum tanks and isolated from environmental noise, with Fabry-Pérot etalons and hollow-cathode lamps (Th-Ne, U-Ne, U-Ar) used for wavelength calibration (A. Quirrenbach et al., 2018, 2020, 2024). This is accompanied with a CARACAL reduction pipeline (J. A. Caballero et al., 2016a), SERVAL (M. Zechmeister et al., 2018), and RACCOON for RV and stellar activity analysis, and an exposure meter that measures photon fluxes for barycentric correction.. All of this enables achieving a RV Precision of $\sim$1 m s^{-1} with long-term stability.

1.5.2 CARMENES Observation Program

The **CARMENES survey** is a high-precision, long-term radial velocity program aimed at detecting low-mass, potentially habitable exoplanets around nearby M dwarfs. Its goals (J. A. Caballero et al., 2025) can be summarised in:

- Detect Earth-mass planets in the habitable zones of $\sim$300 M dwarfs.
- Characterize stellar activity and spectra of M dwarfs.
- Measure planetary masses for transiting planets discovered by *TESS*.
- Perform transmission and emission spectroscopy of exoplanet atmospheres.

The **target sample** consist in $\sim$365 stars covering spectral types M0 to M9, most of them selected from the `CARMENCITA` database of bright, nearby M dwarfs, optimized to maximize RV sensitivity across spectral subtypes (J. A. Caballero et al., 2016b). It is worth mentioning that binaries and unsuitable stars were excluded. Chapter 2–paragraph 2.5.2–includes examples of stars had to be excluded from CARMENCITA database, and also excluded from the analyses performed in Chapter 3 (e.g.:D. Baroch et al. (2018, 2021)).

The **survey phases** of the CARMENES program consist in two for the time being. A first one **GTO (Guaranteed Time Observations)**, from 2016 to 2020 with the observations scheduled by the initial goals of the program, and a subsequent **Legacy+**, from 2021 to 2026, with the consolidation of scientific goals, updated from the initial results, in a joint effort of the GTO observations with the follow-up of TESS and KEPLER discoveries. Along with these two phases, open time allocated for external science projects, have been exploited.

The **Scientific Output** of this very productive project consists, as for now, in over 80 exoplanets discovered or confirmed, including Earth-mass planets in habitable zones. In the CARMENES web page can be read that they are 57 GTO/Legacy/TESS/Kepler around M dwarfs and 12 around earler type (FGK) stars. Among these planets discovered can be mentioned **GJ 3512 b:** a giant planet around an ultra-low-mass star, challenging classical formation models (J. C. Morales et al., 2019), **Teegarden's Star:** a system with multiple Earth-mass planets in or near the habitable zone that during several years was the most similar to Earth exoplanet discovered (M. Zechmeister et al., 2019), or **GJ 357:** a transiting Earth-sized planet with two additional non-transiting companions (R. Luque et al., 2019). In addition to these ones can be mentioned the confirmation of an exoplanet discovery in Barnard's Star, the closest single star to Earth (I. Ribas et al., 2018). Also, other 27 planets confirmed or re-analyzed by CARMENES and notably as mentioned in the same web page, "CARMENES is besides a *planet killer*" performing analysis of a "few systems with challenged exoplanet candidates" (A. Quirrenbach et al., 2022). These exoplanet discoveries have been allowed thanks to the **High-precision RVs** achieved, with a median internal precision of 1.27 m s^{-1} for VIS channel (A. Quirrenbach et al., 2020; J. A. Caballero et al., 2025).In summary, these discoveries are also key contributions to understanding planet formation, occurrence rates, and stellar jitter.

Other goal of the scientific program: performing transmission and emission spectroscopy has rendered fruitful results, with exoplanet atmospheric detection of He I (L. Nortmann et al., 2018; F. J. Alonso-Floriano et al., 2019a; E. Palle et al., 2020), including theoretical modelling as in M. Lampón et al. (2020) Hα, Na I (N. Casasayas-Barris

[1] https://carmenes.caha.es

et al., 2020), K I, Ca II (F. Yan et al., 2019), and H_2O (A. Sánchez-López et al., 2019; F. J. Alonso-Floriano et al., 2019b) via transmission spectroscopy, based on studies of exoplanets on WASP-69, WASP-33, KELT-19 and, over all, HD 189733 and HD 209458.

During the science exploitation of the CARMENES instrument for this survey, and related with the remaining objective of the project mentioned above, the consortium has analysed the chromospheric activity level of the surveyed stars using the different indicators included in the CARMENES spectral range (P. Schöfer et al., 2019, 2022; B. Fuhrmeister et al., 2018, 2019, 2020, 2022, 2023a; B. Toledo-Padrón et al., 2019; E. N. Johnson et al., 2021; M. Lafarga et al., 2020, 2021; S. V. Jeffers et al., 2022), quantified the magnetic field (D. Shulyak et al., 2019; A. Reiners et al., 2022), compared this activity with chromospheric modeling (D. Hintz et al., 2019, 2020, 2023), identified the stars with large activity-induced radial velocity variations (L. Tal-Or et al., 2018) and quantified the impact of activity on radial velocity measurements (S. V. Jeffers et al., 2022; H. L. Ruh et al., 2024), as well as performed measurements of the activity cycles (B. Fuhrmeister et al., 2023b). This thesis is related with the activities performed in this part of the project.

Future Directions

- Complete Legacy+ survey program by 2026.
- Upgrade via **CARMENES+** (R. Varas et al., 2025):
  - New combined VIS+NIR Fabry-Pérot etalon.
  - 24/7 vacuum pump operation.
  - Enhanced fibre switching and calibration routines.
- Support *PLATO* and *JWST* missions for mass and atmosphere characterization.

CARMENES is a benchmark facility for RV detection of exoplanets around M dwarfs. Its innovative dual-channel architecture, exceptional stability, and targeted survey design have made it one of the most productive instruments in exoplanet science over the past decade. It continues to play a vital role in the discovery and characterization of nearby Earth-like worlds.

1.6 Plan of this thesis

The study of chromospheric activity indicators and their flux-flux relationships, need the measurement of the equivalent width (EW) of the excess emission for each activity indicator. This task is intended to be carried out here applying the *spectral subtraction technique*. A Python code (iSTARMOD) has been used, based on a previous FORTRAN one, then in use by the research group. But for obtaining the fluxes of each activity indicator, additional post-processing routines have to be implemented in order to transform the equivalent widths measured on the spectra to Luminosity line to bolometric. The χ factor method (L. M. Walkowicz et al., 2004) has been generalised in this thesis to several other activity indicators than Hα. The methodology of A. Reiners & G. Basri (2008) at determining the line-flux from a series of synthetic spectra in determining the χ factor has been used. In regard to the flux at the continuum near the line for each chromospheric indicator, an analogue of the method of S. T. Douglas et al. (2014) has been used.

The analysis of M-dwarf activity presented in this thesis begins, in Chapter 2, with a description of the spectral subtraction technique, with the prescriptions of `iSTARMOD` code and its additional post-processing. This chapter is based on the paper F. Labarga & D. Montes (2026). In Chapter 3, section 3.3 the resulting flux-flux relationships are presented. They are supplemented in Section 3.4.5 with values of average magnetic field intensity $\langle B \rangle$, metallicity $[Fe/H]$, rotation period $P_{\rm rot}$ and ages. The determination of $P_{\rm rot}$ allows to perform an analysis of the activity in terms of the Rossby Number R_0. The paper ends in Section 3.5 with the conclusions can be obtained from this study in view of the results presented in the previous sections.

1.6.1 Research Purpose

The purpose of this research project is to develop and apply advanced software tools for the analysis of high-resolution stellar spectra obtained from the **CARMENES Observation Program**, with the goal of measuring and characterizing the **chromospheric activity of M-type stars**. This work directly contributes to the study of the effects of stellar magnetic activity on **radial velocity (RV) determinations**, which are essential in the detection and characterization of exoplanets.

One of the outcomes of this project, `iSTARMOD`, is a modern Python-based implementation of the **Spectral Subtraction Technique**–a method that isolates the chromospheric contribution in late-type stars by subtracting the spectrum of a non-active reference star from that of an active one (S. C. Barden, 1985; D. Montes et al., 2000). The technique allows measurement of the excess emission in activity-sensitive lines such as Hα, Ca II H&K, He I D_3,

Na I D_1,D_2, and the Ca II Infrared Triplet (IRT), extending also to He I λ10830 Å and the Paschen series in the near-infrared (F. Labarga & D. Montes, 2026).

By implementing this methodology, the project enables the systematic quantification of chromospheric activity across the CARMENES catalog of M dwarfs and the study of flux-flux relationships among indicators.

1.6.2 General Objectives

This research aims to migrate, extend, and modernize the classic `STARMOD` code (originally in FORTRAN 77) into a Python 3 implementation—`iSTARMOD`—capable of efficiently processing large spectral datasets and integrating into modern astrophysical workflows.
The specific objectives are:

- Migration and modernization of the legacy `STARMOD` code into `Python 3` (`iSTARMOD`), ensuring modularity, maintainability, and compatibility with modern scientific libraries such as `Astropy`, `NumPy`, and `SciPy`.
- Adaptation of spectral reading and preprocessing routines to handle **FITS formats** used by the CARMENES spectrograph and other high-resolution echelle instruments.
- Analysis and validation of the Spectral Subtraction Technique algorithms implemented in Python, including iterative least-squares fitting for radial velocity alignment and rotational broadening via the Gray profile.
- Implementation of automatic equivalent width (EW) measurement and uncertainty estimation following the G. Cayrel de Strobel & M. Spite (1988) formalism, with post-processing routines for chromospheric flux calibration.
- Extension of the method to single and spectroscopic binary systems (SB2), through weighted spectral synthesis and deconvolution for composite spectra.
- Preliminary design of an graphical user interface (GUI) for `iSTARMOD`, improving usability and visualization of spectral subtraction results.
- Automation of large-scale batch processing for the CARMENES dataset, enabling the analysis of extensive samples of M-dwarf spectra.
- Dissemination of the project results through publication in Q1 scientific journals and participation in academic conferences.

1.6.3 Methodology

The project combines software engineering principles with astrophysical modeling techniques to ensure accuracy, reproducibility, and scientific robustness:

1.6.3.1 Software Development Approach

- Requirements analysis, modular software design, version control, and unit testing.
- Integration of configuration management and automatic testing frameworks for reproducible pipelines.
- Continuous validation of algorithmic outputs against benchmark results from `STARMOD` and `CARMENES` data.

1.6.3.2 Spectral Subtraction and Modeling

- Construction of synthetic reference spectra by applying rotational broadening (Gray profile D. F. Gray 2022) and Doppler shifting to inactive star templates of matching spectral type and luminosity class.
- Iterative least-squares minimization of residuals between observed and synthetic spectra, performed order-by-order across echelle spectra to ensure spectral fidelity.
- Quality assurance through residual RMS analysis, ensuring that the subtracted spectra retain emission only at chromospheric-sensitive lines.

1.6.3.3 Data Processing and Calibration

- Support for multiple FITS formats (FOCES, HERMES, CARMENES, etc.).
- Automatic continuum placement and normalization using an adaptation of the `ARES` algorithm (S. G. Sousa et al., 2007, 2015), optimized for late-type stars.
- Calculation of EW uncertainties using the R. Cayrel et al. (2004) formula.
- Conversion of excess equivalent widths to line fluxes normalized to bolometric through newly defined χ-factor calibrations for several chromospheric indicators, covering a wide temperature range (2200-7000 K) (F. Labarga, 2025).
- Determination of several flux-flux relationships, to characterize the chromospheric activity of M-dwarfs.

1.6.3.4 Validation and Scientific Application

- Application of `iSTARMOD` to a representative sample of CARMENES spectra for M-type dwarfs and active binaries.
- Verification of chromospheric flux determinations against classical indices such as $R'_{\rm HK}$ (J. L. Linsky & T. R. Ayres, 1978).
- Analysis of correlations between activity levels, rotation, and other parameters.

1.6.4 Expected Results and Impact

The implementation of `iSTARMOD` will:

- Provide a robust, automated tool for chromospheric activity analysis of M-type stars in large spectroscopic surveys.
- Enable flux-calibrated, wavelength-consistent measurements across multiple chromospheric indicators.
- Facilitate correction of radial velocity variations induced by stellar activity, thereby enhancing the precision of exoplanet searches.
- Contribute an open-source and extensible software package to the astrophysical community, fostering reproducibility and collaboration in stellar activity studies.

In addition to its research applications, `iSTARMOD` will also serve an important **educational role**. The software can be used in university laboratories and graduate-level courses to introduce students to the analysis of stellar spectra, the principles of the spectral subtraction technique, and the study of chromospheric activity in cool stars. Its open-source and modular design makes it ideal for practical sessions, where students can learn how to process real observational data from spectroscopic surveys such as CARMENES, explore the influence of stellar activity on observed spectra, and reproduce professional-grade analyses. This pedagogical use will promote the integration of computational astrophysics and observational techniques in teaching environments, reinforcing both theoretical and practical understanding of stellar activity phenomena.

CHAPTER 2

iSTARMOD: a Python Code to Quantify Chromospheric Activity by Using the Spectral Subtraction Technique

Reference

This chapter is based on Fernando Labarga & David Montes 2026 AJ 171 15 DOI: 10.3847/1538-3881/ae173e
SW available at: 10.5281/zenodo.17329154
Paper published by *The Astronomical Journal, 5th Dec, 2025.*

2.1 Introduction

The spectral subtraction technique (S. C. Barden, 1985; D. Montes et al., 1995a,b, 2000) is one of the most effective methods for quantifying the chromospheric contribution to the radiative outflow in active late-type stars across several activity indicators (D. Montes et al., 2000; M. C. Gálvez et al., 2007, 2009; R. Martínez-Arnáiz et al., 2011; C. J. Marvin et al., 2023). This contribution is typically measured as excess emission –relative to a quiescent reference–in equivalent width (EW) units for specific optical and near-infrared (NIR) spectral lines, which are well-established indicators of chromospheric activity in FGKM-type stars. The excess emission needs to be measured against the photospheric contribution to the radiative outflow:

$$\mathcal{F}'_{\rm line} = \mathcal{F}_{\rm line} - \mathcal{F}_{\rm line,phot} \tag{2.1}$$

where $\mathcal{F}'_{\rm line}$ is the chromospheric excess emission-line flux, $\mathcal{F}_{\rm line}$ is the total flux emitted along this line, and $\mathcal{F}_{\rm line,phot}$ is the photospheric contribution to the outflow along this line. So spectral subtraction requires recovering the continuum through synthesizing a quiescent version of the spectrum from a reference star, and with the same spectral type, radial velocity, and rotational state. Finally, the EW measurement obtained through this method is converted to line flux or, equivalently, line luminosity normalized to bolometric luminosity. For this purpose, the χ-factor method L. M. Walkowicz et al. (2004) applies. This paper describes both spectral subtraction and a series of χ-factor function calibrations. Given the above, the spectral subtraction technique allows us to study magnetically active cool stars, analyze in detail its chromosphere using the information provided for several optical spectroscopic features that are formed at different heights, and discriminate between structures: plages, prominences, flares, and micro-flares. This paper describes methods and tools, by means of `iSTARMOD`, to analyze these features with chromospheric activity indicators, such as the extensively studied Hα along with the rest of Balmer lines in the visible, together with He I D_3 and Na I D_1, D_2, Ca II H and K, and the less studied Ca II infrared triplet (IRT) lines in the NIR (see D. Montes et al. 2000). Further along NIR spectral range can be analyzed Paschen series (Paδ, Paγ and Paβ), together with He I λ10830 (P. Schöfer et al., 2019). All of these lines are included in most of the high-resolution echelle spectra.

Spectral subtraction has been routinely applied to measure chromospheric fluxes of active stars. G. H. Herbig (1985) did so for analyzing Hα emission in F8–G3 stars, and A. Frasca & S. Catalano (1994) applied it in the study of close binaries. D. P. Huenemoerder et al. (1989) explored TiO bands to model the occurrence of spots in the surface of RS CVn stars.

Continuing the work of A. Frasca & S. Catalano (1994), `ROTFIT`, a robust tool for automated spectral classification and activity analysis in late-type stars, was developed. `ROTFIT` is a code written in IDL (interactive data language) designed to determine stellar parameters (effective temperature, surface gravity, and metallicity) by comparing observed spectra with a library of standard-star spectra (A. Frasca et al., 2003, 2006). The tool was used alongside spectral subtraction techniques to isolate chromospheric emission features and characterize the activity levels (P. Guillout et al., 2009). A. Frasca et al. (2018) further used `ROTFIT` to derive stellar parameters ($T_{\rm eff}$, $\log g$, [Fe/H], and $v\sin i$) by fitting observed spectra with a grid of reference star spectra, accounting for rotational broadening. These works show the role of the spectral subtraction technique in enabling the discovery of numerous young, active stars and candidate binaries, with the characterization of their activity based on lithium abundance and chromospheric activity indicators.

Previous to development of `iSTARMOD`, as well as after the significant contribution to early models of extended matter and eclipse behavior in RS CVn binaries, that layed the groundwork for later observational and theoretical efforts (J. C. Hall & L. W. Ramsey, 1992b, 1994), its predecessor, `STARMOD`, has been extensively used in several studies. Among these studies we can mention the observation an analysis of contact binaries, focusing on low mass ratio systems (K. Li et al., 2022; F. Liu et al., 2024, 2025; J.-Y. Wang et al., 2025; Q. Xia et al., 2025; X. Xu et al., 2025); the detailed photometric and spectroscopic studies of W UMa-type binaries (A. Panchal & Y. C. Joshi, 2021; A. Panchal et al., 2022); studies of magnetic and chromospheric activity in RS CVn-type stars: (D.-T. Cao & S.-H. Gu, 2012; D. Cao & S. Gu, 2015, 2024, 2025; D. Cao et al., 2023); studies of extended matter and active binaries, exploring the evolution of magnetic activity and orbital period variations (Q.-f. Pi et al., 2014; L. Zhang et al., 2014a,b; L.-Y.

Zhang, 2018); studies in transmission spectroscopy, to measure or discard activity levels in the studied object (F. J. Alonso-Floriano et al., 2019a); the study of molecular bands to probe starspots properties (D. O'Neal & J. E. Neff, 1997; D. O'Neal et al., 1998, 2001); and finally, studies from our group on activity, kinematics, and age in Single and Binary Late-type Stars (D. Montes et al., 2000, 2004; M. C. Gálvez et al., 2002b, 2006, 2007), rotational modulation of activity (J. López-Santiago et al., 2003a, 2010), and flux-flux relationships (R. Martínez-Arnáiz et al., 2011).

This paper describes and provides the iSTARMOD code for the application of the spectral subtraction technique to all possible activity indicators available in the spectral range being analyzed. Its application is of great scientific interest to characterize the chromospheric activity of FGKM stars, both isolated and binary; to study in detail the temporal variability of especially active stars; and contribute to understanding the different magnetic phenomena that occur in them. Calibrations are also provided to convert the excess chromospheric emission to surface fluxes, facilitating the comparison between different activity indicators measured at different wavelengths that form at different heights in the chromosphere. This allows us to study flux–flux relationships and how they depend on stellar parameters. The method provided with this code and the corresponding flux calibrations allow for the automatic characterization of chromospheric activity in a large number of spectra of a single star, as occurs in spectroscopic surveys such as CARMENES (A. Quirrenbach et al., 2018, 2020; I. Ribas et al., 2023), or in a large number of stars belonging to different clusters or moving groups in large spectroscopic surveys such as the Gaia ESO Survey G. Gilmore et al. 2022). Adequate characterization of chromospheric activity is also of great importance in studies dedicated to the search for exoplanets, in order to mitigate the effect of activity on radial velocities and to rule out false positives.

This paper is structured as follows: Section 2.2 provides a presentation of the spectral subtraction technique and its basic assumptions. Section 2.3 presents the particular implementation of the spectral subtraction technique in iSTARMOD with its workflows, inputs, and improvements. Section 2.4 deals with the χ-factor methodology, to obtain fluxes from the EWs obtained with iSTARMOD, and the calibrations of the χ-function for several chromospheric activity indicators are put in the annexes. Finally, Section 2.5.1 presents some results of the execution of iSTARMOD.

2.2 Spectral Subtraction Technique

The method involves subtracting the spectrum of an active star (the *input* spectrum) from a synthetically constructed *reference* spectrum. This reference is generated by applying artificial rotational broadening and radial velocity shifts to a weighted sum of spectra from inactive *reference* stars that closely match the spectral type and luminosity class of the target star (D. Montes et al., 1995a,b). A key feature of the technique is that subtraction is carried out either order by order in the echelle spectrum or over a predefined wavelength range, allowing for high spectral fidelity.

A major advantage of this method lies in its ability to circumvent the challenge of continuum placement in late-type, cool stars, which exhibit dense forests of absorption lines. By assuming that both the active and reference spectra–being nearly identical in spectral type–share the same pseudo-continuum, the subtraction process effectively isolates the chromospheric emission. This approach greatly reduces systematic uncertainties and simplifies EW measurement of emission features. The core algorithm is implemented as an iterative least-squares optimization to determine the best-fit synthetic spectrum: the one that minimizes the rms of the subtraction residuals. The main stages of the fitting process, for each iteration step, are as follows:

- *Doppler shifting* to align the spectral lines of the input and synthetic spectra.
- *Rotational broadening* using a Gray profile (D. F. Gray, 2022) to simulate the effects of stellar rotation on the reference spectrum.
- *Spectral weighting* of multiple reference stars, where applicable, such as in the case of unresolved binary (SBx) or multiple systems, showing activity.

2.2.1 Radial Velocity Determination

The spectral subtraction technique requires a high-precision spectra alignment of both reference star and active star in each iteration step. This is achieved through Doppler shifting of the reference spectrum. Observed wavelength becomes:

$$\lambda_{\rm obs} = \lambda_0 \left(1 + \frac{v_r}{c}\right) \tag{2.2}$$

where λ_0 is the rest-frame (laboratory) wavelength of the spectral line, $\lambda_{\rm obs}$ is the observed wavelength, v_r is the supposed radial velocity of the star, and c: speed of light.

Here the flux data array of the fits spectrum is shifted by a noninteger amount through performing both an integer and a residual noninteger shift. The combined process allows for subsample shifting of an array, as is commonly used in signal processing where subsample alignment is required. This approach allows the function to be translated smoothly without the discretization artifacts that would arise from integer-only shifts. Conceptually, the operation approximates the continuous transformation $f(x) \longrightarrow f(x - \Delta x)$, where Δx corresponds to the imposed `shift`, thus enabling precise real-space translation of sampled data without resorting to Fourier-space manipulation.

The integer part is handled by direct reindexing, and the fractional part is handled via local Lagrange interpolation. The input `shift` value is determined knowing the step in wavelength value between each pair of consecutive elements in the array, supposed constant throughout the whole spectral order, and transforming this wavelength step into velocity. Then this input value is decomposed into its integer and fractional components. The integer part is

$$\texttt{ishft} = \lfloor \texttt{shft} \rfloor, \tag{2.3}$$

where $\lfloor \cdot \rfloor$ is the floor function, which returns the largest integer not greater than its argument. Then, the fractional part is simply

$$\texttt{fshft} = \texttt{shft} - \texttt{ishft}, \tag{2.4}$$

The integer part of the process reindexes the array with bounds clamping:

$$y[i] = x[\max(0, \min(n-1, i - \texttt{ishft}))]$$

If the noninteger or fractional part $\texttt{fshft} \neq 0$, the residual shift is applied through interpolation. For each index i, an interpolated value is computed at

$$x_{\text{in}} = i - \texttt{fshft}$$

using nearby values $\{(x_j, y_j)\}$ in a local window. The interpolated value is calculated with a Lagrange polynomial:

$$y_{\text{out}} = \sum_{j=0}^{n-1} y_j \cdot \prod_{\substack{i=0 \\ i \neq j}}^{n-1} \frac{x_{\text{in}} - x_i}{x_j - x_i} \tag{2.5}$$

In this implementation, a polynomial of degree 1 (two terms, linear interpolation) is typically used to ensure stability and performance. This technique is well suited for high-precision alignment of an active star and the reference star performed order by order. The alignment requires a least-squares fit that minimizes the residuals between the input spectrum and the shifted reference star spectrum.

2.2.2 Rotational Broadening and the Gray Profile

In stellar spectroscopy, rotational broadening refers to the perturbation of spectral lines caused by Doppler shifts resulting from a star's rotation. Different regions of the stellar surface move toward or away from the observer at different velocities, leading to a spread of the observed wavelengths.

A description of the emitted intensity across the stellar disk is needed to model the effect of stellar rotation on spectral lines. This is where the *Gray profile* (or *Gray rotation profile*) becomes essential. In the theoretical deduction of Gray profile, three main assumptions are made: *solid-body rotation*, that is to say, the entire surface rotates at the same angular velocity, a *simple linear limb-darkening law*, and *neglect of macroturbulence*, implying that large-scale turbulent motions, producing additional patterns of Doppler shifts, are excluded from this theoretical deduction

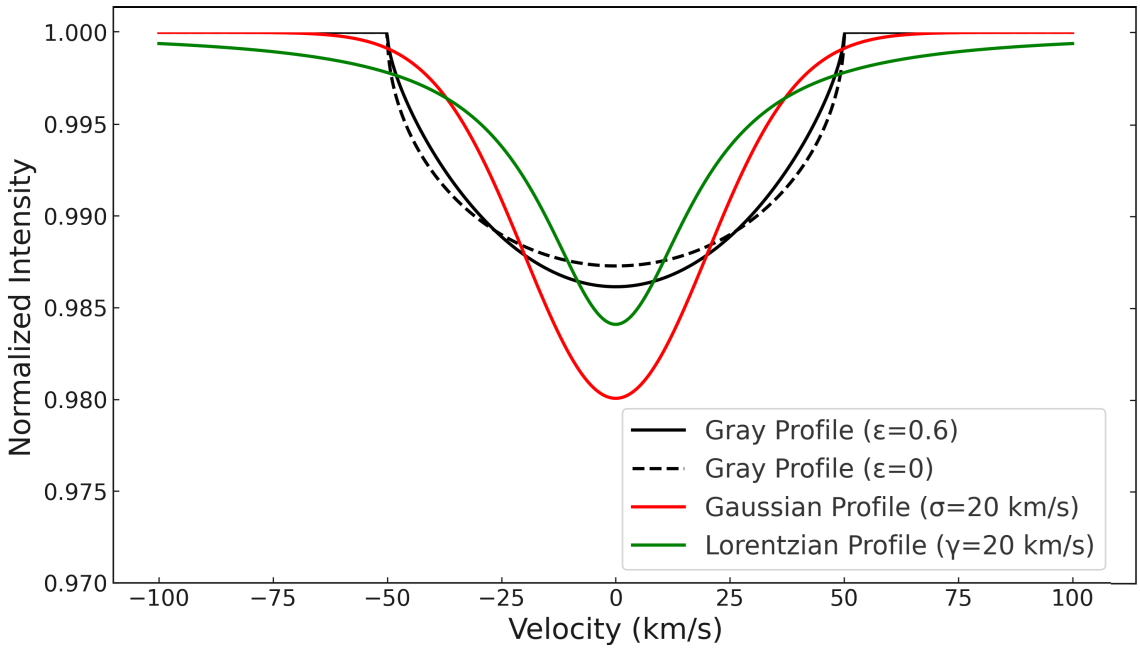

Figure 2.1. Comparison between Gray, Gaussian, and Lorentzian broadening profiles

process, because they are considered already present in the reference star spectrum. Instrumental and macroturbulence effects can also mimic the effect of rotation, but using reference stars' spectra taken with the same instrument, and with the same spectral type, luminosity class, and metallicity, these undesired side effects are avoided. The normalized rotational broadening function $G(v)$ as a function of velocity v (relative to line center) is (D. F. Gray, 2022)

$$G(v) = \frac{2(1-\epsilon)\sqrt{1-\left(\frac{v}{v_{\max}}\right)^2} + \frac{\pi\epsilon}{2}\left(1-\left(\frac{v}{v_{\max}}\right)^2\right)}{\pi v_{\max}(1-\epsilon/3)} \tag{2.6}$$

where $v_{\max} = v \sin i$ is the maximum projected rotational velocity, i is the inclination angle between the rotation axis and the line of sight, and ϵ is the linear limb-darkening coefficient ($0 \leq \epsilon \leq 1$). The domain of the function, as is evident by Equation 2.6, is in the interval $[-v_{\max}, v_{\max}]$, and $G(v) = 0$ outside it ($|v| > v_{\max}$). In the case of no limb darkening ($\epsilon = 0$), the Gray profile reduces to:

$$G(v) = \begin{cases} \dfrac{2}{\pi v_{\max}}\sqrt{1-\left(\dfrac{v}{v_{\max}}\right)^2}, & |v| \leq v_{\max} \\ 0, & |v| > v_{\max} \end{cases} \tag{2.7}$$

This is often referred to as the *classical Gray rotation profile*. However, in iSTARMOD, the Gray profile employed is one defined as in equation 2.6 with $\epsilon = 0.6$ and then this is the Gray parameter for a linear limb-darkening law:

$$\frac{I(\mu = cos\theta)}{I(\mu = 0)} = 1 - \epsilon(1-\mu)$$

where I is the specific intensity. It is worth mentioning that this value for ϵ is the one typical for solar-type stars. It can be different for other types of stars and wavelength ranges (D. F. Gray, 2022).

Other broadening functions relevant for spectral lines and related to other phenomena are the Gaussian (Doppler-thermal broadening) and Lorentzian (pressure broadening). However, they have a very different shape compared to the rotational profile, as it can be seen in Figure 2.1. Gaussian or Lorentzian profiles will always render unphysical wings beyond $\pm v \sin i$ in case of be used for rotational broadening.

The observed stellar line profile $F_{\rm obs}(v)$ is obtained by the convolution of the intrinsic stellar line profile $F_{\rm int}(v)$ with the rotational broadening function $G(v)$:

$$F_{\rm obs}(v) = \int_{-\infty}^{+\infty} F_{\rm int}(v')\, G(v - v')\, dv'. \tag{2.8}$$

Thus, the effect of rotation broadens and redistributes the intrinsic spectral line shape according to the profiles defined here.

The Gray profile describes the distribution of Doppler shifts across the visible stellar disk, where the limb regions exhibit the highest projected velocities $\pm v_{\max}$, while the central regions (near the rotation axis) contribute around $v \approx 0$. Without limb darkening, the contribution depends purely on geometric projection, where limb darkening ($\epsilon > 0$) reduces the flux contribution near the edges. Figure 2.2 summarizes all these effects, when this convolution is applied with several projected rotational velocities ($v$sin$i$).

Macroturbulence refers to large–scale velocity fields in the stellar atmosphere, larger than the photon mean free path, that broaden absorption line profiles beyond the contributions of instrumental, intrinsic and thermal broadening. *It is known that macroturbulence can also mimic the effect of rotation, for low values of ($v \sin i$).*, as described in D. F. Gray (2022). Here, the convolution is performed using a kernel Gaussian profile:

$$M_\zeta(\Delta\lambda) \;=\; \frac{1}{\sqrt{\pi}\,\zeta}\exp\left[-\left(\frac{\Delta v}{\zeta}\right)^2\right] \tag{2.9}$$

with:

$$\int M_\zeta \, d(\Delta v) = 1 \tag{2.10}$$

The velocity fields are defined by ζ, a set of empirical relationships (D. F. Gray 1984, 2010; A. P. Doyle et al. 2014; M. Tsantaki et al. 2018) dependent on $T_{\rm eff}$ and surface gravity log$g$:

$$\zeta = a + B_{\rm n}(T_{\rm eff} - T_{\rm s})^n - c(logg - logg_{\rm s}) \tag{2.11}$$

The normalization condition implies that macroturbulence does not change the EW of absorption-line profiles, only their shape, broadening and reducing their depth. But in spectral subtraction, a small mismatch δT between input and reference star spectrum temperatures and gravity surface therefore could produce residuals dominated by the core depression and wing enhancement pattern. To quantify this, and assess the level of the effect of macroturbulence on spectral subtraction, we will treat δT as a perturbation of the subtracting spectrum. Then, using equation 2.11,

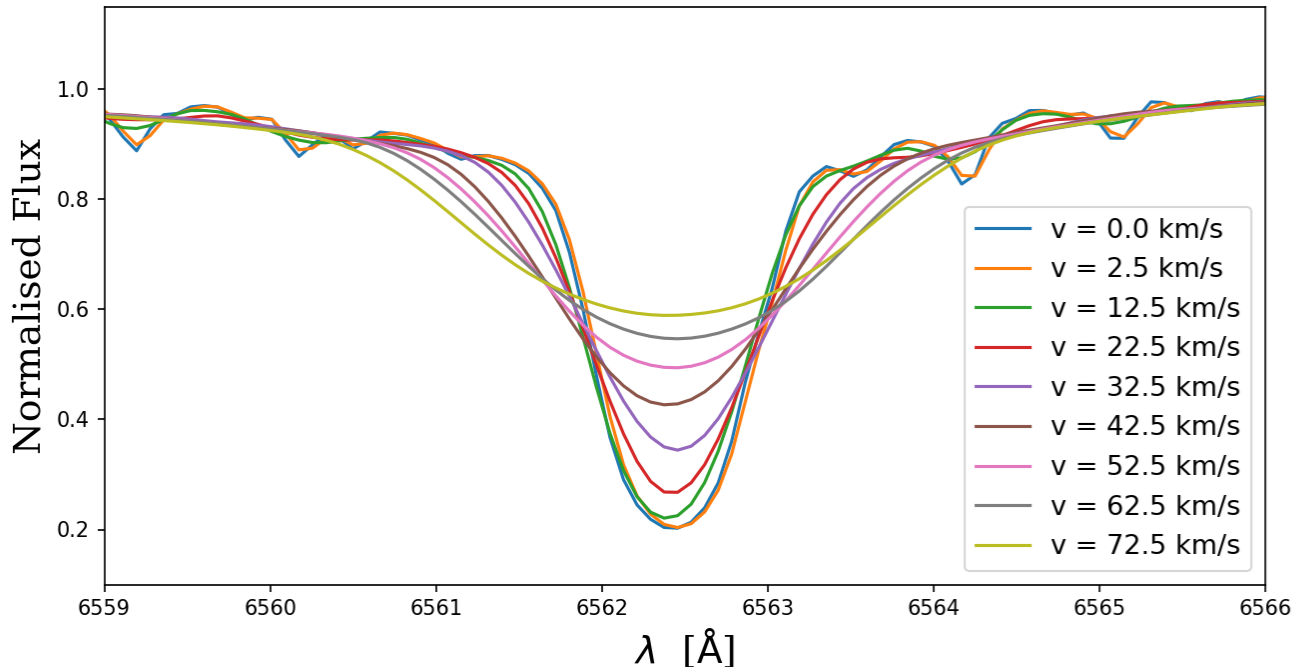

Figure 2.2. Synthetic line profiles with varying rotational velocities ($v \sin i$). The `iSTARMOD` code has been applied to an example Hα absorption line, taken from a quiescent K2V star. Note that minor and noisy features of the intrinsic profile are erased for $v > 10 kms^{-1}$

as derived in A. P. Doyle et al. (2014) to perform the perturbation calculations, the reference star spectrum $F_{\rm orig}$ is convolved with the macroturbulence kernel M_ζ. The first-order perturbation in this convolved spectrum is

$$\delta \left(F_{\rm orig} * M_\zeta \right) \; = \; F_{\rm orig} \; * \; \left(\frac{\partial M}{\partial \zeta} \frac{{\rm d}\zeta}{{\rm d}T_{\rm eff}} \, \delta T \right), \tag{2.12}$$

so the sensitivity kernel is precisely $\partial M / \partial \zeta$ scaled by $d\zeta / dT_{\rm eff}$. Forcing the validity of equation 2.11 outside its effective temperature range ($[5200, 6400]$) in A. P. Doyle et al. (2014) and putting numbers for the examples of Section 2.5.1 (e.g., V1216 Sgr with respect to the reference of Barnard's Star, two M3.5V stars), this scale is $9 \times 10^{-4} \, \delta T$ and the relative perturbation $\delta\zeta/\zeta$ is lower than 8%. Given that an additional convolution with the Gray profile is cumulative, the scale and induced relative error are even lower. This highlights the key point of the choice of a suitable reference star spectrum with comparable $T_{\rm eff}$, luminosity class (then log g) and metallicity.

There are additional features of stars that can be confidently ignored for the case of cool ones: oblateness and the gravity darkening derived from it. *Gravity darkening* is due to the variation in $T_{\rm eff}$ and brightness over the surface of a rotating star due to differences in effective gravity (von Zeipel theorem, see L. B. Lucy 1967), in turn due to oblateness of the body, as

$$T_{\rm eff}(\theta) \simeq \sqrt[4]{g_{\rm eff}(\theta)}$$

where θ is the latitude.

This is important only for very fast rotators (M. Solar et al., 2022), as Be stars, or with intense gravitational fields. Then, for late-type stars, except perhaps the youngest and consequently most active ones, this effect can be safely neglected. To what extent is it negligible? In the majority of cool dwarfs, the rotational velocities are low enough that centrifugal distortion and gravity darkening are insignificant. The oblateness f of a star can be approximated by

$$f \equiv \frac{R_{\rm eq} - R_{\rm pol}}{R_{\rm eq}} \approx \frac{v_{\rm eq}^2 R}{2GM}, \tag{2.13}$$

where $R_{\rm eq}$ is the equatorial radius, $R_{\rm pol}$ is the polar radius, and R is the mean one. Oblateness is typically much less than 1% for stars with $v_{\rm eq} \lesssim 10$ km s^{-1}. Putting the numbers in Equation 2.13 with the parameters of, e.g, EV Lac, a particularly active M3.5Ve flare star, with $v_{\rm eq \, sin} i \approx 5$ km s^{-1}, results in an oblateness parameter of $f \approx 0.009\%$. Similar stars in mass and radius, such as V1274 Her, a BY Dra variable with $v_{\rm eq} \sin i \approx 50$ km s^{-1} yield values for f of around 0.6 %. In such cases, both the deviation from spherical symmetry and the latitudinal temperature variation due to gravity darkening can be safely ignored.

Consequently, for cool stars the use of standard limb-darkened rotation profiles (e.g., Gray profile) assuming a spherical stellar surface is well justified for modeling the rotational broadening of the spectral lines of reference stars.

2.2.3 Weighted Spectra for Binary Systems

The case for binaries requires the third set of parameters specified in Section 2.2: weight of the component stars participating in building the synthetic reference star. Since the spectra are normalized, these weights are applied directly by forming a weighted sum:

$$F_{\rm syn}(\lambda) = w_1 * F_{\rm prim}(\lambda) + w_2 * F_{\rm sec}(\lambda) \tag{2.14}$$

subject to the normalization condition

$$w_1 + w_2 = 1.0 \tag{2.15}$$

The contribution of each component to the total continuum can be obtained from the luminosity ratio in the Hα region of the spectra (D. Montes et al., 1995b), given by

$$\frac{L_1}{L_2} = \left(\frac{R_1}{R_2}\right)^2 \left(\frac{B_{\lambda=\rm H\alpha}(T_{\rm eff,1})}{B_{\lambda=\rm H\alpha}(T_{\rm eff,2})}\right)$$

where $B(\lambda, T_{\rm eff})$ is the Planck function and $R_{1,2}$ are the corresponding radii of each star, where 1,2 refers to the hot and cool components of the binary. Then, the different weights can be calculated as

$$w_1 = \frac{\alpha}{1+\alpha}, \quad w_2 = \frac{1}{1+\alpha}$$

and $\alpha = L_1/L_2$. This normalization of the weights affects the calculation of EWs, as we will see in Section 2.3.2

2.2.4 Quality Tests

Once the three processes mentioned above are executed and optimal radial velocities, $v\sin i$ and spectral weights are determined, the synthetic spectra are finally built and subtracted to the input spectrum. Then, the rms of the residuals are calculated:

$$rms = \sum_{\substack{i=0 \\ i \neq excl}}^{npts} (F_{\rm input}(\lambda) - F_{\rm synth}(\lambda))^2 \tag{2.16}$$

where $i \neq excl$ expresses the condition that points within excluded intervals are not summed.

This suggests an important quality check of this method in the features of the subtracted spectrum: a successful subtraction should yield a near-zero normalized flux level across the spectrum, resulting in a successful alignment of reference and input spectra, except in narrow regions around activity-sensitive lines (measured in Å), which will display residual excess emission (see discussion in Section 2.5.1). Then, in order to put a numerical condition for a successful subtraction performed by iSTARMOD, a limit can be stated where

$$rms \ngeq 0.5$$

depending on the signal-to-noise ratio (S/N) of the spectrum taken.

This approach for spectral subtraction proves particularly valuable for stars with low levels of activity, where chromospheric emission does not significantly rise above the continuum. Hence, the method can be effectively applied across a wide range of stellar activity levels, not only to highly active stars.

2.3 iSTARMOD Code

2.3.1 Overall Description

iSTARMOD constitutes the actual implementation of the spectral subtraction technique for the study of the chromospheric activity in cool stars. iSTARMOD (F. Labarga & D. Montes, 2020) is an updated and extended version of the original STARMOD code developed at Penn State University (S. C. Barden, 1985). Subsequent modifications were introduced by D. Montes et al. (2000) and further developed in the JSTARMOD variant by J. López-Santiago et al. (2010). In this work we present the migration of the code from FORTRAN to Python and implement additional enhancements to improve usability and precision. These upgrades include automated EW measurements (a feature previously not implemented by the code), error estimation routines, and the capability to process large time-series datasets or extensive stellar samples. This functionality is essential at performing, for example, analyses of flux–flux or activity–rotation relationships based on large numbers of spectra-whether for individual stars or for many stars observed in large spectroscopic surveys, such as the CARMENES GTO sample of M stars (A. Quirrenbach et al. 2020 F. Labarga et al. 2023).

The migration of the original FORTRAN STARMOD code to Python was motivated by the need for improved usability, modularity, and integration with modern data analysis workflows. Python provides a versatile programming environment supported by a broad ecosystem of scientific libraries–such as Astropy (Astropy Collaboration et al., 2018),

NumPy (C. R. Harris et al., 2020), and SciPy (P. Virtanen et al., 2020)–that facilitate spectral data handling, numerical optimization, and reproducible research. The Python implementation of iSTARMOD allows for automated processing of large spectral datasets, integration into time-series analysis pipelines, and enhanced flexibility for spectral modeling. The code is publicly available (F. Labarga & D. Montes, 2025) under an open-source license and will be actively maintained by the authors at https://github.com/flabarga/iSTARMOD.

The subtraction is carried out order by order, as mentioned above (section 2.2), in the echelle spectrum to mitigate the effects of instrumental profile and variations across different orders and to optimize memory and computational efficiency.

This order-by-order approach is important in high-resolution echelle spectroscopy owing to the wavelength-dependent sensitivity and instrumental profile that vary across different spectral orders. One of the primary challenges arises from the blaze function, an intrinsic feature of echelle gratings that causes a nonuniform intensity distribution within each order. Although standard reduction pipelines attempt to correct for the blaze response, residual effects often remain and can introduce low-frequency modulation or distortions in the continuum shape. By performing the subtraction within each spectral order independently, iSTARMOD minimizes the propagation of such instrumental artifacts into the final residual spectrum. Furthermore, order-by-order processing allows for local optimization of continuum placement and velocity alignment, improving the accuracy of chromospheric excess emission measurements, especially for narrow spectral lines affected by order-edge distortions or varying S/N across the orders. Moreover, this local optimization of continuum placement makes iSTARMOD especially suitable for the study of chromospheric activity in the NIR channel of the spectrum.

2.3.2 Improvements with Respect to STARMOD

Auxiliary steps are integrated in addition to primary subtraction and fitting procedures:

- Rebinning of spectra that shows variable wavelength step sizes.
- Determination of continuum level using an adaptation of the ARES algorithm (S. G. Sousa et al., 2007, 2015). This is, as mentioned above, particularly important for M dwarfs, where continuum placement is highly uncertain owing to profusion of absorption of atomic and molecular lines.
- Normalization of the spectrum after continuum placement.
- Calculation of the EW by numerical integration over predefined wavelength limits.
- Estimation of EW uncertainties using the Cayrel formula (G. Cayrel de Strobel & M. Spite, 1988; R. Cayrel et al., 2004), based on the full width at half maximum, S/N, and pixel step size (σ_x):

$$\sigma_W = \frac{1.06}{S/N}\sqrt{FWHM \cdot \sigma_x} \tag{2.17}$$

All processing steps are encapsulated in a coherent iterative loop as shown in the workflow depicted in Figure 2.3. The code supports multiple FITS formats produced by high-resolution spectrographs such as FOCES, HERMES and CARMENES, which present their own data structures and spectral characteristics, and the most simple .dat files, where the data arrays of wavelengths and fluxes are extracted, with a format *wvl (space-space) flux*. Execution examples of iSTARMOD are shown in Section 5. for several chromospherica activity indicators.

As previously noted, the algorithm is also suitable for spectroscopic binaries, where each stellar component can be represented by a separate reference spectrum. A composite synthetic spectrum can then be built by a weighted sum of each individually broadened and shifted reference spectra. Here the preliminary calculation of the EWs is performed through the deconvolution of the weighted sum of two Lorentzian profiles. This deconvolution is performed by means of a least-squares fit, implemented via the scipy:optimize:curve_fit function. Subsequently, a numerical integration is performed between two predefined wavelengths, resulting in two EWs values, which must be corrected as

$$EW_{\rm n} = \left(\frac{1}{w_{\rm n}}\right) EW_{\rm n,0}$$

where w_n are the weights, subject to condition eq. 2.15, and n = 1,2 are the *hot* and *cool* components of the binary. In SB2 systems, the weights w1 and w2, which represent the relative flux contributions of each stellar component, are determined internally by iSTARMOD through a least-squares optimization of the composite spectrum, accounting for the spectral type, radial velocity, rotational broadening, and continuum contribution of each component.

Because the individual line profiles are reconstructed through a deconvolution of the observed double-lined spectrum, equivalent widths cannot be measured directly on the observed profile. The assumptions required for applying the G. Cayrel de Strobel & M. Spite (1988) formula are therefore not fulfilled, and this approach is not applicable to SB2 systems.

Instead, EW uncertainties are estimated from the residuals of the subtraction between the observed composite spectrum and the synthetic spectrum obtained as the sum of the two deconvolved stellar components. This residual-based method implicitly includes the uncertainties associated with the determination of w1 and w2, as well as those arising

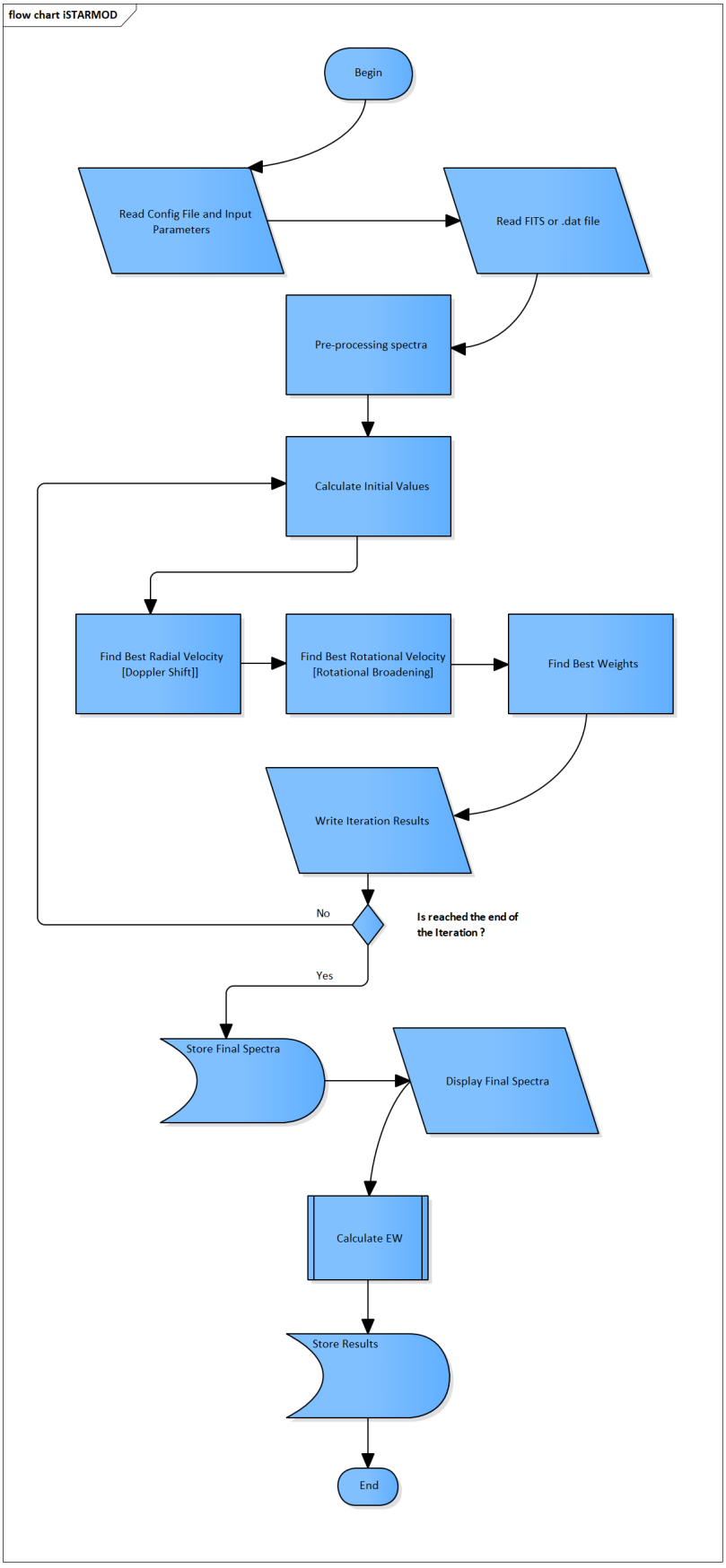

Figure 2.3. Flowchart of iSTARMOD process, showing the implementation of the algorithm of spectral subtraction technique, the steps followed and the information flow

from radial velocities, rotational broadening, template mismatches, and noise. The suitability of this functionality implemented by previous versions of this code was demonstrated in D. Montes et al. (1995a,b, 2000) and most of the studies on spectroscopic binaries mentioned in the introduction, as the `STARMOD` code was made available for the scientific community. See examples of binaries in section 2.5.2

2.3.3 Input Parameters

`iSTARMOD` performs, in the context of *least-squares fitting*, an iterative minimization over spectral segments to best match a synthetic composite of reference spectra to an observed one. The process involves, on one hand, Iterative optimization (`N_ITER`), where parameters like radial velocities, rotational broadening, and weights for primary and secondary components are adjusted to minimize the residuals between observed and synthetic spectra. On the other hand, there is a need to define exclusion zones (`PIX_EXCL`) that allow ignoring regions contaminated by stellar activity or instrumental effects to prevent biasing the fit.

The *least-squares criterion* is used to evaluate the sum of squared residuals within a defined spectral range (`PIX_ZONE`), avoiding specified zones, according to equation 2.16.

Thus, the least-squares fit that the spectral subtraction technique depends on requires a large number of input and configuration parameters, settings for running the `iSTARMOD` tool. These parameters are specified in a configuration file (`inputParameters_filename.sm`) using a `KEYWORD = value` syntax and are organized into several key sections:

1. General Information–defines the input FITS spectrum location and filenames.
2. Output Spectra–specifies output options for synthetic and subtracted spectra.
3. Interpolation Parameters–includes the number of least-squares iterations (`N_ITER`), fitting wavelength ranges, and exclusion zones to ignore during residual summation (e.g., due to stellar activity or edge effects).
4. Primary and Secondary Star Parameters–specifies the Doppler shift (radial velocity), rotational broadening ($v\sin i$), and weights for reference spectra. They will be the initial guesses for the fit process. They can be provided with the option to fix or vary these values during the whole iterative process.
5. Spectra Format–selects the spectral order and line region to analyze, allowing the calculation of EWs.
6. Algorithm and Visualization Parameters–controls display settings and tolerance for identifying emission peaks in subtracted spectra.

In summary, and from the spectral processing perspective, `iSTARMOD` allows precise subtraction of reference spectra from observed ones, enabling detection of excess emission from chromospheric activity. This requires an accurate wavelength calibration and matching of instrumental profiles via Doppler shift and broadening adjustments. Finally, `iSTARMOD` provides post-processing analysis such as EW measurements, with a generation of synthetic (`SYN_NAME`) and subtracted (`SUB_NAME`) spectra to isolate features of interest (e.g., Ca II IRT lines).

Together, these configurations ensure robust, reproducible spectral analysis tailored for stellar activity diagnostics or binary star component separation.

2.4 Calibration of χ Factor Functions for Different Activity Indicators

The ratio between the Hα luminosity and the bolometric luminosity, $L_{\mathrm{H}\alpha}/L_{\mathrm{Bol}}$, is a commonly used measure of chromospheric activity, as Hα represents one of the main radiative channels through which magnetic energy is dissipated in the chromospheres of cool stars. In order to convert the equivalent width (EW) of excess Hα emission, measured as described in the previous section, into an absolute and distance-independent activity indicator, a transformation from EW to line luminosity is required. This transformation is based on the χ factor, originally defined by L. M. Walkowicz et al. (2004) as the ratio between the continuum flux density at the wavelength of the line and the bolometric flux, $\chi = f_{6560}/f_{\mathrm{bol}}$ for Hα. The χ formalism provides a distance-independent method for deriving $L_{\mathrm{H}\alpha}/L_{\mathrm{Bol}}$, minimizing systematic uncertainties associated with stellar radii and distances.

In the original formulation by L. M. Walkowicz et al. (2004), χ values were derived using spectrophotometric observations. Apparent bolometric fluxes were obtained from calibrated photometric data combined with empirical bolometric corrections, while the apparent continuum flux density at the Hα wavelength, f_{6560}, was measured directly from flux-calibrated spectra as the mean continuum level in a narrow spectral window around the line. The χ factor was then computed as the ratio $f_{6560}/f_{\mathrm{bol}}$ over a wide spectral-type range.

Subsequent works adopted the same formal definition of χ but replaced direct spectrophotometric measurements with synthetic stellar atmosphere models to estimate the continuum flux at the line wavelength. In particular, A. Reiners & G. Basri (2008) used DUSTY models after F. Allard et al. (2001), while in this work χ values are computed using BT-Settl synthetic spectra, ensuring consistency with the atmospheric models employed throughout the analysis. In this thesis, the second approach is adopted, avoiding the uncertainties coming the empirical calibrations and

correction, where χ factors are obtained using BT-Settl synthetic spectra, ensuring consistency with the atmospheric models adopted throughout the analysis.

The χ methodology has been widely applied in the literature (e.g. S. T. Douglas et al. 2014; A. Núñez et al. 2024), and has recently been extended to the full Balmer series (A. García Soto et al., 2025). In this study, the approach is further generalized to derive fluxes for additional chromospheric activity indicators. Together with the iSTARMOD code, the calibrations presented here enable extensive and homogeneous studies of chromospheric activity in both single and binary cool stars.

Starting from the relation

$$\log\left(\frac{L_{\rm line}}{L_{\rm Bol}}\right) = \log(\chi) + \log(\mathrm{EW}), \tag{2.18}$$

the line luminosity normalized to the bolometric luminosity can be expressed directly as a function of the measured EW. This ratio is formally equivalent to the ratio between the surface line flux and the bolometric flux, $\mathcal{F}$line/$\mathcal{F}$bol, with the χ factor providing the link between equivalent widths and absolute fluxes.

A set of calibrations $\log\chi = f(T_{\rm eff})$ use synthetic spectra in the temperature range: [2200, 7000] K for most of the chromospheric activity indicators. These temperature ranges cover spectral types from F to M or even early L, of class luminosity V.

A grid of synthetic spectra from the BT-Settl-CIFIST models I. Baraffe et al. (2015), especially suited for low-mass stars, based on F. Allard et al. (2012) and T. O. Husser et al. (2013) was used. The models assume solar metallicity [Fe/H] = 0, visual extinction $A_V = 0$ mag and $\log g$ in the range [4.5, 5.5]. They can be found in the VOSA online repository[1]. The set of synthetic spectra have been degraded in resolution by convolving each spectrum with a Voigt profile (see A. B. McLean et al. 1994), in order to match the spectral resolution of the synthetic spectra ($R \approx 500,000$) to the spectral resolution of, e.g., the CARMENES instrument ($R \approx 85,000$), following E. Marfil et al. (2021). At the resolution of the synthetic spectra, and due to dense forest of atomic and molecular absorption lines, the true continuum is not directly accessible, and continuum estimates become highly sensitive to individual line depths and model details. For this reason, the synthetic spectra are degraded to the instrumental resolution prior to the evaluation of the continuum flux. This degradation is essential to ensure that the continuum definition used to compute the χ factor is consistent with that implicitly adopted in the EW measurements, which are performed on spectra at instrumental resolution. In this thesis, the continuum flux at the line wavelength is defined as the mean flux density measured within narrow spectral windows flanking or near the chromospheric line, chosen to be minimally affected by line cores. No attempt is made to identify a theoretical or absolute continuum, which is not physically accessible in cool-star spectra. Following this definition, the continuum flux at wavelengths near the wavelength of the line under consideration for each $T_{\rm eff}$, are measured.

Once these χ values were calculated, different fits have been obtained, and the coefficients(C_1, α and β) are shown in Table 1 in Appendix 4.5. The curves can be seen in Figure 2.4 for Hα and Figure 1 in Appendix 4.5 for Ca II H & K, He I D_3 + Na I D_1, D_2, Ca II IRT, Paδ, Paγ + He I λ10830 and Paβ.

The fits from these calibrations were obtained proposing a functional form for χ:

$$\chi = C_0 \left(\frac{T_{\rm eff}}{T_s}\right)^{\alpha} 10^{P_5(T_{\rm eff})} \tag{2.19}$$

where Teff is the effective temperature of the star. Equation 2.19 resembles a $\log_{10}$-Schechter-type or Yukawa functions. Taking logs, we end up with

$$log\chi = C_1 + \alpha log T_{\rm eff} + P_5(T_{\rm eff}) \tag{2.20}$$

where

$$P_5(T_{\rm eff}) = \beta_1 T_{\rm eff} + \beta_2 T_{\rm eff}^2 + \beta_3 T_{\rm eff}^3 + \beta_4 T_{\rm eff}^4 + \beta_5 T_{\rm eff}^5 \tag{2.21}$$

and then

$$C_1 = (\log C_0 + \beta_0) - \alpha \log T_s \tag{2.22}$$

The independent term for the polynomial, β_0, and the T_s^{α} have been incorporated into C_1, given that these coefficients cannot be fully determined by any fit.

The first χ factor to be calculated is the one that abounds in the literature: the χ factor corresponding to Hα. To test the limits and accuracy of this methodology, our calibration, spanning the range $[2000, 7000]$, was put together with the model from A. Reiners & G. Basri (2008), which covers the range $[1200, 4000]$. It is important to note that the values from A. Reiners & G. Basri (2008) were originally intended for the study of ML-type stars.

The polynomial defined in A. Reiners & G. Basri (2008), being of fifth degree, exhibits oscillations beyond 4000 K, hence making it unsuitable for extending the calibration up to 7000 K. However both fits match almost perfectly in the range of $T_{\rm eff}(K)$ of [2200, 2700] and remain consistently within [2700, 4000]. Beyond 4000 K the fit of our study extends smoothly. The situation is summarized in Figure 2.4.

The combined EWs of the Ca II H and Ca II K lines allows us to define one the most widely used activity indicators, R'_{HK} (J. L. Linsky & T. R. Ayres, 1978). This parameter is defined as the ratio between Ca II H and K emission and

[1] http://svo2.cab.inta-csic.es/theory/newov2/index.php

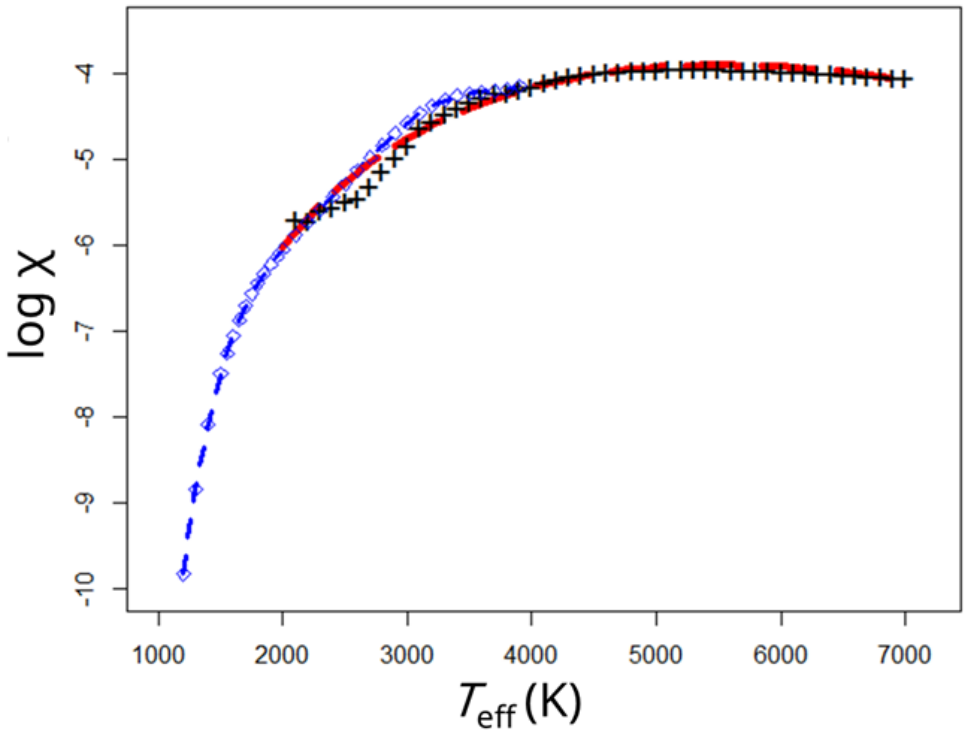

Figure 2.4. Comparison between the polynomial fit provided in A. Reiners & G. Basri (2008) (blue) in the range [1200, 4000] and this paper calculations (red), in the range [2000, 7000]. The points obtained from the set of synthetic spectra are the black crosses.

the stellar bolometric flux (J. L. Linsky et al., 1979),

$$R^{'}_{HK} = \frac{\mathcal{F}'_H + \mathcal{F}'_K}{\sigma T^4_{\rm eff}} \tag{2.23}$$

where the primes denote fluxes where the photospheric contribution has been subtracted as in Eq. 2.1. Considering that

$$\frac{\mathcal{F}_{\rm line}}{\mathcal{F}_{\rm bol}} = \frac{L_{\rm line}}{L_{\rm bol}}$$

both luminosities normalized to bolometric, calculated by means of the χ factor, must be summed up in order to obtain $R^{`}_{\rm HK}$. Hence,

$$R^{'}_{HK} = \frac{L_{\rm Ca\ II\ H}}{L_{\rm Bol}} + \frac{L_{\rm Ca\ II\ K}}{L_{\rm Bol}} = \chi_{\rm HK}(EW(H) + EW(K)) \tag{2.24}$$

As demonstrated in R. Martínez-Arnáiz et al. (2010), the $R^{'}_{HK}$ values obtained by means of the equation 2.24 are equivalent to the ones obtained with the classical Mount Wilson S-index method (A. H. Vaughan et al., 1978).

The lines He I D_3 and Na I D_1, D_2 are clear chromospheric activity indicators. These lines, being sensitive to the chromospheric environment, often mirror the activity observed in Hα, though with differences due to their distinct formation mechanisms and the depth of the chromosphere layer (M. Kumar & R. Fares, 2023). The proximity between the He I D_3 and Na I D_1,D_2 lines allows for a single calibration for all three lines (see the examples in Section 2.5.1), measuring the continuum emission halfway both groups of lines in the synthetic spectra. The values of their fit coefficients are shown in the second column of Table 1 in the Appendix 4.5

All lines of Ca II IRT, Ca II IRT-λ8498, Ca II IRT-λ8542, and Ca II IRT-λ8664, are subject to the same calibration, summarized in top row of Figure 1 and Table 1, both in Annex 4.5. The Ca II IRT is an alternative indicator in the IR of Ca II H and K lines as one of the primary indicators of stellar activity (D. Hintz et al., 2019), and is specially suited for its study in M-type stars.

The fit for He I λ10830 will also apply to the Paγ line. Both lines are very sensitive activity indicators (B. Fuhrmeister et al., 2020). Finally the last calibrations correspond to two lines of the Paschen series: Paδ (bluer λ10052.14 than He I λ10830) and Paβ (on the redder side). The calibrations performed in these spectral ranges, where the position of continuum is difficult to determine for late-type M-dwarfs, make them especially suitable for the study by spectral subtraction technique and `iSTARMOD`.

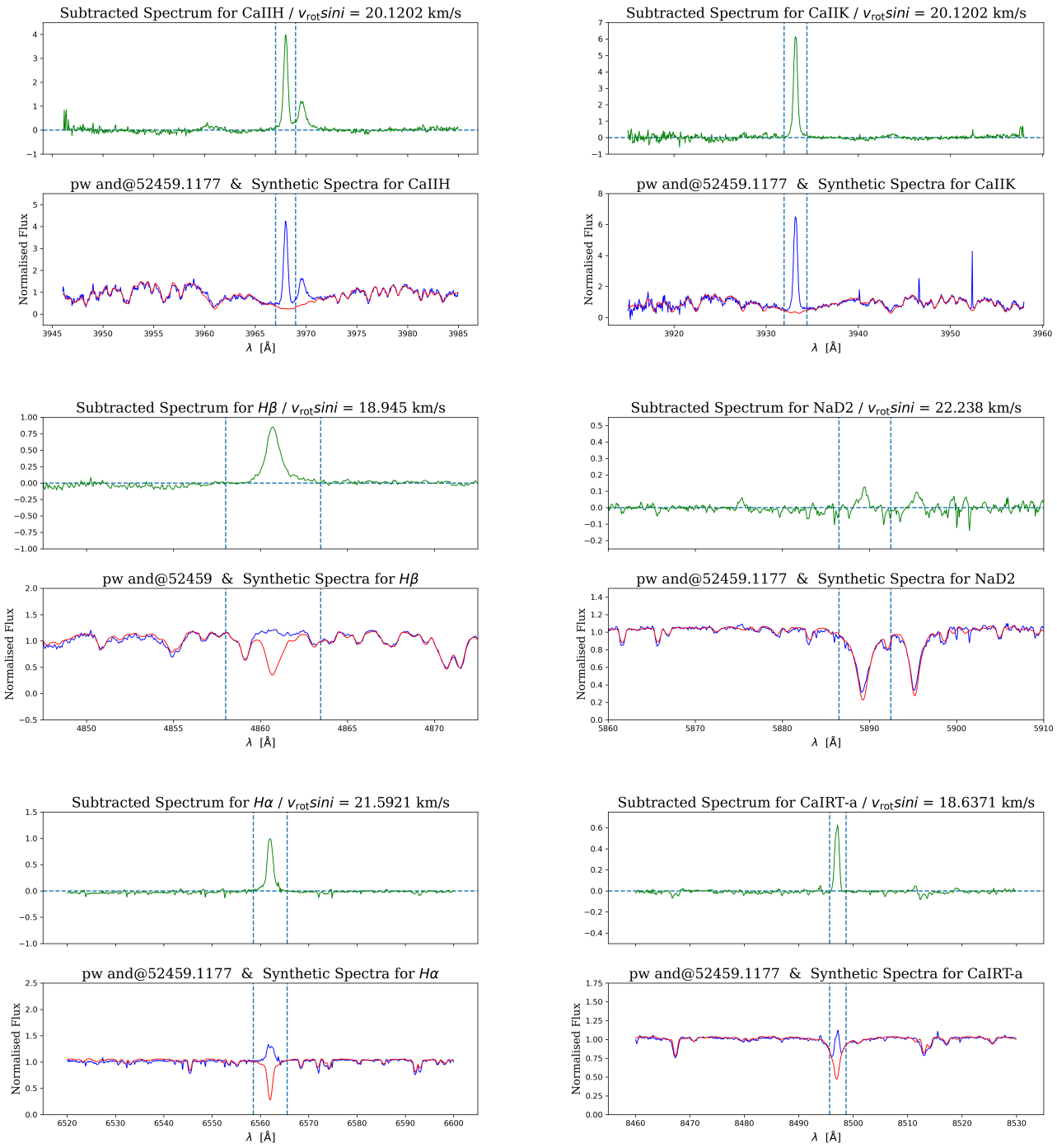

Figure 2.5. Spectral Subtraction Example for PW And, a K2V star observed with FOCES. The different spectra show chromospheric indicators in Ca II H, Ca II K (*top panels*), Hβ and Na I D_2 (*middle panels*), and Hα and Ca II IRT-λ8498 lines (*bottom panels*). Using FOCES provided spectra Lower panel: observed target spectrum (blue) and synthetic spectrum (red), obtained from a reference star spectrum. Upper panel: subtracted spectrum (green). In both panels: the vertical blue dashed lines mark the integration limits for the chromosoheric excess emission EW determination.

2.5 Spectral Subtraction Examples

To illustrate the capabilities of iSTARMOD as an actual implementation of the spectral subtraction technique, we present a selection of stellar spectra that have been processed using the methods described in Section 2.2 and 2.3. These examples demonstrate the softwares effectiveness in extracting chromospheric emission and serve to validate its application to a range of disparate stellar types.

Each spectrum shown below has been selected to highlight specific aspects of the processing pipeline, such as continuum normalization, ability of processing spectra of different sources, and activity indicator extraction.

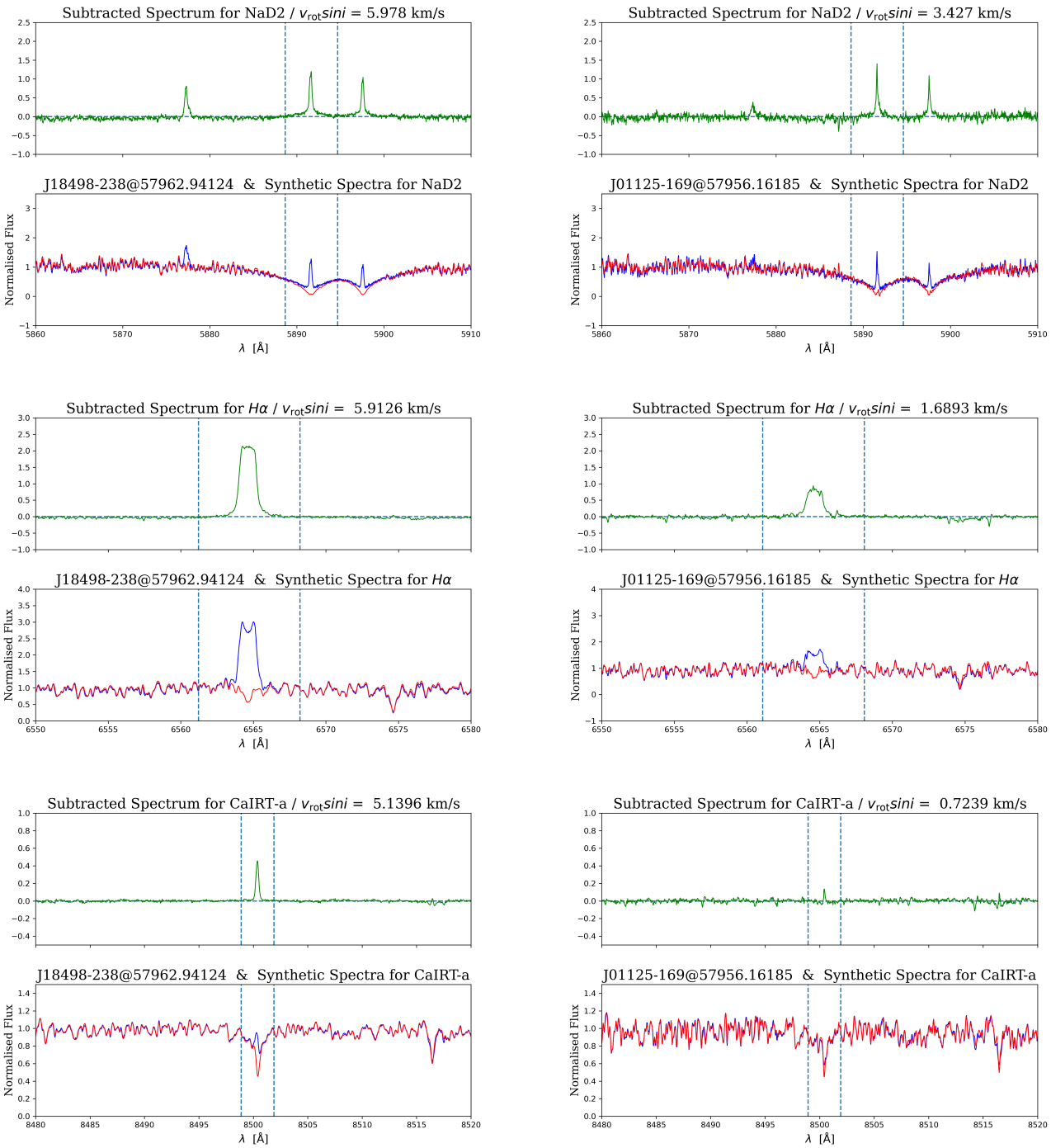

Figure 2.6. Left panels: Spectral Subtraction Example from V1216 Sgr (J18498–238), an M3.5 dwarf, performed with the VIS channel data of CARMENES spectrum, as provided in DR1 (I. Ribas et al., 2023), showing: He I D_3, Na I D_1,D_2 (top), Hα (middle) and Ca II IRT-λ8498 (bottom). Right panels: Spectral Subtraction Example from YZ Cet (J01125-169), an M4.5 dwarf, performed with the VIS channel of a CARMENES spectrum as provided in DR1, showing also He I D_3, Na I D_1,D_2 (top), Hα (middle) and Ca II IRT-λ8498 (bottom). Lines and color codes as in Fig. 2.5.

2.5.1 Case: Spectral Subtraction of Single Stars

Figure 2.5 shows several orders of the same spectrum taken with spectrograph FOCES (M. J. Pfeiffer et al., 1998) at the 2.2 m telescope at Centro Astronómico Hispano en Andalucía (CAHA). The spectrum was that of PW And (HD 1405), a relatively bright star ($m_v = 8.6$) classified as a neighborhood Pleiades-age K2 dwarf with high Li I abundance and a member of the Local Association moving group (D. Montes et al., 2001). It is a fast rotator with a photometric period $P_{\rm phot} = 1.745$ days and $v\sin i = 22.25$ km s^{-1} (J. López-Santiago et al., 2003a; E. Bahar et al., 2024). It is apparent from the figures that the 'quality test' mentioned in Section 2.2 is fulfilled: the rms of the residuals of the least-squares fit process performed are very low. For the case of Ca II H, rms = 0.15, with maximum values $\simeq \pm 0.3$. It is worth mentioning that this line can be resolved against Hϵ, which leads to an error in determining EW of $\leq 9\%$. The rms value for Ca II K is slightly worse rms = 0.26, with maximum values of $\simeq \pm 0.4$. This is likely due to the

stellar flux drop at shorter wavelengths and the consequently lower S/N ratio. The best case is achieved for Hα, where rms = 0.09. In all the above cases the reference, from which the synthetic spectrum have been built is HD166620, a nearby K2V very stable and quiescent star, with spectra also taken with spectrograph FOCES.

A selection of high-resolution spectra from CARMENES Data Release 1 (DR1;I. Ribas et al. 2023; J. A. Caballero et al. 2025) has been used to illustrate the examples presented. CARMENES is a dual-channel spectrograph operating at the 3.5 m telescope of the Calar Alto Observatory, designed for high-precision radial velocity measurements of M dwarfs (A. Quirrenbach et al., 2018, 2020). Figure 2.6 shows subtracted spectra in several orders from spectra of two stars. The left panels of Figure 2.6 corresponds to V1216 Sgr (Ross 154 or J18498–238), a nearby red dwarf star, one of the closest stellar neighbors to our solar system. V1216 Sgr is a UV Ceti type flare star, M3.5V, with strong magnetic activity that is reflected in the figures. The core emission in the He I D_3 and Na I D_1,D_2 lines are clearly visible in the first example analyzed. This example demonstrates the effectiveness of spectral subtraction when several `PIX_EXCL` regions are defined as exclusion intervals–one for each of the three lines present–during the least-squares fit. Across all the spectra taken rms≈0.16 in this order, implying that outside the lines studied the normalized subtracted flux moves within the interval $[-0.2, 0.2]$. Hα presents the same situation achieving an error in EW determination as low as 0.09%. For the case of Ca II IRT-λ4980, $rms = 0.06$ and the error in determining EW is: $e(EW) \approx 0.05\%$. The reference star is the old and relatively quiescent well-known Barnard's Star, with spectral type M3.5V and $T_{\rm eff}$ = 3273 K (after P. Schöfer et al. 2019; I. Ribas et al. 2023) and the spectrum provided by CARMENES DR1 with ID J17578+046. The right panels of Fig. 2.6 corresponds to the CARMENES target YZ Cet (J0115–169), also a nearby red dwarf star but with spectral type M4.5Ve. YZ Cet is a flare star, showing intermittent episodes of magnetic activity. This suggests a slightly lower level of chromospheric activity, as reflected in their levels of Ca II IRT-λ8498 excess emission. However, being a nearby star, the S/N and the values of rms are the same order as in the previous case, and the same applies to the errors obtained in measuring EW. The reference star employed was GJ 1235, with spectral type M4.5V and $T_{\rm eff}$ = 3059 K (after P. Schöfer et al. 2019; E. Marfil et al. 2021), provided by CARMENES DR1 with ID J19216+208.

2.5.2 Case: Spectral Subtraction of Spectroscopic Binaries SB2

Two systems have been chosen as examples of the application of `iSTARMOD` for spectral subtraction in binary stars. The first one, GZ Leo (or 2RE J1101+223), is a chromospherically active binary system classified as K1Ve+K1Ve. It is a double-lined spectroscopic binary (SB2), with its components clearly separated, and has been the subject of several observational studies. Early high-resolution spectroscopic observations were obtained with FOCES (M. J. Pfeiffer et al., 1998) at the 2.2 m telescope at CAHA in 2002 by M. C. Gálvez et al. (2009), who investigated its activity and orbital parameters, using `STARMOD`. One of these spectra has been reprocessed using `iSTARMOD` and the results are shown in the top row of Figure 2.7. The weights were fixed to $w_1 = 0.508$ and $w_2 = 0.492$ in the example for Hα, according to the fact of both components being of the same type, and resulting in a rms = 0.025. This translates for Ca II IRT-λ8498 to weights $w_1 = 0.572$ and $w_2 = 0.428$, resulting in rms = 0.020. The error in EW determination is in both cases $e(EW) \approx 1\%$. As in the case for single stars, the reference stars employed, provided by FOCES, are the G9IV and K0V stars HD 92588 and HD 97004, with similar $T_{\rm eff} \approx 5100$.

More recent observations with the CARMENES spectrograph, from CARMENES Data Release 1 (DR1; I. Ribas et al. 2023; J. A. Caballero et al. 2025) have been included and shown in the bottom row of Figure 2.7. The star is LP 395-8, with spectral type M3.0V+ and $T_{\rm eff,1} = 3600$ K and $T_{\rm eff,2} = 3300$ K, spectral type M3.5V D. Baroch et al. (2018, 2021). Their luminosity ratio $L_2/L_1 = 0.14 \pm 0.01$ in the VIS channel translates in the weights: $w_1 = 0.893$ and $w_2 = 0.107$ for Hα and $w_1 = 0.834$ and $w_2 = 0.166$ for Ca II IRT-λ8498. The error in EW determination is in both cases $e(EW) \approx 2\%$. The reference stars are taken from CARMENES DR1 and referred to in P. Schöfer et al. (2019). They are HO Lib, with spectral type M3.0V and $T_{\rm eff} = 3441K$, and again Barnard's Star (M3.5V).

2.6 Conclusions

`iSTARMOD` tool is a new implementation of the spectral subtraction technique. It is an upgraded and `Python`-coded version of the previous `STARMOD` code, with improved usability, modularity, and integration with modern data analysis workflows. This enhanced implementation of the code allows a more precise determination of radial and rotational projected velocities, as well as an automated calculation of the EWs in the study of single and binary chromospherically active stars. The code is publicly available (F. Labarga & D. Montes, 2025) under an open-source license.

The code is also very useful to identify new lines with a significant chromospheric contribution, apart from well-known activity indicators, and to search for magnetically sensitive spectral lines, which are lines with detectable Zeeman broadening (see D. Montes et al. 2020).

As a companion to the `iSTARMOD` code, a series of calibrations, allowing the determination of its corresponding fitted χ-functions, have been discussed and provided for Hα, Ca II H and K, He I D_3 + Na I D_1,D_2, Ca II IRT, Paδ, Paγ + He I λ10830 and Pβ.

The application of both tools together will allow the calculation of flux–flux relationships F. Labarga (2025) and temporal series, given the ability to process large spectral datasets or extensive stellar samples, and will be the subject of further studies.

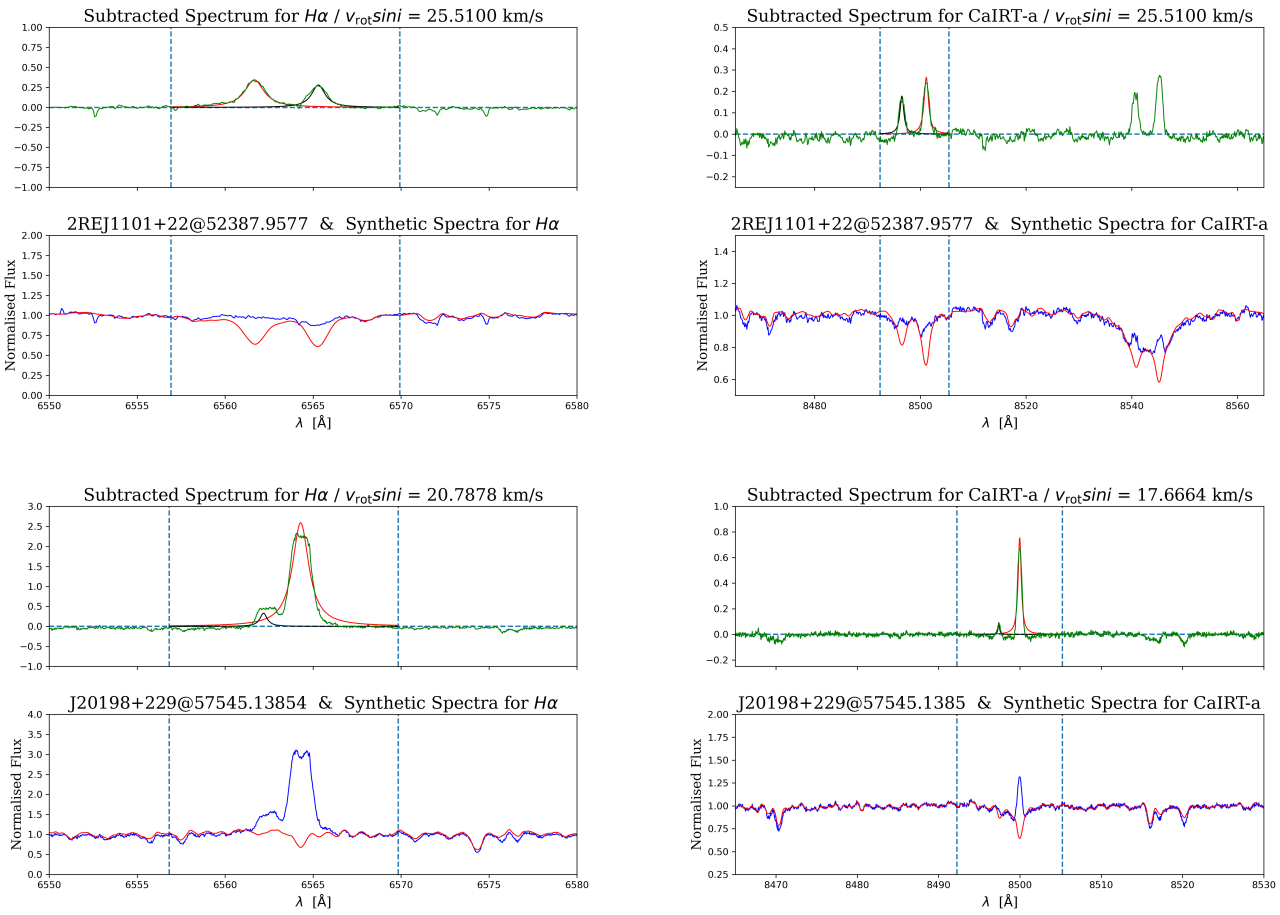

Figure 2.7. Spectral Subtraction examples of two SB2 systems, with H_α order in the left column and Ca II IRT-λ8498 in the right one. *Upper Row*: GZ Leo (2RE J1101+223), a K1V+K1V SB2 star, using FOCES provided spectrum (M. C. Gálvez et al., 2009). *Lower Row* LP 395-8 (J20198+229), a M3.0V+M3.5V SB2 system, using a spectrum taken by the CARMENES spectrograph, from CARMENES Data Release 1 (I. Ribas et al., 2023). Lines and color codes as in Fig. 2.5.

CHAPTER 3

Chromospheric activity of the M-type stars of CARMENES and its Flux-Flux relationships

Reference

This chapter is based on a paper preliminary entitled:
The CARMENES search for exoplanets around M dwarfs. Chromospheric activity and Flux-Flux relationships.
Paper F. Labarga et al. (2026) in preparation, to be submitted to *Astronomy & Astrophysics*.

3.1 Introduction

Stellar activity, ubiquitous among late-type stars (J. C. Hall, 2008), exhibits characteristic features in M dwarfs (T. J. Henry & W.-C. Jao, 2024; N. Meunier et al., 2024; L. Mignon et al., 2023). It is closely linked to rotational state, magnetic-field strength, stellar age, and the depth of the convective zone (A. Reiners & G. Basri, 2009; S. L. Baliunas & A. H. Vaughan, 1985). Since the high-energy radiation emitted by low-mass stars is mediated by magnetic dynamos, stellar activity plays a fundamental role in understanding their evolutionary pathways (M. M. Katsova, 2020).

A clear example of the relevance of activity in stellar evolution is the study of the Vaughan-Preston Gap (A. H. Vaughan & G. W. Preston, 1980), which, as noted by B. R. Durney et al. (1981), is thought to separate two distinct stellar populations. One group displays strong Ca II line fluxes with significant –likely aperiodic– variability, while the other shows weaker fluxes and predominantly cyclic behaviour. These differences may arise from magnetic braking (A. Skumanich, 1972; L. Mestel, 1992; N. Ivanova & R. E. Taam, 2003), which gradually slows stellar rotation and modulates activity levels. Conversely, a weakening of magnetic braking may lead to a "reactivation" or increase in rotation rate in older stars (N. Saunders et al., 2024), suggesting that stars might lose their large-scale magnetic fields more rapidly than previously assumed (T. S. Metcalfe et al., 2024).

Additionally, the depth of the convective zone –set by stellar mass and therefore spectral type and effective temperature– may play a significant role in determining on which side of the gap a star falls. The very existence of the Vaughan-Preston Gap has been questioned by recent studies (S. Boro Saikia et al., 2018), raising the important question of whether the disappearance of the gap would also imply the absence of the underlying stellar populations traditionally associated with it. The analysis of M-dwarf activity presented in this chapter begins with a description of the CARMENES active stars sub-sample used in our study –Section 3.2. Section 3.3 presents the flux-flux relationships determined by means of the methods presented in previous chapters. They are supplemented in Section 3.3 with values of average magnetic field intensity $\langle B \rangle$, metallicity $[Fe/H]$, rotation period $P_{\rm rot}$ and ages. The determination of $P_{\rm rot}$ allows to perform an analysis of the activity in terms of the Rossby Number R_0. Section 3.5 presents the conclusions can be obtained from this study including the new picture of the Vaughan-Preston Gap in view of the results presented in the previous sections.

3.2 The CARMENES sample and the active-star sub-sample

The complete set of stars analyzed in this study is presented in Table 3 for the Active Stars and in Table 6 for the Reference Stars used in the spectral subtraction procedure. Both groups belong to the CARMENES GTO sample, which has previously been employed to investigate activity in M dwarfs. L. Tal-Or et al. (2018) analyzed correlations between radial velocity and various activity indicators, focusing on stars with large RV variability (RV scatter $\geq$ 10 $\mathrm{m\,s^{-1}}$), the so-called RV-loud sample. Their work served as the starting point for the present study. Additional GTO stars showing signs of activitymost of them with $pEW(H\alpha) \leq -0.8$ Å as listed in the CARMENES database (I. Ribas et al., 2023)were further incorporated. The reference stars used in this work are those presented in P. Schöfer et al. (2019). For each spectral subtype, the selected reference star corresponds to the object within the CARMENES GTO sample with the longest known rotation period $P_{\rm rot}$. This choice is motivated by the well-established relationship between chromospheric activity and stellar rotation (S. Mohanty et al., 2002; E. R. Newton et al., 2017; S. V. Jeffers et al., 2018), under the assumption that stars with the longest rotation periods are the least active representatives of their respective spectral types.

An additional selection criterion was the suitability of each star for reliable measurement through the spectral subtraction technique, not only for Hα but also for other chromospheric activity indicators. Spectral subtraction was applied to the adopted set of diagnostics (Hα, Paschen series, Ca II IRT triplet, Na I D_1 & D_2, He I D_3, and He I

λ10830) for most stars in the sample, whereas for some targets only Hα and Ca II IRT measurements were computed specifically for this work.

The final sample comprises 101 stars, including several well-known active late-type stars–such as EV Lac, AU Mic, and YZ CMi–commonly studied in the context of stellar activity. However, other stars in the sample had been largely overlooked in this regard, yet displayed remarkable flare activity during the CARMENES observing campaigns. Examples include J11474+667 (also studied by B. Fuhrmeister et al. 2020 for variability in the He I λ10830 line) and the M8.5-type star J04198+425.

The measurements and analyses reported in this paper are based on observations obtained with the CARMENES instrument (A. Quirrenbach et al., 2018, 2020; J. A. Caballero et al., 2025)–the Calar Alto high-Resolution search for M dwarfs with exo-Earths using Near-infrared and optical Echelle Spectrographs–within its Guaranteed Time Observations (GTO) program. Raw spectra from the CARMENES survey were processed with the dedicated reduction pipeline (J. A. Caballero et al., 2016b; M. Zechmeister et al., 2018), which includes telluric correction (E. Nagel et al., 2023). The resulting dataset, comprising approximately 3000 spectra, forms the basis of the present study. These include spectra not yet publicly released in Data Release 1 (I. Ribas et al., 2023), particularly for the NIR channel, which contains many of the most recently obtained observations.

CARMENES is mounted on the 3.5 m telescope at the Calar Alto Observatory (Almería, Spain) and consists of two cross-dispersed, fibre-fed echelle spectrographs operating simultaneously. The visual (VIS) channel covers $\lambda = 520$–960 nm at a spectral resolution of $R = 94\,600$, while the near-infrared (NIR) channel spans $\lambda = 960$–1710 nm at $R = 80\,400$. Since 2016, the CARMENES survey has monitored more than 300 M dwarfs across all spectral sub-types with the primary goal of detecting exoplanets (A. Reiners et al., 2018). A significant fraction of these data is now available to the scientific community (I. Ribas et al., 2023).

None of the stars in our final sample show evidence of being double-lined spectroscopic binaries (SB2). Some targets that otherwise met our selection criteria were identified as binaries in D. Baroch et al. (2018, 2021). Those classified as SB1 were excluded because, as discussed by D. Montes et al. (1996b), their binarity can significantly affect the spectral subtraction process. SB2 systems were also omitted, as their composite spectra complicate the application of the subtraction technique and may lead to substantial overestimation of chromospheric fluxes.

The complete dataset of line luminosity normalized to bolometric luminosity computed using the methods presented in Chapter 2 taking the measured EW by spectral subtraction is shown in the appendix 4.5, and their mean values in 4.5.

3.3 Flux-Flux Relationships

Empirical flux-flux relationships are widely used in the study of chromospheric activity to understand the correlations, generally through empirical power law functions (D. Montes et al., 1996a), between different activity indicators and their underlying physical mechanisms. These relationships provide insights into stellar magnetic activity (R. de Grijs & D. Kamath, 2021), energy distribution, occurrence of starspots and chromospheric plages (J. López-Santiago et al., 2003b) and evolutionary trends (S. G. Gregory, 2017). Chromospheric activity is often studied using emission lines such as Ca II H& K and IRT lines, Hα, Mg II h & k, He I D_3, Na I D_2 and other lines, identified as activity indicators. Flux-flux relationships help determine how energy is partitioned between these different lines, and how this determines the different channels through which the magnetic energy is dissipated (S. Mohanty et al., 2002). A strong or tight correlation, as we will see below, suggest a common heating mechanism (J. L. Linsky, 2017), likely associated with magnetic activity. Studies of flux-flux relationships, as in R. Martínez-Arnáiz et al. (2011), help to distinguish between different activity regimes, and identify anomalous stars, by detecting ones that deviate from general flux-flux relationships.

3.3.1 Hα vs Ca II IRT-λ8498

The ultimate goal of this work is to obtain flux-flux relationships for the RV loud sample (L. Tal-Or et al., 2018), supplemented with other CARMENES sample stars, also showing conspicuous activity. They are listed, as mentioned above in Appendix 4.5. To this end, the calibrations performed in the previous section will be used. The flux-flux relationships for the CARMENES sample aim to be put in the broader context of the study of activity of cold stars.

The first step to obtain them is measuring the different EW applying the spectral subtraction technique described in Section 2.2. After that, the values obtained are transformed into $L_{\rm line}/L_{\rm Bol}$ (equivalent to flux ratios $\mathcal{F}_{\rm line}/\mathcal{F}_{\rm Bol}$) using the χ factor methodology, as described in Section 2.4. As the very first result, the flux-flux relationships between Ca II IRT-λ8498 and Hα lines is shown in Figure 3.1. There the complete set of measurements are depicted, to evaluate the behaviour of the sequence of points for each supposedly identified group. To complete the analysis, the mean value and the Mean Absolute Deviation (MAD) for each star of the sample has been calculated, and depicted in the left panel of Figure 3.2. This, along with, of course, the levels of excess emission in each line, are the preliminary classification criteria for assign a star to a group.

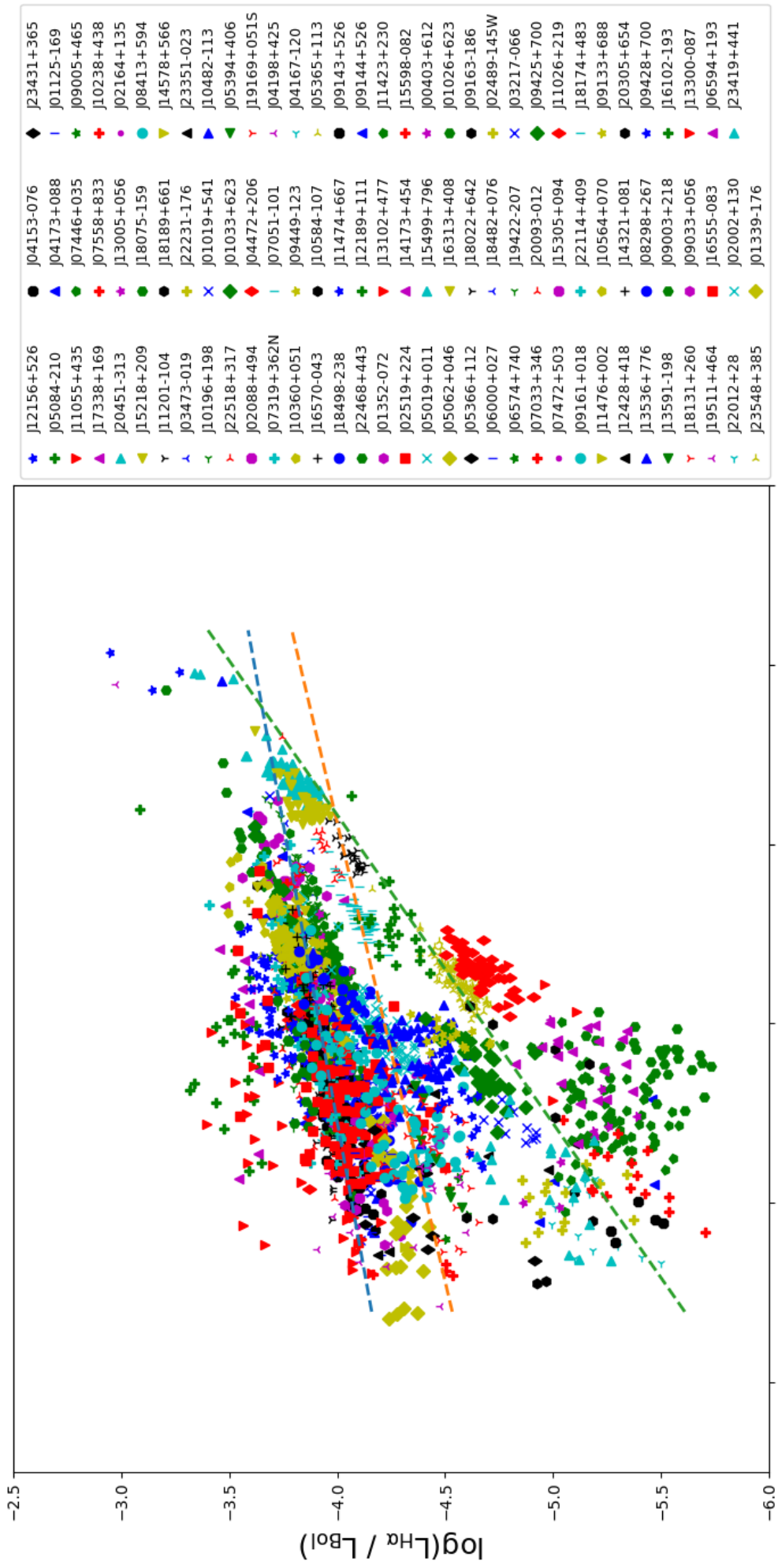

Figure 3.1. $L_{H\alpha}/L_{\rm Bol}$ vs. $L_{\rm Ca\ II\ IRT}/L_{\rm Bol}$. The whole sample set of individual EW measurements, transformed into fluxes ratios by means of χ factor method. The dashed lines are related with the fits of the each emitter population discussed along the paper. The blue dashed line corresponds to **Branch I**, the orange dashed line to **Branch II**, and finally the green one corresponds to **Branch III**. Refer to the text for a detailed explanation of these different emitter populations

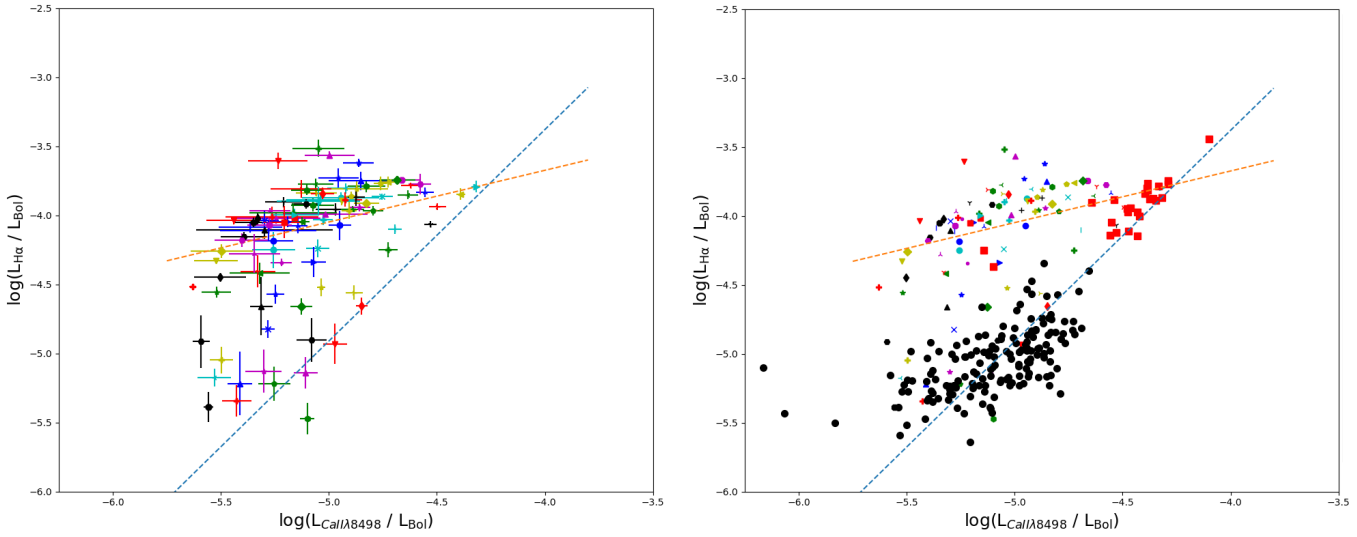

Figure 3.2. Left Panel: Mean values of $L_{H\alpha}/L_{\rm Bol}$ vs. $L_{\rm Ca\ II\ IRT\text{-}\lambda8498}/L_{\rm Bol}$, including the MAD of each star as error bars. Right Panel: Mean values of $L_{H\alpha}/L_{\rm Bol}$ vs. $L_{\rm Ca\ II\ IRT\text{-}\lambda8498}/L_{\rm Bol}$. The whole sample set of mean values of luminosity/flux ratios, including the FGKM stars of R. Martínez-Arnáiz et al. (2011). The read squares correspond to *upper branch* stars (as defined in this reference), while the black dots are the *lower branch* ones. The remaining symbols correspond to the mean values obtained in this study. In the same way, the red dashed line corresponds to the *upper branch* fit, while the blue one to the *lower branch*

A first group of stars, grouping around the blue dashed line in Figure 3.1, and with the highest levels of excess emission in Hα is visible. From a more or less constant level of activity in this line (y-axis), a great variability in the emission of Ca II λ8498 (x-axis), measured in terms of MAD, is seen in the left panel of Figure 3.2. This branch will be mentioned along this paper as **Branch I**. An intermediate group points is also visible with intermediate levels of excess emission in Hα, but very weak emission in Ca II λ8498. They show lower levels of variability in Ca II λ8498 than the previous group. The nature of this group will be discussed later, and will be referred to as **Branch II**. A third group of points, located around the orange dashed line, and with levels of excess emission in both Hα and Ca II λ8498 from intermediate/high to very low is also present. Their variability is almost the same in both axis, being lower as the excess emission is higher. We will refer to them here as **Branch III**.

For comparison and validation purposes, the absolute line fluxes provided in the paper of R. Martínez-Arnáiz et al. (2011) have been translated to line luminosities normalized to bolometric ($L_{\rm line}/L_{\rm Bol}$). Previously, the B-V values provided there have been converted to $T_{\rm eff}$ with the polynomial fit: $\mathrm{T_{eff}} = P_5(B-V)$ described in appendix 4.5, with data from M. J. Pecaut & E. E. Mamajek (2013). So we can incorporate their values to our analyses, in particular of the mean values calculated of the active stars of CARMENES sample. They are shown in the right panel of Figure 3.2.

A clear compatibility between both sets of flux-flux values is apparent. The different branches reported in the literature are visible, resembling the emission dichotomy, due to the different emitter populations, in the Hα vs Ca II IRT excess emission found by J. López-Santiago et al. (2010) and R. Martínez-Arnáiz et al. (2011). Those stars of the *upper branch* (as defined in R. Martínez-Arnáiz et al. (2011) and also in A. H. Vaughan & G. W. Preston (1980)) of the flux-flux relationships, with their values represented here as red squares, are the stars above the supposed Vaughan-Preston gap, believed to be younger and rapidly rotating stars probably with a different dynamo (L. W. Hartmann & R. W. Noyes, 1987; E. Böhm-Vitense, 2007). But the literature values also include points that can be located in our intermediate group. The *lower branch*, as referred to so in that paper, there including also FGK stars and represented in Figure 3.2 with black dots, is visible, overlapping almost exactly with the lower end of Branch III.

Then the behaviour mentioned in B. R. Durney et al. (1981) can be checked. In the Branch I, of highest Hα emission level, a chaotic and wide variability of excess emission values, particularly for Ca II IRT-λ8498, can be found. Then, as the level of Hα emission lowers, the variability in one axis equals the other, suggesting a cyclic behaviour.

This preliminary ascription of the stars of CARMENES sample to the different groups needs to be confirmed by the analyses performed in section 3.4.5.

3.3.2 Ca II IRT-λ8542 vs Ca II IRT-λ8498

The flux-flux relationship of the first two Ca II IRT lines can serve as a reliable testbed for validating the procedure used to derive line fluxes from EWs and empirical calibration relations. Figure 3.3, shows that most of the flux points move along the 1:1 axis, showing that out of the flares both lines of the triplet possess almost the same behaviour. The linear least-squares fit is represented by:

$$log\left(\frac{L_{\rm Ca\ II\ IRT\text{-}\lambda8542}}{L_{\rm Bol}}\right) = a + b\ log\left(\frac{L_{\rm Ca\ II\ IRT\text{-}\lambda8498}}{L_{\rm Bol}}\right) \tag{3.1}$$

and then $a = -0.63 \pm 0.05$, $b = 0.85 \pm 0.01$ and a correlation coefficient R^2 of 0.766. The slight deviation, for an amount of 15 %, from the 1:1 axis is caused by the activity. Also, it is then demonstrated that there are additional effects of activity to consider in Ca II IRT-λ8542 line with respect to Ca II IRT-λ8498. For lower levels of activity this deviation shows that the emission in Ca II IRT-λ8542 is slightly weaker than in Ca II IRT-λ8498. This is inline with J. López-Santiago et al. (2003b), where it is concluded that Ca II IRT-λ8542 is a poorer indicator of the changes in star activity than Ca II IRT-λ8498. A salient feature related to this flux-flux relationship raises considering the ratio EW(Ca II

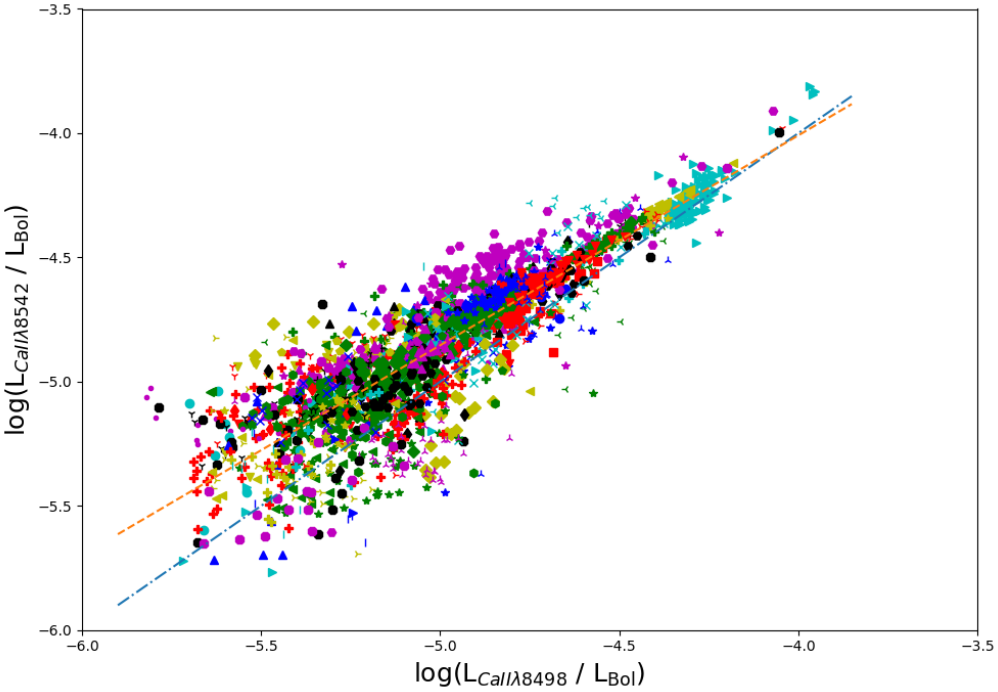

Figure 3.3. Flux-flux relationship for Ca II IRT-λ8542 vs Ca II IRT-λ8498. The codes for the legend are the same as shown in Figure 3.1.The blue dot-dashed line corresponds to the 1:1 axis, while the red dashed line is the fit of eq. 3.1, reported in the text.

IRT-λ8542)/EW(Ca II IRT-λ8498). These kind of ratios as activity indicators were established empirically in J. C. Hall & L. W. Ramsey (1992a) also for Hα and Hβ, using the spectral subtraction technique with the original version of `STARMOD`, applied to RS CVn binaries. There, it were studied the geometrical configuration of chromospheric structures

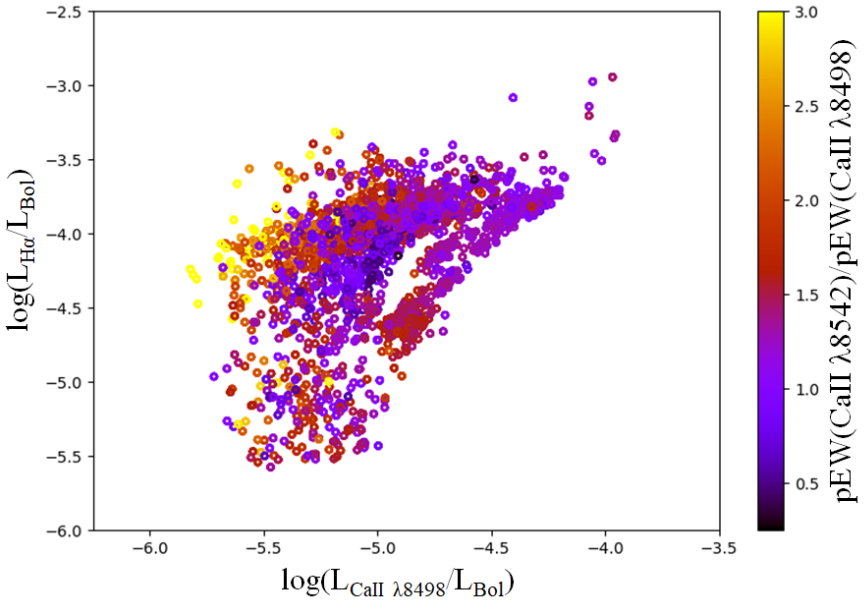

Figure 3.4. $L_{H\alpha}/L_{\rm Bol}$vs. $L_{Ca\ {\rm II}IRT-a}/L_{\rm Bol}$ in log-log graphic. And color coded $EW(Ca\ {\rm II}\lambda 8542)/EW(Ca\ {\rm II}\lambda 8498)$ in the range [0,3]. Ratio values ≥ 3 are depicted also in yellow.

like prominences and plages, and how they are displayed (and measured) from the point of view of the observer when

projected onto the stellar disk centre or at its border. A EW(Ca II IRT-λ8542)/EW(Ca II IRT-λ8498) indicator was used in J. López-Santiago et al. (2003b), using also STARMOD. It was find that for plages, the ratio has a value of $1.5-3$, while for prominences this value is ≈ 9. It is noteworthy that, in Figure 3.4, the maximum values of the ratios are achieved at the lowest values of $L_{\text{Ca II IRT-}\lambda8498}/L_{\text{Bol}}$ (yellow points, above 3.0, in the left side of the group of points). This would seem contrary to the intuition given that the presence of prominences are intimately related with high levels of activity. However, the points with high ratios in EW(Ca II IRT-λ8542)/EW(Ca II IRT-λ8498) mostly belong to stars of the Branch I, reflecting the fact that these stars are the most active. Values of the ratio in the range [1.0, 2.5] are commonly found in the sample related, as seen before, with plages around starspots.

For comparison purposes, the flux values reported by R. Martínez-Arnáiz et al. (2011), originally used to establish flux-flux relationships of the form

$$\log F_{\text{Ca II IRT } \lambda8542} = c_1 + c_2 \log F_{\text{Ca II IRT } \lambda8498}, \tag{3.2}$$

were converted into normalized luminosities, $L_{\text{line}}/L_{\text{Bol}}$. This transformation was performed using the $(B-V)$ colour indices provided in that work and the polynomial calibration $T_{\text{eff}} = f(B-V)$ defined in Appendix 4.5.

A relation of the form

$$\log\left(\frac{L_{\text{Ca II IRT } \lambda8542}}{L_{\text{Bol}}}\right) = a + b, \log\left(\frac{L_{\text{Ca II IRT } \lambda8498}}{L_{\text{Bol}}}\right) \tag{3.3}$$

was then derived. The least-squares fit yields $a = -0.88$ and $b = 0.81$, with a correlation coefficient $R^2 = 0.716$. It is that the obtained slope is consistent with the value derived for the CARMENES sample, and confirming the fact that activity induces a deviation of the relation Ca II IRT-λ8542 vs Ca II IRT-λ8498 from the 1:1 behaviour.

3.3.3 Hα vs R'_{HK}

An analysis of the behaviour of Hα vs Ca II H&K flux-flux relationship has been made for some stars of CARMENES subsample studied in this paper, with archival data collected by V. Perdelwitz et al. (2021). The diagram is presented in Figure 3.5, with the 41–out of 101–mean values collected. A relation for the whole set of data can be defined, as:

$$log\left(\frac{L_{\text{H}\alpha}}{L_{\text{Bol}}}\right) = (-0.51 \pm 0.83) + (0.89 \pm 0.18)\ logR'_{\text{HK}} \tag{3.4}$$

The linear fit yields a correlation coefficient $R^2 = 0.4762$ The associated p-value ($p < 2.2x10^{-}16$) corresponds to the significance of the null hypothesis of zero slope in the linear regression.

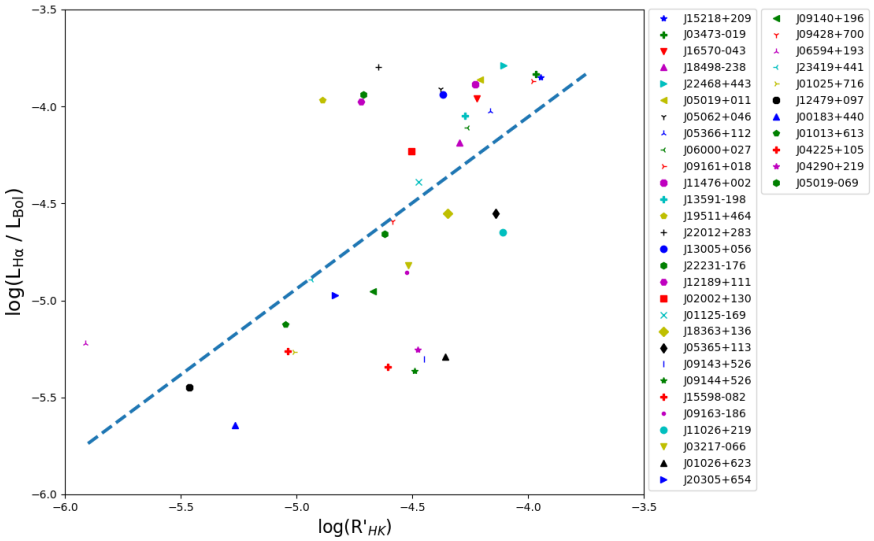

Figure 3.5. Flux-flux relationship for Hα vs R'_{HK}. The blue dashed line corresponds with the linear fit

3.3.4 Hα vs He I D_3 and Hα vs Na I D_2

He I D_3 (λ5878) and Na I $D_{2,1}$ (λ5891 & λ5898) lines are closely related with the bursts of activity in young stars, especially flares (see e.g: (B. Fuhrmeister et al., 2018)). They are located in the same order of the echelle spectra in the VIS channel of CARMENES instrument. However, the $Na_{D1,2}$ lines are severely affected by telluric contamination. This fact jeopardizes the precision required and additionally, for late M-type stars the emission is very weak in this zone of the spectrum. This makes the isolation of the chromospheric contribution less reliable for Na D_1 λ5898 than for the D_2 line.The Na D_2 λ5891 line provides a cleaner diagnostic and has been therefore adopted. However is useful to confirm the correlations in Hα vs He I D_3 and Hα vs Na I D_2 presented in M. Kumar & R. Fares (2023).

Posing a fit for the flux flux relationship as:

$$log\left(\frac{L_{\mathrm{H}\alpha}}{L_{\mathrm{Bol}}}\right) = a + blog\left(\frac{L_{\mathrm{Line}}}{L_{\mathrm{Bol}}}\right) \tag{3.5}$$

where Line can be He I D_3 or Na I D_2, the situation is summarised in Figure 3.6 and in the next Table 3.1:

Table 3.1. Fit coefficients Hα vs He I D_3 and Hα vs Na I D_2 as defined in equation 3.5.

Line	a	b	R^2
He I D_3	-2.34 ± 0.09	0.297 ± 0.016	0.1919
Na I D_2	-2.65 ± 0.08	0.249 ± 0.015	0.1447

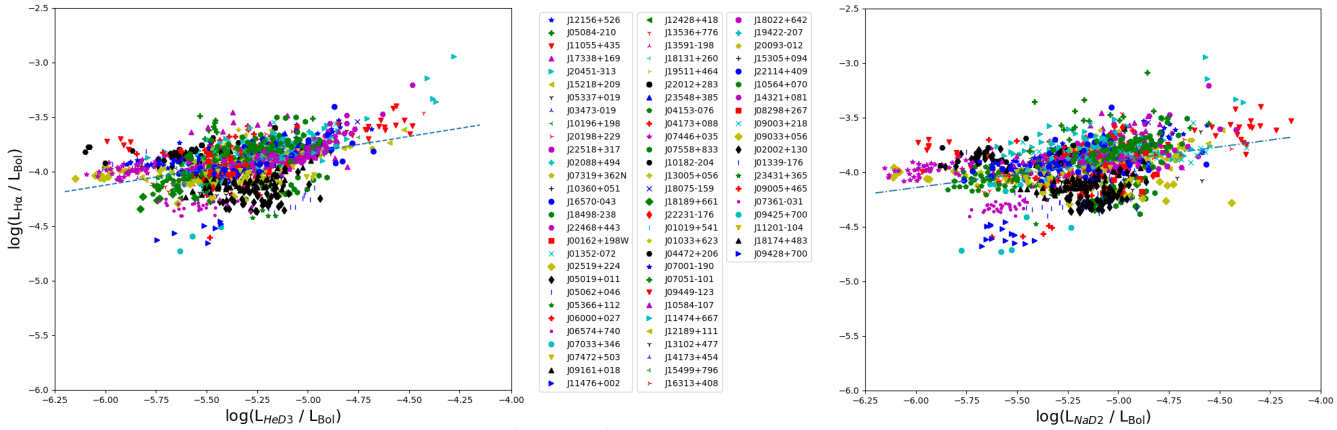

Figure 3.6. Left Panel: Flux-flux relationship for Hα vs He I D_3. Right Panel: Flux-flux relationship for Hα vs Na I D_2. In both cases the blue dashed line represent the respective fits as reported in Table 3.1.

.

3.3.5 He I D_3 vs Na I D_2

Given the fit parameters obtained in the previous section for He I D_3 and Na I D_2, is a good exercise repeating the same analysis of the subsection 3.1. The representation of the points can be seen in the right panel of Figure 3.7. As expected, the dispersion of the points are much higher, given we are dealing with different atomic species, and is apparent that the higher dispersion lies on the side of Na I D_2, due partially to the telluric contamination. The resulting fit is:

$$log\left(\frac{L_{\mathrm{He\ I\ D_3}}}{L_{\mathrm{Bol}}}\right) = (-2.04 \pm 0.10) + (0.63 \pm 0.02)\ log\left(\frac{L_{\mathrm{Na\ I\ D_2}}}{L_{\mathrm{Bol}}}\right) \tag{3.6}$$

with $R^2 = 0.484$ and $p \sim 10^{-16}$.

3.3.6 Hα vs Paschenβ

The Paschenβ line in emission, as mentioned in section 1.3.1.5, is associated with the occurrence of flares in the host M-type stars. It should present a clear correlation between *Paschen*β and Hα lines, as both are hydrogen spectral lines and are influenced by similar physical conditions in stellar chromospheres but in a different layer. In this regards it is important to study how this correlation could be across the different emitter populations, following the program proposed in B. Fuhrmeister et al. (2023a). Figure 3.8 shows that not all the stars of the sample of this study produce emission enough to a measurable effect. Nevertheless, 17 out of 101 stars, mostly in the *upper branch* of the Hα vs Ca II IRT-λ8498 flux-flux relationship, show a profuse flare–and some super-flare–activity. We can see as representatives of this case: the very young (PMS) star M0.5 J20451-313 (AU Mic), studied in many other contexts (B. L. Cale et al., 2021; M. Mallorquín et al., 2024; B. Klein et al., 2022) and wavelengths (S. Bloot et al., 2024), M3.5 J22468+443 (EV Lac) (), M5.0 J11474+667 (B. Fuhrmeister et al., 2023a) but curiously, not J04173+088 (E. N. Johnson et al., 2021). However, no hint of the different emitter populations is seen as there is almost no representation of the Branch III mentioned above. So, we cannot infer any distribution in the different emitter populations. The only noteworthy exception to this is J04198+425. This is a star in the intermediate zone between the Branch I and the Branch III. Their values in both line flux ratios are located in the extremes: from the extreme low values in the quiescent phase, to extremely high value of the only observed superflare.

Given these considerations, two fits had been performed: one with only the fluxes in the quiescent phase ($log(L_{H\alpha}/L_{\mathrm{Bol}}) \leq -3.62$), and other including the values corresponding to the flares. Using the equation 3.5, where Line is Paschenβ, result in the coefficients shown in Table 3.2, being in both cases p-value $\sim 10^{-16}$.

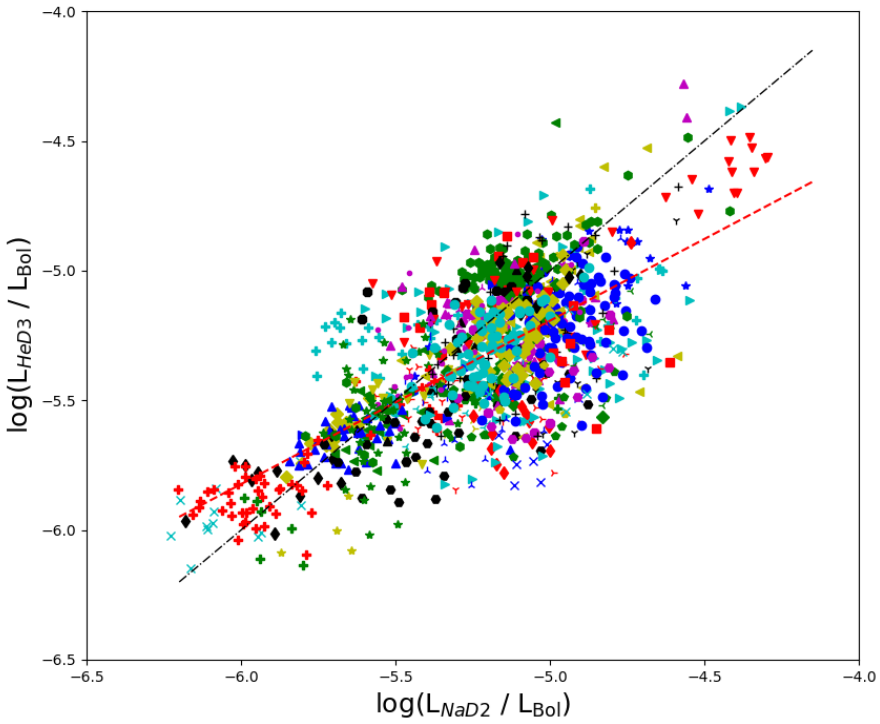

Figure 3.7. Flux-flux relationship for He I D_3 vs Na I D_2. The red dashed line represents the fit of equation 3.6, while the dot-dashed line represents the 1:1 axis.

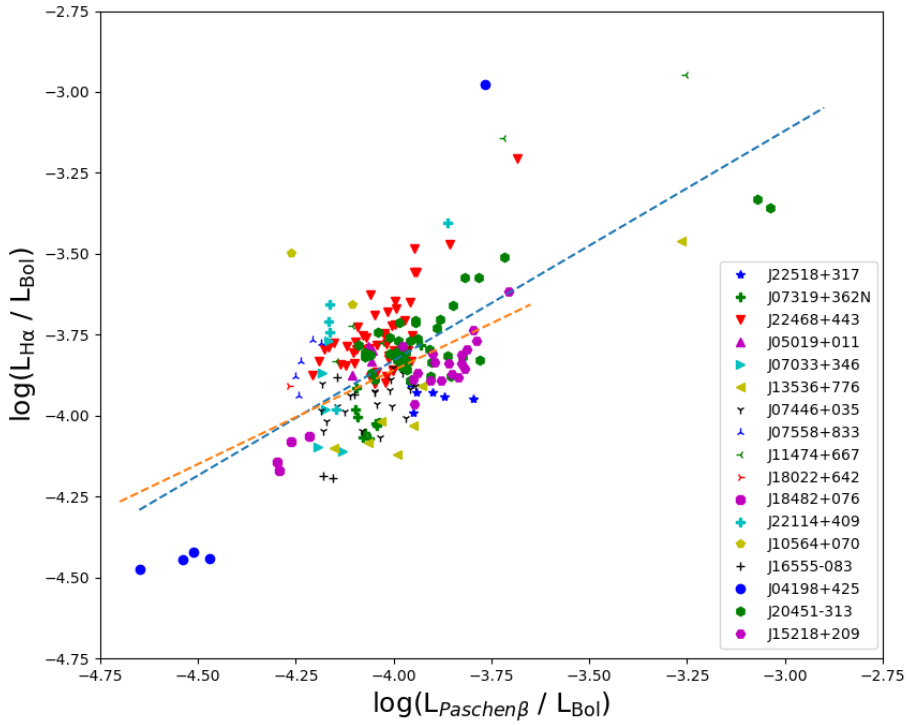

Figure 3.8. Flux-flux relationship for $H\alpha$ vs Paschenβ. The linear fit including the points of flares is depicted as the blue dashed line, while the red dashed line takes into account only the quiescent phases

3.4 Flux-flux Hα vs Ca II IRT-λ8498 relationships in relation to stellar parameters

The flux-flux relationships, that as mentioned in the previous chapter, typically involve chromospheric and coronal emission indicators, such as the Ca II H & K and IRT, Hα, and X-ray emissions, are linked to a variety of processes. These emissions are linked to magnetic dynamo processes, which are governed by a stars rotation and convective properties (A. Skumanich, 1972; P. Charbonneau, 2020). Since stellar activity is known to evolve with age due to rotational braking, an analysis incorporating $P_{\rm rot}$ and age provides a more comprehensive picture of the physical

Table 3.2. Fit coefficients for Hα vs Paschenβ as defined in eq. 3.5

	a	b	R^2
Including Flares	-0.99 ± 0.23	0.71 ± 0.06	0.4312
Only quiescent ph.	-1.54 ± 0.28	0.58 ± 0.07	0.3336

processes involved (S. A. Barnes, 2003, 2007). Furthermore, variations in metallicity may affect opacity, convection efficiency, and consequently, magnetic activity cycles (C. Karoff et al., 2018; A. Bonanno & E. Corsaro, 2022)

In this section the focus is set in the Hα vs Ca II IRT-λ8498 flux-flux relationship, linked with physical parameters such as effetive temperature ($T_{\rm eff}$), rotation period ($P_{\rm rot}$), average magnetic field ($\langle B \rangle$), metallicity ([Fe/H]) and age. It is aimed to refine the understanding of how different stellar properties influence activity correlations, and provide arguments to validate the distribution in branches of different emitter populations detected in section 3.3.1.

3.4.1 Effective Temperature $T_{\rm eff}$

To better understand the behavior of Hα vs. Ca II IRT-a relation, other stellar parameters must be taken into account. This is the case in Figure 3.9, where the flux-flux values are depicted with the data of the effective temperature of each star in colour code, belonging to a range of $T_{\rm eff} \in [2250, 4250]$ K. (The maximum $T_{\rm eff}$ value found among the stars of the sample belongs to the M0.0 star J05365+113 with $T_{\rm eff} = 4067$ K). The $T_{\rm eff}$ come from the database of the CARMENES survey with data from E. Marfil et al. (2021), and are listed in table 3 in appendix 4.5.

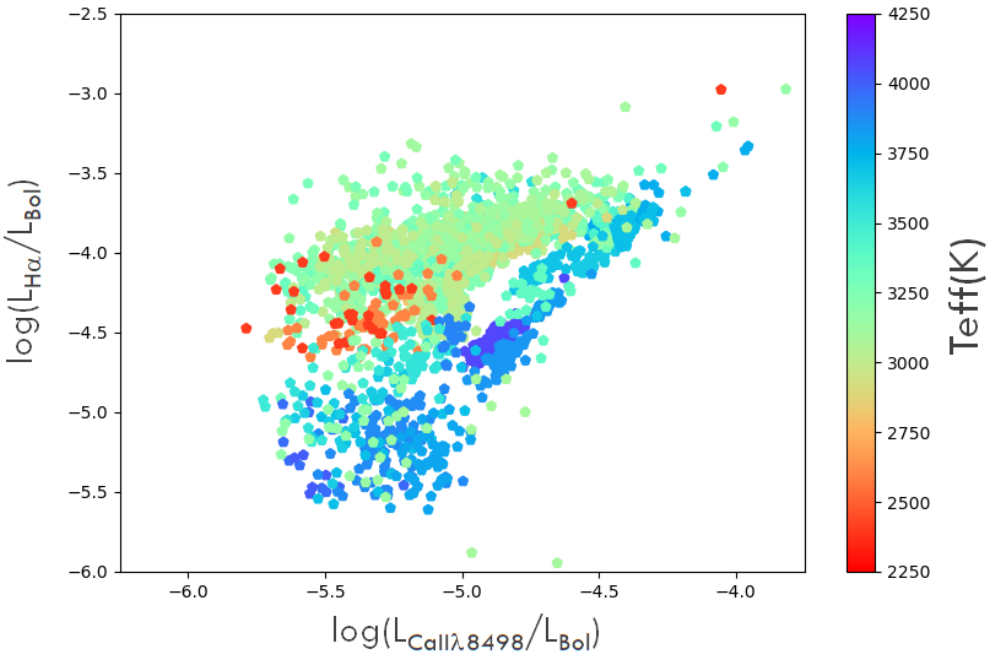

Figure 3.9. $L_{H\alpha}/L_{\rm Bol}$ vs. $L_{\rm Ca\ II\ IRT}/L_{\rm Bol}$ and $T_{\rm eff}(K)$ represented with colour code, in the range [2250, 4250] (K).

Again, three groups are clearly visible. The first one, that could correspond to Branch I of the most active stars, with effective temperature ranging from 2800 to 3450 K, corresponding to spectral types M3.0-M7.0, has the highest levels of emission in both lines. For each level of Ca II IRT-λ8498 these stars have values of Hα above the values corresponding to the stars of the other groups with the exception of values corresponding to the occurrence of flares.

A second group of points, that could correspond to Branch II, have effective temperatures in the wider and cooler range [2400, 3400], corresponding to spectral type M3.5-M8.5, Their intermediate values of emission in Hα relates with the lowest values in Ca II IRT-λ8498.

The third group have point values that are distributed across the whole range of emissions. This group could correspond to Branch III. Their temperatures are in the range [3100, 4100], corresponding to a spectral range M0.0-M5.0.

Then is clearly seen the new arisen situation, where the late-type (lower temperature) stars form a group (Branch II) in between the group of most active stars, according to its level of Hα emission, and the second group of hotter, more massive and less active stars. This feature could be due to the possible damping mechanism of magnetic fields, mentioned in L. M. Walkowicz et al. (2004) (referencing in turn S. Mohanty et al. (2002)), that apparently sets in for very late-type M-dwarfs onward. This must be confirmed by the analysis of the ages of these stars.

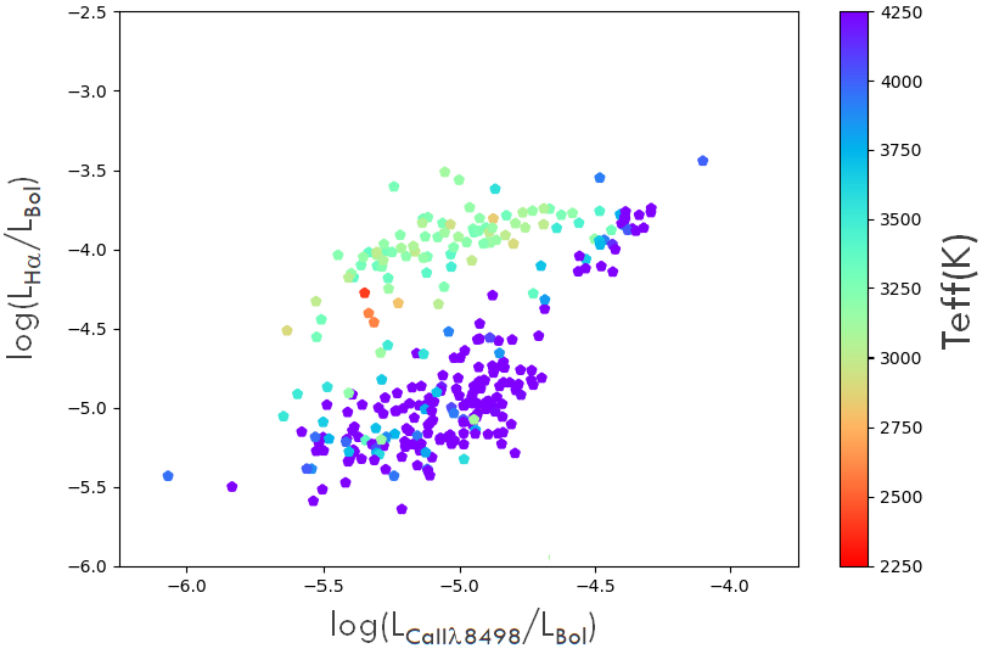

Figure 3.10. The whole sample set of $L_{H\alpha}/L_{\rm Bol}$ vs. $L_{\rm Ca\ II\ IRT}/L_{\rm Bol}$ mean values, including the FGKM stars of R. Martínez-Arnáiz et al. (2011). $T_{\rm eff}(K)$ represented in colour code in the range [2250, 4250] (K). Stars with $T_{\rm eff}$ higher than 4250 K, up to $\sim$ 7000 K cannot be represented with additional colours and they are assigned the highest colour-code value

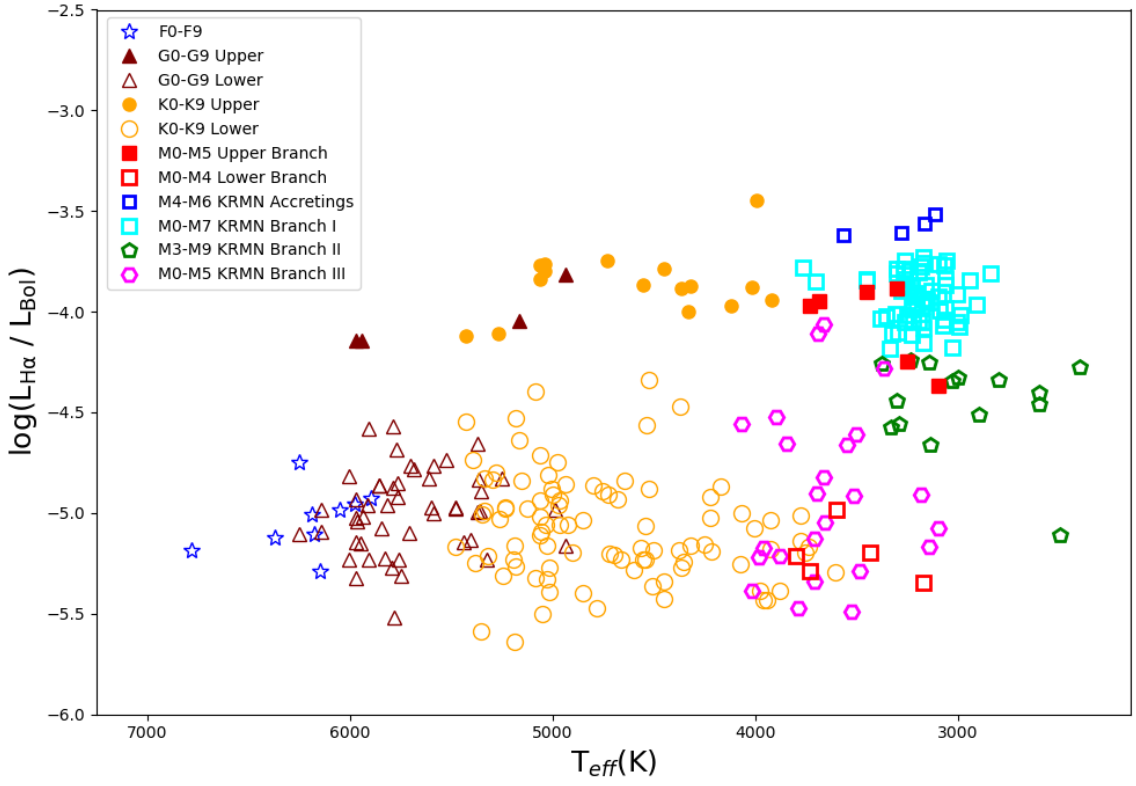

Figure 3.11. $L_{H\alpha}/L_{\rm Bol}$ vs $T_{\rm eff}$ (K). The light-blue squares correspond to the Branch I of most active stars of the CARMENES sample, green pentagons to the intermediate values (Branch II), and the magenta hexagons to the Branch III. The filled symbols belong to *upper branch* R. Martínez-Arnáiz et al. (2011) values, and the rest of empty symbols belong to the *lower branch* values of this reference.

The analysis is the same when considering the mean values, as seen in Figure 3.10. Here the literature values have been included, using again the $T_{\rm eff} = f\,(B-V)$ (see 3.3.1 and Appendix 4.5). Again, the values added for FGK stars (hotter and less active) are located almost all in the lower end of Branch III.

Considering only two of the three parameters above: $\langle L_{H\alpha}/L_{\rm Bol}\rangle$ and $T_{\rm eff}$ (K), Figure 3.11 is obtained. Here the overlapping temperature ranges are clearly shown. Following R. Martínez-Arnáiz et al. (2011), this figure can be interpreted as showing the presumed Vaughan-Preston gap. It is apparent that stars belonging to Branch II and

Branch III fill the gap in the low temperature side of the figure, while most of the Branch I stars cluster densely and in coincidence with most of the literature *upper branch* M-type stars. Compliant with figure 3.9, Branch II and Branch III have more dispersion either in $\langle L_{H\alpha}/L_{Bol}\rangle$ and effective temperatures, allowing their star members to fill the gap, mainly possessing from 3400 K backwards to lower temperatures. The lack of stars in the gap region, those with temperatures typical of K7-M0 types, is remarkable. Taking this into account we can say that the Vaughan-Preston gap is filled partially with M-type stars possessing temperatures up to 3400 k, that is to say: near the boundary of full convection (∼M3.5).

3.4.2 Rotation Period P_{rot}

The data from Rotation Periods P_{rot} provide additional hints to analyse the situation. Here the data for elaborating on Figure 3.12 were collected from from Y. Shan et al. (2024) and listed in table 3 of appendix 4.5, with P_{rot} expressed in days. These data reveals a situation where the shorter periods are located in Branch I, a group of previously presumed faster rotators, while the slower rotators are most grouped in Branch III, which aligns with the expectation of lower rotational velocities. This situation suggests a relationship of rotation period correlated with excess emission in Hα. However, at the lower end of Ca II IRT-λ8498 excess emission in Branch I and within Branch II, some longer rotation periods are also observed. Given the dependence of the rotation period on stellar radius, a more precise analysis can be conducted using the Rossby number. The Rossby number is defined as:

$$R_0 = \frac{P}{\tau_c} \tag{3.7}$$

where P is the rotation period, and τ_c is the convective turnover time, both magnitudes measured in days. So using the N. J. Wright et al. (2018) empirical approximation for τ_c, that makes use of the colour indexes V and K_s, later corrected in S. V. Jeffers et al. (2025):

$$log(\tau_c) = 0.58 + 0.28(V - K_s) \tag{3.8}$$

According with expression 3.7 and 3.8, fits can be proposed as:

$$log\left(\frac{L_{H\alpha}}{L_{\rm Bol}}\right) = a + b log\,(R_0)$$

The two fits of the Figure 3.13 can be summarised in Table 3.3.

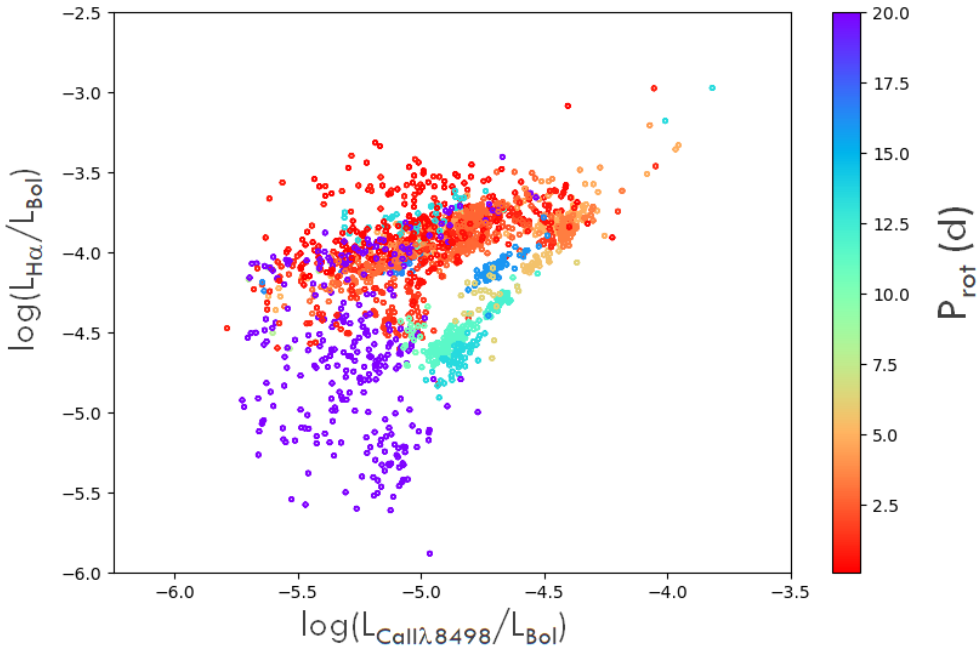

Figure 3.12. A subset (75 out of 101 stars of the sample) of individual measurements of $L_{H\alpha}/L_{\rm Bol}$ vs. $L_{\rm Ca\ II\ IRT\text{-}\lambda8498}/L_{\rm Bol}$ and in colour code the Rotation Period in days. Depicted in the range [0, 20] days, some rotation periods exceed this higher limit.

Although the saturated regime is often described as a plateau in activity, a closer inspection reveals a weak residual dependence of the activity flux on the Rossby number. For Branch I stars, this dependence is characterized by a very shallow slope (b0.05), much smaller than that observed in the unsaturated regime. This result is consistent with the non-zero slopes in the saturated regime have been reported in previous studies (e.g. A. Reiners et al. 2014; A. Frasca et al. 2025). These subtle variations do not contradict the existence of two distinct activity regimes, but instead suggest that saturation represents a regime of strongly reduced, rather than vanishing, Rossby-number dependence.

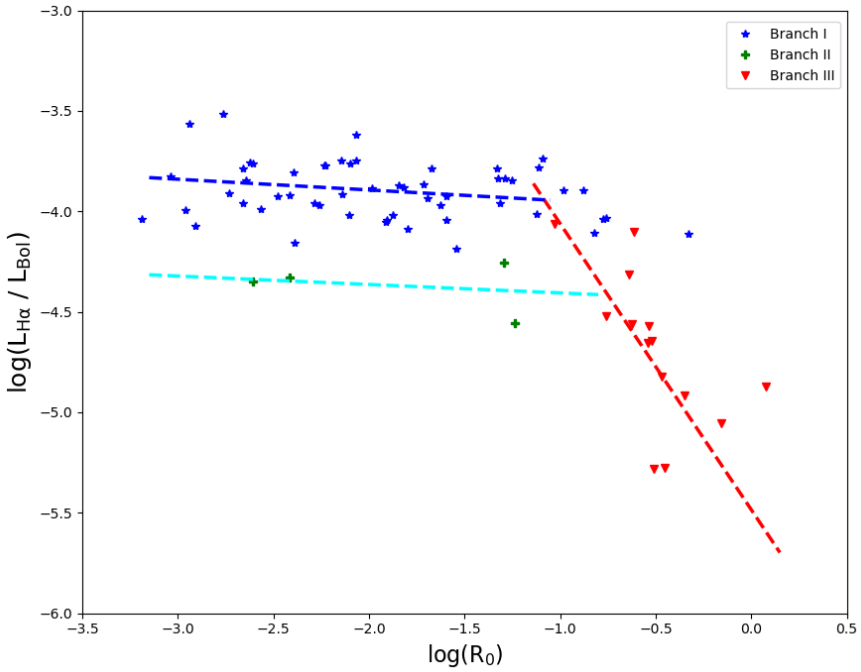

Figure 3.13. $L_{H\alpha}/L_{\rm Bol}$ vs. R_0 (Rossby Number). The same subset (75 out of 101 stars) of measures of H_α line luminosity normalised to bolometric mean values against the Rossby number of each star. Blue symbols corresponds to Branch I, green symbols to Branch II and red symbols to Branch III.

Table 3.3. Fits for the Hα fractional flux vs R_0 relationships

	a	b	R^2
Saturated R.	-4.00 ± 0.06	-0.05 ± 0.02	0.047
Non-saturated R.	-5.48 ± 0.31	-1.42 ± 0.52	0.3503

The saturated regime of fast rotators corresponds almost exclusively to Branch I stars, as expected, while the Branch III of slow rotating stars are framed in the non-saturated regime, thus confirming again the activity-rotation relation. Branch II stars, late-type M-dwarf with intermediate level of activity in Hα, appear in the saturated regime group (green crosses) in Figure 3.13, with Hα flux fraction lower than that of the most active stars. However, due to their limited sample size, a statistically robust fit cannot be established.

The analysis of rotation periods and Rossby numbers confirms the expected activity-rotation correlation. Branch I stars, which are fast rotators, align with the saturated regime, while the slower rotators in Branch III fall within the non-saturated regime. Further gathering of data for Branch II is needed. These results reinforce the role of rotation in regulating magnetic activity.

3.4.3 Average Magnetic Field Intensity: $\langle B \rangle$

Figure 3.14 shows the flux-flux relationship, with the average magnetic field intensity for each star in our sample where data is available colour-coded. The magnetic filed values were taken from A. Reiners et al. (2022) and are listed in table 3 of appendix 4.5. A clear gradient in magnetic field intensity is observed, decreasing from higher to lower levels of Hα flux. As expected, the average magnetic field intensity correlates with stellar activity levels, measured in terms of Hα flux. The Branch I stars forms a clear homogeneous group, with high level of excess emission in Hα satisfactorily related with high levels of average magnetic field. The Branch II stars of our sample, for which we have data available, posses relatively low values of average magnetic field, in the range [900, 1900] G. On the other hand the Branch III stars cover a wider range of values for the average magnetic field: [200, 3400] G. However it is remarkably that, for the same level of emission in Hα, the magnetic field is lower in Branch II than in Branch III.

The previous findings on rotation period and Rossby number align well with the average magnetic field intensity trends observed in our sample. As shown in Figure 3.14, the average magnetic field intensity $\langle B \rangle$ exhibits a clear correlation with activity levels, reinforcing the idea that both rotation and magnetic fields are drivers of chromospheric activity. The Branch I stars form a homogeneous group with strong Hα excess emission and high magnetic field intensities, consistent with their fast-rotating nature. Meanwhile, the Branch II stars, despite having similar levels of Hα emission as some Branch III stars, display slightly lower magnetic field strengths. This suggests that for this emitter population, additional factors beyond just rotation, such as internal stellar structure or evolutionary stage, may influence the magnetic field properties in these stars. However, the remaining stars of Branch III, with lower levels of Hα emission relate with low average magnetic field intensity, as expected.

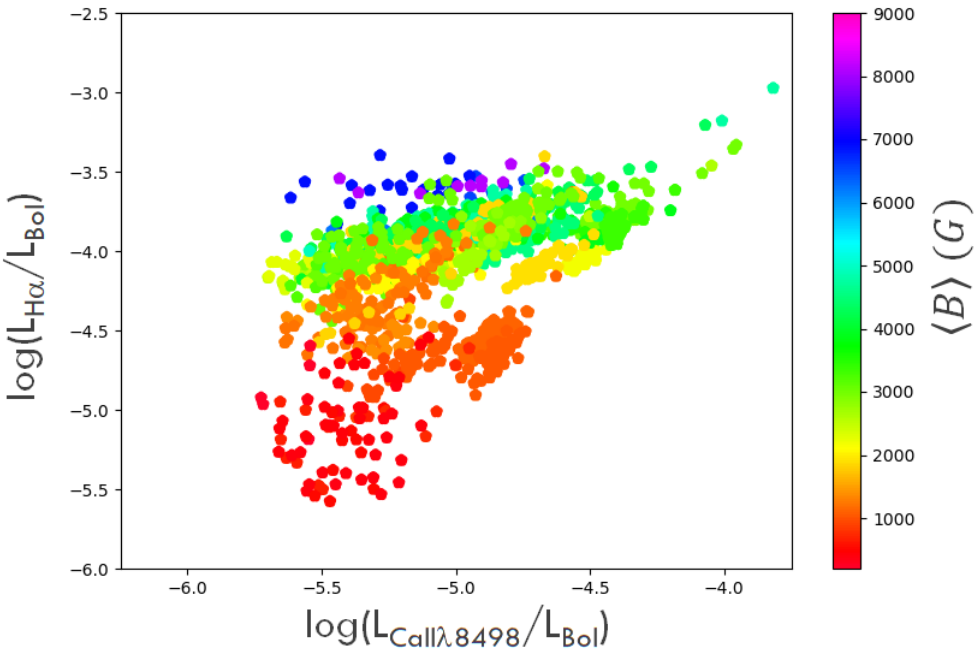

Figure 3.14. $L_{H\alpha}/L_{\rm Bol}$ vs. $L_{CaIIIRT}/L_{\rm Bol}$ + $\langle B \rangle$. The set of individual measurements and in colour code the average magnetic field intensity $\langle B \rangle$ in Gauss, for stars with data from A. Reiners et al. (2022). The data does not cover the complete sample of this study.

3.4.4 Metallicity [Fe/H]

The metallicity values shown in Figure 3.15 were computed by E. Marfil et al. (2021) using the CARMENES template spectra and the StePar Syn code (H. M. Tabernero et al., 2022). The values are listed in table 3 of appendix 4.5 Unlike the clearer trends seen in flux-flux relationships incorporating $T_{\rm eff}$ (Figure 3.9) or $\langle B \rangle$ (Figure 3.14), the distribution of metallicity across different emitter populations appears less well-defined.

The role of metallicity in stellar activity and dynamo processes has been discussed in several previous works, such as A. Bonanno & E. Corsaro (2022), which primarily analysed the dichotomy of stellar activity cycles in cool stars, V. See et al. (2023, 2024) studying a sample of stars of the KEPLER field (F-type to M2-type), and C. Karoff et al. (2018). These studies suggests that metal-poor stars, due to their lower opacity, have higher luminosity and convective efficiency. This could enhance turbulent diffusivity, weakening the large-scale dynamo. Conversely, metal-rich stars, with its increasing opacity have lower luminosity and turbulence diffusivity, strengthening the large-scale dynamo. Given that the presumed Vaughan-Preston gap describes a bimodal distribution of stellar activity, with stars appearing either "active" or "inactive" and few intermediate cases, in A. Bonanno & E. Corsaro (2022) it has been hypothesized that metallicity might influence this gap by affecting the dominant dynamo regime. Under this framework, "active" stars would be associated with the upper branch of the flux-flux distribution, while "inactive" stars would correspond to the lower branch. If metallicity were a determining factor, metal-rich stars should be predominantly found in the inactive group. And notably, there are almost no stars with low metallicity in Branch III. But Branch I contains stars spanning the entire observed metallicity range. However, these results must be interpreted with caution due to potential sample selection biases, as the catalogue primarily includes stars above a certain activity threshold. Nevertheless, as shown in Figure 3.15, the fact that active stars (as measured by $L_{H\alpha}/L_{\rm Bol}$) span a broad range of metallicities, suggests that while metallicity may influence stellar activity and dynamo processes, it does not appear to be the primary factor governing the flux-flux emitter dichotomy. Further studies incorporating larger, unbiased samples and theoretical modelling would be needed to clarify its exact role in shaping stellar activity distributions.

3.4.5 Age. The young stars of the sample

Current theoretical understanding suggests that the *upper branch* stars above the Vaughan-Preston gap consists primarily of highly active, rapidly rotating, and younger stars, whereas the *lower branch* is composed of less active, slowly rotating, and older stars. This implies that stellar activity follows not only an activity-rotation relationship but also an activity-age correlation (S. G. Gregory, 2017). Most activity indicators exhibit a dependence on stellar rotation, and low-mass stars experience rotational braking with age, following Skumanich-type spin-down laws (A. Skumanich, 1972). However, this spin-down may flatten for ages ≤ 3 Ga (L. A. dos Santos et al., 2016).

In M. Cortés-Contreras et al. (2024), candidate young ($\tau \leq 800$ Ma) stars of CARMENES sample are identified, by means of building *ad hoc* kinematic index (KI) and activity index (AI). KI allows ascribing them membership to young star kinematic groups (SKG) performing the assessment using three independent tools: StePar Kin (kinematic

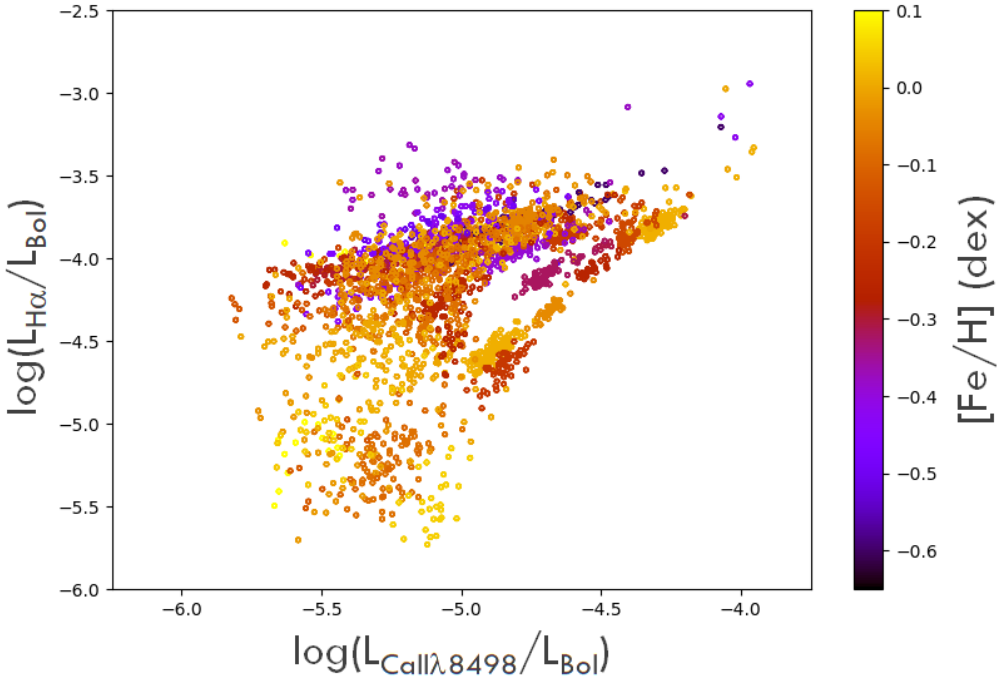

Figure 3.15. The whole set of individual measurements $L_{H\alpha}/L_{\rm Bol}$ vs. $L_{\rm Ca\ II\ IRT\text{-}\lambda8498}/L_{\rm Bol}$ and $[Fe/H]$ is represented colour coded in the range [-0.65, 1.0] dex.

ellipsoid fitting), LACEwING (convergence method) and BANYAN Σ (Bayesian analysis). Additional assessment

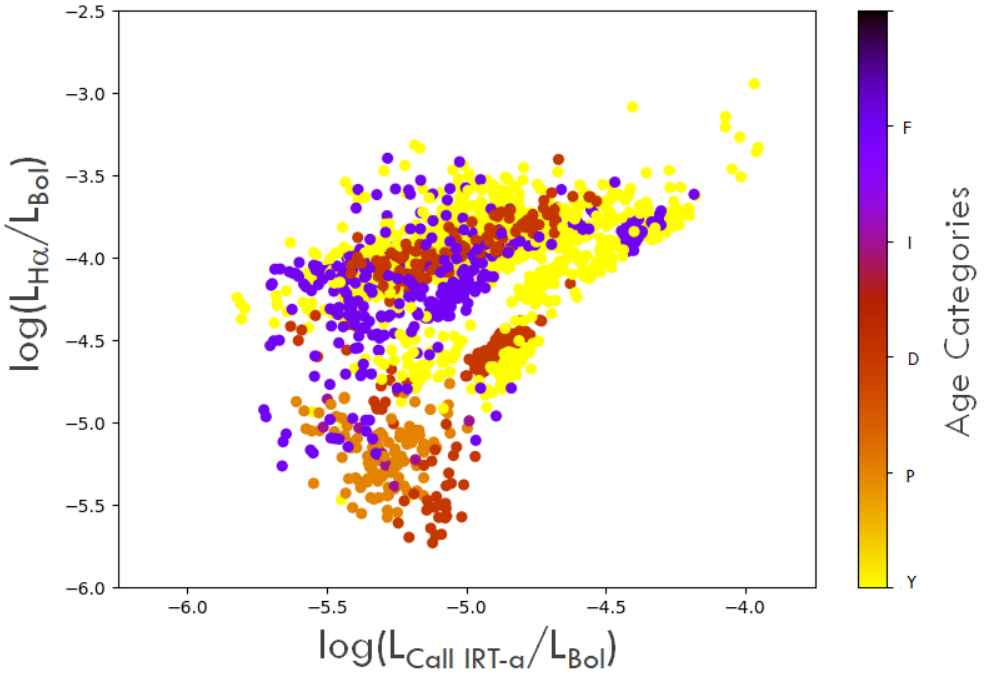

Figure 3.16. A set of individual measurements for the stars of this paper's sample and colour coded the age categories as in M. Cortés-Contreras et al. (2024)

is applied by the AI for those stars not clearly classified via kinematics, the authors apply five activity-color relations as a function of (G–J) color index: rotational period (P), projected rotational velocity (v sin i), X-ray emission ($log(L_X/L_J)$), ultraviolet excess (NUV – J) and Hα excess emission (EW Hα). A star is considered active if it satisfies at least two of these criteria. It is worth mentioning that 7 out of 26 newly identified young candidates in M. Cortés-Contreras et al. (2024) are also present in the sample analysed in this study. The stars are then classified into five categories: "Y" Young, "P" Potentially Young, "D" Dubious, "I" Inconclusive and "F" Field, being the last the category for the supposed older stars.

From this analysis, the categories are applied to the stars of this study in Figure 3.16. This analysis reveals that nearly all stars in Branch I fall into the younger categories: "Y," "P," or "D." Regarding Branch III, although age determination remains uncertain due to potential selection biases and intrinsic uncertainties, the presence of

young stars is unexpected yet evident. A particularly noteworthy observation is that most of the "F" (Field) stars in our sample are located within the intermediate Branch II, reinforcing the distinction between Branch I and this intermediate population. Conversely, compiling the stars of our sample that can *bonafide* be ascribed membership to a SKG, and then a range of age, the Figure 3.17 has been prepared.

This analysis confirms that most stars in Branch I fall within the age range [0–400] Ma, supporting our initial hypothesis regarding their youth. Additionally, the age distribution of stars in Branch III indicates that its leftmost stars are older than those in Branch I. Even within Branch III, a trend emerges: stars exhibiting stronger Hα emission (left side) tend to be younger than those on the right side, which show lower activity levels. Summing up both figures, our analysis supports the hypothesis that stellar activity correlates with both rotation and age,s expected from magnetic braking models. The classification of stars into age categories based on kinematics and activity indicators reveals that Branch I predominantly consists of young and active stars, while Branch III, though exhibiting a broader age distribution, contains both younger and older stars. The intermediate Branch II appears to host a significant number of older "Field" stars, further distinguishing it from Branch I. These findings reinforce the idea that activity levels provide valuable constraints on stellar ages, as in M. Cortés-Contreras et al. (2024), albeit with inherent uncertainties.

3.5 Discussion and Conclusions

In this study, the chromospheric excess flux in Hα, the Ca II IRT lines and other chromospheric activity indicators, for a selection of 101 stars of the CARMENES sample, is derived by subtracting a synthesized inactive star's spectrum from the observed spectrum, using Spectral Subtraction Technique. This allowed the measurement of EW for 3428 spectra of these 101 stars, for Hα and Paschenβ, Ca II IRT, He I D_3 and Na I D_2 lines.

These values were further transformed in fractional luminosities normalized to bolometric using the χ factor method. The application of this method requires the prior derivation of calibration functions for these features, as well as for additional lines such as He I λ10830, Paschenγ and Paschenδ.

Different flux-flux relationship for these lines were analyzed, with more detail in the case of Hα vs Ca II IRT-λ8490. There was confirmed the presence of different emitter populations, as suggested in R. Martínez-Arnáiz et al. (2011), provided the criterion of variability of the fluxes through it Mean Absolute Deviation (MAD) from a calculated Mean Value.

Once we have determined in section 3.3 that Hα vs Ca II IRT is the best indicator for the purposes of our study, in section 3.3 are considered additional parameters, as effective temperature $T_{\rm eff}$, rotation period $P_{\rm rot}$, average magnetic field intensity $\langle B \rangle$, metallicity [Fe/H] and Age, in order to investigate the dependence of the observed behaviors on these parameters. The different emitter populations of active M-dwarfs. From this we can see that we have:

- A first group of stars, mostly in the M3.5-M7.0 type range, which are fully convective. They possess higher levels of Hα emission *for each* Ca II IRT emission level: **Branch I**. This group has a correspondence with the *upper*

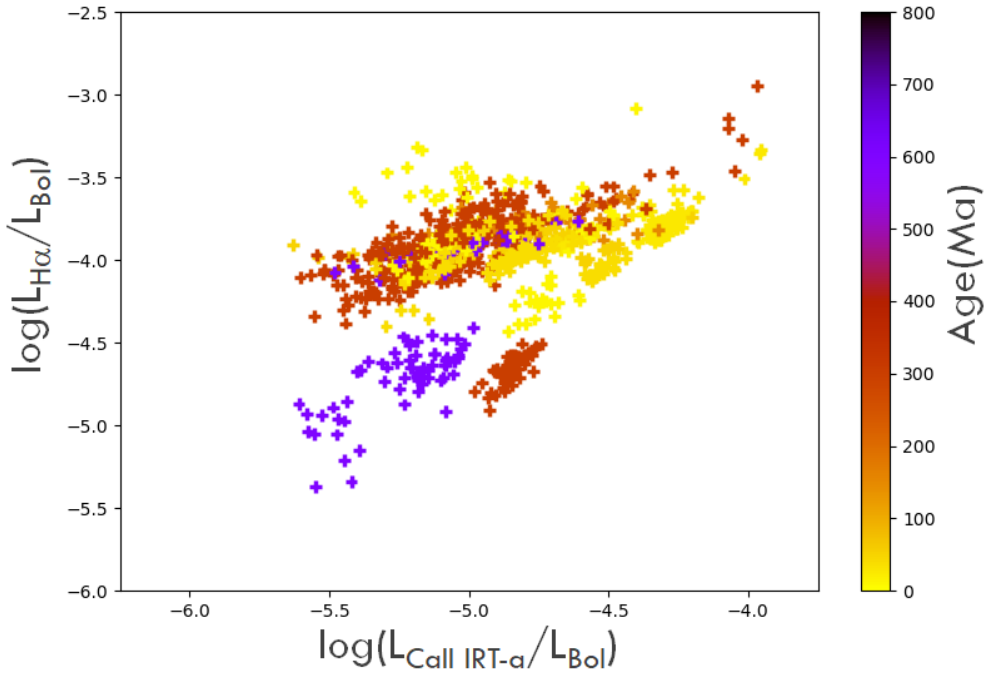

Figure 3.17. $L_{H\alpha}/L_{\rm Bol}$ vs. $L_{\rm Ca\ II\ IRT\text{-}\lambda8498}/L_{\rm Bol}$ + age(Ma). The subset of the individual measures for stars with age determinations is color coded according to their age.

branch emitter populations described in R. Martínez-Arnáiz et al. (2011), but here the values extend to lower levels of Ca II IRT chromospheric excess emission. This group shows stars with high activity and variability in Ca II IRT and fast rotation rates, causing all of them reside in the saturated regime of the Hα-Rossby number diagram. Also, high values for the ratio EW(Ca II IRT-λ8542)/EW(Ca II IRT-λ8498) are most commonly found in this branch, confirming their high level of activity. They posses the highest values of the average magnetic field intensity $\langle B \rangle$. The hypothesis that most of them are younger stars is confirmed by the analysis of section 3.4.5.

- A second group of stars in the M0.0-M5.0 type range, with lower levels of Hα emission for each Ca II IRT emission level: **Branch III**. This group has also a correspondence, in this case almost exactly, with the emitter populations described in R. Martínez-Arnáiz et al. (2011) as *lower branch* for FGK and M-type stars. It represents the stars with relatively low activity, and slower rotation rates. This last feature is confirmed by the fact that all with measured $P_{\rm rot}$ belong to the non-saturated regime of the activity-rotation relationship. Their values of average magnetic field intensity $\langle B \rangle$ are the lowest of the sample. With respect to the age they exhibit a broad age distribution, containing both younger and older stars.

- An intermediate group in the M3.5-M8.5 range, all of them with fully convective interiors, with low average level of Ca II IRT emission but with high variability, and relatively high values of Hα emission for each Ca II IRT emission level. It can be considered a subgroup of Branch I, given its behaviour in the flux-flux phase space, (**Branch II**). These late-type stars are relatively old, and possess a low average magnetic field intensity even in relation with stars of Branch I with comparable levels of emission in Hα.

The results are summarized in Figure 3.18, which also includes a least-squares fit of the type:

$$log\left(\frac{L_{\rm H\alpha}}{L_{\rm Bol}}\right) = a + b\ log\left(\frac{L_{\rm Ca\ II\ IRT\text{-}\lambda 8498}}{L_{\rm Bol}}\right) \tag{3.9}$$

for each identified group, resulting in the values of Table 3.4.

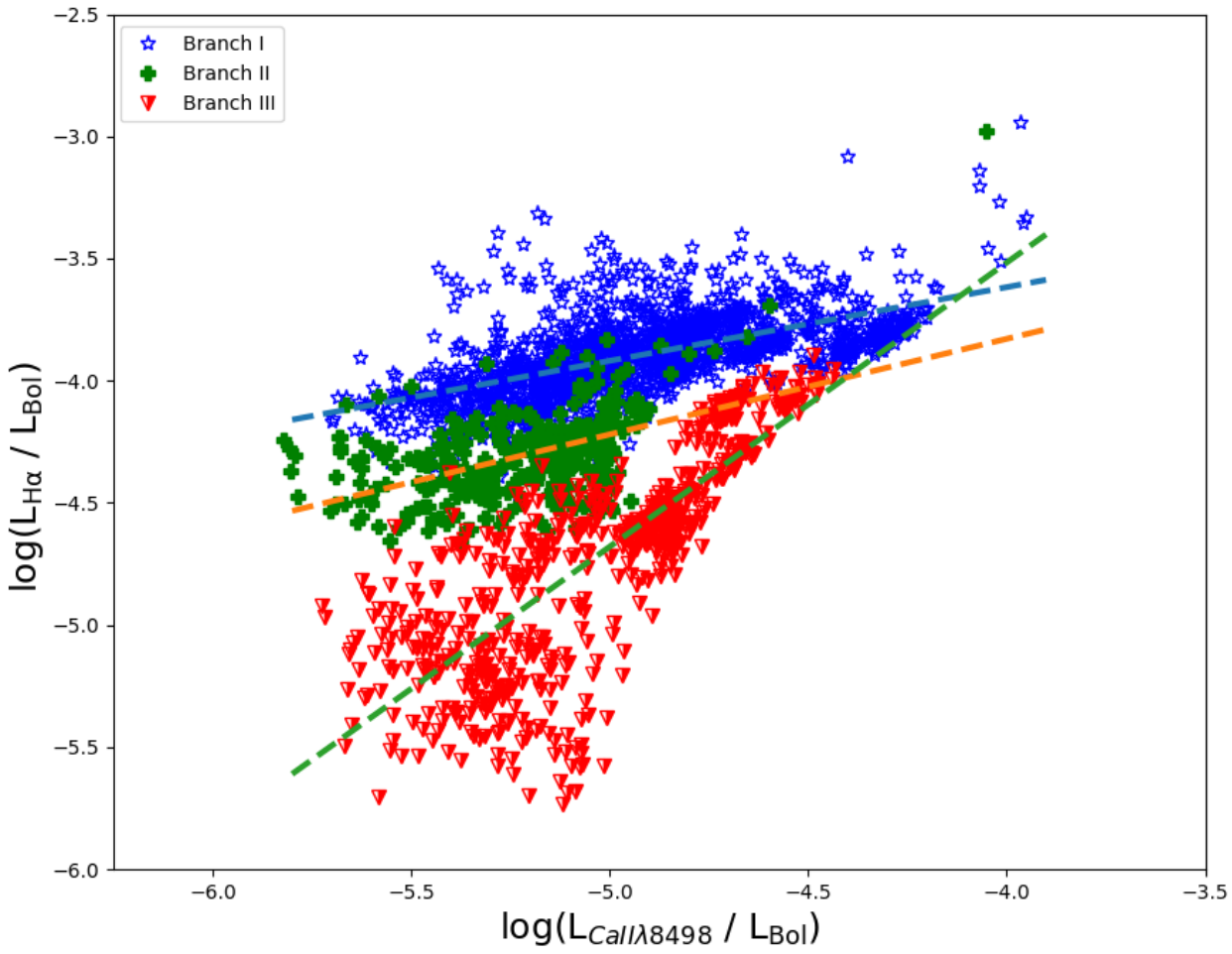

Figure 3.18. Values of $L_{H\alpha}/L_{\rm Bol}$ vs. $L_{\rm Ca\ II\ IRT} - \lambda 8498/L_{\rm Bol}$, showing the different groups identified. Branch I is identified with blue stars, and its fit with dashed blue line. Branch II is identified with green crosses and the fit with the orange dashed line. Branch III has been identified with red triangles, and its fit with the green dashed line.

Table 3.4. Fits for Figure 3.18 of the Hα vs Ca II IRT-λ8498 flux-flux relationships (Equation 3.9)

Branch	a	b	R^2
I	-2.41 ± 0.05	0.30 ± 0.01	0.3055
II	-2.26 ± 0.21	0.39 ± 0.04	0.3311
III	1.13 ± 0.18	1.16 ± 0.04	0.6146

Regarding the existence of two distinct emitter populations, as confirmed by these flux-flux relationships, and its relation to the Vaughan-Preston (VP) gap, the results of this study appear to point toward two seemingly contradictory conclusions.

On one hand, our findings corroborate those of S. Boro Saikia et al. (2018), supporting the argument that the VP gap is effectively filled on the M-type side of the diagram.

On the other hand, the confirmation of two separate emitter populations among stars of different spectral types, distinguished by their effective temperature, suggests distinct behaviours in terms of chromospheric excess emission variability. This, in turn, could imply intrinsic differences in the underlying dynamo mechanisms driving magnetic activity.

In putting all of this together, it can be said that while S. Boro Saikia et al. (2018) argue against a strict VP gap, their findings do not completely rule out the idea of a transition between activity states or even a dichotomy of emitter populations. It is important to mention that this study suggest that the appearance of a gap in smaller samples (like probably this one) may be due to selection biases or insufficient sampling. Our results also reinforce the conclusion of S. Boro Saikia et al. (2018), indicating that prior surveys may have overlooked numerous stars at intermediate activity levels due to similar selection effects. In addition to the above, modern gyrochronology models (e.g., S. A. Barnes (2007)), show a steady decrease in rotation and magnetic activity over billions of years, due to longer evolution times of late-K and M-type stars.

Consequently, these results support an alternative interpretation: that chromospheric activity does not abruptly decline at a particular threshold but instead undergoes a continuous, slow decay, driven by the progressive spin-down and extended evolutionary timescales of M dwarfs. This interpretation along with our results, therefore, argues against the existence of a well-defined VP gap, although favoring instead the existence of different emitter populations.

In summary, this picture of three groups in the $L_{H\alpha}/L_{\rm Bol}$ vs. $L_{\rm Ca\ II\ IRT\text{-}\lambda8498}/L_{\rm Bol}$ flux-flux phase space seems to indicate that the most important driver to differentiate the behaviour of the different emitter population of active stars is their internal structure, between partially and fully convective. This could force a dichotomy in the dynamo mechanism responsible of the activity of these stars.

On the other hand, the overlap in spectral type range between Branch I and Branch II, along with the identification of older stars in the latter, suggests that stars evolve from Branch I to Branch II as they age. It is worth mentioning that the analysis of the results provided in section 3.4.4 and 3.4.5 highlights the need of further studies of these two parameters to clarify their exact role in shaping stellar activity.

CHAPTER 4

Conclusions

The work presented in this thesis has focused on the development, validation, and astrophysical application of the `iSTARMOD` tool–an advanced Python-based reimplementation of the classic `STARMOD` code. This modernization effort, together with its scientific applications, has led to a set of significant methodological and astrophysical results that contribute to the study of chromospheric activity in M-type stars.

4.1 iSTARMOD: A Modern Tool for Spectral Subtraction and Activity Analysis

`iSTARMOD` constitutes a fully modular and extensible software package implementing the spectral subtraction technique for stellar activity studies. It integrates seamlessly with contemporary Python scientific libraries such as `NumPy`, `SciPy`, and `Astropy`, and introduces automation, batch processing, and improved precision in the determination of radial and rotational velocities, as well as equivalent widths (EWs) of chromospheric lines in single and binary systems.

Its open-source distribution (F. Labarga & D. Montes, 2026) ensures reproducibility and accessibility, providing the community with a modern, flexible, and user-friendly framework for the processing of large stellar spectral datasets, such as those produced by the CARMENES spectrograph. Beyond replicating the core functionality of the original code, `iSTARMOD` enables the detection of additional magnetically sensitive and chromospheric lines–those with significant Zeeman broadening signatures–thus extending its scientific reach to magnetic field diagnostics. The description of the code has been published in (F. Labarga & D. Montes, 2026) and the software is available at F. Labarga & D. Montes (2025).

Complementary absolute surface flux calibration routines have been developed for key spectral features–Hα, Ca II H and K, He I D_3 + Na I D_1, D_2, Ca II IRT, and the Paschen lines (Paδ, Paγ, and Paβ, including He I λ10830)–enabling quantitative flux determination and the computation of chromospheric excesses emission. Together, these calibrations and the `iSTARMOD` pipeline form a coherent framework for analyzing chromospheric emission in large samples, supporting the derivation of flux–flux relationships and time-domain studies of activity variability.

4.2 Flux–Flux Relationships and the Nature of M-Dwarf Activity

Following the development of `iSTARMOD`, it was employed in this thesis to study chromospheric activity through the spectral subtraction of 3428 spectra corresponding to 101 M-type stars from the CARMENES sample. The study derived the chromospheric excess EWs in Hα, Ca II IRT, He I D_3, Na I D_2, and Paschen lines, converting them into fractional luminosities normalized to the bolometric luminosity via the χ-factor method.

The complete set of fractional luminosities–or equivalently, fractional fluxes–data, used in this thesis applying the methodology, have been gathered in Annex 4.5, and its mean values in Annex 4.5

A detailed statistical analysis of flux–flux relationships revealed the existence of three distinct emitter populations, primarily characterized through the $L_{\mathrm{H}\alpha}/L_{\mathrm{Bol}}$ versus $L_{\mathrm{Ca\,II\,IRT\text{-}a}}/L_{\mathrm{Bol}}$ relationship. The results are summarized in Fig. 3.18, and the best-fit parameters are given in Table 3.4. Three main branches were identified:

- **Branch I:** Highly active, fast-rotating M3.5–M7.0 stars located beyond the fully convective boundary. These stars exhibit enhanced Hα emission, with high activity and variability in Ca II IRT in contrast with a reduced variability in Hα, strong magnetic fields, and occupy the saturated regime of the Hα–Rossby relation. They are likely young objects with intense dynamo action.

- **Branch II:** Intermediate stars, also beyond the fully convective limit but typically older and less magnetically intense, showing moderate emission levels and significant variability. Their properties suggest an evolutionary link between Branch I and less active stars.

- **Branch III:** Earlier-type M0–M5 dwarfs with comparatively low activity, slower rotation, and weaker magnetic fields. They fall in the non-saturated regime, corresponding to more evolved and magnetically quieter stars.

The derived least-squares fits (Eq. 3.9) for these three groups displaying distinct slopes, and the analysis of the dependence with the different stellar parameters, underscore systematic differences in their chromospheric energy dissipation mechanisms. These results provide robust evidence that stellar internal structure–particularly the transition from partially to fully convective interiors–plays a central role in shaping chromospheric activity patterns.

4.3 Implications for the Vaughan–Preston Gap and Magnetic Evolution

The presence of distinct emitter branches bears direct relevance to the long-debated Vaughan–Preston (VP) gap. While the results confirm two broad regimes of chromospheric emission, they also indicate that the "gap" is not an absence of stars but rather a continuum populated by intermediate objects–consistent with the findings of S. Boro Saikia et al. (2018). The apparent bimodality often reported in smaller samples may thus result from selection effects or incomplete sampling.

Our findings further align with modern gyrochronology models (S. A. Barnes, 2007), which predict a gradual decay of magnetic activity due to stellar spin-down over gigayear timescales. The observed flux–flux distributions suggest that chromospheric emission does not decline abruptly but undergoes a smooth, continuous evolution, driven by both rotational braking and long-term dynamo evolution. Consequently, the VP gap likely reflects evolutionary transitions rather than a true dichotomy in magnetic behavior.

4.4 Summary of Contributions

The main outcomes and contributions of this thesis can be summarized as follows:

- Development of `iSTARMOD`, a Python-based, modular, and open-source reimplementation of the classical `STARMOD` code for spectral subtraction and chromospheric activity studies.
- Design of calibration functions for Hα, Ca II H&K, Ca II IRT, He I, Na I, and Paschen lines, enabling accurate flux and χ-factor determinations.
- Large-scale application to 3428 CARMENES spectra of 101 M dwarfs, resulting in precise measurements of chromospheric excess fluxes and equivalent widths.
- Identification of three distinct chromospheric emitter populations (Branches I–III) with different magnetic, rotational, and evolutionary properties.
- Evidence supporting a continuous evolution of magnetic activity across the M-type sequence, rather than a discrete Vaughan–Preston gap.
- Establishment of a methodological and computational foundation for future large-sample studies of magnetic activity, variability, and stellar evolution in cool stars.

4.5 Future Work

The outcomes of this thesis establish a solid foundation for subsequent investigations. The `iSTARMOD` framework opens pathways to:

- Expand flux–flux analyses to additional chromospheric and transition-region indicators. With the data available from CARMENES, the primary target is a further analysis of NIR channel.
- To carry out a detailed study of the magnetic activity of particular interesting M stars of the CARMENES sample (as young stars, rapid rotators, etc...) taking advantage of the large number of spectra available throughout the instrument's operating period in order to characterize possible activity cycles and perform flare statistics.
- Explore correlations with metallicity, age, and magnetic topology to better understand dynamo diversity among M dwarfs.
- Analyze in detail the chromospheric activity of the components of the binary systems (SB1 and SB2) that have been identified in the CARMENES survey using the `iSTARMOD` code that is specially prepared for this purpose.

Moreover, the open-source nature of `iSTARMOD` ensures its applicability beyond this work, both as a scientific tool for stellar activity research and as an educational platform for teaching spectral analysis techniques in observational astrophysics.

In summary, this thesis has not only modernized a cornerstone tool for chromospheric studies but also contributed new insights into the magnetic and rotational evolution of low-mass stars. The combination of technological innovation and astrophysical interpretation presented here underscores the importance of integrating software development with fundamental stellar physics.

Further Acknowledgments

Acknowledgments

Part of the spectral subtraction examples in this work have been elaborated on using spectra from the CARMENES project. CARMENES is an instrument at the Centro Astronómico Hispano en Andalucia (CAHA) in Calar Alto Observatory, operated jointly by the Junta de Andalucía and the Instituto de Astrofísica de Andalucía (CSIC). We used data from the CARMENES data archive at CAB (CSIC-INTA), made publicly available in CARMENES Data Release 1 (DR1).

We acknowledge financial support from the Universidad Complutense de Madrid (UCM) and the Agencia Estatal de Investigación (AEI/10.13039/501100011033) of the Ministerio de Ciencia e Innovación and the ERDF "A way of making Europe" through project PID2022-137241NB-C4[4]

We appreciate our anonymous referee for helpful suggestions that greatly improved the quality of the paper 2.

The author gratefully acknowledges the CARMENES Consortium for providing access to high-quality spectroscopic data and for continuous scientific support. Special thanks are extended to the project supervisors, collaborators, and colleagues whose discussions and insights greatly enriched this research. The development of `iSTARMOD` also benefited from the contributions of the open-source astrophysics community, whose tools and libraries were essential for this work.

Facilities

Calar Alto Observatory (CAHA)

Software

ARES is available at this webpage: http://www.astro.up.pt/ sousasag/ares/.
Astropy (Astropy Collaboration et al., 2018) is available at GitHub: https://github.com/astropy/astropy.
Numpy (C. R. Harris et al., 2020) is available at GitHub: https://github.com/numpy/numpy.
Scipy (P. Virtanen et al., 2020) is available at GitHub: https://github.com/scipy/scipy.
TeXstudio A LaTeX Editor. Available at: https://www.texstudio.org/ (accessed May 20, 2025).

Bibliography

Allard, F., Hauschildt, P. H., Alexander, D. R., Tamanai, A., & Schweitzer, A. 2001, The Limiting Effects of Dust in Brown Dwarf Model Atmospheres, ApJ, 556, 357, doi: 10.1086/321547

Allard, F., Homeier, D., & Freytag, B. 2012, Models of very-low-mass stars, brown dwarfs and exoplanets, Philosophical Transactions of the Royal Society of London Series A, 370, 2765, doi: 10.1098/rsta.2011.0269

Alonso-Floriano, F. J., Snellen, I. A. G., Czesla, S., et al. 2019a, He I λ 10 830 Å in the transmission spectrum of HD209458 b, A&A, 629, A110, doi: 10.1051/0004-6361/201935979

Alonso-Floriano, F. J., Sánchez-López, A., Snellen, I. A. G., et al. 2019b, Multiple water band detections in the CARMENES near-infrared transmission spectrum of HD 189733 b, A&A, 621, A74, doi: 10.1051/0004-6361/201834339

Aoyama, Y., Marleau, G.-D., Ikoma, M., & Mordasini, C. 2021, Comparison of Planetary Hα-emission Models: A New Correlation with Accretion Luminosity, ApJL, 917, L30, doi: 10.3847/2041-8213/ac19bd

Astropy Collaboration, Price-Whelan, A. M., Sipőcz, B. M., et al. 2018, The Astropy Project: Building an Open-science Project and Status of the v2.0 Core Package, AJ, 156, 123, doi: 10.3847/1538-3881/aabc4f

Bahar, E., Şenavcı, H. V., Işık, E., et al. 2024, First Chromospheric Activity and Doppler Imaging Study of PW And Using a New Doppler Imaging Code: SpotDIPy, ApJ, 960, 60, doi: 10.3847/1538-4357/ad055d

Baliunas, S. L., & Vaughan, A. H. 1985, Stellar activity cycles., Annu. Rev. Astron. Astrophys, 23, 379, doi: 10.1146/annurev.aa.23.090185.002115

Baraffe, I., & Chabrier, G. 2018, A closer look at the transition between fully convective and partly radiative low-mass stars, A&A, 619, A177, doi: 10.1051/0004-6361/201834062

Baraffe, I., Homeier, D., Allard, F., & Chabrier, G. 2015, New evolutionary models for pre-main sequence and main sequence low-mass stars down to the hydrogen-burning limit, A&A, 577, A42, doi: 10.1051/0004-6361/201425481

Baranne, A., Queloz, D., Mayor, M., et al. 1996, ELODIE: A spectrograph for accurate radial velocity measurements., A&AS, 119, 373

Barden, S. C. 1985, A study of short-period RS Canum Venaticorum and W Ursae Majoris binary systems : the global nature of H alpha., ApJ, 295, 162, doi: 10.1086/163361

Barnes, S. A. 2003, On the Rotational Evolution of Solar- and Late-Type Stars, Its Magnetic Origins, and the Possibility of Stellar Gyrochronology, ApJ, 586, 464, doi: 10.1086/367639

Barnes, S. A. 2007, Ages for Illustrative Field Stars Using Gyrochronology: Viability, Limitations, and Errors, ApJ, 669, 1167, doi: 10.1086/519295

Baroch, D., Morales, J. C., Ribas, I., et al. 2018, The CARMENES search for exoplanets around M dwarfs. Nine new double-line spectroscopic binary stars, A&A, 619, A32, doi: 10.1051/0004-6361/201833440

Baroch, D., Morales, J. C., Ribas, I., et al. 2021, The CARMENES search for exoplanets around M dwarfs. Spectroscopic orbits of nine M-dwarf multiple systems, including two triples, two brown dwarf candidates, and one close M-dwarf-white dwarf binary, A&A, 653, A49, doi: 10.1051/0004-6361/202141031

Bellotti, S., & Morin, J. 2025, Solar and Stellar Activity, arXiv e-prints, arXiv:2509.20202, doi: 10.48550/arXiv.2509.20202

Bloot, S., Callingham, J. R., Vedantham, H. K., et al. 2024, Phenomenology and periodicity of radio emission from the stellar system AU Microscopii, A&A, 682, A170, doi: 10.1051/0004-6361/202348065

Böhm-Vitense, E. 2007, Chromospheric Activity in G and K Main-Sequence Stars, and What It Tells Us about Stellar Dynamos, ApJ, 657, 486, doi: 10.1086/510482

Boisse, I., Oshagh, M., Lovis, C., et al. 2013, in IAU Symposium, Vol. 294, Solar and Astrophysical Dynamos and Magnetic Activity, ed. A. G. Kosovichev, E. de Gouveia Dal Pino, & Y. Yan, 471–475, doi: 10.1017/S1743921313002937

Bonanno, A., & Corsaro, E. 2022, On the Origin of the Dichotomy of Stellar Activity Cycles, ApJL, 939, L26, doi: 10.3847/2041-8213/ac9c05

Boro Saikia, S., Marvin, C. J., Jeffers, S. V., et al. 2018, Chromospheric activity catalogue of 4454 cool stars. Questioning the active branch of stellar activity cycles, A&A, 616, A108, doi: 10.1051/0004-6361/201629518

Buccino, A. P., & Mauas, P. J. D. 2008, Mg II h+k emission lines as stellar activity indicators of main sequence F-K stars, A&A, 483, 903, doi: 10.1051/0004-6361:20078925

Burke, E. 2015, A Philosophical Enquiry into the Origin of Our Ideas of the Sublime and the Beautiful, 2nd edn., ed. P. Guyer, Oxford World's Classics (Oxford: Oxford University Press), 208

Caballero, J. A., Seifert, W., Quirrenbach, A., et al. 2025, CARMENES as an Instrument for Exoplanet Research, arXiv e-prints, arXiv:2503.05501, doi: 10.48550/arXiv.2503.05501

Caballero, J. A., Guàrdia, J., López del Fresno, M., et al. 2016a, in Society of Photo-Optical Instrumentation Engineers (SPIE) Conference Series, Vol. 9910, Observatory Operations: Strategies, Processes, and Systems VI, ed. A. B. Peck, R. L. Seaman, & C. R. Benn, 99100E, doi: 10.1117/12.2233574

Caballero, J. A., Cortés-Contreras, M., Alonso-Floriano, F. J., et al. 2016b, in 19th Cambridge Workshop on Cool Stars, Stellar Systems, and the Sun (CS19), Cambridge Workshop on Cool Stars, Stellar Systems, and the Sun, 148, doi: 10.5281/zenodo.60060

Cale, B. L., Reefe, M., Plavchan, P., et al. 2021, Diving Beneath the Sea of Stellar Activity: Chromatic Radial Velocities of the Young AU Mic Planetary System, AJ, 162, 295, doi: 10.3847/1538-3881/ac2c80

Canet, A., & Gómez de Castro, A. I. 2021, Evolution of Earth-like extended exospheres orbiting solar-like stars, MNRAS, 502, 6170, doi: 10.1093/mnras/stab492

Canet, A., Varela, J., & Gómez de Castro, A. I. 2024, Stellar wind impact on early atmospheres around unmagnetized Earth-like planets, MNRAS, 531, 2626, doi: 10.1093/mnras/stae1267

Cao, D., & Gu, S. 2015, Chromospheric activity and rotational modulation of the RS Canum Venaticorum binary V711 Tauri during 1998-2004, MNRAS, 449, 1380, doi: 10.1093/mnras/stv110

Cao, D., & Gu, S. 2024, Red Asymmetry of H_α Line Profiles during the Flares on the Active RS CVn-type Star II Pegasi, ApJ, 963, 13, doi: 10.3847/1538-4357/ad1928

Cao, D., & Gu, S. 2025, Further Investigation on Chromospheric Activity Patterns of the RS Canum Venaticorum Star V711 Tauri, AJ, 169, 198, doi: 10.3847/1538-3881/adb5fe

Cao, D., Gu, S., Wolter, U., et al. 2023, Prominence detection and chromosphere feature on the prototype RS CVn of active binary systems, MNRAS, 523, 4146, doi: 10.1093/mnras/stad1700

Cao, D.-T., & Gu, S.-H. 2012, New observations of chromospheric and prominence activity on the RS CVn-type binary SZ Piscium, A&A, 538, A130, doi: 10.1051/0004-6361/201118184

Cao, W. 2015, Physics 320: Lecture 18: Solar Magnetism – Dynamo„ https://web.njit.edu/~cao/Phys320_L18.pdf

Casasayas-Barris, N., Pallé, E., Yan, F., et al. 2020, Is there Na I in the atmosphere of HD 209458b?. Effect of the centre-to-limb variation and Rossiter-McLaughlin effect in transmission spectroscopy studies, A&A, 635, A206, doi: 10.1051/0004-6361/201937221

Catanzaro, G. 2014, Spectral Lines Analysis: Rotational Velocity and Velocity Fields, ed. E. Niemczura, B. Smalley, & W. Pych (Cham: Springer International Publishing), 121–130, doi: 10.1007/978-3-319-06956-2_11

Cayrel, R., Depagne, E., Spite, M., et al. 2004, First stars V - Abundance patterns from C to Zn and supernova yields in the early Galaxy, A&A, 416, 1117, doi: 10.1051/0004-6361:20034074

Cayrel de Strobel, G., & Spite, M., eds. 1988, IAU Symposium, Vol. 132, The impact of very high S/N spectroscopy on stellar physics: proceedings of the 132nd Symposium of the International Astronomical Union held in Paris, France, June 29-July 3, 1987.

Chabrier, G., & Baraffe, I. 1997, Structure and evolution of low-mass stars, A&A, 327, 1039, doi: 10.48550/arXiv.astro-ph/9704118

Charbonneau, P. 2020, Dynamo models of the solar cycle, Living Reviews in Solar Physics, 17, 4, doi: 10.1007/s41116-020-00025-6

Cifuentes, C., Caballero, J. A., Cortés-Contreras, M., et al. 2020, CARMENES input catalogue of M dwarfs. V. Luminosities, colours, and spectral energy distributions, A&A, 642, A115, doi: 10.1051/0004-6361/202038295

Cifuentes, C., Caballero, J. A., González-Payo, J., et al. 2025, CARMENES input catalogue of M dwarfs: IX. Multiplicity from close spectroscopic binaries to ultra-wide systems, A&A, 693, A228, doi: 10.1051/0004-6361/202452527

Corrales, L., Stassun, K. G., Cunningham, T., et al. 2023, The life cycle of stars and their planets from the high energy perspective, arXiv e-prints, arXiv:2311.07674, doi: 10.48550/arXiv.2311.07674

Cortés-Contreras, M., Caballero, J. A., Montes, D., et al. 2024, CARMENES input catalogue of M dwarfs: VIII. Kinematics in the solar neighbourhood, A&A, 692, A206, doi: 10.1051/0004-6361/202451585

Costes, J. C., Watson, C. A., de Mooij, E., et al. 2021, Long-term stellar activity variations and their effect on radial-velocity measurements, MNRAS, 505, 830, doi: 10.1093/mnras/stab1183

Cram, L. E., & Giampapa, M. S. 1987, Formation of Chromospheric Lines in Cool Dwarf Stars, ApJ, 323, 316, doi: 10.1086/165829

Crivellari, L., Simón-Díaz, S., & Arévalo, M. J. 2019, Radiative Transfer in Stellar and Planetary Atmospheres (Cambridge University Press), doi: 10.1017/9781108583572

Davenport, J. R. A. 2016, The Kepler Catalog of Stellar Flares, ApJ, 829, 23, doi: 10.3847/0004-637X/829/1/23

de Grijs, R., & Kamath, D. 2021, Stellar Chromospheric Variability, Universe, 7, 440, doi: 10.3390/universe7110440

Donati, J.-F., & Landstreet, J. D. 2009, Magnetic Fields of Nondegenerate Stars, Annu. Rev. Astron. Astrophys, 47, 333, doi: 10.1146/annurev-astro-082708-101833

Donati, J.-F., Morin, J., Petit, P., et al. 2008, Large-scale magnetic topologies of early M dwarfs, MNRAS, 390, 545, doi: 10.1111/j.1365-2966.2008.13799.x

dos Santos, L. A., Meléndez, J., do Nascimento, J.-D., et al. 2016, The Solar Twin Planet Search. IV. The Sun as a typical rotator and evidence for a new rotational braking law for Sun-like stars, A&A, 592, A156, doi: 10.1051/0004-6361/201628558

Douglas, S. T., Agüeros, M. A., Covey, K. R., et al. 2014, The Factory and the Beehive. II. Activity and Rotation in Praesepe and the Hyades, ApJ, 795, 161, doi: 10.1088/0004-637X/795/2/161

Doyle, A. P., Davies, G. R., Smoker, J. V., & Smalley, B. 2014, Macroturbulence in slowly rotating solar-type stars, Monthly Notices of the Royal Astronomical Society, 444, 3592, doi: 10.1093/mnras/stu1692

Dumusque, X. 2018, Measuring precise radial velocities on individual spectral lines. I. Validation of the method and application to mitigate stellar activity, A&A, 620, A47, doi: 10.1051/0004-6361/201833795

Durney, B. R., Mihalas, D., & Robinson, R. D. 1981, A preliminary interpretation of stellar chromospheric CA II emission variations within the framework of stellar dynamo theory., PASP, 93, 537, doi: 10.1086/130878

Folsom, C. P., Petit, P., Bouvier, J., et al. 2016, The evolution of surface magnetic fields in young solar-type stars - I. The first 250 Myr, MNRAS, 457, 580, doi: 10.1093/mnras/stv2924

Frasca, A., Alcalá, J. M., Covino, E., et al. 2003, Further identification of ROSAT all-sky survey sources in Orion, A&A, 405, 149, doi: 10.1051/0004-6361:20030644

Frasca, A., Alonso-Santiago, J., Catanzaro, G., et al. 2023, TIC 43152097 The first eclipsing binary in NGC 2232, A&A, 677, A154, doi: 10.1051/0004-6361/202347226

Frasca, A., & Catalano, S. 1994, Hα survey of late-type active binaries., A&A, 284, 883

Frasca, A., Guillout, P., Klutsch, A., et al. 2018, A spectroscopic survey of the youngest field stars in the solar neighborhood . II. The optically faint sample, A&A, 612, A96, doi: 10.1051/0004-6361/201732028

Frasca, A., Guillout, P., Marilli, E., et al. 2006, Newly discovered active binaries in the RasTyc sample of stellar X-ray sources. I. Orbital and physical parameters of six new binaries, A&A, 454, 301, doi: 10.1051/0004-6361:20054573

Frasca, A., Zhang, J. Y., Alonso-Santiago, J., et al. 2025, LAMOST medium-resolution observations of the Pleiades, A&A, 698, A7, doi: 10.1051/0004-6361/202553673

Fry, S. 2024, Stephen Fry's Greek Myths, Vol. 4, Odyssey (London: Michael Joseph), 416

Fuhrmeister, B., Czesla, S., Schmitt, J. H. M. M., et al. 2018, The CARMENES search for exoplanets around M dwarfs. Wing asymmetries of Hα, Na I D, and He I lines, A&A, 615, A14, doi: 10.1051/0004-6361/201732204

Fuhrmeister, B., Czesla, S., Schmitt, J. H. M. M., et al. 2019, The CARMENES search for exoplanets around M dwarfs. Period search in Hα, Na I D, and Ca II IRT lines, A&A, 623, A24, doi: 10.1051/0004-6361/201834483

Fuhrmeister, B., Czesla, S., Hildebrandt, L., et al. 2020, The CARMENES search for exoplanets around M dwarfs. Variability of the He I line at 10 830 Å, A&A, 640, A52, doi: 10.1051/0004-6361/202038279

Fuhrmeister, B., Czesla, S., Nagel, E., et al. 2022, The CARMENES search for exoplanets around M dwarfs. Diagnostic capabilities of strong K I lines for photosphere and chromosphere, A&A, 657, A125, doi: 10.1051/0004-6361/202141733

Fuhrmeister, B., Czesla, S., Schmitt, J. H. M. M., et al. 2023a, The CARMENES search for exoplanets around M dwarfs. Behaviour of the Paschen lines during flares and quiescence, A&A, 678, A1, doi: 10.1051/0004-6361/202347161

Fuhrmeister, B., Czesla, S., Perdelwitz, V., et al. 2023b, The CARMENES search for exoplanets around M dwarfs. Variability on long timescales as seen in chromospheric indicators, A&A, 670, A71, doi: 10.1051/0004-6361/202244829

Gálvez, M. C., Montes, D., Fernández-Figueroa, M. J., de Castro, E., & Cornide, M. 2007, Multiwavelength optical observations of chromospherically active binary systems. V. FF UMa (2RE J0933+624): a system with orbital period variation, A&A, 472, 587, doi: 10.1051/0004-6361:20067015

Gálvez, M. C., Montes, D., Fernández-Figueroa, M. J., De Castro, E., & Cornide, M. 2009, Multiwavelength Optical Observations of Two Chromospherically Active Binary Systems: V789 Mon and GZ Leo, AJ, 137, 3965, doi: 10.1088/0004-6256/137/4/3965

Gálvez, M. C., Montes, D., Fernández-Figueroa, M. J., & López-Santiago, J. 2006, Chromospheric Activity and Orbital Solution of Six New Late-type Spectroscopic Binary Systems, Astrophysics and Space Science, 304, 59, doi: 10.1007/s10509-006-9074-3

Gálvez, M. C., Montes, D., Fernández-Figueroa, M. J., et al. 2002a, Multiwavelength optical observations of chromospherically active binary systems. IV. The X-ray/EUV selected binary BK Psc (2RE J0039+103), A&A, 389, 524, doi: 10.1051/0004-6361:20020644

Gálvez, M. C., Montes, D., Fernández-Figueroa, M. J., et al. 2002b, Multiwavelength optical observations of chromospherically active binary systems. IV. The X-ray/EUV selected binary BK Psc (2RE J0039+103), A&A, 389, 524, doi: 10.1051/0004-6361:20020644

García Soto, A., Duvvuri, G. M., Newton, E. R., et al. 2025, Short-term Balmer Line Emission Variability in M Dwarfs, ApJ, 982, 98, doi: 10.3847/1538-4357/adb615

Gilmore, G., Randich, S., Worley, C. C., et al. 2022, The Gaia-ESO Public Spectroscopic Survey: Motivation, implementation, GIRAFFE data processing, analysis, and final data products, A&A, 666, A120, doi: 10.1051/0004-6361/202243134

Golimowski, D. A., Leggett, S. K., Marley, M. S., et al. 2004, L' and M' Photometry of Ultracool Dwarfs, AJ, 127, 3516, doi: 10.1086/420709

Gray, D. F. 1984, The observation and analysis of stellar photospheric velocity fields. I - Effects of macroturbulence and rotation on line profiles, Astrophysical Journal, 281, 719, doi: 10.1086/162149

Gray, D. F. 2010, Empirical Decoding of the Shapes of Spectral-Line Bisectors, ApJ, 710, 1003, doi: 10.1088/0004-637X/710/2/1003

Gray, D. F. 2022, The observation and analysis of stellar photospheres (Cambridge University Press), doi: 10.1017/9781009082136

Gregory, S. G. 2017, in IAU Symposium, Vol. 328, Living Around Active Stars, ed. D. Nandy, A. Valio, & P. Petit, 252–263, doi: 10.1017/S1743921317003891

Guillout, P., Klutsch, A., Frasca, A., et al. 2009, A spectroscopic survey of the youngest field stars in the solar neighbourhood. I. The optically bright sample, A&A, 504, 829, doi: 10.1051/0004-6361/200811313

Hall, J. C. 2008, Stellar Chromospheric Activity, Living Reviews in Solar Physics, 5, 2, doi: 10.12942/lrsp-2008-2

Hall, J. C., & Ramsey, L. W. 1992a, Eclipse Observations of RS CVn Binaries. I. A Survey for Extended Matter, AJ, 104, 1942, doi: 10.1086/116370

Hall, J. C., & Ramsey, L. W. 1992b, Eclipse Observations of RS CVn Binaries. I. A Survey for Extended Matter, AJ, 104, 1942, doi: 10.1086/116370

Hall, J. C., & Ramsey, L. W. 1994, Eclipse Observations of RS CVN Binaries II. A Parametric Model of Extended Matter, AJ, 107, 1149, doi: 10.1086/116927

Harris, C. R., Millman, K. J., van der Walt, S. J., et al. 2020, Array programming with NumPy, Nature, 585, 357, doi: 10.1038/s41586-020-2649-2

Hartmann, L. W., & Noyes, R. W. 1987, Rotation and magnetic activity in main-sequence stars., Annu. Rev. Astron. Astrophys, 25, 271, doi: 10.1146/annurev.aa.25.090187.001415

Hawley, S. L., Allred, J. C., Johns-Krull, C. M., et al. 2003, Multiwavelength Observations of Flares on AD Leonis, ApJ, 597, 535, doi: 10.1086/378351

Henry, T. J., & Jao, W.-C. 2024, The Character of M Dwarfs, Annu. Rev. Astron. Astrophys, 62, 593, doi: 10.1146/annurev-astro-052722-102740

Herbig, G. H. 1985, Chromospheric H alpha emission in F8-G3 dwarfs and its connection with the T Tauri stars., ApJ, 289, 269, doi: 10.1086/162887

Hintz, D., Fuhrmeister, B., Czesla, S., et al. 2019, The CARMENES search for exoplanets around M dwarfs. Chromospheric modeling of M 2-3 V stars with PHOENIX, A&A, 623, A136, doi: 10.1051/0004-6361/201834788

Hintz, D., Fuhrmeister, B., Czesla, S., et al. 2020, The CARMENES search for exoplanets around M dwarfs. The He I infrared triplet lines in PHOENIX models of M 2-3 V stars, A&A, 638, A115, doi: 10.1051/0004-6361/202037596

Hintz, D., Peacock, S., Barman, T., et al. 2023, Modeling the Chromosphere and Transition Region of Planet-hosting Star GJ 436, ApJ, 954, 73, doi: 10.3847/1538-4357/ace103

Huenemoerder, D. P., Ramsey, L. W., & Buzasi, D. L. 1989, Titanium Oxide Variations in II Pegasi, AJ, 98, 2264, doi: 10.1086/115295

Husser, T. O., Wende-von Berg, S., Dreizler, S., et al. 2013, A new extensive library of PHOENIX stellar atmospheres and synthetic spectra, A&A, 553, A6, doi: 10.1051/0004-6361/201219058

Ibañez Bustos, R. V., Buccino, A. P., Flores, M., Martinez, C. F., & Mauas, P. J. D. 2023, Correlation between activity indicators: Hα and Ca II lines in M-dwarf stars, A&A, 672, A37, doi: 10.1051/0004-6361/202245352

Ibañez Bustos, R. V., Buccino, A. P., Nardetto, N., et al. 2025, Characterisation of magnetic activity of M dwarfs: Possible impact on surface brightness, A&A, 696, A230, doi: 10.1051/0004-6361/202450348

Ivanova, N., & Taam, R. E. 2003, Magnetic Braking Revisited, ApJ, 599, 516, doi: 10.1086/379192

Jao, W.-C., Henry, T. J., Gies, D. R., & Hambly, N. C. 2018, A Gap in the Lower Main Sequence Revealed by Gaia Data Release 2, ApJL, 861, L11, doi: 10.3847/2041-8213/aacdf6

Jeffers, S. V., Schöfer, P., Lamert, A., et al. 2018, CARMENES input catalogue of M dwarfs. III. Rotation and activity from high-resolution spectroscopic observations, A&A, 614, A76, doi: 10.1051/0004-6361/201629599

Jeffers, S. V., Barnes, J. R., Schöfer, P., et al. 2022, The CARMENES search for exoplanets around M dwarfs. Benchmarking the impact of activity in high-precision radial velocity measurements, A&A, 663, A27, doi: 10.1051/0004-6361/202141880

Jeffers, S. V., Barnes, J. R., Schöfer, P., et al. 2025, The CARMENES search for exoplanets around M dwarfs: Understanding the wavelength dependence of radial velocity measurements, A&A, 696, A27, doi: 10.1051/0004-6361/202347510

Johnson, E. N., Czesla, S., Fuhrmeister, B., et al. 2021, Simultaneous photometric and CARMENES spectroscopic monitoring of fast-rotating M dwarf GJ 3270. Discovery of a post-flare corotating feature, A&A, 651, A105, doi: 10.1051/0004-6361/202040159

Kaminski, A., Sabotta, S., Kemmer, J., et al. 2025, The CARMENES search for exoplanets around M dwarfs: Occurrence rates of Earth-like planets around very low-mass stars, A&A, 696, A101, doi: 10.1051/0004-6361/202453381

Karoff, C., Metcalfe, T. S., Santos, Â. R. G., et al. 2018, The Influence of Metallicity on Stellar Differential Rotation and Magnetic Activity, ApJ, 852, 46, doi: 10.3847/1538-4357/aaa026

Katsova, M. M. 2020, The evolution of the solar-stellar activity, Journal of Atmospheric and Solar-Terrestrial Physics, 211, 105456, doi: 10.1016/j.jastp.2020.105456

Klein, B., Zicher, N., Kavanagh, R. D., et al. 2022, One year of AU Mic with HARPS - II. Stellar activity and star-planet interaction, MNRAS, 512, 5067, doi: 10.1093/mnras/stac761

Kossakowski, D., Kürster, M., Henning, T., et al. 2022, The CARMENES search for exoplanets around M dwarfs. Stable radial-velocity variations at the rotation period of AD Leonis: A test case study of current limitations to treating stellar activity, A&A, 666, A143, doi: 10.1051/0004-6361/202243773

Kraft, R. P. 1967, Studies of Stellar Rotation. V. The Dependence of Rotation on Age among Solar-Type Stars, ApJ, 150, 551, doi: 10.1086/149359

Kumar, M., & Fares, R. 2023, A study of the magnetic activity and variability of GJ 436, MNRAS, 518, 3147, doi: 10.1093/mnras/stac2766

Labarga, F. 2025, PhD thesis, Universidad Complutense de Madrid (UCM)

Labarga, F., & Montes, D. 2020, in XIV.0 Scientific Meeting (virtual) of the Spanish Astronomical Society, 153

Labarga, F., & Montes, D. 2025, iSTARMOD: a Python Code to Quantify Chromospheric Activity by Using Spectral Subtraction Technique (10.0), Zenodo, doi: 10.5281/zenodo.17329154

Labarga, F., & Montes, D. 2026, iSTARMOD: a Python Code to Quantify Chromospheric Activity by Using Spectral Subtraction Technique, AJ, 171, 14, doi: 10.3847/1538-3881/ae173e

Labarga, F., Montes, D., Duque-Arribas, C., et al. 2023, in Highlights on Spanish Astrophysics XI, ed. M. Manteiga, L. Bellot, P. Benavidez, A. de Lorenzo-Cáceres, M. A. Fuente, M. J. Martínez, M. Vázquez Acosta, & C. Dafonte, 272, doi: 10.5281/zenodo.7668217

Labarga, F., Montes, D., Duque-Arribas, C., et al. 2026, The CARMENES search for exoplanets around M dwarfs. Chromospheric activity and Flux-Flux relationships, to be submitted to A&A

Lafarga, M., Ribas, I., Lovis, C., et al. 2020, The CARMENES search for exoplanets around M dwarfs. Radial velocities and activity indicators from cross-correlation functions with weighted binary masks, A&A, 636, A36, doi: 10.1051/0004-6361/201937222

Lafarga, M., Ribas, I., Reiners, A., et al. 2021, The CARMENES search for exoplanets around M dwarfs. Mapping stellar activity indicators across the M dwarf domain, A&A, 652, A28, doi: 10.1051/0004-6361/202140605

Lagg, A., Lites, B., Harvey, J., Gosain, S., & Centeno, R. 2017, Measurements of Photospheric and Chromospheric Magnetic Fields, Space Science Rev., 210, 37, doi: 10.1007/s11214-015-0219-y

Lampón, M., López-Puertas, M., Lara, L. M., et al. 2020, Modelling the He I triplet absorption at 10 830 Å in the atmosphere of HD 209458 b, A&A, 636, A13, doi: 10.1051/0004-6361/201937175

Landman, D. A. 1981, Measurements of He D3 profiles in solar plages, ApJ, 244, 345, doi: 10.1086/158712

Laughlin, G., Bodenheimer, P., & Adams, F. C. 1997, The End of the Main Sequence, ApJ, 482, 420, doi: 10.1086/304125

Li, K., Gao, X., Liu, X.-Y., et al. 2022, Extremely Low Mass Ratio Contact Binaries. I. The First Photometric and Spectroscopic Investigations of Ten Systems, AJ, 164, 202, doi: 10.3847/1538-3881/ac8ff2

Lindegren, L., & Dravins, D. 2003, The fundamental definition of "radial velocity", A&A, 401, 1185, doi: 10.1051/0004-6361:20030181

Linsky, J. L. 1980, Stellar chromospheres, Annu. Rev. Astron. Astrophys, 18, 439, doi: 10.1146/annurev.aa.18.090180.002255

Linsky, J. L. 2017, Stellar Model Chromospheres and Spectroscopic Diagnostics, Annu. Rev. Astron. Astrophys, 55, 159, doi: 10.1146/annurev-astro-091916-055327

Linsky, J. L., & Avrett, E. H. 1970, The Solar H and K Lines, PASP, 82, 169, doi: 10.1086/128904

Linsky, J. L., & Ayres, T. R. 1978, Stellar model chromospheres. VI. Empirical estimates of the chromospheric radiative losses of late-type stars., ApJ, 220, 619, doi: 10.1086/155945

Linsky, J. L., Worden, S. P., McClintock, W., & Robertson, R. M. 1979, Stellar model chromospheres. X. High-resolution, absolute flux profiles of the Ca II H and K lines in stars of spectral types F0 - M2., ApJS, 41, 47, doi: 10.1086/190607

Linsky, J. L., Wood, B. E., Youngblood, A., et al. 2020, The Relative Emission from Chromospheres and Coronae: Dependence on Spectral Type and Age, ApJ, 902, 3, doi: 10.3847/1538-4357/abb36f

Liu, F., Li, K., Gao, X., et al. 2024, The first analysis of three long-period low mass-ratio contact binaries, MNRAS, 527, 6406, doi: 10.1093/mnras/stad3591

Liu, F., Li, K., Gao, X., et al. 2025, Extremely Low Mass Ratio Contact Binaries. II. The First Photometric and Spectroscopic Investigations of Six Systems with Orbital Periods Longer than 0.5 days, MNRAS, doi: 10.1093/mnras/staf763

López Santiago, J. 2005, PhD thesis, Complutense University of Madrid, Spain

López-Santiago, J., Montes, D., Fernández-Figueroa, M. J., & Ramsey, L. W. 2003a, Rotational modulation of the photospheric and chromospheric activity in the young, single K2-dwarf PW And, A&A, 411, 489, doi: 10.1051/0004-6361:20031377

López-Santiago, J., Montes, D., Fernández-Figueroa, M. J., & Ramsey, L. W. 2003b, Rotational modulation of the photospheric and chromospheric activity in the young, single K2-dwarf PW And, A&A, 411, 489, doi: 10.1051/0004-6361:20031377

López-Santiago, J., Montes, D., Gálvez-Ortiz, M. C., et al. 2010, A high-resolution spectroscopic survey of late-type stars: chromospheric activity, rotation, kinematics, and age, A&A, 514, A97, doi: 10.1051/0004-6361/200913437

Lucy, L. B. 1967, Gravity-Darkening for Stars with Convective Envelopes, Zeitschrift für Astrophysik, 65, 89

Luque, R., Pallé, E., Kossakowski, D., et al. 2019, Planetary system around the nearby M dwarf GJ 357 including a transiting, hot, Earth-sized planet optimal for atmospheric characterization, A&A, 628, A39, doi: 10.1051/0004-6361/201935801

MacDonald, J., & Gizis, J. 2018, An explanation for the gap in the Gaia HRD for M dwarfs, MNRAS, 480, 1711, doi: 10.1093/mnras/sty1888

Mallorquín, M., Béjar, V. J. S., Lodieu, N., et al. 2024, Revisiting the dynamical masses of the transiting planets in the young AU Mic system: Potential AU Mic b inflation at 20 Myr, A&A, 689, A132, doi: 10.1051/0004-6361/202450047

Marfil, E., Tabernero, H. M., Montes, D., et al. 2021, The CARMENES search for exoplanets around M dwarfs. Stellar atmospheric parameters of target stars with SteParSyn, A&A, 656, A162, doi: 10.1051/0004-6361/202141980

Marleau, G. D., Aoyama, Y., Kuiper, R., et al. 2022, Accreting protoplanets: Spectral signatures and magnitude of gas and dust extinction at H α, A&A, 657, A38, doi: 10.1051/0004-6361/202037494

Martin, J., Fuhrmeister, B., Mittag, M., et al. 2017, The Ca II infrared triplet's performance as an activity indicator compared to Ca II H and K. Empirical relations to convert Ca II infrared triplet measurements to common activity indices, A&A, 605, A113, doi: 10.1051/0004-6361/201630298

Martínez-Arnáiz, R., López-Santiago, J., Crespo-Chacón, I., & Montes, D. 2011, Effect of magnetic activity saturation in chromospheric flux-flux relationships, MNRAS, 414, 2629, doi: 10.1111/j.1365-2966.2011.18584.x

Martínez-Arnáiz, R., Maldonado, J., Montes, D., Eiroa, C., & Montesinos, B. 2010, Chromospheric activity and rotation of FGK stars in the solar vicinity. An estimation of the radial velocity jitter, A&A, 520, A79, doi: 10.1051/0004-6361/200913725

Marvin, C. J., Reiners, A., Anglada-Escudé, G., Jeffers, S. V., & Boro Saikia, S. 2023, Absolute Ca II H & K and H-alpha flux measurements of low-mass stars: Extending R'$_{HK}$ to M dwarfs, A&A, 671, A162, doi: 10.1051/0004-6361/201937306

Maxted, P. F. L. 2022, Limb darkening measurements from TESS and Kepler light curves of transiting exoplanets, Monthly Notices of the Royal Astronomical Society, 519, 3723, doi: 10.1093/mnras/stac3741

McLean, A. B., Mitchell, C. E. J., & Swanston, D. M. 1994, Implementation of an efficient analytical approximation to the Voigt function for photoemission lineshape analysis, Journal of Electron Spectroscopy and Related Phenomena, 69, 125, doi: 10.1016/0368-2048(94)02189-7

Mestel, L. 1992, The solar-stellar connection - Magnetic braking and stellar activity, Proc Astr Soc Australia, 10, 3, doi: 10.1017/S132335800001910X

Metcalfe, T. S., Buccino, A. P., Brown, B. P., et al. 2013, Magnetic Activity Cycles in the Exoplanet Host Star epsilon Eridani, ApJL, 763, L26, doi: 10.1088/2041-8205/763/2/L26

Metcalfe, T. S., Strassmeier, K. G., Ilyin, I. V., et al. 2024, Weakened Magnetic Braking in the Exoplanet Host Star 51 Peg, ApJL, 960, L6, doi: 10.3847/2041-8213/ad0a95

Meunier, N., Mignon, L., Kretzschmar, M., & Delfosse, X. 2024, Characterisation of the stellar activity of M dwarfs. II. Relationship between Ca, Hα, and Na chromospheric emissions, A&A, 684, A106, doi: 10.1051/0004-6361/202347362

Mignon, L., Meunier, N., Delfosse, X., et al. 2023, Characterisation of stellar activity of M dwarfs. I. Long-timescale variability in a large sample and detection of new cycles, A&A, 675, A168, doi: 10.1051/0004-6361/202244249

Mohanty, S., Basri, G., Shu, F., Allard, F., & Chabrier, G. 2002, Activity in Very Cool Stars: Magnetic Dissipation in Late M and L Dwarf Atmospheres, ApJ, 571, 469, doi: 10.1086/339911

Montes, D. 1995, PhD thesis, Complutense University of Madrid, Department of Astronomy

Montes, D., Crespo-Chacón, I., Gálvez, M. C., et al. 2004, in Lecture Notes and Essays in Astrophysics, ed. A. Ulla & M. Manteiga, Vol. 1 (Real Sociedad Española de Física), 119–132

Montes, D., de Castro, E., Fernandez-Figueroa, M. J., & Cornide, M. 1995a, Application of the spectral subtraction technique to the CA II H & K and H lines in a sample of chromospherically active binaries., A&AS, 114, 287

Montes, D., Fernandez-Figueroa, M. J., Cornide, M., & de Castro, E. 1996a, in Astronomical Society of the Pacific Conference Series, Vol. 109, Cool Stars, Stellar Systems, and the Sun, ed. R. Pallavicini & A. K. Dupree, 657, doi: 10.48550/arXiv.astro-ph/9506025

Montes, D., Fernandez-Figueroa, M. J., Cornide, M., & de Castro, E. 1996b, The behaviour of the excess CA II H and K and H emissions in chromospherically active binaries., A&A, 312, 221, doi: 10.48550/arXiv.astro-ph/9511125

Montes, D., Fernandez-Figueroa, M. J., de Castro, E., & Cornide, M. 1995b, Excess Hα emission in chromospherically active binaries., A&A, 294, 165

Montes, D., Fernández-Figueroa, M. J., De Castro, E., et al. 2000, Multiwavelength optical observations of chromospherically active binary systems. III. High resolution echelle spectra from Ca II H & K to Ca II IRT, A&AS, 146, 103, doi: 10.1051/aas:2000359

Montes, D., López-Santiago, J., Fernández-Figueroa, M. J., & Gálvez, M. C. 2001, Chromospheric activity, lithium and radial velocities of single late-type stars possible members of young moving groups, A&A, 379, 976, doi: 10.1051/0004-6361:20011385

Montes, D., López-Gallifa, A., Labarga, F., et al. 2020, in XIV.0 Scientific Meeting (virtual) of the Spanish Astronomical Society, 168

Morales, J. C., Mustill, A. J., Ribas, I., et al. 2019, A giant exoplanet orbiting a very-low-mass star challenges planet formation models, Science, 365, 1441, doi: 10.1126/science.aax3198

Morales, J. C., Ribas, I., Reffert, S., et al. 2025, The CARMENES search for exoplanets around M dwarfs: Revisiting the GJ 317, GJ463, and GJ 3512 systems and two newly discovered planets orbiting GJ9773 and GJ 508.2, A&A, 700, A242, doi: 10.1051/0004-6361/202554992

Morin, J., Donati, J.-F., Petit, P., et al. 2008, Large-scale magnetic topologies of mid M dwarfs, MNRAS, 390, 567, doi: 10.1111/j.1365-2966.2008.13809.x

Musielak, Z. E. 2004, in IAU Symposium, Vol. 219, Stars as Suns : Activity, Evolution and Planets, ed. A. K. Dupree & A. O. Benz, 437

Musielak, Z. E., Rosner, R., Stein, R. F., & Ulmschneider, P. 1994, On Sound Generation by Turbulent Convection: A New Look at Old Results, ApJ, 423, 474, doi: 10.1086/173825

Nagel, E., Czesla, S., Kaminski, A., et al. 2023, The CARMENES search for exoplanets around M dwarfs. Telluric absorption corrected high S/N optical and near-infrared template spectra of 382 M dwarf stars, A&A, 680, A73, doi: 10.1051/0004-6361/202346524

Newton, E. R., Irwin, J., Charbonneau, D., et al. 2017, The Hα Emission of Nearby M Dwarfs and its Relation to Stellar Rotation, ApJ, 834, 85, doi: 10.3847/1538-4357/834/1/85

Nortmann, L., Pallé, E., Salz, M., et al. 2018, Ground-based detection of an extended helium atmosphere in the Saturn-mass exoplanet WASP-69b, Science, 362, 1388, doi: 10.1126/science.aat5348

Noyes, R. W., Hartmann, L. W., Baliunas, S. L., Duncan, D. K., & Vaughan, A. H. 1984, Rotation, convection, and magnetic activity in lower main-sequence stars., ApJ, 279, 763, doi: 10.1086/161945

Núñez, A., Agüeros, M. A., Curtis, J. L., et al. 2024, The Factory and the Beehive. V. Chromospheric and Coronal Activity and Its Dependence on Rotation in Praesepe and the Hyades, ApJ, 962, 12, doi: 10.3847/1538-4357/ad117e

of Sciences Engineering, N. A., & Medicine". 2025, "Solar and Space Physics for the Nation: An Overview of the 20242033 Decadal Survey" ("Washington, DC": "The National Academies Press"), doi: 10.17226/29150

O'Neal, D., & Neff, J. E. 1997, OH 1.563 micron Absorption from Starspots on Active Stars, AJ, 113, 1129, doi: 10.1086/118331

O'Neal, D., Neff, J. E., Saar, S. H., & Mines, J. K. 2001, Hydroxyl 1.563 Micron Absorption from Starspots on Active Stars, AJ, 122, 1954, doi: 10.1086/323093

O'Neal, D., Saar, S. H., & Neff, J. E. 1998, Spectroscopic Evidence for Nonuniform Starspot Properties on II Pegasi, ApJL, 501, L73, doi: 10.1086/311441

Owen, J. E., & Mohanty, S. 2016, Habitability of terrestrial-mass planets in the HZ of M Dwarfs - I. H/He-dominated atmospheres, MNRAS, 459, 4088, doi: 10.1093/mnras/stw959

Palle, E., Nortmann, L., Casasayas-Barris, N., et al. 2020, A He I upper atmosphere around the warm Neptune GJ 3470 b, A&A, 638, A61, doi: 10.1051/0004-6361/202037719

Panchal, A., & Joshi, Y. C. 2021, Photometric and Spectroscopic Analysis of Four Contact Binaries, AJ, 161, 221, doi: 10.3847/1538-3881/abea0c

Panchal, A., Joshi, Y. C., De Cat, P., & Tiwari, S. N. 2022, Long-term Photometric and Low-resolution Spectroscopic Analysis of Five Contact Binaries, ApJ, 927, 12, doi: 10.3847/1538-4357/ac45fb

Parker, E. N. 1955, Hydromagnetic Dynamo Models., ApJ, 122, 293, doi: 10.1086/146087

Pecaut, M. J., & Mamajek, E. E. 2013, Intrinsic Colors, Temperatures, and Bolometric Corrections of Pre-main-sequence Stars, ApJS, 208, 9, doi: 10.1088/0067-0049/208/1/9

Perdelwitz, V., Chaikin-Lifshitz, A., Ofir, A., & Aharonson, O. 2025, The Influence of Stellar Chromospheres and Coronae on Exoplanet Transmission Spectroscopy, ApJL, 980, L42, doi: 10.3847/2041-8213/adb158

Perdelwitz, V., Mittag, M., Tal-Or, L., et al. 2021, CARMENES input catalog of M dwarfs. VI. A time-resolved Ca II H&K catalog from archival data, A&A, 652, A116, doi: 10.1051/0004-6361/202140889

Pfeiffer, M. J., Frank, C., Baumueller, D., Fuhrmann, K., & Gehren, T. 1998, FOCES - a fibre optics Cassegrain Echelle spectrograph, A&AS, 130, 381, doi: 10.1051/aas:1998231

Pi, Q.-f., Zhang, L.-Y., Li, Z.-m., & Zhang, X.-l. 2014, Magnetic Activity and Orbital Period Variation of the Short-period Eclipsing Binary DV Psc, AJ, 147, 50, doi: 10.1088/0004-6256/147/3/50

Quirrenbach, A., Amado, P. J., Ribas, I., et al. 2018, in Society of Photo-Optical Instrumentation Engineers (SPIE) Conference Series, Vol. 10702, Ground-based and Airborne Instrumentation for Astronomy VII, ed. C. J. Evans, L. Simard, & H. Takami, 107020W, doi: 10.1117/12.2313689

Quirrenbach, A., CARMENES Consortium, Amado, P. J., et al. 2020, in Society of Photo-Optical Instrumentation Engineers (SPIE) Conference Series, Vol. 11447, Ground-based and Airborne Instrumentation for Astronomy VIII, ed. C. J. Evans, J. J. Bryant, & K. Motohara, 114473C, doi: 10.1117/12.2561380

Quirrenbach, A., Passegger, V. M., Trifonov, T., et al. 2022, The CARMENES search for exoplanets around M dwarfs. Two Saturn-mass planets orbiting active stars, A&A, 663, A48, doi: 10.1051/0004-6361/202142915

Quirrenbach, A., Aceituno, J., Agüí Fernández, J. F., et al. 2024, in Society of Photo-Optical Instrumentation Engineers (SPIE) Conference Series, Vol. 13098, Observatory Operations: Strategies, Processes, and Systems X, ed. C. R. Benn, A. Chrysostomou, & L. J. Storrie-Lombardi, 1309825, doi: 10.1117/12.3023682

Reiners, A. 2009, Activity-induced radial velocity jitter in a flaring M dwarf, A&A, 498, 853, doi: 10.1051/0004-6361/200810257

Reiners, A. 2012, Observations of Cool-Star Magnetic Fields, Living Reviews in Solar Physics, 9, 1, doi: 10.12942/lrsp-2012-1

Reiners, A., & Basri, G. 2008, Chromospheric Activity, Rotation, and Rotational Braking in M and L Dwarfs, ApJ, 684, 1390, doi: 10.1086/590073

Reiners, A., & Basri, G. 2009, On the magnetic topology of partially and fully convective stars, A&A, 496, 787, doi: 10.1051/0004-6361:200811450

Reiners, A., Basri, G., & Browning, M. 2009, Evidence for Magnetic Flux Saturation in Rapidly Rotating M Stars, ApJ, 692, 538, doi: 10.1088/0004-637X/692/1/538

Reiners, A., Schüssler, M., & Passegger, V. M. 2014, Generalized Investigation of the Rotation-Activity Relation: Favoring Rotation Period instead of Rossby Number, ApJ, 794, 144, doi: 10.1088/0004-637X/794/2/144

Reiners, A., Shulyak, D., Anglada-Escudé, G., et al. 2013, Radial velocity signatures of Zeeman broadening, A&A, 552, A103, doi: 10.1051/0004-6361/201220437

Reiners, A., Zechmeister, M., Caballero, J. A., et al. 2018, The CARMENES search for exoplanets around M dwarfs. High-resolution optical and near-infrared spectroscopy of 324 survey stars, A&A, 612, A49, doi: 10.1051/0004-6361/201732054

Reiners, A., Shulyak, D., Käpylä, P. J., et al. 2022, Magnetism, rotation, and nonthermal emission in cool stars. Average magnetic field measurements in 292 M dwarfs, A&A, 662, A41, doi: 10.1051/0004-6361/202243251

Ribas, I., Tuomi, M., Reiners, A., et al. 2018, A candidate super-Earth planet orbiting near the snow line of Barnard's star, Nature, 563, 365, doi: 10.1038/s41586-018-0677-y

Ribas, I., Reiners, A., Zechmeister, M., et al. 2023, The CARMENES search for exoplanets around M dwarfs. Guaranteed time observations Data Release 1 (2016-2020), A&A, 670, A139, doi: 10.1051/0004-6361/202244879

Robrade, J., & Schmitt, J. H. M. M. 2009, X-ray emission from the M9 dwarf 1RXS J115928.5-524717. Quasi-quiescent coronal activity at the end of the main-sequence, A&A, 496, 229, doi: 10.1051/0004-6361/200811224

Ruh, H. L., Zechmeister, M., Reiners, A., et al. 2024, The CARMENES search for exoplanets around M dwarfs: The impact of rotation and magnetic fields on the radial velocity jitter in cool stars, A&A, 692, A138, doi: 10.1051/0004-6361/202450836

Saar, S., & Brandenburg, A. 2001, in Astronomical Society of the Pacific Conference Series, Vol. 248, Magnetic Fields Across the Hertzsprung-Russell Diagram, ed. G. Mathys, S. K. Solanki, & D. T. Wickramasinghe, 231, doi: 10.48550/arXiv.astro-ph/0105070

Saar, S. H., & Brandenburg, A. 1999, Time Evolution of the Magnetic Activity Cycle Period. II. Results for an Expanded Stellar Sample, ApJ, 524, 295, doi: 10.1086/307794

Saar, S. H., Huovelin, J., Osten, R. A., & Shcherbakov, A. G. 1997, HeI D3 absorption and its relation to rotation and activity in G and K dwarfs., A&A, 326, 741

Sabotta, S., Schlecker, M., Chaturvedi, P., et al. 2021, The CARMENES search for exoplanets around M dwarfs. Planet occurrence rates from a subsample of 71 stars, A&A, 653, A114, doi: 10.1051/0004-6361/202140968

Salz, M., Czesla, S., Schneider, P. C., et al. 2018, Detection of He I λ10830 Å absorption on HD 189733 b with CARMENES high-resolution transmission spectroscopy, A&A, 620, A97, doi: 10.1051/0004-6361/201833694

Sánchez-López, A., Alonso-Floriano, F. J., López-Puertas, M., et al. 2019, Water vapor detection in the transmission spectra of HD 209458 b with the CARMENES NIR channel, A&A, 630, A53, doi: 10.1051/0004-6361/201936084

Saunders, N., van Saders, J. L., Lyttle, A. J., et al. 2024, Stellar Cruise Control: Weakened Magnetic Braking Leads to Sustained Rapid Rotation of Old Stars, ApJ, 962, 138, doi: 10.3847/1538-4357/ad1516

Schmidt, S. J., Kowalski, A. F., Hawley, S. L., et al. 2012, Probing the Flare Atmospheres of M Dwarfs Using Infrared Emission Lines, ApJ, 745, 14, doi: 10.1088/0004-637X/745/1/14

Schmidt, S. J., West, A. A., Bochanski, J. J., Hawley, S. L., & Kielty, C. 2014, Calibrating Ultracool Dwarfs: Optical Template Spectra, Bolometric Corrections, and χ Values, PASP, 126, 642, doi: 10.1086/677403

Schmitt, J. H. M. M. 1997, Coronae on solar-like stars., A&A, 318, 215

Schöfer, P., Jeffers, S. V., Reiners, A., et al. 2019, The CARMENES search for exoplanets around M dwarfs. Activity indicators at visible and near-infrared wavelengths, A&A, 623, A44, doi: 10.1051/0004-6361/201834114

Schöfer, P., Jeffers, S. V., Reiners, A., et al. 2022, The CARMENES search for exoplanets around M dwarfs. Rotational variation in activity indicators of Ross 318, YZ CMi, TYC 3529-1437-1, and EV Lac, A&A, 663, A68, doi: 10.1051/0004-6361/201936102

Schrijver, C. J. 1987, in Cool Stars, Stellar Systems and the Sun, ed. J. L. Linsky & R. E. Stencel, Vol. 291 (Springer), 135–145, doi: 10.1007/3-540-18653-0_120

See, V., Lu, Y. L., Amard, L., & Roquette, J. 2024, The impact of stellar metallicity on rotation and activity evolution in the Kepler field using gyro-kinematic ages, MNRAS, 533, 1290, doi: 10.1093/mnras/stae1828

See, V., Roquette, J., Amard, L., & Matt, S. 2023, Further evidence of the link between activity and metallicity using the flaring properties of stars in the Kepler field, MNRAS, 524, 5781, doi: 10.1093/mnras/stad2020

See, V., Jardine, M., Vidotto, A. A., et al. 2016, The connection between stellar activity cycles and magnetic field topology, MNRAS, 462, 4442, doi: 10.1093/mnras/stw2010

Segura, A., Walkowicz, L. M., Meadows, V., Kasting, J., & Hawley, S. 2010, The Effect of a Strong Stellar Flare on the Atmospheric Chemistry of an Earth-like Planet Orbiting an M Dwarf, Astrobiology, 10, 751, doi: 10.1089/ast.2009.0376

Sekiguchi, M., & Fukugita, M. 2000, A Study of the B-V Color-Temperature Relation, AJ, 120, 1072, doi: 10.1086/301490

Shan, Y., Revilla, D., Skrzypinski, S. L., et al. 2024, CARMENES input catalog of M dwarfs. VII. New rotation periods for the survey stars and their correlations with stellar activity, A&A, 684, A9, doi: 10.1051/0004-6361/202346794

Sheminova, V. A. 2017, Fourier analysis of spectra of solar-type stars, Kinematics and Physics of Celestial Bodies, 33, 217, doi: 10.3103/S0884591317050063

Shulyak, D., Reiners, A., Engeln, A., et al. 2017, Strong dipole magnetic fields in fast rotating fully convective stars, Nature Astronomy, 1, 0184, doi: 10.1038/s41550-017-0184

Shulyak, D., Reiners, A., Seemann, U., Kochukhov, O., & Piskunov, N. 2014, Exploring the magnetic field complexity in M dwarfs at the boundary to full convection, A&A, 563, A35, doi: 10.1051/0004-6361/201322136

Shulyak, D., Reiners, A., Nagel, E., et al. 2019, Magnetic fields in M dwarfs from the CARMENES survey, A&A, 626, A86, doi: 10.1051/0004-6361/201935315

Skumanich, A. 1972, Time Scales for Ca II Emission Decay, Rotational Braking, and Lithium Depletion, ApJ, 171, 565, doi: 10.1086/151310

Skumanich, A., Smythe, C., & Frazier, E. N. 1975, On the statistical desription of inhomogeneities in the quiet solar atmosphere. I. Linear regression analysis and absolute calibration of multichannel observations of the Ca^+ emission network., ApJ, 200, 747, doi: 10.1086/153846

Solar, M., Arcos, C., Curé, M., Levenhagen, R. S., & Araya, I. 2022, Automatic algorithm to obtain v sin i values via Fourier transform in the BeSOS database, MNRAS, 511, 4404, doi: 10.1093/mnras/stac202

Sousa, S. G., Santos, N. C., Adibekyan, V., Delgado-Mena, E., & Israelian, G. 2015, ARES v2: new features and improved performance, A&A, 577, A67, doi: 10.1051/0004-6361/201425463

Sousa, S. G., Santos, N. C., Israelian, G., Mayor, M., & Monteiro, M. J. P. F. G. 2007, A new code for automatic determination of equivalent widths: Automatic Routine for line Equivalent widths in stellar Spectra (ARES), A&A, 469, 783, doi: 10.1051/0004-6361:20077288

Stassun, K. G., Hebb, L., Covey, K., et al. 2011, in Astronomical Society of the Pacific Conference Series, Vol. 448, 16th Cambridge Workshop on Cool Stars, Stellar Systems, and the Sun, ed. C. Johns-Krull, M. K. Browning, & A. A. West, 505, doi: 10.48550/arXiv.1012.2580

Tabernero, H. M., Marfil, E., Montes, D., & González Hernández, J. I. 2022, STEPARSYN: A Bayesian code to infer stellar atmospheric parameters using spectral synthesis, A&A, 657, A66, doi: 10.1051/0004-6361/202141763

Tal-Or, L., Zechmeister, M., Reiners, A., et al. 2018, The CARMENES search for exoplanets around M dwarfs. Radial-velocity variations of active stars in visual-channel spectra, A&A, 614, A122, doi: 10.1051/0004-6361/201732362

Toledo-Padrón, B., González Hernández, J. I., Rodríguez-López, C., et al. 2019, Stellar activity analysis of Barnard's Star: very slow rotation and evidence for long-term activity cycle, MNRAS, 488, 5145, doi: 10.1093/mnras/stz1975

Tsantaki, M., Sousa, S. G., Adibekyan, V. Z., et al. 2018, Macroturbulent and rotational velocities for FGK dwarfs and subgiants: calibration and implications, Monthly Notices of the Royal Astronomical Society, 473, 5066, doi: 10.1093/mnras/stx2719

Ulmschneider, P. 1970, On Frequency and Strength of Shock Waves in the Solar Atmosphere, Solar Physics, 12, 403, doi: 10.1007/BF00148023

Vaiana, G. S., Cassinelli, J. P., Fabbiano, G., et al. 1981, Results from an extensive Einstein stellar survey., ApJ, 245, 163, doi: 10.1086/158797

Varas, R., Calvo-Ortega, R., Amado, P. J., et al. 2025, Improving radial velocity precision with CARMENES-PLUS: An upgrade of the near-infrared spectrograph cooling system, Experimental Astronomy, 60, 10, doi: 10.1007/s10686-025-10020-0

Vaughan, A. H., & Preston, G. W. 1980, A survey of chromospheric CA II H and K emission in field stars of the solar neighborhood., PASP, 92, 385, doi: 10.1086/130683

Vaughan, A. H., Preston, G. W., & Wilson, O. C. 1978, Flux measurements of Ca II and K emission., PASP, 90, 267, doi: 10.1086/130324

Vidotto, A. A., Gregory, S. G., Jardine, M., et al. 2014, Stellar magnetism: empirical trends with age and rotation, MNRAS, 441, 2361, doi: 10.1093/mnras/stu728

Virtanen, P., Gommers, R., Oliphant, T. E., et al. 2020, SciPy 1.0: fundamental algorithms for scientific computing in Python, Nature Methods, 17, 261, doi: 10.1038/s41592-019-0686-2

Walkowicz, L. M., & Hawley, S. L. 2009, Tracers of Chromospheric Structure. I. Observations of Ca II K and Hα in M Dwarfs, AJ, 137, 3297, doi: 10.1088/0004-6256/137/2/3297

Walkowicz, L. M., Hawley, S. L., & West, A. A. 2004, The χ Factor: Determining the Strength of Activity in Low-Mass Dwarfs, PASP, 116, 1105, doi: 10.1086/426792

Wang, J.-Y., Li, K., Gao, X., et al. 2025, Search for and Analysis of Eclipsing Binaries in the LAMOST Medium-resolution Survey Field. I. R.A.: $23^h01^m51^s$, Decl.: +34°36'45", ApJ, 979, 69, doi: 10.3847/1538-4357/ad9929

West, A. A., Hawley, S. L., Walkowicz, L. M., & Covey, K. R. 2004, in IAU Symposium, Vol. 219, Stars as Suns : Activity, Evolution and Planets, ed. A. K. Dupree & A. O. Benz, 935

Winters, J. G., Henry, T. J., Jao, W.-C., et al. 2019, The Solar Neighborhood. XLV. The Stellar Multiplicity Rate of M Dwarfs Within 25 pc, AJ, 157, 216, doi: 10.3847/1538-3881/ab05dc

Wright, J. T., & Gaudi, B. S. 2013, in Planets, Stars and Stellar Systems. Volume 3: Solar and Stellar Planetary Systems, ed. T. D. Oswalt, L. M. French, & P. Kalas (Springer), 489, doi: 10.1007/978-94-007-5606-9_10

Wright, N. J., Newton, E. R., Williams, P. K. G., Drake, J. J., & Yadav, R. K. 2018, The stellar rotation-activity relationship in fully convective M dwarfs, MNRAS, 479, 2351, doi: 10.1093/mnras/sty1670

Xia, Q., Wang, X., Li, K., et al. 2025, Minute-cadence Observations of the LAMOST Fields with the TMTS. VI. Physical Parameters of Contact Binaries, AJ, 169, 139, doi: 10.3847/1538-3881/ada7eb

Xu, X., Li, K., Liu, F., et al. 2025, Photometric and Spectroscopic Investigations of Three Large Amplitude Contact Binaries, AJ, 169, 85, doi: 10.3847/1538-3881/ad9a59

Yan, F., Casasayas-Barris, N., Molaverdikhani, K., et al. 2019, Ionized calcium in the atmospheres of two ultra-hot exoplanets WASP-33b and KELT-9b, A&A, 632, A69, doi: 10.1051/0004-6361/201936396

Zechmeister, M., Reiners, A., Amado, P. J., et al. 2018, Spectrum radial velocity analyser (SERVAL). High-precision radial velocities and two alternative spectral indicators, A&A, 609, A12, doi: 10.1051/0004-6361/201731483

Zechmeister, M., Dreizler, S., Ribas, I., et al. 2019, The CARMENES search for exoplanets around M dwarfs. Two temperate Earth-mass planet candidates around Teegarden's Star, A&A, 627, A49, doi: 10.1051/0004-6361/201935460

Zhang, L., Pi, Q., Yang, Y., & Li, Z. 2014a, Magnetic activity and orbital period variation of the eclipsing binary KV Gem, New Astronomy, 27, 81, doi: 10.1016/j.newast.2013.09.002

Zhang, L., Pi, Q., Zhu, Z., Zhang, X., & Li, Z. 2014b, Chromospheric activity on late-type star LQ Hya, New Astronomy, 32, 1, doi: 10.1016/j.newast.2014.02.010

Zhang, L.-Y. 2018, Photospheric and chromospheric activity of the short period X-ray and Algol eclipsing binary UX CrB, Astrophysics and Space Science, 363, 174, doi: 10.1007/s10509-018-3395-x

Appendices

Calibrations curves of logχ for the most important chromospheric activity indicators

The following Tables 1 and 2 and Fig. 1 show the fit parameters of the χ-functions mentioned in Section 2.4 of the main text. For all these calibrations, along with the corresponding to H$_\alpha$, presented in the main text, follow the procedures described in 2.4.

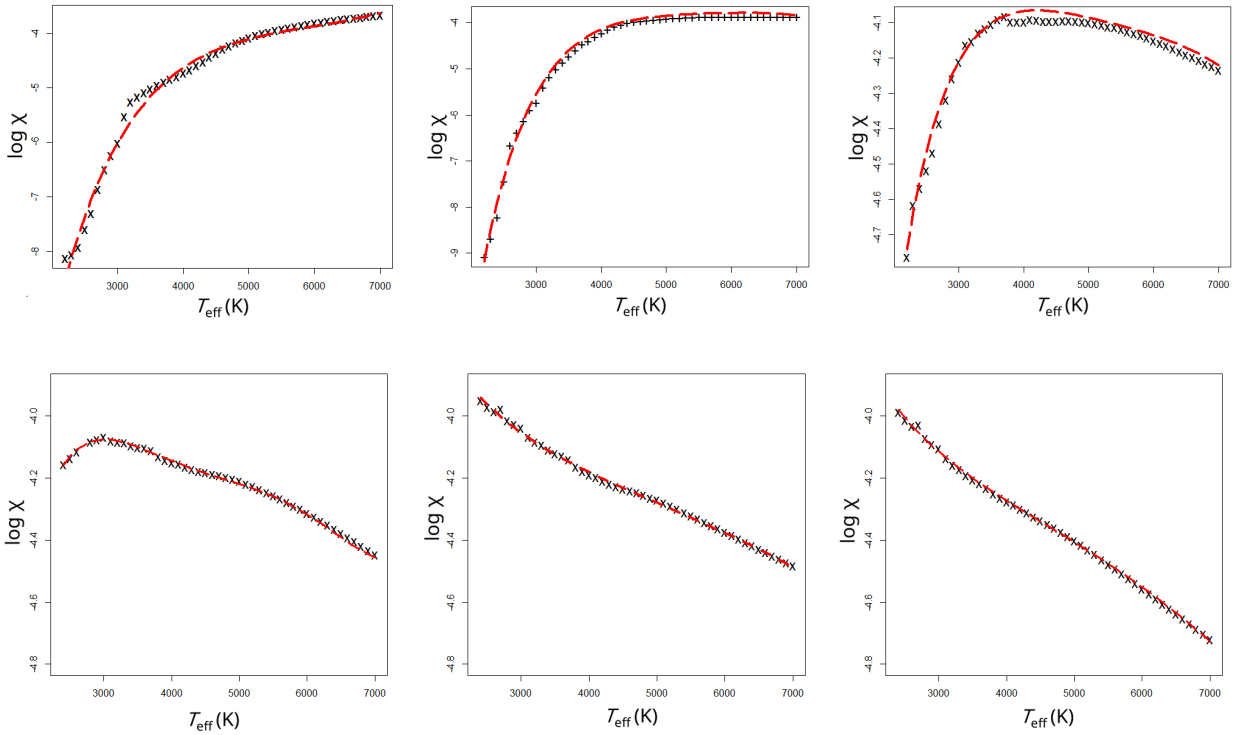

Figure 1. Calibration for Ca II H&K doublet (left panel), He I D3 and also Na I D_1 & Na I D_2 (middle panel), and Ca II IRT lines (right panel). In the second row, the curves for Paschen δ (left panel), Paschen γ + He I λ10830 (middle panel) and Paschen β (right panel).All in the range of effective temperatures [2200, 7000] K. The calibration curve for Hα can be seen in the Figure 2.4

Table 1. Parameters of the fit for $\log\chi = C_1 + \alpha \log T_{\rm eff} + P_5(T_{\rm eff})$ for the lines in the VIS channel of CARMENES. This includes Ca II H&K, He I D$_3$, Na I D$_{1,2}$ and Hα in the visible and Ca II IRT in the infrared.

Coefficient	Ca II H&K (1)	He I D$_3$ & Na I D$_{1,2}$ (2)	Hα (3)	Ca II IRT (4)
10^{-2} C_1	-1.747 ± 0.134	-4.471 ± 0.346	-0.4629 ± 0.018	-0.8953 ± 0.0688
10^{-1} α	5.434 ± 0.454	14.91 ± 1.24	1.281 ± 0.006	2.917 ± 0.245
10^{3} β_1	-7.759 ± 0.953	-33.28 ± 3.97	-1.006 ± 0.060	-7.107 ± 0.783
10^{7} β_2	3.356 ± 0.544	28.88 ± 4.670	0	6.628 ± 0.920
10^{10} β_3	0	-1.125 ± 0.235	0	-0.2619 ± 0.0461
10^{14} β_4	0	0	0	0
10^{18} β_5	0	0	0	0
Adj. Param. R^2	0.9893	0.9969	0.9712	0.9895

Table 2. Parameters of the fit for $\log \chi = C_1 + \alpha \log T_{\rm eff} + P_5(T_{\rm eff})$ for the lines in the NIR channel of CARMENES. This includes Paschenδ, Paschenγ and Paschenβ of the Paschen series, along with He I λ10830. All of them in the infrared.

Coefficient	Paschenδ (5)	He I λ10830 & Paschenγ (6)	Paschenβ (7)
10^{-2} C_1	-0.1169 ± 0.039	0.04525 ± 0.00859	0.06372 ± 0.00757
10^{-1} α	2.917 ± 0.245	-0.2733 ± 0.0289	-0.3364 ± 0.0255
10^{3} β_1	8.538 ± 0.475	0.3790 ± 0.0586	0.5096 ± 0.0516
10^{7} β_2	-37.00 ± 2.19	-0.2360 ± 0.0325	-0.3533 ± 0.0287
10^{10} β_3	7.774 ± 0.495	0	0
10^{14} β_4	-7.984 ± 0.536	0	0
10^{18} β_5	3.202 ± 0.228	0	0
Adj. Param. R^2	0.9986	0.9995	0.9995

iSTARMOD Input Parameters and Configuration file

As shown in the Figure 2.3, the first step is to provide the algorithm a very large set of parameters, that are specified in an input `inputParameters.sm` file with the syntax `KEYWORD = value`.

The parameters are grouped in the following sections. whose names are kept as in `STARMOD` for historical reasons and retro-compatibility

- `GENERAL INFORMATION`
  - `IM_PATH =v.\path\` # This is the path where the input FITS spectrum is located. Can be a relative path.
  - `OBJ_NAME = name_of_file.fits` # Name of the input FITS file(s). If there are several files, wildcards can be used.
- `OUTPUT SPECTRA`: All these files will be generated in the same path as defined by `IM_PATH`
  - `SYN_SPEC = VALUE` # write output spectra: only admits YES/NO
  - `SYN_NAME = name_of_synth` # name of the synthetic spectrum (if SYN_SPEC =YES)
  - `SUB_NAME = name_of_subtr` # name of subtracted spectrum (if SYN_SPEC =YES)
- `INTERPOLATION PARAMETERS`: In this group, the number of executions of the least squares iterative loop is defined as well as the wavelength range in Å, for the order to be analyzed, as well as the wavelength intervals to be excluded of the sum of the residuals for the least squares. The intervals are typically those affected by activity, where the lines present excess emission instead or absorption. If the radial velocities are large, it is prudent to also exclude the blue or red ends of the spectrum.
  - `N_ITER = 8` # number of iterations: integer
  - `PIX_ZONE = XXXX YYYY wvl` # 'pixel' range for the fit: 2 integers
  - `PIX_EXCL = ZZZ1 ZZZ2 wvl` # Blue/Red exclusion skip subrange: 2 integers (optional)
  - `PIX_EXCL = ZZZ3 ZZZ4 wvl` # Line Zone skip subrange: 2 integers (optional)
  - `PIX_EXCL = ZZZ5 ZZZ6 Wvl` # skip subrange: 2 integers (optional)
  - `PIX_EXCL =` # skip subrange: 2 integers (optional)
  - `PIX_EXCL =` # skip subrange: 2 integers (optional)
- `PRIMARY STAR`. Reference star parameters. The radial velocity, *vsini*, and weight values for the initial guesses can be fixed so that they do not vary across loop iterations, or allowed to vary freely from those initial guesses.
  - `REF_PATH = .\path\` # path (absolute or relative) of fits spectrum for primary star of reference
  - `PRM_NAME = name_of_file.fits` # primary filename
  - `PRM_RAD = X.xxx var/fix` # doppler shift: float, keyword (var/fix)
  - `PRM_ROT = Y.yyy var/fix` # doppler broadening: float, keyword (var/fix)
  - `PRM_WGT = Z.zzz var/fix` # weight: float, keyword (var/fix).
- `SECONDARY STAR`. The same as previous. In this case for the secondary star.
  - `SEC_PATH = .\path\` # path (absolute or relative) of fits spectrum for primary star of reference
  - `SEC_NAME = name_of_file.fits` # secondary filename: Name /NONE
  - `SEC_RAD = X.xxx var/fix` # doppler shift: float, keyword (var/fix)
  - `SEC_ROT = Y.yyy var/fix` # doppler broadening: float, keyword (var/fix)
  - `SEC_WGT = Z.zzz var/fix` # weight: float, keyword (var/fix).
- `SPECTRA FORMAT`. To define the order of the input spectrum to analyze. The `LINE` parameter must be compliant with the specification of a configuration file `lambdas.dat`. If `NONE` the tool will not perform any calculation
  - `MODE = ech` # NOT USED
  - `APERTURE = 46` # aperture number/ Order : integer
  - `BAND =` # NOT USED
  - `LINE = CaIRT-a` # To specify the LINE for measuring the equivalent width
- `ALGORITHM & VISUALISATION PARAMS`. To define the maximum value of the y-axis in each of the window of the created figure. The FINDMAX_TOLERANCE restricts the wavelength interval where the emission maximum is to be searched.
  - `MAXFLUXDISP_OBJ = X.xx` # Maximum y-value to display in the object+ref spectra window
  - `MAXFLUXDISP_SUB = X.xx` # Maximum y-value to display in the subtracted spectrum window
  - `FINDMAX_TOLERANCE = 0.00x` # to find the maximum of the subtracted spectra when calculating the integral

Preliminary implementation of iSTARMOD Graphical User Interface (GUI)

The below figures depicts the preliminary implementation of the GUI for the iSTARMOD SW in python Tcl/Tk.

Concept of Operation

The design of this GUI follows the operative of the SW execution.

1. Read the .sm file with the input parameters to the algorithm, as specified in 4.5
2. Modify, add or delete these parameters.
3. Run iSTARMOD

To this end, the left panel shows the list of parameters read from the .sm file. Selecting a line of the read file in the panel, values of the trio [KEYWORD = value # comment] are shown in three edit boxes in the bottom. This allows to modify/add/delete input parameters. Clicking on action buttons make these changes apply to the list or be saved to the file. The right panel shows the result of the execution of a python script corresponding to the action prescribed by a menu option or a keyboard command (accelerator).

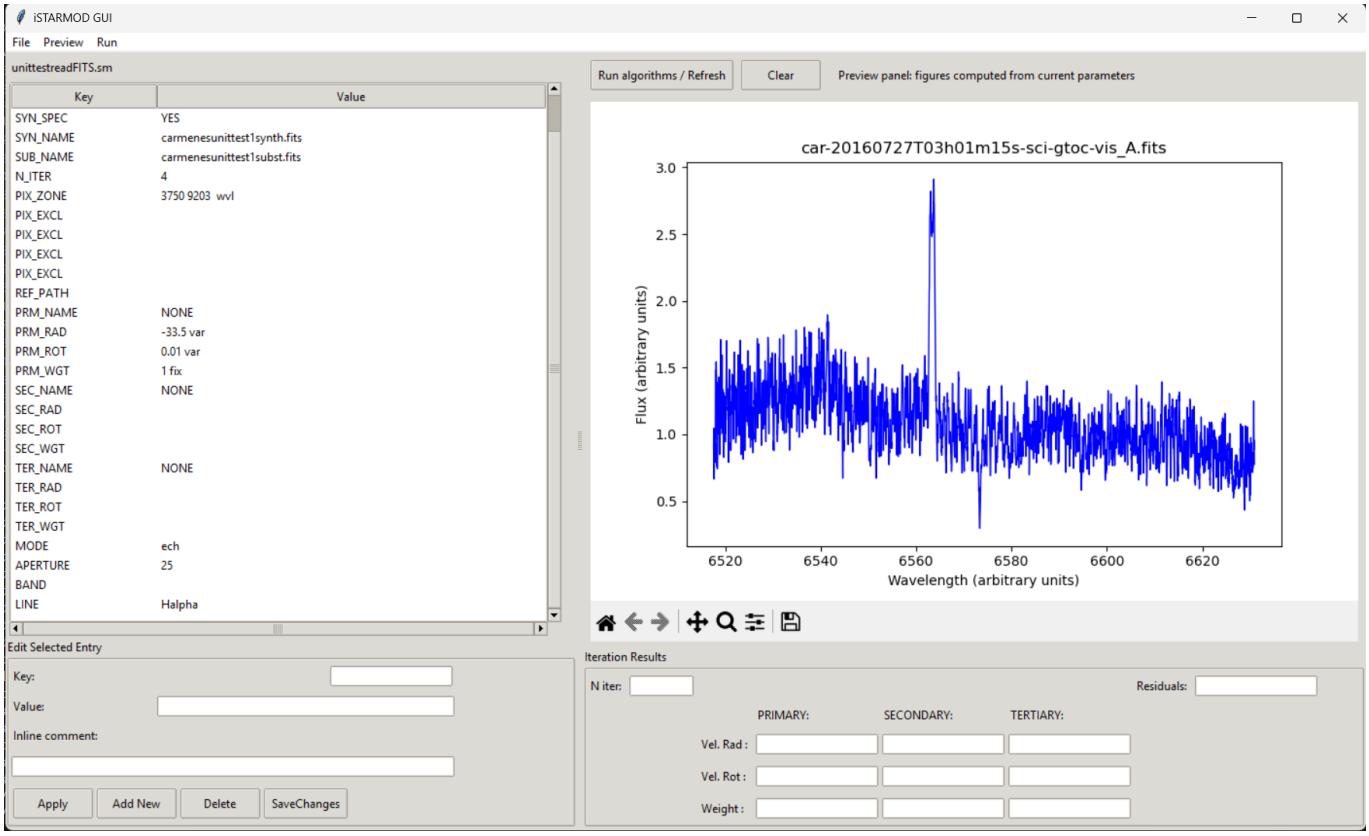

Figure 2. Pre-view of the order 25 of a CARMENES provided spectrum, corresponding to TZ Ari a M3.5V star

Previous to the execution of iSTARMOD, a preview of the PIX_EXCL intervals, based on the reading of the .sm file can be draw on the right panel.

When is executed the iSTARMOD algorithm, a series of edit boxes show the values of each iteration at the bottom of the right panel. These boxes cannot be edited. Once the figure is sent to the window within the panel, matplotlib functionality can be used to zoom/pane or save to a file the figure drawn.

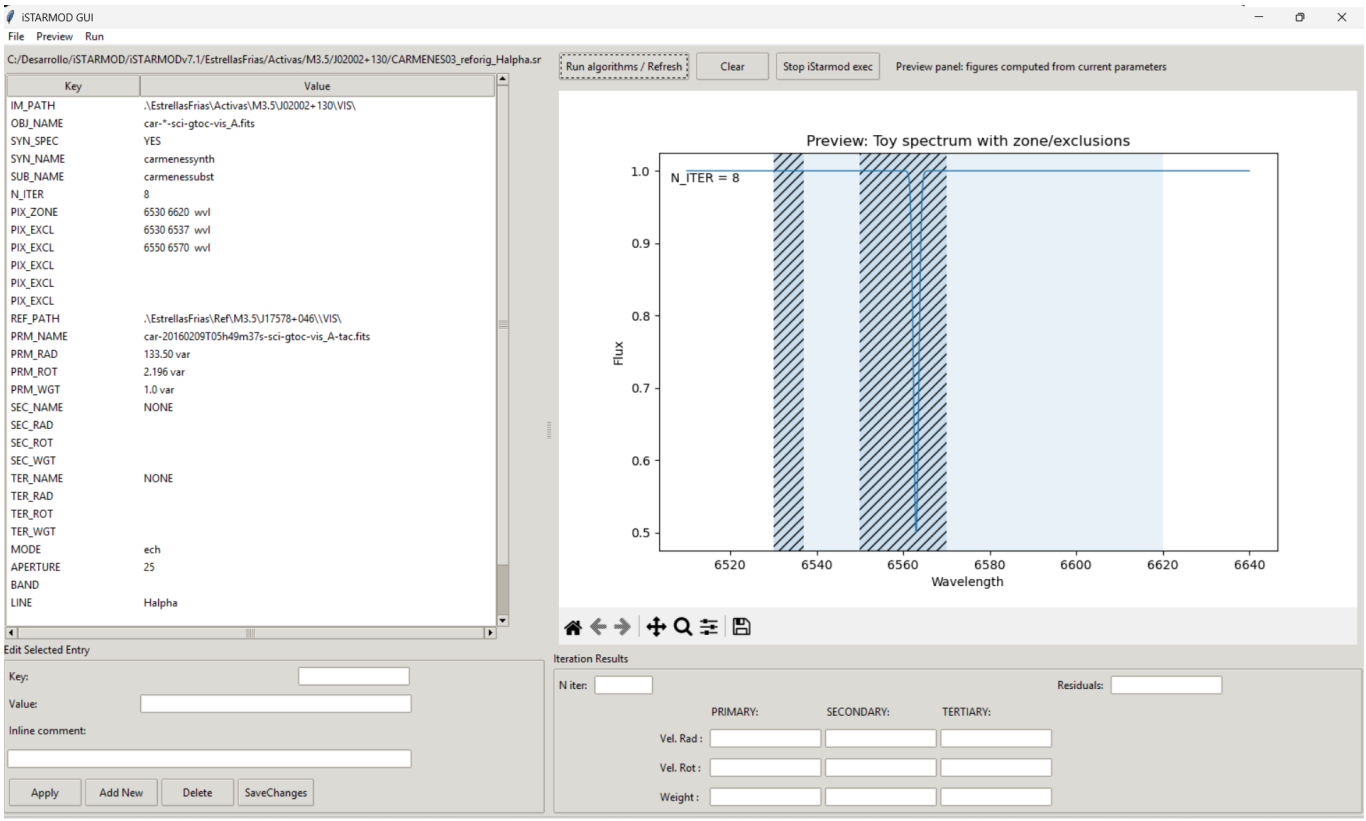

Figure 3. Preview of PIX_EXCL intervals as appear in the .sm file the application have just read

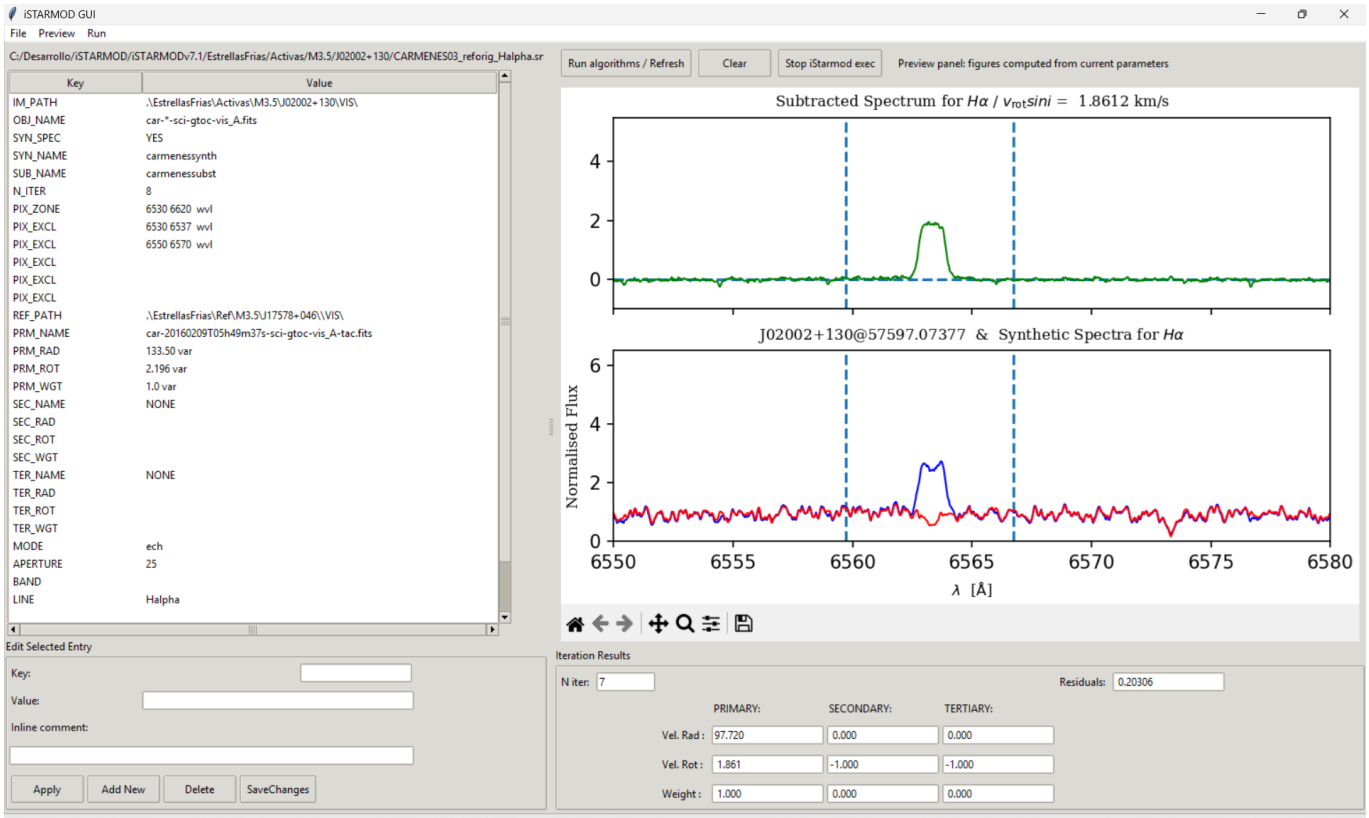

Figure 4. iSTARMOD GUI showing the result of performing the spectral subtraction to a CARMENES provided spectrum of TZ Ari, a M3.5V star. The spectral subtraction was executed on the spectral order containing Hα. The reference star' spectrum corresponds to another M3.5V star: Barnard' Star in a quiescent phase

Catalogue of Active Stars

The following table shows the complete sample of stars used in our study.

Table 3. Catalogue of studied Active Stars

KarmnID	Name	α [J2000]	δ [J2000]	J [mag]	Sp. Type	$T_{\rm eff}$ [K]	Mag.Field $\langle B \rangle$ [G]	[Fe/H] [dex]	$P_{\rm rot}$ [d]	vsini $[kms^{-1}]$	Avail. spectra
J12156+526[1]	StKM 2-809	12:15:39.36	+52:39:08.8	8.588 ± 0.024	M4.0V	3568 ± 7	6530 ± 680	−0.19 ± 0.14	0.73	35.3 ± 3.5	13
J05084-210	2MASS J05082729-2101444	05:08:27.30	-21:01:44.4	9.716 ± 0.024	M5.0V	3115 ± 29		−0.38 ± 0.07	0.28	25.2 ± 2.5	26
J11055+435	WX UMa	11:05:30.89	+43:31:17.9	8.742 ± 0.026	M5.5V	3278 ± 86	6880 ± 140	−0.36 ± 0.25		8.2 ± 2.7	20
J17338+169[1]	1RXS J173353.5+165515	17:33:53.18	+16:55:13.1	8.895 ± 0.027	M5.5V	3165 ± 302	8130 ± 940	−0.02 ± 0.06	0.27	41.5 ± 7.7	12
J20451-313	AU Mic	20:45:09.53	-31:20:27.2	5.436 ± 0.017	M0.5V	3768 ± 20	3010 ± 220	+0.01 ± 0.06	4.89	9.3 ± 1.2	100
J15218+209[1]	OT Ser	15:21:52.93	+20:58:39.9	6.610 ± 0.021	M1.5V	3706 ± 302	3360 ± 100	−0.16 ± 0.09	3.35	4.3 ± 1.5	48
J11201-104	LP 733-099	11:20:06.10	-10:29:46.7	7.814 ± 0.026	M2.0V	3661 ± 9	2170 ± 160	−0.26 ± 0.06	5.64	3.6 ± 1.5	27
J03473-019[1]	G 80-021	03:47:23.34	-01:58:19.9	7.804 ± 0.026	M3.0V	3451 ± 121	3490 ± 200	−0.18 ± 0.15	3.88	5.2 ± 1.5	11
J10196+198	AD Leo	10:19:36.28	+19:52:12.0	5.449 ± 0.027	M3.0V	3455 ± 5	3570 ± 90	−0.19 ± 0.12		4.3 ± 0.0	64
J22518+317[1]	GT Peg	22:51:53.54	+31:45:15.2	7.697 ± 0.020	M3.0V	3173 ± 95	3870 ± 340	−0.31 ± 0.18		13.2 ± 0.9	12
J02088+494[1]	G 173-039	02:08:53.62	+49:26:56.4	8.423 ± 0.023	M3.5V	3265 ± 114		−0.16 ± 0.19	0.75	24.1 ± 2.4	16
J07319+362N	V* BL Lyn	07:31:57.32	+36:13:47.4	7.571 ± 0.020	M3.5V	3384 ± 7	2530 ± 140	−0.09 ± 0.09		2.0	37
J10360+051	RY Sex	10:36:01.22	+05:07:12.8	8.463 ± 0.024	M3.5V	3268 ± 16	4820 ± 140	−0.62 ± 0.07	6.90	2.9 ± 1.6	7
J16570-043[1]	LP 686-027	16:57:05.74	-04:20:56.3	7.971 ± 0.023	M3.5V	3206 ± 14	3660 ± 380	−0.60 ± 0.03		10.1 ± 1.5	15
J18498-238[1]	V1216 Sgr	18:49:49.36	-23:50:10.4	6.222 ± 0.018	M3.5V	3340 ± 30	2080 ± 220	−0.43 ± 0.1		3.0 ± 1.5	36
J22468+443[1]	EV Lac	22:46:49.73	+44:20:02.4	6.106 ± 0.030	M3.5V	3306 ± 30	4320 ± 110	−0.60 ± 0.09	4.35	3.5 ± 1.5	101
J01352-072[1]	Barta 161 12	01:35:13.92	-07:12:51.5	8.964 ± 0.021	M4.0V	3184 ± 29		−0.02 ± 0.08	0.70	59.8 ± 6.9	11
J02519+224	RBS 365	02:51:54.10	+22:27:29.9	8.919 ± 0.024	M4.0V	2990 ± 30		−0.03 ± 0.19		27.2 ± 2.7	13
J05019+011	1RXS J050156.7+010845	05:01:56.66	+01:08:42.9	8.526 ± 0.026	M4.0V	3066 ± 30	3320 ± 250	−0.20 ± 0.26	2.08	6.5 ± 1.5	19
J05062+046	RX J0506.2+0439	05:06:12.93	+04:39:27.2	8.909 ± 0.020	M4.0V	3006 ± 30	3070 ± 490	+0.10 ± 0.16	0.89	24.9 ± 2.5	13
J05366+112	PM J05366+1117	05:36:38.46	+11:17:48.8	8.266 ± 0.032	M4.0V	3355 ± 23	2520 ± 180	−0.20 ± 0.1	5.44	2.4 ± 1.5	14
J06000+027[1]	G 99-049	06:00:03.50	+02:42:23.6	6.905 ± 0.011	M4.0V	3296 ± 19	2490 ± 220	−0.20 ± 0.13	1.81	4.9 ± 1.5	15
J06574+740	2MASS J06572616+7405265	06:57:26.12	+74:05:26.6	8.926 ± 0.024	M4.0V	3137 ± 17	3330 ± 830	−0.06 ± 0.06	0.61	27.1 ± 2.7	12
J07033+346	LP 255-011	07:03:23.17	+34:41:51.4	8.773 ± 0.020	M4.0V	3310 ± 26	2430 ± 160	−0.24 ± 0.11	8.00	2.0	14
J07472+503	2MASS J07471385+5020386	07:47:13.87	+50:20:38.5	8.855 ± 0.023	M4.0V	3251 ± 59	2940 ± 290	−0.08 ± 0.18	1.32	10.1 ± 1.5	15
J09161+018	RX J0916.1+0153	09:16:10.18	+01:53:08.8	8.770 ± 0.026	M4.0V	3237 ± 60	3900 ± 360	−0.08 ± 0.21	1.43	10.4 ± 1.5	9
J11476+002	LP 613-49A	11:47:40.75	+00:15:20.1	8.991 ± 0.035	M4.0V	3282 ± 19	3720 ± 180	−0.35 ± 0.12		2.4 ± 1.5	6
J12428+418	G 123-055	12:42:49.88	+41:53:47.1	8.118 ± 0.020	M4.0V	3328 ± 25	2350 ± 170	−0.08 ± 0.09		2.0	7
J13536+776	RX J1353.6+7737	13:53:38.79	+77:37:08.2	8.635 ± 0.019	M4.0V	3198 ± 83	2630 ± 400	+0.00 ± 0.3	1.23	8.9 ± 1.5	25
J13591-198	LP 799-007	13:59:10.41	-19:50:03.7	8.334 ± 0.037	M4.0V	3261 ± 20	1910 ± 240	−0.15 ± 0.07	3.32	3.2 ± 1.5	17
J18131+260	LP 390-16	18:13:06.57	+26:01:51.9	8.899 ± 0.020	M4.0V	3271 ± 63	4490 ± 270	−0.36 ± 0.13	2.28	5.9 ± 1.5	11
J19511+464[1]	G 208-042	19:51:09.32	+46:29:00.2	8.586 ± 0.023	M4.0V	3177 ± 39	4210 ± 620	+0.16 ± 0.19	0.59	22.1 ± 0.9	14
J22012+283[1]	V374 Peg	22:01:13.12	+28:18:24.9	7.635 ± 0.026	M4.0V	3195 ± 29	3630 ± 880	+0.03 ± 0.11		36.9 ± 0.7	11
J23548+385	RX J2354.8+3831	23:54:51.46	+38:31:36.2	8.937 ± 0.034	M4.0V	3263 ± 16	4900 ± 130	−0.55 ± 0.09	4.80	3.6 ± 1.5	12
J04153-076	omi02 Eri C	04:15:21.54	-07:39:20.7	6.747 ± 0.020	M4.5V	3179 ± 61	3020 ± 140	−0.30 ± 0.17	8.56	2.1 ± 1.5	50
J04173+088	LTT 11392	04:17:18.53	+08:49:22.0	9.030 ± 0.026	M4.5V	3100 ± 50		0.00	0.37	35.3 ± 3.5	39
J07446+035[1]	YZ CMi	07:44:40.17	+03:33:08.9	6.581 ± 0.024	M4.5V	2908 ± 98	4540 ± 150	−0.39 ± 0.24	2.78	4.0 ± 1.5	51
J07558+833	GJ 1101	07:55:53.93	+83:23:04.9	8.744 ± 0.026	M4.5:V	3252 ± 55	3610 ± 480	−0.24 ± 0.21	1.11	12.1 ± 1.5	14
J13005+056	FN Vir	13:00:33.52	+05:41:08.0	8.553 ± 0.035	M4.5V	3158 ± 38	3830 ± 620	−0.36 ± 0.11	0.60	16.4 ± 1.6	12
J18075-159	GJ 1224	18:07:32.84	-15:57:47.1	8.639 ± 0.024	M4.5V	3220 ± 22	3190 ± 160	−0.37 ± 0.13		2.2 ± 1.5	9
J18189+661[1]	LP 71-165	18:18:57.23	+66:11:33.3	8.740 ± 0.021	M4.5V	3172 ± 45	3960 ± 740	−0.46 ± 0.16	0.52	15.3 ± 1.5	13
J22231-176	LP 820-012	22:23:07.00	-17:36:26.3	8.242 ± 0.027	M4.5V	3228 ± 19	2150 ± 240	−0.12 ± 0.14	4.57	2.0	12
J01019+541	G 218-020	01:01:59.49	+54:10:57.7	9.778 ± 0.022	M5.0V	3070 ± 13		−0.20 ± 0.06		30.6 ± 3.1	21
J01033+623[1]	V* V388 Cas	01:03:19.84	+62:21:55.8	8.611 ± 0.027	M5.0V	3057 ± 49		−0.24 ± 0.24	1.02	10.5 ± 1.5	13
J04472+206[1]	RX J0447.2+2038	04:47:12.25	+20:38:10.8	9.380 ± 0.022	M5.0V	2943 ± 98	6230±1540	−0.06 ± 0.04		47.6±26.8	12
J07051-101	2MASS J07051194-1007528	07:05:11.96	-10:07:52.8	10.196 ± 0.024	M5.0V	3100 ± 50		0.00			5
J09449-123[1]	G 161-071	09:44:54.19	-12:20:54.4	8.496 ± 0.024	M5.0V	2842 ± 99	4860 ± 990	−0.14 ± 0.07	0.44	31.2 ± 3.1	10
J10584-107	LP 731-076	10:58:27.99	-10:46:30.5	9.512 ± 0.023	M5.0V	3218 ± 23	4100 ± 170	−0.31 ± 0.17		3.2 ± 1.5	53
J11474+667	1RXS J114728.8+664405	11:47:28.57	+66:44:02.7	9.684 ± 0.022	M5.0V	3171 ± 14	4770 ± 140	−0.42 ± 0.19	13.30	2.7 ± 1.5	54
J12189+111[1]	GL Vir	12:18:59.40	+11:07:33.8	8.525 ± 0.027	M5.0V	3064 ± 32	3970 ± 460	−0.27 ± 0.22		15.5 ± 1.6	13
J13102+477	G 177-025	13:10:12.63	+47:45:18.7	9.584 ± 0.020	M5.0V	3221 ± 21	2290 ± 170	−0.25 ± 0.13	29.06	2.0	34
J14173+454[1]	RX J1417.3+4525	14:17:22.10	+45:25:46.0	9.467 ± 0.019	M5.0V	3222 ± 24	5850 ± 500	−0.51 ± 0.07	0.37	15.9 ± 1.6	12
J15499+796[1]	LP 022-420	15:49:55.14	+79:39:51.6	9.721 ± 0.021	M5.0V	3095 ± 15	3240±1040	−0.17 ± 0.09	0.19	26.9 ± 2.7	15
J16313+408[1]	G 180-060	16:31:18.79	+40:51:51.7	9.461 ± 0.023	M5.0V	3170 ± 42	4170 ± 380	−0.47 ± 0.11	0.51	7.1 ± 1.5	14
J18022+642[1]	LP 071-082	18:02:16.60	+64:15:44.2	8.541 ± 0.024	M5.0V	3213 ± 43	4930 ± 310	−0.46 ± 0.15	0.28	11.3 ± 1.5	28
J18482+076	G 141-036	18:48:17.54	+07:41:21.2	8.853 ± 0.024	M5.0V	3175 ± 39	1190 ± 230	−0.12 ± 0.13		2.4 ± 1.5	54
J19422-207	2MASS J19421282-2045477	19:42:12.82	-20:45:48.0	9.598 ± 0.024	M5.1V	3241 ± 54	3840 ± 350	−0.49 ± 0.1	1.34	6.2 ± 1.5	12
J20093-012[1]	2MASS J20091824- 01133774	20:09:18.25	-01:13:38.3	9.403 ± 0.026	M5.0V	3301 ± 90	3670 ± 190	−0.51 ± 0.15	1.37	4.3 ± 1.5	12
J15305+094	NLTT 40406	15:30:30.33	+09:26:01.4	9.569 ± 0.025	M5.5V	3073 ± 15	4780 ± 600	−0.29 ± 0.08		16.3 ± 1.6	6
J22114+409	1RXS J221124.3+410000	22:11:24.16	+40:59:58.7	9.725 ± 0.020	M5.5V	3132 ± 30	1880 ± 210	−0.04 ± 0.12		2.0	56
J10564+070	CN Leo	10:56:28.92	+07:00:53.0	7.085 ± 0.024	M6.0V	3071 ± 24	3010 ± 160	−0.05 ± 0.2		2.0	77

KarmnID	Name	α [J2000]	δ [J2000]	J [mag]	Sp. Type	$T_{\rm eff}$ [K]	Mag.Field $\langle B \rangle$ [2] [G]	[Fe/H] [dex]	$P_{\rm rot}$ [3] [d]	vsini [$km s^{-1}$]	Avail. spectra
J14321+081	LP 560-035	14:32:08.51	+08:11:31.2	10.108 ± 0.024	M6.0V	3161 ± 86	2840 ± 370	−0.08 ± 0.32		6.3 ± 1.5	22
J08298+267[1]	DX Cnc	08:29:49.35	+26:46:33.6	8.235 ± 0.021	M6.5V	2997 ± 49	2680 ± 440	+0.01 ± 0.19		10.5 ± 1.5	25
J09003+218	LP 368-128	09:00:23.55	+21:50:04.9	9.436 ± 0.020	M6.5V	3061 ± 43	4270 ± 370	+0.00 ± 0.18		14.3 ± 1.5	21
J09033+056	NLTT 20861	09:03:20.96	+05:40:14.6	10.766 ± 0.024	M7.0V	3027 ± 19	3220 ± 480	−0.25 ± 0.12		9.7 ± 1.5	29
J16555-083[1]	VB 8	16:55:35.26	-08:23:40.8	9.776 ± 0.029	M7.0V	3005 ± 21	3020 ± 200	−0.04 ± 0.09		5.4 ± 1.5	128
J02002+130	TZ Ari	02:00:12.96	+13:03:07.0	7.514 ± 0.017	M3.5:V	3237 ± 32		−0.25 ± 0.14	2.00	2.0	59
J01339-176	LP 768-113	01:33:58.00	-17:38:23.8	8.842 ± 0.025	M4.0V	3376 ± 34		−0.13 ± 0.08	7.75	2.0	31
J23431+365	GJ 1289	23:43:06.31	+36:32:13.1	8.110 ± 0.029	M4.0V	3301 ± 30	1360 ± 190	−0.10 ± 0.1		2.0	18
J01125-169	YZ Cet	01:12:30.64	-16:59:56.4	7.258 ± 0.020	M4.5V	3228 ± 46		−0.39 ± 0.2	70.10	2.0	48
J09005+465	GJ 1119	09:00:32.48	+46:35:11.1	8.604 ± 0.023	M4.5V	3293 ± 30		−0.03 ± 0.08		2.0	7
J10238+438	LP 212-062	10:23:51.86	+43:53:33.1	10.039 ± 0.022	M5.0V	2900 ± 50		0.00			7
J02164+135	LP 469-206	02:16:29.85	+13:35:12.8	9.871 ± 0.021	M5.5V	2800 ± 50		0.00		12.4	8
J08413+594	LP 090-018	08:41:20.13	+59:29:50.4	9.615 ± 0.023	M5.5V	3141 ± 38	1280 ± 210	−0.07 ± 0.16		2.0	173
J14578+566	GJ 1187	14:57:53.73	+56:39:24.5	10.207 ± 0.029	M5.5V	3000 ± 50		0.00		8.6 ± 0.1	7
J23351-023	GJ 1286	23:35:10.46	-02:23:20.6	9.148 ± 0.021	M5.5V	3136 ± 38	910 ± 160	−0.13 ± 0.17		2.0	72
J10482-113	LP 731-058	10:48:12.61	-11:20:09.6	8.857 ± 0.021	M6.5V	3029 ± 25		−0.08 ± 0.17		2.1 ± 1.5	78
J05394+406	LSR J0539+4038	05:39:24.80	+40:38:42.8	11.109 ± 0.021	M8.0V	2600 ± 50	1830 ± 380	0.00		4.1 ± 1.5	18
J19169+051S[1]	V1298 Aql	19:16:57.61	+05:09:01.6	9.908 ± 0.025	M8.0V	2600 ± 50	1210 ± 180	0.00		2.7 ± 2.7	41
J04198+425	LSR J0419+4233	04:19:52.13	+42:33:30.4	11.094 ± 0.022	M8.5V	2400 ± 38		0.00	0.99	3.6 ± 2.3	32
J04167-120	LP 714-47	04:16:45.60	-12:05:02.5	9.493 ± 0.024	M0.0V	3961 ± 13	650 ± 140	+0.15 ± 0.04			34
J05365+113[1]	V2689 Ori	05:36:30.99	+11:19:40.3	6.126 ± 0.023	M0.0V	4067 ± 14	1110 ± 60	+0.01 ± 0.03	11.75	3.8 ± 1.5	128
J09143+526	HD 79210	09:14:22.77	+52:41:11.8	4.889 ± 0.037	M0.0V	4015 ± 16	400 ± 50	−0.12 ± 0.05	17.54	2.9 ± 1.2	28
J09144+526	HD 79211	09:14:24.68	+52:41:10.9	4.779 ± 0.174	M0.0V	3983 ± 12	340 ± 40	−0.03 ± 0.04	16.88	2.3 ± 1.5	48
J11423+230	LP 375-23	11:42:18.37	+23:01:36.7	8.649 ± 0.026	M0.5V	3868 ± 4		−0.08 ± 0.03			87
J15598-082	BD-07 4156	15:59:53.38	-08:15:11.5	7.185 ± 0.030	M1.0V	3707 ± 14	520 ± 100	−0.02 ± 0.04		2.0	15
J00403+612	2MASS J00402129+6112490	00:40:21.29	+61:12:49.1	10.154 ± 0.024	m1.5V	3709 ± 11		+0.00 ± 0.03			17
J01026+623	BD+61 195	01:02:38.87	+62:20:42.2	6.230 ± 0.021	M1.5V	3791 ± 19		+0.05 ± 0.06	18.82	2.0	83
J09163-186	LP 787-052	09:16:20.64	-18:37:32.9	7.351 ± 0.021	M1.5V	3697 ± 14	740 ± 150	−0.03 ± 0.06		2.0	5
J02489-145W	PM J02489-1432W	02:48:59.27	-14:32:14.9	9.528 ± 0.042	m2.0V	3655 ± 25		+0.04 ± 0.05			34
J03217-066	G 77-046	03:21:46.92	-06:40:24.2	7.857 ± 0.026	M2.0V	3661 ± 17	930 ± 110	+0.01 ± 0.04	21.00	2.0	11
J09425+700	GJ 360	09:42:34.84	+70:02:02.0	6.917 ± 0.018	M2.0V	3547 ± 23	1030 ± 110	+0.00 ± 0.03		2.0	35
J11026+219	DS Leo	11:02:38.34	+21:58:01.7	6.522 ± 0.020	M1.0V	3846 ± 84	1040 ± 60	−0.20 ± 0.14	14.26	2.6 ± 1.5	51
J18174+483	TYC 3529-1437-1	18:17:25.13	+48:22:02.3	7.770 ± 0.017	M2.0V	3692 ± 300	1910 ± 100	−0.32 ± 0.11	15.83	2.0	68
J09133+688	G 234-57A	09:13:23.86	+68:52:31.0	7.775 ± 0.019	M2.5V	3900 ± 168		−0.25 ± 0.09		2.0	16
J20305+654	GJ 793	20:30:32.05	+65:26:58.4	6.735 ± 0.021	M2.5V	3514 ± 23	220 ± 110	−0.03 ± 0.06		2.0	53
J09428+700	GJ 362	09:42:51.73	+70:02:21.9	7.326 ± 0.020	M3.0V	3504 ± 30	1390 ± 140	+0.02 ± 0.05	24.33	2.0	18
J16102-193	K2-33	16:10:15	-19:19:09.4	11.095 ± 0.023	M3.0	3365 ± 72		−0.02 ± 0.07		7.3 ± 1.5	23
J13300-087	Ross 476	13:30:02.80	-08:42:25.5	9.599 ± 0.022	M4.0V	3100 ± 50		0.00			7
J06594+193	GJ 1093	06:59:28.82	+19:20:55.9	9.160 ± 0.024	M5.0V	3146 ± 38	390 ± 120	−0.10 ± 0.19		2.0	26
J23419+441	HH And	23:41:55.04	+44:10:38.8	6.884 ± 0.026	M5.0V	3186 ± 41	410 ± 100	+0.04 ± 0.17		2.0	49
Total number of spectra available											3428

(1) Stars in the RV-loud sample of L. Tal-Or et al. (2018), with data from A. Reiners et al. (2018)

Reference Stars for Spectral Subtraction

The reference stars used in this work are those presented in P. Schöfer et al. (2019). For each spectral subtype, the selected reference star corresponds to the object within the CARMENES GTO sample with the longest known rotation period $P_{\rm rot}$. This choice is motivated by the well-established relationship between chromospheric activity and stellar rotation (S. Mohanty et al., 2002; E. R. Newton et al., 2017; S. V. Jeffers et al., 2018), under the assumption that stars with the longest rotation periods are the least active representatives of their respective spectral types. For stars of spectral type later than M6.0 is almost impossible to obtain reference stars showing little or null activity. So from the large number of spectra of Teegarden's Star obtained for M. Zechmeister et al. (2019), it has been possible to select one spectrum in a relatively quiescent phase, in order to perform the spectral subtraction technique.

Table 6. Catalogue of Reference Stars. Values taken from P. Schöfer et al. (2019)

KarmnID	Name	α [$J2000$]	δ [$J2000$]	J [mag]	Sp.Type	Teff [($\pm$51) K]	EW(Hα) [Å^{-1}]	[Fe/H] dex
J14257+236W	BD+24 2733A	14:25:43.49	+23:37:01.1	6.769	M0.0V	4024	0.000	+0.07
J18051-030	HD 165222	18:05:07.56	−03:01:52.4	6.161	M1.0V	3663	0.000	−0.20
J16254+543	GJ 625	16:25:24.59	+54:18:14.9	6.608	M1.5V	3525	0.000	−0.28
J04429+189	HD 285968	04:42:55.81	+18:57:28.5	6.462	M2.0V	3574	0.003	+0.00
J15194-077	HO Lib	15:19:26.89	−07:43:20.1	6.706	M3.0V	3441	0.000	−0.08
J17578+046	Barnard's Star	17:57:48.49	+04:41:40.5	5.244	M3.5V	3273	0.000	−0.57
J11477+008	FI Vir	11:47:44.40	+00:48:16.4	6.505	M4.0V	3264	0.000	−0.10
J19216+208	GJ 1235	19:21:38.68	+20:52:02.8	8.796	M4.5V	3059	0.000	−0.17
J03133+047	CD Cet	03:13:22.99	+04:46:29.4	8.775	M5.0V	3204	0.000	−0.06
J00067-075	GJ 1002	00:06:43.26	−07:32:14.7	8.323	M5.5V	3061	0.000	−0.15
J07403-174	LP 783-002	07:40:19.22	−17:24:44.9	10.155	M6.0V	2964	0.000	+0.04
J02530+168	Teegardens Star	02:53:00.89	+16:52:52.6	8.390	M7.0V	3034	−0.500	−0.11

For comparison and confirmation purposes, it has been incorporated the mean flux values of FGKM stars taken from R. Martínez-Arnáiz et al. (2011). There, (B-V) values were used instead of $T_{\rm eff}$. So, they must be *translated* to the current study calculations, to obtain $L_{\rm Line}/L_{\rm Bol}$ implementing the χ-factor methodology.

Instead of using the conversions provided in D. A. Golimowski et al. (2004), as it is widely done in previous studies, the more recent data of M. J. Pecaut & E. E. Mamajek (2013)[1] has been followed to obtain a conversion function. The subset of (B-V) values range of [0.295, 2.170] in this reference, equivalent to a range of spectral types from F0 to M9, can be used to perform a polynomial fit:

$$T_{\rm eff} = P_n((B-V)) \tag{1}$$

and making n=5, the parameters of Table 8 are obtained. This polynomial fit has then been incorporated as a special function to the processing SW. Doing so computational resources are saved in regard to the application of a interpolation schema.

Table 8. Polynomial fit $T_{\rm eff} = P_5(B-V)$ from data of M. J. Pecaut & E. E. Mamajek (2013)

Coefficient	Value	Std. Error
a	10348.7	4.0370e+02
b	−15608.6	2.3086e+03
c	22479.1	4.7448e+03
d	−18763.4	4.4273e+03
e	7518.7	1.9112e+03
f	−1.139.2	3.0990e+02
Adj. Param.R^2	0.9982	

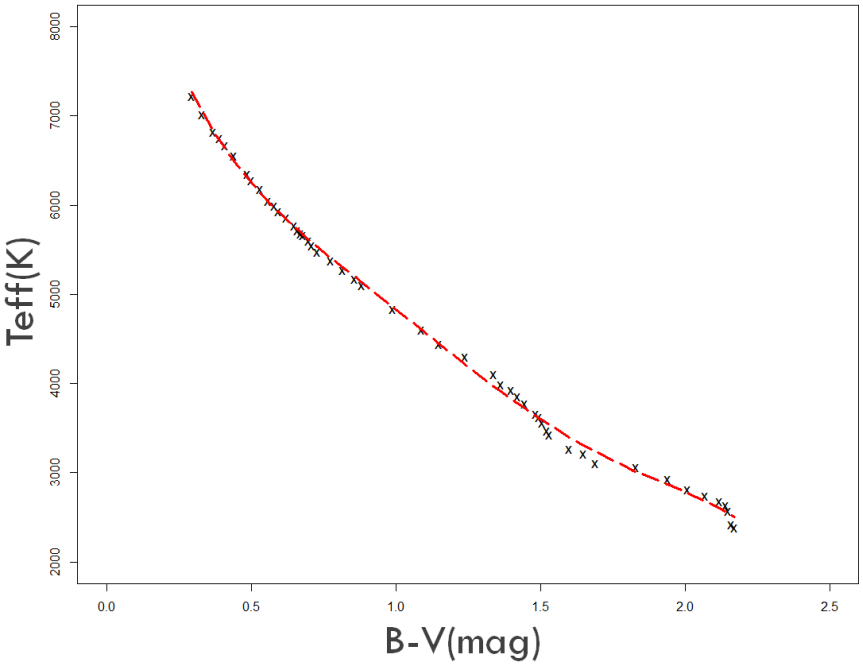

Figure 5. Fit B-V vs $T_{\rm eff}$ to transform literature values of R. Martínez-Arnáiz et al. (2011) to present paper calculations. From data of M. J. Pecaut & E. E. Mamajek (2013), compatible with Fig. 3 of the more precise calibration, but functionally complex, of M. Sekiguchi & M. Fukugita (2000). The values provided are the black crosses, while the red dashed line is the performed fit.

[1]Data used of the updated version (2022.04.16) of Table 5, downloaded from "Stellar Color/Teff Table" in `http://www.pas.rochester.edu/~emamajek/EEM_dwarf_UBVIJHK_colors_Teff`

Flux Data of Catalogue Stars

Table 9 presents the merged datasets containing all individual of chromospheric activity indicators for the analyzed sample of M-type stars. Each multicolumn group corresponds to a specific spectral region or activity indicator, while the columns within each group provide, the first the measured line luminosity normalized to bolometric luminosity and the second, its associated uncertainty. Blank cells indicate epochs for which no useful data were available in a given dataset. This comprehensive table serves as the foundation for the subsequent analysis of stellar activity trends performed in Section 3.

The calculated fluxes are based on the EWs measured from CARMENES spectra (see e.g. I. Ribas et al. 2023). The relation between the line luminosity normalized to bolometric luminosity the measured EW is given by

$$log\left(\frac{L_{\rm line}}{L_{\rm Bol}}\right) = log(\chi) + log(EW) \tag{2}$$

where the χ-factor is used to convert the measured equivalent width into the corresponding flux ratio. The χ-factor methodology described by L. M. Walkowicz et al. (2004); A. Reiners & G. Basri (2008) was applied as outlined in Section 2.

Table 9. Collected line luminosities normalized to bolometric luminosity by star and MJD. Blank cells indicate missing data.

// Star	MJD	Hα		Ca II IRT-a		Ca II IRT-b		He I D_3		Na I D_2		Paβ		Paδ	
		$log\left(\frac{L_{line}}{L_{Bol}}\right)$	δ	$log\left(\frac{L_{line}}{L_{Bol}}\right)$	δ	$log\left(\frac{L_{line}}{L_{Bol}}\right)$	δ	$log\left(\frac{L_{line}}{L_{Bol}}\right)$	δ	$log\left(\frac{L_{line}}{L_{Bol}}\right)$	δ	$log\left(\frac{L_{line}}{L_{Bol}}\right)$	δ	$log\left(\frac{L_{line}}{L_{Bol}}\right)$	δ
J12156+526	57449	-3.52925	-0.00056	-4.92495	0.06685	-4.8289	0.07498	-4.8467	0.0715	-4.87423	0.072				
J12156+526	57488.99788	-3.63017	-0.00078	-4.86551	0.06987	-4.76359	0.07708	-4.87784	0.06093	-5.0262	0.06241				
J12156+526	57511.94105	-3.65015	-0.00076	-4.81555	0.07206	-4.85154	0.07418	-4.95278	0.06549	-4.67848	0.07813				
J12156+526	57529.92663	-3.60652	-0.00076	-4.57481	0.07969	-4.79564	0.077	-4.68576	0.07416	-4.486	0.07515				
J12156+526	57557.93039	-3.5929	-0.00072	-5.01458	0.06163	-4.78795	0.07633	-4.84132	0.06725	-4.77455	0.06866				
J12156+526	57747.16475	-3.55512	-0.00069	-4.745	0.07475	-4.80529	0.07583	-4.84382	0.06937	-4.74704	0.07302				
J12156+526	57752.25231	-3.69081	-0.00089	-4.93556	0.06628	-4.95364	0.06999	-5.14752	0.04793	-4.87246	0.05532				
J12156+526	57755.13126	-3.66821	-0.00086	-4.83986	0.07097	-4.91922	0.07151	-4.88603	0.06761	-4.75334	0.07426				
J12156+526	57760.20877	-3.66136	-0.00087	-4.94608	0.06577	-4.95742	0.06981	-5.12395	0.04442	-4.78642	0.06886				
J12156+526	57801.03313	-3.63999	-0.00068	-5.02496	0.06094	-4.86856	0.07355	-4.89251	0.07074	-4.73586	0.07662				
J12156+526	57813.98907	-3.61025	-0.00058	-4.81027	0.07295	-4.93826	0.07145	-4.8856	0.0728	-4.71794	0.07924				
J05084-210	57754.92514	-3.5623	-0.00057	-4.9695	0.2725	-4.70257	0.28709								
J05084-210	57759.89999	-3.52168	-0.00053	-5.02719	0.26824	-4.78586	0.28398			-5.1735	0.25635				
J05084-210	57761.89316	-3.58334	-0.00061	-5.1558	0.2567	-4.83339	0.28189	-5.46607	0.23678	-5.21426	0.25192				
J05084-210	58034.15906	-3.61076	-0.00062	-5.2131	0.2502	-4.83616	0.28176			-5.22824	0.25124				
J05084-210	58050.13464	-3.58947	-0.00061	-4.87261	0.27835	-4.98741	0.27333			-4.64657	0.28917				
J05084-210	58052.08864	-3.56669	-0.00059	-5.03363	0.26795	-4.79722	0.28346			-5.28353	0.24576				
J05084-210	58056.11427	-3.49134	-0.00049	-4.9891	0.27127	-4.76929	0.28465	-5.53315	0.23443	-4.97772	0.27389				
J05084-210	58059.09531	-3.52394	-0.00053	-4.84981	0.27961	-4.76624	0.28473			-4.99508	0.27207				
J05084-210	58092.02434	-3.58937	-0.00063	-5.41197	0.22081	-4.80056	0.28331								
J05084-210	58094.01065	-3.08563	-0.00029	-4.40315	0.29404	-4.39445	0.29467			-4.85828	0.27988			-4.39649	0.28753
J05084-210	58109.95193	-3.47286	-0.0005	-5.29458	0.24004	-4.8182	0.28258			-5.04058	0.26838				
J05084-210	58111.95446	-3.33656	-0.00037	-5.16625	0.25579	-4.82654	0.28216			-5.16902	0.25726				
J05084-210	58135.86432	-3.52918	-0.00055	-4.79666	0.28235	-4.76417	0.28486	-5.45853	0.23445	-5.14531	0.25996				
J05084-210	58391.17209	-3.43892	-0.00051	-5.00963	0.26978	-4.76049	0.28496			-5.21474	0.25439				
J05084-210	58396.17503	-3.5072	-0.00052	-4.98986	0.27128	-4.68868	0.28759			-4.78249	0.28438				
J05084-210	58426.09754	-3.60604	-0.00063	-5.09494	0.26287	-4.77942	0.28424	-5.45869	0.22686	-5.27067	0.24546				
J05084-210	58434.08257	-3.51193	-0.00051	-4.85998	0.27917	-4.61313	0.28989	-4.97633	0.27924	-3.89765	0.29961				
J05084-210	58450.0361	-3.62077	-0.00067	-5.00527	0.2701	-4.74365	0.28565	-5.49213	0.22044	-4.97109	0.27339				
J05084-210	58458.0411	-3.63412	-0.00068	-5.12298	0.26017	-4.72297	0.28637	-5.4524	0.23997						
J05084-210	58469.9868	-3.64697	-0.00068	-5.38782	0.22503	-4.8861	0.2793								
J05084-210	58475.96651	-3.44023	-0.00047	-5.22002	0.24981	-4.90768	0.27809			-4.82623	0.28186				
J05084-210	58483.95443	-3.31592	-0.00035	-5.18474	0.25378	-4.65675	0.28858								
J05084-210	58489.9203	-3.69801	-0.00077	-5.06599	0.26532	-4.76639	0.28473	-5.51026	0.22621	-5.24259	0.24954				
J05084-210	58494.89777	-3.46779	-0.00049	-5.04801	0.26688	-4.74531	0.28555								
J11055+435	57418	-3.8337	-0.0015	-5.44215	0.02031	-5.25438	0.03854			-4.37011	0.06167				
J11055+435	57472.03545	-3.61407	-0.00091	-5.11998	0.04762	-5.00515	0.05927	-4.7174	0.05689	-4.62505	0.04896				
J11055+435	57502.97557	-3.57655	-0.00084	-5.00123	0.0512	-4.97579	0.06031	-4.56748	0.06039	-4.30127	0.06657				
J11055+435	57529.8644	-3.72774	-0.00118	-5.16339	0.03581	-5.11393	0.05432			-4.38335	0.06467				
J11055+435	57557.88002	-3.65064	-0.00099	-5.06727	0.0558	-5.00111	0.05977	-4.49591	0.06244	-4.41469	0.06472				
J11055+435	57748.1985	-3.58907	-0.00085	-5.20584	0.0484	-5.01461	0.05995	-4.62061	0.06195	-4.33884	0.06651				
J11055+435	57754.17961	-3.69958	-0.00099	-5.39445	0.01475	-5.18936	0.05202	-4.70136	0.05952	-4.39411	0.06378				
J11055+435	57763.17222	-3.58648	-0.00085	-5.38748	0.02761	-5.06756	0.05817	-4.64869	0.05867	-4.53925	0.06456				
J11055+435	57766.17244	-3.56427	-0.00081	-5.56206	-0.02226	-5.16973	0.05349	-4.85208	0.0525	-4.44715	0.06049				
J11055+435	57787.0886	-3.61536	-0.00093	-5.20001	0.04098	-5.06705	0.05691	-4.70595	0.05594	-4.21953	0.06456				
J11055+435	57801.00962	-3.3969	-0.00045	-5.28165	0.04356	-5.07788	0.05921	-4.56346	0.06437	-4.29667	0.0685				
J11055+435	57813.91903	-3.4187	-0.00046	-5.02357	0.05952	-5.03114	0.06062	-4.57958	0.06384	-4.42223	0.06717				
J11055+435	57819.17485	-3.61788	-0.00088	-5.32032	0.02267	-5.04948	0.05796	-4.61702	0.05935	-4.41203	0.05931				
J11055+435	57820.97231	-3.52712	-0.00055	-4.94836	0.06024	-4.9474	0.0635	-4.63829	0.0647	-4.14713	0.0704				
J11055+435	57822.91579	-3.58317	-0.00064	-5.25321	0.03667	-5.17796	0.05652	-4.70141	0.06297	-4.40443	0.06802				
J11055+435	57831.94119	-3.53036	-0.00064	-5.163	0.05145	-5.12484	0.05686	-4.52488	0.06413	-4.34671	0.06732				
J11055+435	57847.98522	-3.58133	-0.00077	-5.05801	0.05608	-4.98566	0.06086	-4.48376	0.0653	-4.35333	0.06738				
J11055+435	57852.98405	-3.66461	-0.0009	-5.61517	-0.02533	-5.13253	0.054	-4.78056	0.05772	-4.51903	0.05844				
J11055+435	57890.88638	-3.74611	-0.00125	-5.28342	0.02369	-5.18082	0.05331			-4.36594	0.06517				
J17338+169	57499.10519	-3.56782	0.00021	-4.82345	0.07066	-4.78721	0.07392	-5.24989	0.03386	-5.13753	0.04134				
J17338+169	57528.08331	-3.59414	0.00014	-4.9048	0.06574					-5.07711	0.05635				
J17338+169	57558.01363	-3.59214	0.00016	-4.99303	0.05945	-4.94837	0.0649								
J17338+169	57570.96625	-3.63253	6e-05	-5.36218	0.01304	-4.957	0.06432	-5.41967	0.01403	-5.03686	0.06107				
J17338+169	57602.87785	-3.45267	0.00033	-4.79398	0.0721	-4.77509	0.07447	-5.37079	0.02939	-5.08397	0.06126				
J17338+169	57802.19513	-3.55702	0.00024	-4.90352	0.06588	-4.78799	0.07388	-5.18677	0.05274	-4.79721	0.07234				
J17338+169	57818.19657	-3.63679	0.00014	-5.13262	0.04636	-5.01853	0.0598	-5.57537	0.02288						

Continued on next page

// Star	MJD	Hα		Ca II IRT-a		Ca II IRT-b		He I D_3		Na I D_2		Paβ		Paδ	
		$log\left(\frac{L_{line}}{L_{Bol}}\right)$	δ	$log\left(\frac{L_{line}}{L_{Bol}}\right)$	δ	$log\left(\frac{L_{line}}{L_{Bol}}\right)$	δ	$log\left(\frac{L_{line}}{L_{Bol}}\right)$	δ	$log\left(\frac{L_{line}}{L_{Bol}}\right)$	δ	$log\left(\frac{L_{line}}{L_{Bol}}\right)$	δ	$log\left(\frac{L_{line}}{L_{Bol}}\right)$	δ
J17338+169	57821.18485	-3.58877	0.00024	-4.94519	0.06299	-4.71852	0.07685	-5.49521	0.03768	-4.97008	0.08942				
J17338+169	57823.17747	-3.48028	0.00045	-4.67168	0.07893	-4.60397	0.08115	-5.10167	0.07245	-4.85359	0.08152				
J17338+169	57833.15373	-3.54308	0.00023	-5.43275	-0.00106	-5.05943	0.05643	-5.3698	0.03426	-4.92225	0.08811				
J20451-313	58678.05758	-3.68406	-0.00046	-4.27218	0.10429	-4.23117	0.10447	-5.04517	0.09051	-5.06952	0.07936	-3.94297	0.09078	-5.46393	0.07416
J20451-313	58678.06251	-3.68947	-0.00047	-4.2731	0.1043	-4.26094	0.10436	-4.97286	0.09339	-4.9002	0.08796	-3.94293	0.09078	-5.60404	0.06204
J20451-313	58679.02686	-3.36395	-0.00024	-4.02639	0.10505	-3.84473	0.10537	-4.36662	0.10365	-4.3813	0.10404	-3.03839	0.10255	-3.95692	0.10302
J20451-313	58679.03162	-3.33843	-0.00023	-4.0219	0.10506	-3.83277	0.10538	-4.38386	0.10352	-4.41807	0.10389	-3.07095	0.10249	-3.9949	0.10292
J20451-313	58680.02227	-3.57367	-0.00036	-4.25317	0.10438	-4.17096	0.10466	-4.90543	0.09454	-4.95803	0.08539	-3.78156	0.0954	-5.40474	0.04987
J20451-313	58680.03216	-3.5788	-0.00036	-4.25298	0.10439	-4.17777	0.10462	-4.90649	0.09451	-5.34178	0.05613	-3.81762	0.09448	-5.38825	0.05196
J20451-313	58684.05787	-3.86019	-0.00069	-4.34467	0.10407	-4.3507	0.10395	-5.26585	0.07963	-4.68762	0.09494			-5.5758	0.06481
J20451-313	58684.06264	-3.85299	-0.00068	-4.34772	0.10404	-4.35243	0.10394	-5.12746	0.08683	-5.25385	0.06527			-5.71167	0.04968
J20451-313	58686.03792	-3.80799	-0.00062	-4.34408	0.104	-4.29578	0.10419	-5.32306	0.07592	-5.28484	0.06226			-5.72443	0.048
J20451-313	58686.04243	-3.79816	-0.0006	-4.33782	0.10403	-4.28958	0.10422	-5.21397	0.0826	-5.10993	0.07676	-3.93908	0.09107	-5.48127	0.07287
J20451-313	58687.06846	-3.81333	-0.00061	-4.34691	0.10399	-4.31104	0.10413	-5.29702	0.07767	-5.13617	0.07494	-4.05847	0.08641	-5.54586	0.06755
J20451-313	58687.07298	-3.80484	-0.0006	-4.35735	0.10394	-4.32324	0.10409	-5.08186	0.08874	-5.42614	0.04544	-3.95913	0.09042	-5.60679	0.06176
J20451-313	58688.06959	-3.79501	-0.00059	-4.32343	0.10413	-4.27423	0.10427	-4.99494	0.09182	-4.6394	0.0961			-5.89266	0.02056
J20451-313	58688.08316	-3.76741	-0.00051									-3.98855	0.08972	-5.71209	0.04962
J20451-313	58690.04664	-3.70586	-0.00048	-4.26899	0.1044	-4.18242	0.10466	-4.80837	0.10003	-5.07241	0.09773	-3.88118	0.09267	-5.81377	0.03475
J20451-313	58690.05145	-3.70162	-0.00047	-4.26516	0.10441	-4.15709	0.10474	-4.89415	0.09869			-3.98406	0.0891	-5.78098	0.03993
J20451-313	58690.99451	-3.84712	-0.00068	-4.36542	0.10384	-4.33151	0.10388	-5.43277	0.06727	-4.80588	0.09148	-3.78046	0.09543	-5.88006	0.023
J20451-313	58690.9999	-3.89556	-0.00075	-4.35738	0.1039	-4.35508	0.10382	-5.30187	0.07735	-4.76714	0.09275	-3.82264	0.09435	-5.70667	0.05032
J20451-313	58693.03857	-3.83291	-0.00064	-4.34332	0.10404	-4.30193	0.1042	-5.20466	0.0831			-4.07404	0.08521	-5.8886	0.02135
J20451-313	58693.04377	-3.83125	-0.00064	-4.34282	0.10419	-4.3225	0.1041	-5.1021	0.08791			-3.9876	0.08913	-5.89729	0.02142
J20451-313	58694.08506	-3.8323	-0.00064	-4.33034	0.10408	-4.2951	0.1042	-5.38535	0.07116	-4.86158	0.08949	-4.07311	0.08519	-5.84244	0.02989
J20451-313	58694.09012	-3.8301	-0.00063	-4.33431	0.10406	-4.26452	0.1043	-5.33737	0.07481	-4.85771	0.08964	-3.90755	0.09179		
J20451-313	58695.02809	-3.91849	-0.00078	-4.34819	0.10402	-4.36779	0.10369	-5.27766	0.0789	-4.73343	0.09376			-5.66219	0.05574
J20451-313	58695.03416	-3.86408	-0.00069	-4.36544	0.1039	-4.44157	0.10343			-4.67521	0.0953	-3.98054	0.08924		
J20451-313	58696.01248	-3.83673	-0.00065	-4.35518	0.10391	-4.30979	0.1041	-5.30289	0.07728	-5.16027	0.07317	-3.86114	0.09327	-5.78491	0.03933
J20451-313	58696.01693	-3.84933	-0.00066	-4.36786	0.10387	-4.34573	0.10394	-5.27694	0.07895	-4.8063	0.09147	-3.90323	0.09197	-5.6625	0.05571
J20451-313	58698.00833	-3.87056	-0.0007	-4.34368	0.10404	-4.32507	0.10407	-5.29377	0.07788	-5.02121	0.08216	-3.98965	0.08883	-5.80237	0.0366
J20451-313	58698.01292	-3.83335	-0.00064	-4.33891	0.10406	-4.30713	0.10415	-5.24475	0.08088						
J20451-313	58698.97379	-3.79336	-0.00058	-4.324	0.10409	-4.32516	0.10407	-5.38601	0.07123	-5.01689	0.0824			-5.80074	0.03686
J20451-313	58698.97829	-3.82386	-0.00062	-4.3317	0.10407	-4.27603	0.10427	-5.33901	0.07479	-4.91097	0.08751			-5.7448	0.04521
J20451-313	58699.96672	-3.87635	-0.0007	-4.33371	0.10408	-4.32346	0.10404	-5.29426	0.07775	-5.07875	0.07879				
J20451-313	58699.9713	-3.87724	-0.0007	-4.32737	0.10409	-4.27318	0.10427	-5.40426	0.06961	-5.56445	0.02273			-5.88927	0.02122
J20451-313	58701.99389	-3.76233	-0.00054	-4.28438	0.10424	-4.24088	0.10441	-5.22692	0.08588	-4.94657	0.08593				
J20451-313	58703.97878	-3.76426	-0.00054	-4.29418	0.10428	-4.25017	0.10439	-5.2083	0.08283					-5.7277	0.04756
J20451-313	58703.9843	-3.79012	-0.00057	-4.27773	0.10432	-4.26866	0.10433	-5.14603	0.08592	-5.59905	0.01582	-4.009	0.08846	-5.78063	0.03998
J20451-313	58705.98539	-3.87583	-0.00071	-4.34698	0.10395	-4.36533	0.10268	-5.34368	0.07446	-4.65395	0.09581			-5.60613	0.06183
J20451-313	58705.9965	-3.86038	-0.00068	-4.34425	0.10394	-4.36729	0.10366	-5.49204	0.06161	-4.77612	0.09259			-5.80939	0.03546
J20451-313	58710.93479	-3.72284	-0.00051	-4.28259	0.10425	-4.24283	0.10431	-5.0877	0.09004	-5.53159	0.0288	-3.88826	0.09308		
J20451-313	58710.93962	-3.66778	-0.00044	-4.2977	0.10419	-4.20939	0.10445	-5.01512	0.09605			-3.84761	0.09378		
J20451-313	58711.94244	-3.86236	-0.00069	-4.35693	0.10396	-4.32195	0.10401			-4.84653	0.09006			-5.80702	0.03585
J20451-313	58711.94699	-3.86444	-0.00069	-4.37156	0.10389	-4.28593	0.10417	-5.54581	0.05559	-5.48658	0.0364	-3.96683	0.08976	-5.77112	0.04141
J20451-313	58713.99719	-3.69161	-0.00046	-4.28066	0.10429	-4.19472	0.10456	-5.21917	0.08712	-5.46373	0.03996				
J20451-313	58714.00196	-3.79106	-0.00058	-4.2764	0.10432	-4.23494	0.10443	-5.22719	0.08375	-4.84746	0.09002			-5.81741	0.03415
J20451-313	58714.9439	-3.84119	-0.00066	-4.3557	0.104	-4.30474	0.10416	-5.13977	0.08628			-3.90631	0.09197	-5.66802	0.05506
J20451-313	58714.94888	-3.83003	-0.00064	-4.3552	0.10404	-4.29729	0.10415	-5.15834	0.08541	-5.41872	0.04646	-3.85495	0.09341		
J20451-313	58717.93962	-3.81656	-0.00062	-4.32479	0.10418	-4.22832	0.10448	-5.22437	0.0826	-4.93843	0.0863			-5.7463	0.045
J20451-313	58717.94471	-3.82074	-0.00062	-4.31689	0.10419	-4.23378	0.10446	-5.24078	0.08153	-4.95439	0.08556	-3.97741	0.0893		
J20451-313	58722.95418	-3.82999	-0.00063	-4.33821	0.10408	-4.30947	0.1041	-5.54102	0.05648						
J20451-313	58722.95855	-3.83228	-0.00064	-4.34587	0.10405	-4.29439	0.10415	-5.70747	0.0331	-4.86153	0.0895			-5.86252	0.02628
J20451-313	58723.91027	-3.8119	-0.00061	-4.36181	0.10398	-4.33149	0.10399	-5.79071	0.0177					-5.86521	0.02579
J20451-313	58723.91526	-3.88767	-0.00073	-4.35287	0.10402	-4.31604	0.10406	-5.63337	0.04454	-5.17357	0.07215				
J20451-313	58726.96739	-3.8228	-0.00063	-4.30514	0.10422	-4.27635	0.10421	-5.47977	0.0627					-5.88326	0.02239
J20451-313	58741.88597	-3.78653	-0.00057	-4.299	0.10425	-4.21655	0.10452	-5.16377	0.08748					-5.73897	0.04602
J20451-313	58741.89027	-3.80441	-0.00059	-4.30302	0.10425	-4.20175	0.10457	-5.17883	0.08734			-4.08854	0.08501	-5.81239	0.03498
J20451-313	58742.8609	-3.82972	-0.00063	-4.34347	0.10408	-4.27355	0.10425	-5.46156	0.0649			-4.01	0.08866	-5.92076	0.01485
J20451-313	58742.86531	-3.85176	-0.00066	-4.35956	0.104	-4.27714	0.10424	-5.16244	0.08522					-5.89039	0.021
J20451-313	58743.84435	-3.88016	-0.00071	-4.34426	0.10407	-4.25095	0.10434	-5.40676	0.0694						
J20451-313	58743.84873	-3.86571	-0.00069	-4.3425	0.10406	-4.28649	0.1042	-5.23344	0.08153					-5.8589	0.02695
J20451-313	58744.88619	-3.78651	-0.00058	-4.32703	0.10404	-4.26833	0.10423	-5.12298	0.08741					-5.61735	0.06067
J20451-313	58744.8912	-3.75063	-0.00053	-4.32926	0.10403	-4.2367	0.10437	-5.27976	0.08034					-5.81475	0.03459
J20451-313	58754.89375	-3.74153	-0.00052	-4.32858	0.10407	-4.19926	0.10457	-5.05744	0.09497					-5.84661	0.02915

Continued on next page

// Star	MJD	Hα		Ca II IRT-a		Ca II IRT-b		He I D_3		Na I D_2		Paβ		Paδ	
		$log\left(\frac{L_{line}}{L_{Bol}}\right)$	δ	$log\left(\frac{L_{line}}{L_{Bol}}\right)$	δ	$log\left(\frac{L_{line}}{L_{Bol}}\right)$	δ	$log\left(\frac{L_{line}}{L_{Bol}}\right)$	δ	$log\left(\frac{L_{line}}{L_{Bol}}\right)$	δ	$log\left(\frac{L_{line}}{L_{Bol}}\right)$	δ	$log\left(\frac{L_{line}}{L_{Bol}}\right)$	δ
J20451-313	58756.86725	-3.76412	-0.00055	-4.28138	0.10435	-4.16159	0.10467	-5.06092	0.08955						
J20451-313	58756.87238	-3.78489	-0.00057	-4.29972	0.10426	-4.24552	0.10441	-5.24756	0.08072					-5.22284	0.08773
J20451-313	58758.86225	-3.82683	-0.00063	-4.35512	0.10395	-4.25173	0.10435	-5.1845	0.08414					-5.78894	0.03871
J20451-313	58758.86677	-3.81598	-0.00061	-4.33701	0.10405	-4.2356	0.10443	-5.12803	0.0868					-5.76032	0.043
J20451-313	58759.80163	-3.78328	-0.00057	-4.32829	0.10407	-4.20694	0.10454	-5.06037	0.09257						
J20451-313	58759.80651	-3.76004	-0.00054	-4.31947	0.10411	-4.23246	0.10444	-5.11627	0.08757					-5.68847	0.05261
J20451-313	58760.84353	-3.80533	-0.00059	-4.34582	0.10403	-4.30859	0.10414	-5.34587	0.0743					-5.33967	0.08208
J20451-313	58760.8483	-3.75482	-0.00053	-4.33364	0.10408	-4.23436	0.10443	-5.34159	0.07461					-5.72738	0.0476
J20451-313	58762.82919	-3.81103	-0.0006	-4.31655	0.10418	-4.18037	0.10463	-5.21653	0.08238					-5.853	0.02801
J20451-313	58762.83432	-3.81907	-0.00061	-4.30707	0.10423	-4.21604	0.10452	-5.15275	0.08602					-5.93425	0.01197
J20451-313	58764.82188	-3.691	-0.00046	-4.30665	0.10415	-4.18451	0.10456	-5.10747	0.08763					-5.66123	0.05585
J20451-313	58764.82663	-3.68151	-0.00045	-4.29552	0.1042	-4.1722	0.1046	-5.08505	0.08855					-5.80646	0.03594
J20451-313	58765.82326	-3.73845	-0.00051	-4.26985	0.10436	-4.16637	0.10466	-5.14449	0.08599					-5.69619	0.05165
J20451-313	58765.82811	-3.73235	-0.0005	-4.27963	0.10432	-4.1391	0.10474	-5.15573	0.08554					-5.77339	0.04108
J20451-313	59049.03792	-3.83434	-0.00065	-4.35898	0.10395	-4.31616	0.10411	-5.06301	0.08947					-5.32969	0.08263
J20451-313	59050.05488	-3.86839	-0.0007	-4.37809	0.10388	-4.31521	0.10411	-5.20526	0.08306					-5.36975	0.08037
J20451-313	59051.04034	-3.67032	-0.00044	-4.1981	0.10465	-4.15711	0.10476	-4.85015	0.09782	-5.1673	0.07384			-5.37641	0.08318
J20451-313	59059.0093	-3.80002	-0.0006	-4.34208	0.10403	-4.34005	0.10398	-5.48213	0.06246	-5.51775	0.03122	-3.99026	0.08926	-5.60004	0.06244
J20451-313	59060.05626	-3.83916	-0.00066	-4.35855	0.10393	-4.30023	0.10411			-4.69544	0.09474				
J20451-313	59061.0093	-3.85894	-0.00067	-4.31838	0.10422	-4.34973	0.10403	-5.43322	0.06723	-5.07634	0.07894				
J20451-313	59067.00806	-3.85789	-0.00067	-4.35985	0.10393	-4.30132	0.10414	-5.38081	0.07164	-4.82281	0.0909	-3.98291	0.08965	-5.8498	0.02859
J20451-313	59069.98418	-3.90736	-0.00075	-4.35967	0.10393	-4.3705	0.1037			-4.93548	0.08656	-4.0478	0.08695	-5.86388	0.02604
J20451-313	59075.97176	-3.74496	-0.00052	-4.23546	0.10453	-4.14694	0.10478	-5.06774	0.09347	-5.32574	0.07246	-4.03919	0.0872		
J20451-313	59077.97497	-3.76436	-0.00054	-4.32568	0.10408	-4.27769	0.1043	-5.19267	0.08425					-5.71001	0.04989
J20451-313	59079.00424	-3.81767	-0.00062	-4.33537	0.10408	-4.23202	0.10447	-5.18141	0.08524	-5.53197	0.02873	-3.99271	0.08933		
J20451-313	59080.93558	-3.82522	-0.00063	-4.34302	0.10408	-4.31216	0.10409	-5.34203	0.07468	-5.1486	0.07404	-3.96999	0.08997		
J20451-313	59084.97838	-3.91625	-0.00077	-4.38224	0.1039	-4.33686	0.10398	-5.35648	0.07351	-5.27569	0.06317	-3.95677	0.09092		
J20451-313	59085.96302	-3.88063	-0.00072	-4.3726	0.1039	-4.32491	0.10403	-5.32728	0.07562	-5.00896	0.08283	-3.96767	0.09027	-5.70506	0.05053
J20451-313	59086.94063	-3.87206	-0.0007	-4.3468	0.10399	-4.27176	0.10428	-5.23608	0.08495	-5.37414	0.05227			-5.81709	0.0342
J20451-313	59094.95562	-3.83255	-0.00063	-4.35289	0.10404	-4.28544	0.10417	-5.70949	0.03276			-3.96589	0.09012	-5.77819	0.04035
J20451-313	59097.94071	-3.74785	-0.00053	-4.33072	0.10411	-4.24509	0.10436	-5.41782	0.07023			-3.99356	0.08913	-5.92398	0.01417
J20451-313	59098.9068	-3.85713	-0.00068	-4.39227	0.10377	-4.33865	0.10392	-5.63894	0.04374			-4.05659	0.08676	-5.85123	0.02833
J20451-313	59112.90971	-3.77947	-0.00056	-4.35804	0.10394	-4.22837	0.10445	-5.11388	0.08742	-4.54924	0.09803				
J20451-313	59147.79921	-3.89563	-0.00074	-4.35076	0.10406	-4.17106	0.10469	-4.92829	0.09396	-4.9203	0.08711			-5.8184	0.03399
J20451-313	59153.79522	-3.79154	-0.00057	-4.33878	0.10404	-4.12382	0.10474	-5.3235	0.07579						
J20451-313	59160.77166	-3.51941	-0.00032	-4.03752	0.10505	-3.94623	0.10524	-4.7065	0.10148	-5.01982	0.09847	-3.71671	0.10092	-5.34645	0.05692
J20451-313	59169.75795	-3.86887	-0.00069	-4.36061	0.104	-4.21399	0.1045	-5.22044	0.08281					-5.82393	0.03306
J15218+209	57537.0249	-3.86008	-4.00E-05	-4.41944	0.04421	-4.30586	0.04476	-5.2444	-0.01243	-5.00062	0.03162				
J15218+209	57538.96742	-3.87892	-9.00E-05	-4.43516	0.04411	-4.34067	0.04456	-5.23114	-0.0105	-4.9465	0.03279				
J15218+209	57542.96668	-3.78533	0.00032	-4.33259	0.04519	-4.25455	0.04544	-4.91076	0.03725	-4.76637	0.04082				
J15218+209	57549.9175	-3.85183	-2.00E-05	-4.42517	0.04415	-4.31827	0.04468	-5.23392	-0.00971	-5.0221	0.03076				
J15218+209	57552.92199	-3.87238	-7.00E-05	-4.42199	0.04424	-4.35232	0.04451	-5.26671	-0.01752						
J15218+209	57554.95146	-3.87091	-7.00E-05	-4.40839	0.04434	-4.32147	0.04468	-5.23129	-0.00699	-4.86025	0.03412				
J15218+209	57567.92922	-3.91253	-3.00E-05	-4.42484	0.04431	-4.33673	0.04471	-5.24077	-0.00154	-4.85297	0.03813				
J15218+209	57586.90083	-3.91491	0.00017	-4.40644	0.04486	-4.33902	0.0451	-5.12894	0.02469	-4.98692	0.03753				
J15218+209	57607.82604	-3.86351	0.00022	-4.41226	0.04481	-4.32754	0.04514	-5.20073	0.02116	-4.94897	0.03527				
J15218+209	57752.20402	-3.73505	0.00023	-4.30591	0.04476	-4.24586	0.04501	-4.59695	0.04043	-4.55628	0.04183	-3.79709	0.03734	-5.33694	-0.01277
J15218+209	57755.22383	-3.78226	0.00012	-4.39963	0.04429	-4.32034	0.04465	-5.06047	0.01529	-4.67857	0.03928				
J15218+209	57759.26367	-3.80769	7e-05	-4.42329	0.04416	-4.32727	0.04465	-5.06816	0.02716	-4.97107	0.03196	-3.89976	0.03503		
J15218+209	57762.209	-3.8379	0	-4.44315	0.04403	-4.34867	0.04452	-4.96458	0.0159	-4.79937	0.03692	-3.86067	0.03594		
J15218+209	57779.2736	-3.87118	-7.00E-05	-4.43078	0.04411	-4.33643	0.04458	-5.0935	0.0245	-4.70733	0.04402	-3.85079	0.0363		
J15218+209	57787.20785	-3.81934	5e-05	-4.38963	0.04437	-4.28453	0.04485	-4.99632	0.01481						
J15218+209	57798.17951	-3.89011	-1.00E-05	-4.42378	0.04434	-4.32887	0.04477	-5.15352	0.00639	-5.01281	0.03276	-3.87952	0.0352		
J15218+209	57941.94633	-3.80189	8e-05	-4.30086	0.04486	-4.22568	0.04514	-4.92909	0.02698	-4.91733	0.03472				
J15218+209	57941.96024	-3.76864	0.00015	-4.31023	0.04481	-4.22918	0.04512	-4.80065	0.03178	-4.69583	0.03962				
J15218+209	57942.92713	-3.87923	0.00018	-4.40066	0.04491	-4.30729	0.04523	-5.22875	0.0061	-4.97625	0.03639			-5.09652	0.01368
J15218+209	57943.90294	-3.83947	0.00033	-4.36885	0.04525	-4.27531	0.04551	-5.03983	0.03505	-4.81564	0.04094	-3.82727	0.03945		
J15218+209	57944.04399	-3.88327	0.00027	-4.39264	0.04511	-4.2994	0.04539	-5.12547	0.02425	-5.05859	0.02982	-3.83508	0.03668		
J15218+209	57944.88546	-3.87309	0.00024	-4.38881	0.04509	-4.2976	0.0454	-5.11303	0.03176	-4.76531	0.04108				
J15218+209	57944.98442	-3.87431	0.00026	-4.38773	0.04512	-4.29705	0.0454	-5.11635	0.02843	-4.76938	0.041				
J15218+209	57945.88411	-3.93427	0.00011	-4.40323	0.04498	-4.31071	0.0453	-5.09723	0.02409	-4.9056	0.03863				
J15218+209	57946.02234	-3.78349	0.00037	-4.33368	0.04524	-4.25083	0.04549	-5.00809	0.02838	-4.85684	0.0383				
J15218+209	57946.88259	-3.91819	0.00011	-4.43056	0.04477	-4.33767	0.0451	-5.3523	-0.00831	-4.84277	0.03914				
J15218+209	57946.99198	-3.96318	-0.00031	-4.42195	0.04419	-4.32944	0.04462	-5.1436	0.002	-4.74744	0.02858	-3.94725	0.03364		

Continued on next page

// Star	MJD	Hα		Ca II IRT-a		Ca II IRT-b		He I D_3		Na I D_2		Paβ		Paδ	
		$log\left(\frac{L_{line}}{L_{Bol}}\right)$	δ	$log\left(\frac{L_{line}}{L_{Bol}}\right)$	δ	$log\left(\frac{L_{line}}{L_{Bol}}\right)$	δ	$log\left(\frac{L_{line}}{L_{Bol}}\right)$	δ	$log\left(\frac{L_{line}}{L_{Bol}}\right)$	δ	$log\left(\frac{L_{line}}{L_{Bol}}\right)$	δ	$log\left(\frac{L_{line}}{L_{Bol}}\right)$	δ
J15218+209	57947.90545	-3.89257	0.00024	-4.43109	0.04494	-4.33233	0.0453	-5.22608	0.01405	-4.97336	0.03766				
J15218+209	57947.99949	-3.90555	-0.00015	-4.39203	0.04434	-4.30685	0.04474	-5.0949	0.01799	-4.87314	0.03547				
J15218+209	57948.89083	-3.89232	0.00026	-4.41892	0.04506	-4.32523	0.04537	-5.13235	0.02699	-4.85636	0.0401	-3.90573	0.0361		
J15218+209	57949.01998	-3.85492	3e-05	-4.38334	0.04449	-4.30063	0.04486	-4.94599	0.0297	-4.71565	0.03877	-3.81943	0.03704		
J15218+209	57949.9111	-3.90592	0.00024	-4.40691	0.04509	-4.31003	0.04542	-5.19228	0.02086	-4.92949	0.03902				
J15218+209	57949.99885	-3.61591	0.00059	-4.18278	0.04582	-4.11821	0.04597	-4.5273	0.04349	-4.48714	0.04417	-3.70646	0.03907	-4.75883	0.0312
J15218+209	57950.90751	-3.78649	0.00041	-4.33538	0.04538	-4.25562	0.04562	-4.82478	0.03988	-4.75954	0.04167				
J15218+209	57951.01083	-3.85303	0.0002	-4.37474	0.04491	-4.29268	0.04522	-5.16627	0.01977	-4.73048	0.03981				
J15218+209	57952.88851	-3.88233	-8.00E-05	-4.38384	0.04441	-4.29547	0.04483	-5.1802	0.01299	-4.92419	0.03382				
J15218+209	57952.8973	-3.85028	0.0003	-4.3699	0.04521	-4.286	0.04547	-5.15378	0.0305	-4.79259	0.04086				
J15218+209	58171.16676	-3.76769	0.00015	-4.38153	0.04448	-4.29573	0.04481	-4.94341	0.03185	-4.74878	0.03829	-3.78901	0.03772		
J15218+209	58179.14544	-3.78531	0.0002	-4.39233	0.04458	-4.30815	0.0449	-5.16915	0.00327	-4.71472	0.03971	-3.97731	0.03222		
J15218+209	58212.06576	-3.83437	2e-05	-4.41787	0.0442	-4.32741	0.04465	-5.1057	0.00316	-4.8235	0.03674	-3.89373	0.03506		
J15218+209	58213.18109	-3.88996	0.0002	-4.42449	0.04491	-4.33536	0.04524	-5.26307	0.00879	-4.94567	0.03767	-3.94897	0.03428		
J15218+209	58215.06026	-3.86945	0.0002	-4.39576	0.04496	-4.32825	0.04521	-5.25166	0.0088	-4.69785	0.04164	-3.94017	0.03487		
J15218+209	58236.98901	-3.71638	0.00024	-4.30095	0.04487	-4.22785	0.04514	-4.87346	0.03467	-4.95289	0.03417				
J15218+209	58237.97139	-3.79525	0.0001	-4.41829	0.04417	-4.31997	0.04467	-4.98217	0.02348	-4.9569	0.03279	-3.81296	0.03719		
J15218+209	58261.92869	-3.78844	0.00011	-4.42362	0.04412	-4.32079	0.04465	-5.09102	0.01836	-4.9736	0.03147				
J15218+209	58294.95528	-3.81243	0.00035	-4.42082	0.04495	-4.32063	0.04531	-5.18926	0.02281	-4.99359	0.03721	-3.82673	0.03772		
J15218+209	58316.96004	-3.95707	-0.00029	-4.39921	0.04434	-4.3062	0.04475	-5.14512	0.00604	-4.87994	0.03509				
J15218+209	58318.90875	-3.92761	-0.00014	-4.42512	0.0442	-4.33996	0.04462	-5.23936	-0.00646	-4.77715	0.03851				
J11201-104	57492.93411	-4.10946	-0.00151	-4.5673	0.08966	-4.44999	0.09024	-5.13468	0.05674	-5.22183	0.03563			-5.6115	0.04406
J11201-104	57509.91378	-4.04487	-0.00131	-4.48126	0.09021	-4.40184	0.09051	-5.00793	0.07654	-5.45622	0.00081				
J11201-104	58093.25124	-4.06651	-0.00104	-4.54708	0.0905	-4.4513	0.09084	-5.22883	0.05735	-5.5589	0.05633				
J11201-104	58235.91774	-4.00815	-0.00086	-4.47639	0.09103	-4.3807	0.09134	-5.2931	0.07019	-5.36939	0.0464			-5.61784	0.05225
J11201-104	58237.90864	-4.02387	-0.00124	-4.53339	0.08982	-4.41333	0.09048	-5.50642	0.00815					-5.74581	0.02675
J11201-104	58242.89495	-4.08374	-0.0014	-4.5846	0.08955	-4.45621	0.09027			-5.44661	-0.00326			-5.57842	0.04794
J11201-104	58244.83035	-4.10292	-0.00128	-4.56452	0.09013	-4.47731	0.09053							-5.67716	0.04191
J11201-104	58557.04699	-3.95347	-0.00083	-4.4357	0.09105	-4.33656	0.09136	-5.07569	0.07895	-5.04226	0.08251			-5.66384	0.0431
J11201-104	58558.956	-3.98777	-0.00114	-4.48319	0.09039	-4.37836	0.09084	-5.33504	0.04912	-5.06755	0.07863			-5.66457	0.0377
J11201-104	58571.0067	-4.11657	-0.00155	-4.57724	0.08952	-4.44676	0.09028	-5.20348	0.0507	-5.38745	0.009			-5.65084	0.03976
J11201-104	58572.03917	-4.09048	-0.00145	-4.56757	0.08959	-4.44785	0.09025	-5.31635	0.03791					-5.70929	0.0317
J11201-104	58576.02477	-4.06628	-0.00137	-4.52914	0.08988	-4.44564	0.09029	-5.21939	0.04925	-5.45867	0.00337			-5.77032	0.02245
J11201-104	58588.99356	-4.09244	-0.00145	-4.55096	0.08972	-4.46824	0.09014	-5.15666	0.05486	-4.90405	0.08234			-5.69409	0.03419
J11201-104	58589.94023	-4.07986	-0.00142	-4.53215	0.08986	-4.41706	0.09044	-5.31226	0.04415	-5.24373	0.05121			-5.66421	0.0381
J11201-104	58596.97487	-4.05668	-0.00135	-4.5228	0.08993	-4.4518	0.09023	-4.97623	0.06783	-4.93275	0.08073				
J11201-104	58601.934	-3.99192	-0.00097	-4.43933	0.09096	-4.34888	0.09123	-5.44603	0.03613	-5.50453	0.05857			-5.77576	0.02477
J11201-104	58603.95562	-4.12702	-0.00136	-4.55914	0.09014	-4.45449	0.09058	-5.35634	0.03268	-5.34921	0.01616			-5.69435	0.03415
J11201-104	58604.95687	-4.08542	-0.00142	-4.51807	0.08996	-4.43682	0.09037	-5.37208	0.03046					-5.73598	0.02781
J11201-104	58607.9403	-4.09119	-0.00142	-4.56232	0.08993	-4.45049	0.09047	-5.56544	-0.00293					-5.68218	0.03541
J11201-104	58617.93693	-4.01542	-0.00109	-4.50022	0.09034	-4.40576	0.09076	-5.3015	0.06248	-5.27601	0.07136			-5.64348	0.04032
J11201-104	58628.88654	-4.07871	-0.00141	-4.5405	0.08986	-4.43713	0.09036	-5.2411	0.04681					-5.65504	0.0389
J11201-104	58629.88015	-4.05973	-0.00135	-4.47836	0.09027	-4.3944	0.09061	-5.23154	0.04801					-5.75086	0.02554
J11201-104	58632.85401	-4.1005	-0.00148	-4.57138	0.08956	-4.45872	0.09016	-5.40658	0.02529	-5.45174	-0.00386			-5.68926	0.03446
J11201-104	58638.86175	-4.10477	-0.00149	-4.56098	0.0897	-4.44139	0.09027	-5.33566	0.0354					-5.72213	0.03027
J11201-104	58828.2022	-4.10993	-0.00138	-4.55076	0.09013	-4.45715	0.09048	-5.4562	0.01764	-5.35443	0.01774			-5.66825	0.0383
J11201-104	58832.20584	-4.05825	-0.00135	-4.52226	0.08988	-4.3996	0.0905	-5.30875	0.04423	-5.34501	0.06281			-5.68867	0.03492
J11201-104	58915.98404	-4.03096	-0.00125	-4.52854	0.08986	-4.41512	0.09045	-4.97187	0.07384					-5.79017	0.01915
J03473-019	57630.18403	-3.86937	-0.00074	-4.57514	0.10743	-4.46875	0.10798			-5.00722	0.10253				
J03473-019	57677.09698	-3.76674	-0.00057	-4.49847	0.10811	-4.31832	0.10893	-4.87357	0.10452	-4.77329	0.10668				
J03473-019	57695.03985	-3.85372	-0.00071	-4.556	0.10767	-4.48018	0.10799	-5.08965	0.09979	-5.01931	0.1022				
J03473-019	57701.01902	-3.76782	-0.00058	-4.49866	0.10806	-4.39317	0.10852	-5.04319	0.10093	-4.91225	0.10392				
J03473-019	57703.01826	-3.88065	-0.00075	-4.51817	0.10797	-4.52522	0.10769	-5.03848	0.10099	-4.99225	0.10296				
J03473-019	57752.84094	-3.84591	-0.00069	-4.56072	0.10766	-4.39346	0.10856	-5.13419	0.09308	-5.08736	0.10123				
J03473-019	57753.85242	-3.83578	-0.00068	-4.57598	0.10751	-4.45768	0.10817			-5.16074	0.09974				
J03473-019	57754.89358	-3.89822	-0.00078	-4.68174	0.10651	-4.40552	0.10845	-5.1048	0.09928	-5.18689	0.09848				
J03473-019	57760.85	-3.8977	-0.00079	-4.63969	0.10692	-4.43045	0.1083	-5.15189	0.09782	-5.0612	0.1018				
J03473-019	57761.92292	-3.82135	-0.00066	-4.56089	0.10755	-4.39725	0.10854	-5.1245	0.09345	-5.05728	0.10196				
J03473-019	57765.81422	-3.75797	-0.00057	-4.44086	0.10843	-4.30066	0.109	-4.95286	0.10255	-4.92793	0.10416				
J10196+198	58198.80401	-3.80032	-0.0007	-4.63108	0.06532	-4.53597	0.06675	-4.99847	0.06023	-5.17924	0.05831				
J10196+198	58198.92783	-3.86644	-0.00082	-4.64418	0.06521	-4.60281	0.06615	-5.05727	0.05925	-4.9031	0.06352				
J10196+198	58199.02747	-3.83106	-0.00076	-4.74826	0.06387	-5.02774	0.05975	-5.04788	0.05958	-5.491	0.04357				
J10196+198	58199.801	-3.87807	-0.00084	-4.67482	0.06486	-4.73983	0.06476	-5.07947	0.05884	-5.43165	0.0484				
J10196+198	58199.82912	-3.82723	-0.00075	-4.59447	0.06579	-4.54025	0.06675	-4.89022	0.06292	-5.22428	0.05686				

Continued on next page

// Star	MJD	Hα		Ca II IRT-a		Ca II IRT-b		He I D_3		Na I D_2		Paβ		Paδ	
		$log\left(\frac{L_{line}}{L_{Bol}}\right)$	δ	$log\left(\frac{L_{line}}{L_{Bol}}\right)$	δ	$log\left(\frac{L_{line}}{L_{Bol}}\right)$	δ	$log\left(\frac{L_{line}}{L_{Bol}}\right)$	δ	$log\left(\frac{L_{line}}{L_{Bol}}\right)$	δ	$log\left(\frac{L_{line}}{L_{Bol}}\right)$	δ	$log\left(\frac{L_{line}}{L_{Bol}}\right)$	δ
J10196+198	58200.02075	-3.73046	-0.00061	-4.41378	0.0671	-4.4309	0.06741	-4.69932	0.06549	-4.81521	0.06492				
J10196+198	58204.83157	-3.85128	-0.00079	-4.61753	0.06572	-4.48202	0.06711	-5.13848	0.05746	-5.32065	0.05327				
J10196+198	58204.92522	-3.82582	-0.00075	-4.5905	0.06616	-4.55279	0.0666	-5.02051	0.06035	-5.29853	0.05419				
J10196+198	58205.06375	-3.77202	-0.00067	-4.49524	0.06692	-4.44203	0.06734	-4.9124	0.06281	-5.12517	0.05977				
J10196+198	58208.85005	-3.83901	-0.00077	-4.58067	0.06598	-4.63617	0.06587	-5.04029	0.06011	-5.1408	0.059				
J10196+198	58208.9694	-3.69165	-0.00056	-4.38627	0.06739	-4.37502	0.06774	-4.7509	0.0649	-4.78639	0.06538				
J10196+198	58209.80836	-3.81859	-0.00074	-4.53889	0.06622	-4.44682	0.06735	-5.01862	0.05976	-5.42251	0.04108				
J10196+198	58210.82621	-3.84121	-0.00077	-4.61889	0.06548	-4.70227	0.06504	-5.26634	0.05229	-5.04253	0.05966				
J10196+198	58210.82975	-3.85823	-0.0008	-4.58935	0.06575	-4.41196	0.06754	-5.05003	0.05958	-5.25112	0.05602				
J10196+198	58211.85497	-3.86159	-0.00081	-4.66719	0.06502	-4.49107	0.06707	-5.089	0.05894	-5.09377	0.06013				
J10196+198	58212.06093	-3.90231	-0.00089	-4.71248	0.06428	-4.62446	0.06602	-5.38862	0.04785	-4.99667	0.06211				
J10196+198	58212.90527	-3.73964	-0.00062	-4.42559	0.06719	-4.36029	0.06781	-4.87089	0.06316	-4.99792	0.0623				
J10196+198	58213.00849	-3.79522	-0.0007	-4.54871	0.06616	-4.4287	0.06746	-5.0215	0.06042	-5.13486	0.05954				
J10196+198	58214.80961	-3.8463	-0.00078	-4.62582	0.06577	-4.60588	0.06615	-5.08282	0.05905	-5.24658	0.0559				
J10196+198	58214.93629	-3.80269	-0.00068	-4.53306	0.06664	-4.39214	0.06763	-4.94544	0.06192	-5.07075	0.06064				
J10196+198	58215.04171	-3.82209	-0.00074	-4.63714	0.06536	-4.53518	0.06662	-5.17663	0.0564	-5.14108	0.05858				
J10196+198	58215.86118	-3.87255	-0.00083	-4.71655	0.0643	-4.80945	0.0637	-5.03449	0.05863						
J10196+198	58216.85196	-3.81663	-0.00073	-4.53208	0.06627	-4.75713	0.06437	-4.89993	0.06221	-4.98128	0.0623				
J10196+198	58217.84948	-3.84423	-0.00077	-4.6474	0.06518	-4.51362	0.06699	-4.92395	0.06135	-4.9293	0.06238				
J10196+198	58224.83786	-3.75544	-0.00062	-4.51373	0.06679	-4.4369	0.06741	-4.97028	0.06167	-5.01929	0.06198				
J10196+198	58225.06994	-3.8256	-0.00075	-4.64775	0.06517	-4.53443	0.06671	-5.15844	0.05637	-5.03122	0.06146				
J10196+198	59704.971	-3.94764	-0.00098	-4.69612	0.06468										
J10196+198	59705.89247	-3.91743	-0.00092	-4.70403	0.06447										
J10196+198	59705.98249	-3.87022	-0.00083	-4.627	0.0654										
J10196+198	59706.89347	-3.89385	-0.00088	-4.68505	0.0647										
J10196+198	59707.00182	-3.8657	-0.00082	-4.60935	0.06564										
J10196+198	59708.89403	-3.90586	-0.0009	-4.66541	0.06497										
J10196+198	59709.85337	-3.85225	-0.0008	-4.633	0.06533										
J10196+198	59711.84733	-3.86507	-0.00082	-4.71396	0.06446										
J10196+198	59713.90042	-3.87314	-0.00083	-4.67094	0.06491										
J10196+198	59717.85384	-3.87336	-0.00084	-4.67959	0.06477										
J10196+198	59717.94078	-3.85033	-0.00079	-4.68191	0.06474										
J10196+198	59718.86368	-3.9141	-0.00091	-4.67159	0.06479										
J10196+198	59718.9377	-3.86082	-0.00082	-4.63592	0.0652										
J10196+198	59719.88252	-3.84563	-0.00078	-4.61942	0.06545										
J10196+198	59720.90675	-3.85586	-0.0008	-4.56827	0.06604										
J10196+198	59721.87895	-3.81495	-0.00073	-4.59648	0.06568										
J10196+198	59722.86665	-3.90992	-0.0009	-4.66946	0.06489										
J10196+198	59723.93408	-3.83565	-0.00077	-4.69336	0.0646										
J10196+198	59724.85862	-3.87641	-0.00084	-4.7005	0.06455										
J10196+198	59725.85361	-3.90813	-0.00076	-4.69244	0.06565										
J10196+198	59726.85548	-3.66239	-0.00052	-4.371	0.06745										
J10196+198	59727.85473	-3.87531	-0.00084	-4.63223	0.06561										
J10196+198	59729.85103	-3.91565	-0.00092	-4.68756	0.06467										
J10196+198	59730.87944	-3.89266	-0.00087	-4.67594	0.06485										
J10196+198	59733.86102	-3.85873	-0.00081	-4.62724	0.0654										
J10196+198	59735.86318	-3.89974	-0.0008	-4.69229	0.06523										
J10196+198	59736.87657	-3.89278	-0.00087	-4.73643	0.06404										
J10196+198	59737.85715	-3.89577	-0.0007	-4.68308	0.06586										
J10196+198	59738.87383	-3.89522	-0.00087	-4.79947	0.06246										
J10196+198	59739.87403	-3.89342	-0.00087	-4.71326	0.06447										
J10196+198	59740.86471	-3.8811	-0.00079	-4.72755	0.06441										
J10196+198	59741.8712	-3.90086	-0.00089	-4.64459	0.06521										
J10196+198	59742.86812	-3.8889	-0.00086	-4.71994	0.0643										
J10196+198	59746.86476	-3.8794	-0.00085	-4.62164	0.06536										
J10196+198	59747.88014	-3.83733	-0.00077	-4.63825	0.06524										
J10196+198	59748.86434	-3.86443	-0.00082	-4.66475	0.06494										
J10196+198	59749.88955	-3.91893	-0.00092	-4.74783	0.06379										
J22518+317	57587.08898	-3.90124	-0.00052	-4.46608	0.07479	-4.38229	0.07554	-5.3709	0.0699	-5.42752	0.0697	-3.95784	0.06635	-5.53551	0.03522
J22518+317	57592.12865	-3.91785	-0.00053	-4.49059	0.07462	-4.39242	0.07546	-5.50644	0.06782	-5.40656	0.06984			-5.6963	0.01646
J22518+317	57605.0767	-3.92895	-0.00055	-4.50646	0.07452	-4.40179	0.07542	-5.4727	0.06746	-5.32447	0.07112	-3.90164	0.06686	-5.61895	0.02615
J22518+317	57631.13382	-3.99204	-0.00064	-4.57177	0.07375	-4.42596	0.07522	-5.49641	0.06682	-5.45242	0.06838	-3.95022	0.06541	-5.58177	0.03041
J22518+317	57633.11922	-3.94879	-0.00058	-4.50084	0.07446	-4.33998	0.07564	-5.42105	0.06949	-5.30973	0.07153	-3.79726	0.0694	-5.66232	0.02071
J22518+317	57689.00384	-3.9289	-0.00055	-4.46245	0.0749	-4.34775	0.07576	-5.49278	0.06782	-5.30129	0.07174	-3.94287	0.06559	-5.64918	0.02279

Continued on next page

// Star	MJD	Hα		Ca II IRT-a		Ca II IRT-b		He I D_3		Na I D_2		Paβ		Paδ	
		$log\left(\frac{L_{line}}{L_{Bol}}\right)$	δ	$log\left(\frac{L_{line}}{L_{Bol}}\right)$	δ	$log\left(\frac{L_{line}}{L_{Bol}}\right)$	δ	$log\left(\frac{L_{line}}{L_{Bol}}\right)$	δ	$log\left(\frac{L_{line}}{L_{Bol}}\right)$	δ	$log\left(\frac{L_{line}}{L_{Bol}}\right)$	δ	$log\left(\frac{L_{line}}{L_{Bol}}\right)$	δ
J22518+317	57694.83792	-3.94054	-0.00057	-4.51811	0.07427	-4.42361	0.07524	-5.29533	0.0713	-5.44577	0.06887	-3.87166	0.06755	-5.57876	0.03074
J22518+317	57737.84053	-4.00796	-0.00067	-4.58113	0.0736	-4.46587	0.07495	-5.63292	0.06168	-5.43667	0.06857				
J22518+317	57753.80443	-3.9229	-0.00055	-4.48176	0.07467	-4.3796	0.0755	-5.41567	0.06913	-5.33385	0.07128			-5.57416	0.03155
J22518+317	57754.83571	-3.98721	-0.00063	-4.59984	0.07346	-4.4662	0.07487	-5.59693	0.06427	-5.48492	0.06809			-5.60956	0.02761
J22518+317	57761.77686	-3.74402	-0.00037	-4.19975	0.07637	-4.14132	0.07664	-5.17588	0.07307	-5.0738	0.07456			-5.49264	0.0395
J22518+317	57765.79848	-4.01897	-0.00068	-4.58602	0.07353	-4.45505	0.07497	-5.48231	0.06672	-5.56588	0.0657			-5.56403	0.03262
J02088+494	57621.14226	-3.65833	-0.00036	-4.50069	0.05125	-4.51174	0.05059	-5.17487	0.04538	-4.99055	0.04929				
J02088+494	57688.00021	-3.76701	-0.00045	-4.84098	0.03645	-4.56511	0.04573	-5.20963	0.04488	-5.14474	0.04725				
J02088+494	57691.02801	-3.65079	-0.00034	-4.42995	0.05251	-4.40567	0.05265	-4.97897	0.04997	-5.01376	0.04981				
J02088+494	57710.93462	-3.77435	-0.00046	-4.754	0.03996	-4.49967	0.04723	-5.18242	0.04513	-5.21673	0.04647				
J02088+494	57945.1208	-3.78502	-0.00047	-4.7546	0.04319	-4.67789	0.04775	-5.24501	0.04382	-5.28746	0.04157				
J02088+494	57954.11049	-3.77088	-0.00044	-4.64077	0.04849	-4.66223	0.04818	-5.21769	0.04474	-5.02811	0.04812				
J02088+494	57956.0877	-3.73766	-0.00042	-4.66301	0.04917	-4.47455	0.04991	-5.11635	0.04716	-5.15212	0.04551				
J02088+494	57958.09309	-3.80182	-0.00048	-4.75027	0.04071	-4.61001	0.04558	-5.1996	0.04464	-4.95824	0.04786				
J02088+494	57960.0886	-3.78536	-0.00047	-4.83882	0.04615	-4.65576	0.0481	-5.25016	0.04333	-5.22348	0.04033				
J02088+494	57965.08378	-3.75238	-0.00043	-4.6032	0.04958	-4.58908	0.04526	-5.10373	0.04687	-5.12936	0.04585				
J02088+494	57968.07182	-3.72447	-0.00041	-4.66734	0.0429	-4.5241	0.04658	-5.19936	0.04495	-5.02878	0.04794				
J02088+494	57970.07363	-3.80771	-0.00049	-4.60323	0.04484	-4.60695	0.0468	-5.17445	0.04649	-5.24592	0.04319				
J02088+494	57975.08655	-3.7724	-0.00045	-4.79342	0.04163	-4.59482	0.04534	-5.16445	0.04589	-5.27019	0.04213				
J02088+494	57979.09153	-3.75762	-0.00044	-4.60102	0.04507	-4.51519	0.04684	-5.1706	0.04554	-5.13214	0.04591				
J02088+494	57981.03679	-3.76972	-0.00045	-4.74295	0.04133	-4.59143	0.04916	-5.21709	0.04465	-5.19794	0.04426				
J02088+494	57987.08852	-3.63289	-0.00033	-4.42204	0.05258	-4.38119	0.05278	-4.99465	0.04981	-5.01573	0.04928				
J07319+362N	57442	-4.13035	-0.00116	-5.07698	0.05135	-4.91198	0.05415	-5.45704	0.0082					-5.33298	0.03319
J07319+362N	57444	-4.09221	-0.00107	-5.09382	0.05129	-4.92113	0.05415	-5.4295	0.01293					-5.46993	0.02325
J07319+362N	57449	-3.78162	-0.00055	-4.50135	0.05765	-4.41755	0.05803	-4.683	0.05605	-4.87227	0.05516	-3.93186	0.04758	-5.38904	0.03109
J07319+362N	57467.95902	-4.11624	-0.00112	-5.07926	0.05149	-4.88208	0.05436	-5.26727	0.0265	-5.60774	-0.03522			-5.41495	0.02762
J07319+362N	57475.86734	-4.06926	-0.00102	-4.99793	0.05264	-4.88471	0.05433	-5.39444	0.02595					-5.46686	0.02374
J07319+362N	57635.16297	-4.13494	-0.00118	-5.10267	0.0515	-4.94348	0.05351	-5.3434	0.02166					-5.43961	0.02595
J07319+362N	57656.16477	-3.99734	-0.00086	-5.05165	0.05201	-4.8356	0.05499	-5.30622	0.02808	-5.36101	0.01195			-5.51365	0.01935
J07319+362N	57756.02141	-4.10748	-0.0011	-5.21725	0.04805	-4.99117	0.05275	-5.18983	0.03179	-5.36712	0.04728			-5.40167	0.0288
J07319+362N	57813.94624	-4.01713	-0.00084	-5.0204	0.05281	-4.87233	0.05494	-5.27749	0.04672	-5.7078	0.02988			-5.41354	0.03194
J07319+362N	57814.93117	-4.1261	-0.0011	-5.15854	0.04946	-5.02113	0.05272	-5.48311	0.01193					-5.35753	0.03515
J07319+362N	57830.83512	-3.98106	-0.00075	-5.03094	0.05288	-4.82064	0.05561	-5.21934	0.04889	-5.58908	0.03107	-4.097	0.0463	-5.39791	0.03293
J07319+362N	57851.92799	-3.911	-0.00071	-4.78937	0.05559	-4.65405	0.05673	-5.16857	0.04791	-5.29882	0.04185			-5.40043	0.02868
J07319+362N	57852.87742	-4.03185	-0.0009	-5.02874	0.05267	-4.90745	0.05433	-5.42661	0.02656					-5.40403	0.03172
J07319+362N	58009.16015	-4.00407	-0.00087	-5.10818	0.05081	-4.86924	0.05453	-5.31754	0.04296			-4.09275	0.04223	-5.42057	0.02741
J07319+362N	58021.15978	-4.02428	-0.00087	-5.07825	0.05197	-4.87285	0.05494	-5.40474	0.02073	-5.75585	-0.00419	-4.04567	0.04811	-5.41929	0.03242
J07319+362N	58047.13385	-3.91509	-0.00071	-4.88836	0.05499	-4.74359	0.0562	-5.17509	0.04905			-4.09588	0.0466	-5.38258	0.03407
J07319+362N	58122.89129	-4.06775	-0.001	-5.05832	0.05198	-4.90597	0.05417	-5.26078	0.03144	-5.38897	0.04396			-5.40798	0.03209
J07319+362N	58174.94719	-3.96577	-0.00075	-4.88735	0.05488	-4.8141	0.05568	-5.26054	0.0476					-5.37622	0.0329
J07319+362N	58391.14022	-3.99399	-0.00085	-5.0011	0.05251	-4.82749	0.05498	-5.13538	0.04857					-5.33339	0.03614
J07319+362N	58394.13367	-4.0204	-0.00089	-5.07014	0.05202	-4.86121	0.05507	-5.23373	0.03788			-4.03621	0.04809	-5.3546	0.0355
J07319+362N	58397.14438	-4.05437	-0.00097	-5.09263	0.05122	-4.87826	0.05464	-5.31809	0.02542			-4.07316	0.04693	-5.38138	0.03375
J07319+362N	58399.13447	-4.05438	-0.00097	-5.07013	0.05158	-4.86106	0.05468	-5.21439	0.03377	-5.72919	-0.02782			-5.35261	0.0325
J07319+362N	58416.11176	-4.06809	-0.001	-5.0976	0.05074	-4.9259	0.05383	-5.38968	0.01643			-4.07859	0.04662	-5.38968	0.03244
J07319+362N	58480.20931	-4.00761	-0.00085	-4.98419	0.0536	-4.83227	0.05539	-5.21401	0.03903	-5.3934	0.04506			-5.36944	0.03427
J07319+362N	58486.12249	-4.02989	-0.00092	-5.0667	0.05138	-4.87223	0.0546	-5.1613	0.04116	-5.67818	0.03154	-4.04365	0.04718	-5.36936	0.03351
J07319+362N	58491.21744	-4.02188	-0.00091	-4.99515	0.05284	-4.86105	0.05485	-5.15723	0.03718					-5.38901	0.02949
J07319+362N	58492.0872	-4.07105	-0.00101	-5.16172	0.04949	-4.91478	0.05411	-5.28128	0.02674	-5.65906	0.03067	-4.06326	0.0461	-5.40602	0.02973
J07319+362N	58493.11784	-3.97058	-0.0008	-4.97112	0.05329	-4.80372	0.05539	-5.31877	0.04274	-5.47802	0.04128			-5.36491	0.03133
J07319+362N	58498.18554	-4.04113	-0.00095	-5.0438	0.0519	-4.87164	0.05472	-5.30842	0.03207	-5.75777	0.02659			-5.35221	0.03216
J07319+362N	58538.09857	-4.0706	-0.00102	-5.0459	0.05195	-4.9022	0.05416	-5.55186	0.03048					-5.38116	0.03004
J07319+362N	58757.09434	-4.01429	-0.00089	-4.96649	0.05372	-4.83141	0.05529	-5.25696	0.03368	-5.55449	0.02517			-5.41993	0.0311
J07319+362N	58769.05502	-4.10571	-0.0011	-5.10703	0.05151	-4.9185	0.0545	-5.20634	0.03466	-5.42991	-0.00121			-5.36607	0.0356
J07319+362N	58772.09584	-4.04823	-0.00096	-5.06701	0.05173	-4.88285	0.05459	-5.37776	0.0166	-5.60608	-3.00E-05			-5.37733	0.0336
J07319+362N	58773.1306	-4.00167	-0.00087	-5.00113	0.05281	-4.83276	0.05507	-5.21789	0.04657	-5.68057	0.01401			-5.34022	0.03576
J07319+362N	58783.13888	-4.11826	-0.00114	-5.03496	0.05273	-4.83691	0.05529	-5.20044	0.04081	-5.69855	0.01802			-5.40948	0.03095
J10360+051	57754.163	-3.91499	-0.00061	-4.98137	0.05587	-4.83245	0.06137	-5.42459	0.03656	-5.35431	0.05685				
J10360+051	58117.16935	-3.88855	-0.00057	-4.98078	0.05297	-4.83028	0.06125	-5.34003	0.0429	-5.35529	0.05697				
J10360+051	58122.05925	-3.92728	-0.00062	-4.99455	0.05531	-4.76021	0.06223	-5.19947	0.04984	-5.28575	0.06185				
J10360+051	58235.86863	-3.79875	-0.00047	-4.76131	0.06172	-4.64854	0.06325	-5.14435	0.05536	-5.22466	0.05852				
J10360+051	58237.88561	-3.82928	-0.0005	-4.77758	0.06143	-4.65264	0.06305	-5.05535	0.05756	-5.09859	0.05773				
J10360+051	58240.85951	-3.83253	-0.0005	-4.82293	0.05942	-4.75418	0.06234	-4.98693	0.05694						
J10360+051	58262.84421	-3.86635	-0.00054	-4.96375	0.05371	-4.74079	0.06216	-5.14626	0.05151	-5.1678	0.05566				

Continued on next page

// Star	MJD	Hα		Ca II IRT-a		Ca II IRT-b		He I D_3		Na I D_2		Paβ		Paδ	
		$log\left(\frac{L_{line}}{L_{Bol}}\right)$	δ	$log\left(\frac{L_{line}}{L_{Bol}}\right)$	δ	$log\left(\frac{L_{line}}{L_{Bol}}\right)$	δ	$log\left(\frac{L_{line}}{L_{Bol}}\right)$	δ	$log\left(\frac{L_{line}}{L_{Bol}}\right)$	δ	$log\left(\frac{L_{line}}{L_{Bol}}\right)$	δ	$log\left(\frac{L_{line}}{L_{Bol}}\right)$	δ
J16570-043	57477.18343	-4.00706	-0.00068	-5.03891	0.06876	-4.81784	0.07239	-5.47187	0.06165	-5.36843	0.06855				
J16570-043	57489.11536	-3.99805	-0.00066	-5.08694	0.06638	-4.83262	0.07339	-5.45297	0.0608						
J16570-043	57509.11966	-3.9499	-0.00061	-4.98855	0.06777	-4.84192	0.07278	-5.32317	0.06817	-5.31426	0.05808				
J16570-043	57511.12225	-3.89668	-0.00053	-4.85558	0.07424	-4.73911	0.0754	-5.46015	0.06291	-5.31189	0.07228				
J16570-043	57540.04626	-4.01228	-0.00069	-5.05661	0.06625	-4.84328	0.07212	-5.58985	0.05283	-5.38444	0.06782				
J16570-043	57553.99024	-3.96872	-0.00062	-4.96266	0.07099	-4.74244	0.07536	-5.44777	0.06057	-5.36786	0.07049				
J16570-043	57573.95353	-3.9393	-0.0006	-4.85746	0.07345	-4.67194	0.07634	-5.17318	0.07121	-5.17833	0.07392				
J16570-043	57802.21862	-4.01853	-0.0007	-5.08246	0.06458	-4.89435	0.07134	-5.63726	0.05344	-5.35247	0.06908				
J16570-043	57818.14447	-4.06172	-0.00078	-5.1283	0.06275	-4.90302	0.07104	-5.50555	0.05825	-5.50398	0.0633				
J16570-043	57822.20022	-3.74861	-0.00038	-4.72235	0.07606	-4.60152	0.0772	-5.19794	0.07438	-5.1769	0.07409				
J16570-043	57832.14896	-4.02911	-0.00072	-5.03767	0.06665	-4.90786	0.07053	-5.45238	0.0626	-5.51075	0.06467				
J16570-043	57848.13701	-3.98266	-0.00065	-4.94373	0.06975	-4.86016	0.07039	-5.46567	0.06195	-5.45613	0.0666				
J16570-043	57850.08836	-3.86031	-0.00049	-4.87736	0.07293	-4.73996	0.07493	-5.31601	0.06788	-5.25335	0.072				
J16570-043	57853.11142	-3.92094	-0.00055	-4.89147	0.07365	-4.76292	0.0755	-5.37872	0.06606	-5.33058	0.07072				
J16570-043	57856.10292	-3.9612	-0.00062	-4.99842	0.07013	-4.81943	0.07455	-5.43813	0.06808	-5.32857	0.06968				
J18498-238	57947.98086	-4.07402	-0.00097	-5.15834	0.03235	-4.87819	0.03845			-4.96386	0.03869				
J18498-238	57949.01007	-4.30769	-0.00169	-5.37414	0.00427	-5.0885	0.03279			-4.91414	0.03624				
J18498-238	57949.9765	-4.2383	-0.0014	-5.32393	0.00971	-5.04965	0.03526			-4.97385	0.03616				
J18498-238	57950.99397	-4.23726	-0.00142	-5.37014	0.00481	-5.01262	0.0342			-4.96551	0.0268				
J18498-238	57952.98628	-4.15011	-0.00112	-4.90854	0.0304	-5.36542	0.00975								
J18498-238	57957.94936	-4.30443	-0.00164	-5.45051	-0.0021	-5.11295	0.0334			-5.01367	0.03492				
J18498-238	57959.96927	-4.18709	-0.00119	-5.2188	0.02415	-4.98583	0.03689	-5.05339	0.02996	-4.87426	0.03804				
J18498-238	57960.94644	-4.38281	-0.002	-5.44043	-0.00228	-5.18516	0.02093			-4.89398	0.03784				
J18498-238	57961.93626	-4.21709	-0.00134	-5.40467	0.00157	-5.0413	0.03477	-5.14115	0.02685	-4.98201	0.03784				
J18498-238	57962.94124	-4.07212	-0.00095	-4.95378	0.03767	-4.77965	0.03994	-4.97292	0.03239	-4.89595	0.03934				
J18498-238	57963.93201	-4.22905	-0.00139	-5.38534	0.00341	-5.11747	0.033			-4.93452	0.03797				
J18498-238	57964.93515	-4.11916	-0.00098	-5.30664	0.01788	-4.98712	0.03745	-5.08446	0.02888	-4.96851	0.03757				
J18498-238	57967.93063	-4.20615	-0.00129	-5.34525	0.01496	-5.0687	0.03496	-5.11096	0.02791	-5.02586	0.03666				
J18498-238	57973.89941	-4.15678	-0.00115	-5.23575	0.03072	-4.93358	0.03795	-5.17329	0.02515	-5.04301	0.03605				
J18498-238	57974.91041	-4.05157	-0.00093	-4.9193	0.0379	-4.7488	0.03988	-4.90557	0.0355	-4.91247	0.03929				
J18498-238	57975.90212	-4.10349	-0.00102	-5.15588	0.03305	-4.93423	0.03769	-5.12338	0.02754	-4.94767	0.03821				
J18498-238	57976.90796	-4.13118	-0.00096	-5.19614	0.03258	-4.92056	0.03851	-5.22586	0.02331	-5.02703	0.03672				
J18498-238	57978.94174	-4.05259	-0.00091	-5.10747	0.03383	-4.88085	0.0383	-5.05068	0.03001	-4.86897	0.03871				
J18498-238	57980.86992	-4.23701	-0.00144	-5.28707	0.02194	-5.05627	0.03504	-5.19004	0.02477	-4.86704	0.03573				
J18498-238	57981.89022	-4.18977	-0.00114	-5.26484	0.01863	-5.01749	0.03635	-5.09826	0.0285	-4.99768	0.03602				
J18498-238	57985.87488	-4.17049	-0.00114	-5.27517	0.02126	-5.04599	0.03658			-4.86247	0.03768				
J18498-238	57986.91098	-4.27311	-0.00152	-5.43345	-0.00154	-5.1799	0.03198			-4.99017	0.03158				
J18498-238	57988.85613	-4.18715	-0.00125	-5.20455	0.0254	-4.92683	0.03754	-5.13484	0.02671	-4.82166	0.03904				
J18498-238	57989.90971	-4.13091	-0.00107	-5.18364	0.03325	-4.91885	0.03847			-5.06815	0.03583				
J18498-238	58001.83994	-4.23407	-0.00139	-5.44048	-0.00105	-5.07708	0.03416			-5.06852	0.03497				
J18498-238	58006.82244	-4.244	-0.00143	-5.24677	0.01503	-5.05823	0.03517			-4.9697	0.03618				
J18498-238	58007.88443	-4.19607	-0.00125	-5.33463	0.01145			-5.09057	0.02867	-5.07391	0.03519			-5.68057	-0.01737
J18498-238	58008.83829	-4.11414	-0.00104	-5.17029	0.03158	-4.94336	0.03736			-4.95121	0.03769				
J18498-238	58009.81046	-4.15699	-0.00118	-5.20336	0.03131	-5.01625	0.03591	-5.0694	0.02933	-5.07159	0.03564				
J18498-238	58016.80903	-4.18673	-0.00102	-5.34106	0.02789	-5.02767	0.03745			-5.07906	0.03508				
J18498-238	58017.79987	-4.33798	-0.00175	-5.55323	-0.01601	-5.17692	0.02587								
J18498-238	58021.78947	-4.19255	-0.00117	-5.26869	0.01687	-5.00988	0.03633			-4.99377	0.03632				
J18498-238	58028.78942	-4.18965	-0.00126	-5.35785	0.0059	-4.98276	0.03615			-5.04168	0.03493				
J18498-238	58032.78545	-4.03298	-0.00088	-4.92156	0.03812	-4.73555	0.04017	-4.94607	0.0331	-4.91476	0.03949				
J18498-238	58033.78265	-4.15885	-0.00117	-5.2777	0.02184	-4.95333	0.0372	-5.00462	0.03141	-5.01951	0.03644				
J22468+443	57575.16418	-3.86413	-0.0004	-4.94351	0.03523	-4.70268	0.03761	-5.03226	0.03503	-5.2774	0.03402			-5.04332	0.0274
J22468+443	57592.12059	-3.86669	-0.00053	-5.04981	0.02866	-4.62662	0.03612	-5.10287	0.02969	-5.3939	0.02731			-5.03803	0.02757
J22468+443	57611.10403	-3.84181	-0.00054	-4.93406	0.02843	-4.54548	0.03778	-5.07638	0.02988	-5.36149	0.02715				
J22468+443	57613.99302	-3.79668	-0.00049	-4.83544	0.03483	-4.54045	0.03803	-5.02869	0.03103	-5.11192	0.03358	-4.06953	0.022	-5.36829	0.0086
J22468+443	57620.00519	-3.89797	-0.00062	-4.90218	0.03121	-4.54027	0.03636	-5.04205	0.02952	-5.05748	0.03391				
J22468+443	57626.03733	-3.67053	-0.00037	-4.51985	0.03807	-4.32947	0.03912	-4.91498	0.03576	-4.84674	0.03721	-3.99275	0.02618	-5.67059	-0.02553
J22468+443	57632.12897	-3.5568	-0.0003	-4.51023	0.03799	-4.32233	0.03906	-4.80766	0.03683	-4.86876	0.03676	-3.94235	0.02531	-4.68029	0.0249
J22468+443	57632.96715	-3.2069	-0.00014	-4.07033	0.03997	-3.91018	0.04029	-4.48473	0.03898	-4.55419	0.03905	-3.6844	0.03197	-4.25171	0.0356
J22468+443	57634.1314	-3.79853	-0.0005	-4.981	0.03181	-4.6401	0.037	-4.99823	0.03167	-5.14682	0.03173			-5.66383	-0.02527
J22468+443	57634.96616	-3.7886	-0.00048	-4.8866	0.03355	-4.62405	0.03509	-4.966	0.03231	-5.1432	0.03298			-5.46521	-0.00094
J22468+443	57635.95998	-3.90744	-0.00063	-4.88038	0.03012	-4.60155	0.03371			-5.06432	0.0331			-5.53019	-0.00771
J22468+443	57643.87608	-3.79297	-0.00048	-4.87262	0.03417	-4.80256	0.03158	-5.07187	0.02822						
J22468+443	57643.90119	-3.83346	-0.00053	-4.85831	0.03226	-4.56814	0.03761	-5.07549	0.0297	-5.06606	0.03397			-5.36246	0.00789
J22468+443	57644.9948	-3.86563	-0.00057	-4.97194	0.02701	-4.46879	0.03841	-5.00196	0.03163	-5.19683	0.03122			-5.01243	0.02621

Continued on next page

// Star	MJD	Hα		Ca II IRT-a		Ca II IRT-b		He I D_3		Na I D_2		Paβ		Paδ	
		$log\left(\frac{L_{line}}{L_{Bol}}\right)$	δ	$log\left(\frac{L_{line}}{L_{Bol}}\right)$	δ	$log\left(\frac{L_{line}}{L_{Bol}}\right)$	δ	$log\left(\frac{L_{line}}{L_{Bol}}\right)$	δ	$log\left(\frac{L_{line}}{L_{Bol}}\right)$	δ	$log\left(\frac{L_{line}}{L_{Bol}}\right)$	δ	$log\left(\frac{L_{line}}{L_{Bol}}\right)$	δ
J22468+443	57645.98485	-3.76869	-0.00046	-4.83861	0.03448	-4.45585	0.03847			-5.11392	0.03424			-5.00561	0.02644
J22468+443	57645.98846	-3.76855	-0.00047	-4.75217	0.03566	-4.4376	0.03861	-5.00967	0.03136	-5.11554	0.03352			-5.02647	0.02573
J22468+443	57646.87303	-3.71885	-0.00041	-4.70103	0.03651	-4.31184	0.03923	-4.86079	0.03618	-4.94583	0.03594	-3.99509	0.02305		
J22468+443	57650.0369	-3.48528	-0.00025	-4.35399	0.03905	-4.19627	0.03965	-4.80769	0.03703	-4.84814	0.03744	-3.94827	0.02934	-4.51051	0.0307
J22468+443	57654.90045	-3.85053	-0.00055	-4.93881	0.02836	-4.57903	0.03758	-5.02913	0.02941	-5.05062	0.0344			-5.26248	0.0147
J22468+443	57656.10409	-3.77493	-0.00047	-4.77804	0.03564	-4.44474	0.03857	-5.00119	0.03135	-4.94081	0.03626			-5.48138	-0.00254
J22468+443	57656.89272	-3.7527	-0.00044	-4.72561	0.03605	-4.4333	0.03866	-4.99391	0.0316	-4.97664	0.03589			-5.06537	0.0243
J22468+443	57657.01595	-3.60141	-0.00031	-4.57758	0.03779	-4.33381	0.03899	-5.0563	0.03003	-4.49854	0.03607			-4.75057	0.03291
J22468+443	57677.84494	-3.83996	-0.00054	-4.78048	0.03543	-4.54004	0.038	-5.05103	0.03029	-5.10649	0.03346			-5.51146	-0.00539
J22468+443	57678.8023	-3.80557	-0.00049	-4.82086	0.03489	-4.49957	0.0382	-4.95779	0.03259	-5.10546	0.03288			-5.33126	0.01037
J22468+443	57683.87778	-3.7467	-0.00044	-4.67344	0.03675	-4.50539	0.03814	-5.10668	0.02859	-5.10278	0.03409			-5.08456	0.02344
J22468+443	57684.84596	-3.83188	-0.00052	-5.05905	0.02382	-4.74985	0.0317	-5.08119	0.02799	-5.11451	0.03251	-4.19149	0.01247	-5.68671	-0.02925
J22468+443	57688.80128	-3.86357	-0.00057	-5.03198	0.02486	-4.74122	0.0309	-5.04691	0.02896	-5.0944	0.03236			-5.16387	0.02004
J22468+443	57692.99867	-3.85945	-0.00056	-4.93656	0.02791	-4.62149	0.03587	-5.06936	0.02824	-5.2743	0.02867			-5.06478	0.02422
J22468+443	57694.83475	-3.85994	-0.00056	-4.98767	0.03188	-4.54577	0.03789	-4.96745	0.03087	-5.25972	0.02993			-5.32021	0.01079
J22468+443	57697.87892	-3.8044	-0.00049	-4.87719	0.03003	-4.5229	0.0379	-4.96354	0.031	-5.17943	0.02555				
J22468+443	57703.91154	-3.77141	-0.00047	-4.82196	0.03414	-4.48129	0.03827	-5.02021	0.03123	-5.10319	0.03347			-5.64842	-0.02332
J22468+443	57704.80118	-3.80679	-0.0005	-4.89101	0.03353	-4.49402	0.03821	-4.96903	0.0309	-5.23271	0.03001	-4.104	0.01961	-5.14155	0.02166
J22468+443	57710.78384	-3.81882	-0.00051	-4.82477	0.03463	-4.53944	0.03796	-4.95185	0.03126	-5.15582	0.03241			-5.12648	0.02166
J22468+443	57751.82581	-3.75112	-0.00044	-4.85027	0.03257	-4.40491	0.0388	-4.94797	0.03267	-5.1794	0.03259	-4.02239	0.02408	-5.04808	0.02495
J22468+443	57752.7774	-3.83722	-0.00054	-4.94944	0.02792	-4.61284	0.0373	-5.18511	0.02399	-5.23634	0.03029	-4.0995	0.01852	-4.97279	0.0275
J22468+443	57753.77517	-3.76052	-0.00045	-4.81947	0.03486	-4.54528	0.03799	-4.913	0.03282	-5.15336	0.03298	-4.06956	0.02002	-5.01958	0.02597
J22468+443	57754.80977	-3.82263	-0.00052	-4.99307	0.02893	-4.66821	0.0368	-5.03123	0.02942	-5.11796	0.0334			-5.02195	0.02588
J22468+443	57760.86144	-3.85074	-0.00055	-5.01655	0.02504	-4.60566	0.03728	-5.03731	0.02916	-5.1975	0.03091			-5.15403	0.02051
J22468+443	57761.79296	-3.81578	-0.00051	-4.86892	0.03439	-4.4955	0.03832	-4.91643	0.0321	-5.19496	0.03228				
J22468+443	57762.78459	-3.8588	-0.00056	-4.95634	0.02757	-4.56819	0.03767	-5.00746	0.03006	-5.22202	0.03006			-4.98733	0.02704
J22468+443	57766.82932	-3.73449	-0.00043	-4.70413	0.0364	-4.50044	0.03833	-4.85686	0.03417	-5.20286	0.03234			-5.10755	0.0228
J22468+443	57853.18319	-3.78844	-0.00047	-4.80039	0.03503	-4.4635	0.03849	-4.98945	0.03208	-5.04746	0.03524	-4.16709	0.02158	-5.15341	0.02136
J22468+443	57855.18728	-3.83983	-0.00054	-4.94132	0.02835	-4.56567	0.03774	-5.0251	0.03094	-5.06944	0.0342			-5.44834	0.00065
J22468+443	57862.16933	-3.79573	-0.00049	-4.84676	0.0343	-4.48786	0.03821	-5.25738	0.0235	-5.0439	0.03436	-4.17822	0.0192	-5.29836	0.01244
J22468+443	57882.15213	-3.85404	-0.00055	-4.94297	0.03284	-4.68246	0.0368	-5.06898	0.02926	-5.24607	0.03025			-5.47632	-0.00104
J22468+443	57888.10537	-3.83006	-0.00053	-4.84913	0.03474	-4.51235	0.03816	-5.04575	0.03061	-5.09932	0.03295			-5.54833	-0.0095
J22468+443	57892.115	-3.78169	-0.00044	-4.82927	0.03537	-4.56609	0.03806	-4.94968	0.03387	-5.07028	0.03498	-4.04245	0.02997	-5.02819	0.02805
J22468+443	57914.15322	-3.83381	-0.00048	-4.88385	0.03467	-4.59225	0.03652	-5.02307	0.03231	-5.24566	0.032			-5.06141	0.0273
J22468+443	57918.16778	-3.77719	-0.0004	-4.899	0.03438	-4.56224	0.03693	-5.02183	0.03385	-5.17896	0.03344	-4.15258	0.02661	-5.14069	0.02593
J22468+443	57922.14339	-3.8486	-0.00049	-4.90385	0.03449	-4.5823	0.03668	-5.0224	0.03243	-5.22882	0.03252			-5.00039	0.0291
J22468+443	57931.16262	-3.64986	-0.00036	-4.53321	0.03802	-4.36134	0.039	-4.78647	0.03741	-4.99605	0.03579	-3.95876	0.03114	-4.98237	0.02823
J22468+443	57934.07882	-3.83256	-0.00053	-4.83469	0.03509	-4.48208	0.03838	-5.08648	0.02885	-5.11373	0.03056			-5.05998	0.02763
J22468+443	57939.14602	-3.79878	-0.00045	-4.85232	0.03522	-4.57159	0.03794	-4.98838	0.03367	-5.22224	0.03256	-3.99911	0.03058	-5.10866	0.03241
J22468+443	57942.07424	-3.68903	-0.00038	-4.59181	0.03765	-4.41792	0.0388	-4.97226	0.03219	-5.0155	0.03538	-4.04843	0.02259	-5.37965	0.00656
J22468+443	57953.16432	-3.78583	-0.00043	-4.83327	0.03536	-4.54065	0.0381	-5.00615	0.03365	-5.28556	0.03168	-4.12047	0.02806	-5.4472	0.00747
J22468+443	57960.93911	-3.84947	-0.00054	-4.95987	0.03292	-4.59335	0.03625	-5.05547	0.02978	-5.38361	0.02637			-5.39569	0.01307
J22468+443	57963.06537	-3.8002	-0.00049	-4.85217	0.03438	-4.46001	0.03842	-5.00779	0.03141	-5.21419	0.0312			-5.14967	0.0213
J22468+443	57967.92108	-3.55671	-0.00027	-4.48176	0.03849	-4.30702	0.03932	-4.89224	0.0366	-5.0228	0.03566	-3.94641	0.0318	-4.99372	0.02912
J22468+443	57974.00558	-3.77116	-0.00044	-4.76804	0.03619	-4.48707	0.03853	-5.01411	0.0329	-5.03269	0.03598	-4.0983	0.02805	-5.28586	0.01628
J22468+443	57988.8465	-3.80257	-0.0005	-4.86809	0.03206	-4.60229	0.03532	-5.07648	0.02852	-5.02274	0.03418			-5.22503	0.01687
J22468+443	57989.91948	-3.8139	-0.00049	-4.86402	0.03441	-4.53945	0.03801	-5.01558	0.03245	-5.06484	0.03474	-4.0137	0.0308	-5.04708	0.02775
J22468+443	57990.09311	-3.8576	-0.0005	-5.03153	0.02615	-4.65032	0.03519	-5.04867	0.03162	-5.16596	0.03271			-5.11684	0.02565
J22468+443	57996.86032	-3.79133	-0.00046	-4.81932	0.03535	-4.4916	0.03837	-5.00315	0.0353	-5.09959	0.03448	-4.06265	0.02954	-5.35184	0.01408
J22468+443	57997.11056	-3.79615	-0.00043	-4.85542	0.03496	-4.51574	0.03831	-4.95259	0.03661	-5.07258	0.03576	-4.094	0.02848	-5.35364	0.01471
J22468+443	57997.94145	-3.80923	-0.00047	-4.83933	0.03467	-4.48934	0.03838	-4.97781	0.03363	-5.12231	0.03431	-4.06741	0.02965	-5.33964	0.01392
J22468+443	57998.85889	-3.62814	-0.00031	-4.47273	0.03872	-4.29987	0.03945	-4.89901	0.03668	-4.92115	0.03731	-4.06026	0.02969	-5.61882	-0.00982
J22468+443	57999.18375	-3.72618	-0.00031	-4.76705	0.03677	-4.49726	0.03877	-4.92149	0.0357	-5.08066	0.03624	-4.09162	0.02656	-5.09887	0.02627
J22468+443	57999.91701	-3.84229	-0.0005	-4.96137	0.03066	-4.68268	0.03694	-5.03478	0.03261	-5.13872	0.03386	-4.13707	0.02712	-5.5632	-0.00461
J22468+443	58000.13245	-3.88104	-0.00059	-4.98486	0.02666	-4.64296	0.03473	-5.14429	0.02569	-5.23834	0.03013	-4.05799	0.02612	-5.38192	0.00677
J22468+443	58001.12241	-3.84481	-0.00045	-4.87141	0.03303	-4.5875	0.03791	-5.01048	0.03431	-5.17554	0.03464	-4.12301	0.02724	-5.58277	-0.00672
J22468+443	58001.91486	-3.78044	-0.00043	-4.82721	0.03519	-4.51762	0.03828	-4.90946	0.03485	-5.16196	0.03397	-4.01773	0.03062	-5.59303	-0.00753
J22468+443	58006.81385	-3.87108	-0.00055	-4.97854	0.02792	-4.62799	0.03736	-4.97877	0.03191	-5.14211	0.03307			-5.6016	-0.0085
J22468+443	58006.99696	-3.75282	-0.0004	-4.77742	0.03587	-4.516	0.03836	-4.9296	0.03494	-5.03766	0.03583	-4.07921	0.02885	-5.57163	-0.00489
J22468+443	58007.19421	-3.78521	-0.00045	-4.7576	0.0358	-4.49669	0.03817	-4.98597	0.03278	-5.0104	0.03599			-5.40154	0.0104
J22468+443	58007.81844	-3.85745	-0.00053	-4.97693	0.02783	-4.56753	0.03587	-5.025	0.03145	-5.07424	0.03438	-4.00049	0.03115	-5.46526	0.00532
J22468+443	58007.9969	-3.90936	-0.00055	-5.00869	0.02691	-4.67175	0.03465	-5.12632	0.03009	-5.1918	0.03355			-5.47671	0.00412
J22468+443	58008.18476	-3.83356	-0.00053	-4.81533	0.03492	-4.54226	0.03791	-5.00905	0.03141	-5.1365	0.03315			-5.35243	0.00865
J22468+443	58008.85385	-3.89839	-0.00057	-4.95333	0.03105	-4.60354	0.03762	-5.02345	0.03147	-5.11821	0.03429	-4.02142	0.03091	-5.5008	0.00254

Continued on next page

// Star	MJD	Hα		Ca II IRT-a		Ca II IRT-b		He I D_3		Na I D_2		Paβ		Paδ	
		$log\left(\frac{L_{line}}{L_{Bol}}\right)$	δ	$log\left(\frac{L_{line}}{L_{Bol}}\right)$	δ	$log\left(\frac{L_{line}}{L_{Bol}}\right)$	δ	$log\left(\frac{L_{line}}{L_{Bol}}\right)$	δ	$log\left(\frac{L_{line}}{L_{Bol}}\right)$	δ	$log\left(\frac{L_{line}}{L_{Bol}}\right)$	δ	$log\left(\frac{L_{line}}{L_{Bol}}\right)$	δ
J22468+443	58009.02359	-3.87889	-0.00054	-4.96356	0.02803	-4.63616	0.03723	-5.03957	0.03201	-5.12787	0.03429	-4.01802	0.0307	-5.44012	0.00687
J22468+443	58009.18564	-3.8898	-0.0006	-4.95392	0.02805	-4.55572	0.03566	-5.05528	0.02916	-5.25018	0.0292			-5.51257	-0.00578
J22468+443	58026.86804	-3.90196	-0.00053	-5.02201	0.03253	-4.58442	0.03592	-5.05916	0.03185	-5.15739	0.0343	-4.04855	0.03062	-5.40592	0.01114
J22468+443	58027.1208	-3.87503	-0.00046	-5.0077	0.02867	-4.54739	0.03634	-5.03466	0.03227	-5.05363	0.03592	-4.20594	0.02151	-5.58992	-0.00783
J22468+443	58028.12541	-3.72101	-0.00035	-4.6083	0.03785	-4.39934	0.03902	-4.89253	0.03504	-4.8736	0.03761	-4.00382	0.02888	-5.60806	-0.01092
J22468+443	58028.9301	-3.7465	-0.00035	-4.71626	0.03681	-4.40076	0.0391	-4.96286	0.03504	-5.03201	0.03672	-4.02414	0.03072	-5.26396	0.01901
J22468+443	58029.16798	-3.80618	-0.00047	-4.85873	0.0347	-4.65724	0.03432	-4.96925	0.03098	-5.15006	0.03285	-4.06234	0.02004	-5.12739	0.02173
J22468+443	58029.89117	-3.8667	-0.00053	-5.00041	0.0271	-4.6392	0.03736	-5.02565	0.03167	-5.1587	0.03393	-4.04423	0.02966	-5.33918	0.01323
J22468+443	58030.90125	-3.86187	-0.0005	-4.95646	0.0289	-4.59628	0.03782	-5.02419	0.03216	-5.19439	0.03374	-4.00215	0.03091	-5.44197	0.0065
J22468+443	58031.12353	-3.91452	-0.00055	-4.96824	0.02905	-4.6194	0.03774	-5.03075	0.0312	-5.15796	0.03403			-5.01174	0.00961
J22468+443	58031.92972	-3.47052	-0.00022	-4.27205	0.03938	-4.13216	0.03985	-4.62987	0.03878	-4.74807	0.03846	-3.85791	0.03364	-4.53521	0.03078
J22468+443	58032.10293	-3.64621	-0.00029	-4.48284	0.03855	-4.32743	0.03934	-4.82004	0.03772	-4.88337	0.0377	-3.99622	0.02985	-5.1615	0.02351
J22468+443	58032.85466	-3.76707	-0.00043	-4.77938	0.03558	-4.45565	0.0386	-5.01455	0.03289	-5.09152	0.03499			-5.06416	0.02654
J22468+443	58033.08041	-3.70487	-0.00028	-4.64649	0.03786	-4.35877	0.03946	-4.94853	0.0358	-4.98911	0.03747	-3.97222	0.03007	-5.38093	0.01122
J22468+443	58033.89512	-3.82399	-0.00045	-4.90194	0.03387	-4.6288	0.03754	-4.99811	0.0327	-5.17937	0.03401	-4.01141	0.03077	-5.50311	0.00154
J22468+443	58034.09258	-3.79955	-0.00041	-4.82456	0.03533	-4.5007	0.03852	-5.01223	0.03369	-5.18596	0.03421	-3.96419	0.0289	-5.22398	0.01707
J22468+443	58034.97137	-3.83331	-0.00048	-4.94607	0.03304	-4.45488	0.03862	-4.97526	0.03303	-5.204	0.03338	-3.95627	0.03221	-5.67589	-0.01773
J22468+443	58059.78601	-3.85199	-0.00055	-4.88543	0.03169	-4.50827	0.03812	-5.02048	0.03083	-5.26742	0.03072			-5.12148	0.02297
J22468+443	58080.91031	-3.6781	-0.00038	-4.58049	0.03765	-4.34861	0.03909	-4.86618	0.03397	-4.98011	0.03518	-4.01527	0.02223	-5.19924	0.0295
J22468+443	58095.77422	-3.75102	-0.00045	-4.73718	0.0364	-4.50356	0.03824	-4.86007	0.03621	-5.07398	0.035	-3.9514	0.02476	-5.003	0.02686
J22468+443	58098.77408	-3.82138	-0.00052	-4.89218	0.02936	-4.60622	0.03727	-4.91856	0.03209					-5.13977	0.02117
J01352-072	57622.16272	-3.82054	-0.00077	-4.59342	0.0538	-4.46206	0.05725	-5.21826	0.04905	-5.42158	0.02838				
J01352-072	57642.12351	-3.7266	-0.00057	-4.48182	0.05736	-4.28844	0.06046	-4.96896	0.05675	-5.08764	0.05346				
J01352-072	57688.01895	-3.7047	-0.00057	-4.4964	0.05681	-4.45856	0.05732	-4.94519	0.05689	-5.1665	0.0635				
J01352-072	57689.94375	-3.72311	-0.00061	-4.37603	0.06156	-4.36382	0.05972	-4.94801	0.05865	-5.05497	0.05738				
J01352-072	57690.03199	-3.86948	-0.00087	-4.56597	0.05461	-4.41074	0.05833	-5.08525	0.05184	-5.34203	0.06129				
J01352-072	57694.94953	-3.95014	-0.00102	-4.64458	0.05218	-4.37599	0.059	-5.13025	0.04717	-5.38588	0.06102				
J01352-072	57702.92905	-3.72015	-0.00064	-4.68796	0.05056	-4.4808	0.0568	-5.17798	0.04582	-5.47218	0.05296				
J01352-072	57734.84006	-3.56017	-0.00049	-4.5927	0.05747	-4.69284	0.05037	-4.86456	0.059	-5.13881	0.06352				
J01352-072	57751.83365	-3.83555	-0.00081	-4.75308	0.0479	-4.48215	0.05676	-5.32424	0.03617	-5.34966	0.03564				
J01352-072	57761.82791	-3.80467	-0.00081	-4.56063	0.05476	-4.43837	0.05776	-5.08014	0.05438	-5.39224	0.06093				
J01352-072	57762.81995	-3.79585	-0.0008	-4.61224	0.05322	-4.44745	0.05757	-5.07129	0.04893	-5.13591	0.06345				
J02519+224	57626.16677	-3.99461	-0.00071	-5.00513	0.04076	-4.78454	0.04917	-5.83907	0.03772	-6.08178	-0.00947				
J02519+224	57690.08409	-4.05905	-0.00082	-5.5183	-0.00292	-4.89244	0.04611	-6.02569	0.02894	-5.94615	0.04781				
J02519+224	57693.00903	-3.98414	-0.0007	-5.10632	0.03563	-4.766	0.04962	-5.88318	0.03669						
J02519+224	57974.0981	-3.99592	-0.00071	-5.35512	0.01679	-4.75773	0.04981	-5.90256	0.03588	-5.80646	0.05394				
J02519+224	57976.09926	-3.99147	-0.00071	-5.02946	0.03965	-4.95637	0.04391	-5.73353	0.04428	-5.81077	0.0434				
J02519+224	57981.06061	-3.95556	-0.00065	-4.80887	0.04771	-4.67863	0.05151	-5.999	0.02945	-6.11003	0.02738				
J02519+224	57987.1486	-4.03663	-0.00075	-5.25615	0.02559	-4.80011	0.04877	-6.05162	0.01808						
J02519+224	57990.16815	-4.03652	-0.00079	-5.13963	0.03369	-4.74111	0.0502	-6.02021	0.02375						
J02519+224	57999.13104	-4.04355	-0.00077	-5.09929	0.03602	-4.8576	0.04718	-5.9864	0.03121	-6.11357	-0.00894				
J02519+224	58001.1303	-3.9849	-0.0007	-4.97313	0.04207	-4.7266	0.05052	-5.92738	0.03618	-6.08821	0.03019				
J02519+224	58008.0402	-4.00639	-0.00073	-5.11688	0.03511	-4.70711	0.05094	-5.97475	0.03023	-6.09307	0.0276				
J02519+224	58010.09383	-4.0603	-0.00081	-5.18823	0.03067	-4.76483	0.04965	-6.00895	0.02217	-5.93477	0.05248				
J02519+224	58017.07661	-4.06103	-0.00081	-5.46706	0.00408	-4.76515	0.04964	-6.14813	0.00945						
J05019+011	57647.13757	-3.90429	-0.00063	-4.82155	0.03991	-4.65095	0.03633	-5.63018	0.03242	-5.58761	0.03839				
J05019+011	57690.06177	-3.94954	-0.0007	-4.89238	0.03894	-4.65689	0.036	-5.67239	0.03168	-5.72433	0.0323				
J05019+011	58010.16542	-3.87065	-0.00059	-4.73174	0.04109	-4.57423	0.0379	-5.65021	0.03193	-5.70725	0.03504				
J05019+011	58026.15237	-3.79806	-0.0005	-4.6946	0.04152	-4.57949	0.04173	-5.55077	0.03457	-5.69041	0.03246	-4.05397	0.03198		
J05019+011	58034.10272	-3.88223	-0.0006	-4.74651	0.04095	-4.61662	0.03905	-5.61419	0.03327	-5.71474	0.03305				
J05019+011	58054.06653	-3.87977	-0.0006	-4.69604	0.04157	-4.55773	0.04198	-5.59073	0.03338	-5.62341	0.03763				
J05019+011	58080.00014	-3.94119	-0.00064	-4.86909	0.0394	-4.65221	0.03613	-5.74286	0.03131	-5.80262	0.03049				
J05019+011	58084.02435	-3.87711	-0.00059	-4.74629	0.04095	-4.60727	0.04152	-5.6019	0.03328	-5.65973	0.03109				
J05019+011	58109.92629	-3.85069	-0.00056	-4.74224	0.041	-4.58644	0.04178	-5.58181	0.03477	-5.65966	0.03332				
J05019+011	58111.90164	-3.85913	-0.00057	-4.79109	0.04037	-4.65743	0.03613	-5.67856	0.03209	-5.70327	0.02757				
J05019+011	58123.90783	-3.94675	-0.00069	-4.79577	0.04047	-4.63752	0.03646	-5.79387	0.02402	-5.85521	0.01712				
J05019+011	58131.89659	-3.84037	-0.00054	-4.78066	0.04054	-4.62176	0.03683	-5.6512	0.03327	-5.69943	0.02523				
J05019+011	58139.88792	-3.83071	-0.00054	-4.7594	0.04087	-4.62365	0.03915	-5.58466	0.03352	-5.687	0.02519	-4.05598	0.03191		
J05019+011	58208.82581	-3.82889	-0.00053	-4.75321	0.04095	-4.58785	0.0418	-5.66323	0.0312	-5.77709	0.01908				
J05019+011	58211.80509	-3.84405	-0.00056	-4.64415	0.04193	-4.43728	0.04301	-5.41103	0.03693						
J05019+011	58212.81089	-3.83049	-0.00054	-4.74029	0.04099	-4.54445	0.04045	-5.60277	0.03332						
J05019+011	58392.1436	-3.84005	-0.00055	-4.6683	0.04187	-4.64801	0.04114	-5.60341	0.03378	-5.62377	0.03644				
J05019+011	58487.90805	-3.87457	-0.00059	-4.81396	0.04019	-4.63081	0.03661	-5.66634	0.03124	-5.72616	0.02483	-4.10657	0.03017		
J05019+011	58847.88172	-3.78399	-0.00046	-4.61719	0.04233	-4.51084	0.04246	-5.48911	0.03712	-5.5835	0.03633	-4.06573	0.03183		

Continued on next page

// Star	MJD	Hα		Ca II IRT-a		Ca II IRT-b		He I D_3		Na I D_2		Paβ		Paδ	
		$log\left(\frac{L_{line}}{L_{Bol}}\right)$	δ	$log\left(\frac{L_{line}}{L_{Bol}}\right)$	δ	$log\left(\frac{L_{line}}{L_{Bol}}\right)$	δ	$log\left(\frac{L_{line}}{L_{Bol}}\right)$	δ	$log\left(\frac{L_{line}}{L_{Bol}}\right)$	δ	$log\left(\frac{L_{line}}{L_{Bol}}\right)$	δ	$log\left(\frac{L_{line}}{L_{Bol}}\right)$	δ
J05062+046	57689.03941	-3.93706	-0.00064	-4.80834	0.06838	-4.77734	0.07017	-5.76848	0.06228	-5.88466	0.06898				
J05062+046	57694.02834	-3.83681	-0.00049	-4.72382	0.07079	-4.50826	0.07564	-5.63131	0.06854	-5.70592	0.07632				
J05062+046	58008.16049	-3.93027	-0.00063	-4.87201	0.06623	-4.63616	0.07346	-5.96434	0.05177						
J05062+046	58019.18607	-3.93053	-0.00061	-4.84111	0.06732	-4.68732	0.07239	-5.73426	0.06398						
J05062+046	58029.14333	-3.92871	-0.00062	-4.81735	0.06818	-4.52126	0.07544	-5.77688	0.06203	-5.94578	0.06073				
J05062+046	58049.12283	-3.9658	-0.00068	-4.98281	0.06177	-4.8274	0.06873	-5.86676	0.05697	-5.80834	0.076				
J05062+046	58081.03293	-3.9148	-0.0006	-4.75989	0.06989	-4.63697	0.07344	-5.75192	0.0639	-5.98602	0.07217				
J05062+046	58111.86991	-3.9432	-0.00064	-4.8552	0.06692	-4.65142	0.07315	-5.8057	0.06004	-5.96705	0.0545				
J05062+046	58123.88495	-3.88274	-0.00058	-4.87628	0.06617	-4.70248	0.07205	-5.62179	0.06685	-5.62641	0.07805				
J05062+046	58134.89778	-3.81172	-0.0005	-4.71498	0.07108	-4.61985	0.07385	-5.79932	0.06155	-5.75137	0.06777				
J05062+046	58208.80267	-3.9742	-0.00072	-4.91086	0.06486	-4.68319	0.07248	-6.01387	0.04004	-5.89221	0.07495				
J05062+046	58211.82838	-3.91002	-0.00061	-4.81498	0.06825	-4.70094	0.07208	-5.81854	0.05706	-5.67699	0.05956				
J05062+046	58212.83345	-3.90795	-0.0006	-4.75372	0.07006	-4.76131	0.07064	-5.72482	0.06434	-5.70247	0.0773				
J05366+112	57419	-4.12809	-0.00142	-5.56009	0.03934	-5.34783	0.05724	-5.52182	0.07866	-5.51272	0.0675				
J05366+112	57652.11294	-4.12743	-0.00163	-5.33368	0.06813	-5.14944	0.07673	-5.50468	0.06138	-5.41232	0.08695				
J05366+112	57672.10125	-4.00755	-0.00123	-5.30607	0.07837	-5.08713	0.08637	-5.43456	0.07983	-5.27951	0.09751				
J05366+112	58033.19492	-4.08686	-0.00114	-5.45776	0.0613	-5.17131	0.08045	-5.51809	0.08567	-5.52604	0.08897				
J05366+112	58041.16691	-3.96698	-0.00077	-5.22233	0.10105	-4.92909	0.10122	-5.25297	0.10071	-5.38913	0.09892				
J05366+112	58049.14581	-3.85992	-0.00069	-4.93629	0.10597	-4.74513	0.1083	-5.18902	0.10031	-5.20127	0.10421				
J05366+112	58080.14526	-4.00334	-0.00105	-5.34915	0.06954	-5.06191	0.08596	-5.42022	0.08748	-5.46997	0.08479				
J05366+112	58104.96164	-4.04257	-0.00117	-5.35199	0.06721			-5.56923	0.07646	-5.64598	0.0479				
J05366+112	58108.98126	-3.94479	-0.00104	-5.19914	0.08986	-4.88174	0.10553	-5.14565	0.09839	-5.28734	0.0899				
J05366+112	58526.81075	-4.05201	-0.00137	-5.50788	0.04599			-5.44792	0.0671	-5.44443	0.06176				
J05366+112	58774.14675	-4.01034	-0.00124	-5.39216	0.06371	-5.17584	0.07988	-5.43215	0.08299	-5.44863	0.09587				
J06000+027	57397	-3.95941	-0.00104	-5.06988	0.04831	-4.86256	0.05582	-5.18558	0.03908	-5.64551	0.01197				
J06000+027	57400	-4.06893	-0.00135	-5.42009	0.01637	-5.00638	0.04636	-5.36302	0.02313	-5.39332	0.02257				
J06000+027	57475.8384	-4.13738	-0.00137	-5.53603	0.00438	-5.15684	0.04896	-5.31895	0.03522	-5.36524	0.03553				
J06000+027	57650.15787	-4.15221	-0.00161	-5.57269	-0.00326	-5.04935	0.04726	-5.47452	0.01178	-5.24757	0.02101				
J06000+027	57677.18953	-4.11082	-0.00144	-5.28055	0.02918	-4.95685	0.05428	-5.29121	0.02925	-5.23287	0.04878				
J06000+027	57692.14587	-4.04971	-0.00126	-5.35829	0.02323	-4.9477	0.05459	-5.25743	0.04415	-5.40437	0.03985				
J06000+027	57693.14223	-4.2018	-0.00183	-5.6448	-0.01523	-5.11576	0.0414	-5.37618	0.02231						
J06000+027	57694.17426	-4.06863	-0.00135	-5.34294	0.02396	-5.01305	0.05307	-5.30165	0.03298	-5.3128	0.04244				
J06000+027	57699.1356	-4.03002	-0.00123	-5.18583	0.03807	-4.89924	0.0553	-5.34285	0.03995	-5.53949	0.03174				
J06000+027	57704.07801	-4.07428	-0.00135	-5.28687	0.02869	-4.99661	0.05329	-5.58982	0.00704	-5.29787	0.04275				
J06000+027	57706.10552	-4.14208	-0.00156	-5.4782	0.0097	-5.01996	0.04583	-5.6447	-0.01047	-5.3192	0.00961				
J06000+027	57712.06712	-4.04997	-0.00127	-5.18538	0.0479	-4.89044	0.05591	-5.20243	0.03972	-5.41117	0.0392				
J06574+740	57492.85078	-3.98662	-0.00089	-5.0522	0.04405	-4.77765	0.05881	-5.56914	0.04208	-5.35168	0.05536				
J06574+740	57689.97234	-3.96712	-0.00085	-4.83472	0.05427	-4.89354	0.05538	-5.53132	0.04781	-5.39117	0.05835				
J06574+740	57694.00378	-3.96159	-0.00084	-4.92038	0.05079	-4.61706	0.06227	-5.42522	0.0519	-5.3753	0.05743				
J06574+740	57706.13877	-3.91149	-0.00074	-4.69933	0.05849	-4.59737	0.06261	-5.45173	0.05165	-5.41386	0.05817				
J06574+740	58035.15313	-3.97618	-0.00086	-4.95755	0.04907	-4.78175	0.0587	-5.51401	0.04997	-5.48536	0.05395				
J06574+740	58048.17898	-3.94018	-0.0008	-4.84241	0.05399	-4.82693	0.05746	-5.4557	0.05168	-5.40243	0.06535				
J06574+740	58056.15006	-3.98387	-0.00078	-5.05886	0.04357	-4.97193	0.05249	-5.61585	0.04966	-5.36834	0.06662				
J06574+740	58065.13132	-3.93944	-0.00078	-4.91272	0.05112	-4.67509	0.06116	-5.55121	0.0503	-5.39928	0.0658				
J06574+740	58091.01664	-3.92088	-0.00076	-4.79227	0.05574	-4.72449	0.0601	-5.38196	0.05467	-5.39017	0.05748				
J06574+740	58094.11794	-3.96157	-0.00084	-4.86702	0.05301	-4.92379	0.05433	-5.55545	0.04754	-5.37157	0.05838				
J06574+740	58135.92408	-3.96458	-0.00083	-4.85972	0.05334	-4.84785	0.05684	-5.58623	0.04376	-5.38542	0.05887				
J07033+346	57665.12331	-4.06056	-0.0013	-5.36897	0.09823	-4.99048	0.12882	-5.41055	0.10915	-5.46609	0.10109				
J07033+346	57689.19624	-3.95285	-0.00103	-4.9551	0.12939	-4.80288	0.13169	-5.35554	0.11692	-5.25299	0.11677				
J07033+346	57693.17966	-4.09663	-0.00144	-5.6194	0.06399	-5.03823	0.12706	-5.43807	0.10528	-5.39003	0.11006	-4.19344	0.11417		
J07033+346	57735.06463	-4.10986	-0.00149	-5.35945	0.09637	-5.09127	0.12604	-5.66142	0.08051	-5.60988	0.1024				
J07033+346	58032.19107	-3.86917	-0.00085	-4.91802	0.13008	-4.69188	0.13281	-5.33303	0.11871	-5.10974	0.12222	-4.18194	0.11477		
J07033+346	58049.20458	-4.16762	-0.00168	-5.69915	0.04779	-5.08744	0.12605	-5.51299	0.10477	-5.55948	0.1237				
J07033+346	58122.96075	-3.9618	-0.00105	-5.24284	0.1216	-4.95706	0.12963	-5.35427	0.11467	-5.35657	0.12015				
J07033+346	58135.01436	-3.98006	-0.0011	-5.16096	0.12381	-4.89361	0.13028	-5.32404	0.11448	-5.44768	0.11405	-4.1747	0.11568		
J07033+346	58847.06815	-3.99011	-0.00111	-5.26392	0.1211	-4.98132	0.12913	-5.48356	0.10555	-5.49475	0.1086				
J07033+346	58849.89536	-3.94617	-0.00104	-4.98476	0.12778	-4.77419	0.13181	-5.24517	0.11986	-5.28526	0.12231				
J07033+346	58856.91187	-3.76893	-0.00069	-4.8243	0.13137	-4.63303	0.13341	-4.85993	0.13005	-5.10628	0.1273	-4.16617	0.11627		
J07033+346	58880.86083	-4.05904	-0.00131	-5.27415	0.10445	-4.95612	0.12911	-5.47191	0.10761	-5.35194	0.11244				
J07033+346	58890.88325	-4.1102	-0.00148	-5.6008	0.06587	-5.1687	0.12434	-5.53248	0.10043	-5.6357	0.0606	-4.12963	0.11724		
J07033+346	58893.97112	-4.11597	-0.00149	-5.41373	0.09096	-5.05962	0.12715	-5.60981	0.08589	-5.48566	0.10224				
J07472+503	57673.16994	-4.08815	-0.00129	-5.31722	0.02474	-4.90387	0.05007	-5.54445	0.03608						
J07472+503	58005.16492	-3.94569	-0.00092	-5.12927	0.03972	-4.73975	0.05508	-5.48599	0.03429						
J07472+503	58031.141	-4.04943	-0.00121	-5.317	0.02476	-4.8524	0.05185	-5.50452	0.03637						

Continued on next page

// Star	MJD	Hα		Ca II IRT-a		Ca II IRT-b		He I D_3		Na I D_2		Paβ		Paδ	
		$log\left(\frac{L_{line}}{L_{Bol}}\right)$	δ	$log\left(\frac{L_{line}}{L_{Bol}}\right)$	δ	$log\left(\frac{L_{line}}{L_{Bol}}\right)$	δ	$log\left(\frac{L_{line}}{L_{Bol}}\right)$	δ	$log\left(\frac{L_{line}}{L_{Bol}}\right)$	δ	$log\left(\frac{L_{line}}{L_{Bol}}\right)$	δ	$log\left(\frac{L_{line}}{L_{Bol}}\right)$	δ
J07472+503	58051.1612	-4.07698	-0.0011	-5.3129	0.02515	-4.87987	0.05093	-5.53042	0.04408						
J07472+503	58081.06146	-3.84691	-0.00076	-4.98395	0.04685	-4.76571	0.05441	-5.46669	0.04119						
J07472+503	58109.04382	-4.07789	-0.00128	-5.31844	0.02462	-4.93928	0.04872	-5.63608	0.02312	-5.53063	0.026				
J07472+503	58846.00363	-4.00186	-0.00105	-5.06501	0.04292	-4.81621	0.05298	-5.48952	0.04211	-5.52118	0.03855				
J07472+503	58857.01316	-4.10851	-0.00135	-5.406	0.01538	-4.93476	0.0489	-5.64086	0.02624	-5.59884	0.01557				
J07472+503	58862.02024	-4.03975	-0.00116	-5.18769	0.03538	-4.8385	0.0523	-5.55717	0.03358	-5.56963	0.0297				
J07472+503	58881.94252	-3.92255	-0.0009	-5.07431	0.04242	-4.81405	0.05305	-5.46267	0.03753	-5.44197	0.04456				
J07472+503	58890.91386	-4.08462	-0.00128	-5.5209	5e-05	-4.92155	0.04941	-5.52378	0.03716	-5.50758	0.04178				
J07472+503	58893.93532	-4.0895	-0.00126	-5.56659	-0.00727	-4.9393	0.04872	-5.54342	0.03686	-5.50466	0.04534				
J07472+503	58896.87102	-3.98088	-0.00105	-4.89348	0.05417	-4.64072	0.05731	-5.20604	0.05203	-5.23223	0.05396				
J07472+503	58902.91347	-3.92265	-0.00088	-5.03483	0.04447	-4.75577	0.05467	-5.46058	0.04247	-5.38292	0.04922				
J07472+503	58919.92359	-4.05826	-0.0012	-5.51588	0.00081	-4.93095	0.04905	-5.49863	0.03699	-5.5122	0.04248				
J09161+018	57712.15892	-3.80852	-0.00069	-4.56851	0.05158	-4.47221	0.05246	-5.03268	0.04706						
J09161+018	58091.09964	-3.91748	-0.00086	-5.04456	0.02898	-4.74491	0.04245	-5.45029	0.03224						
J09161+018	58105.17222	-3.86003	-0.00076	-4.83598	0.03928	-4.8014	0.04061	-5.33769	0.03767						
J09161+018	58110.13328	-3.9059	-0.00077	-4.95249	0.0342	-4.76545	0.04183	-5.46711	0.03774	-5.39018	0.03618				
J09161+018	58138.9445	-3.94296	-0.00092	-5.30899	0.00647	-4.76529	0.04184	-5.49224	0.029	-5.54134	0.0253				
J09161+018	58527.9098	-3.81003	-0.00068	-4.77137	0.04878	-4.62611	0.05095	-5.38239	0.03748	-5.331	0.03987				
J09161+018	58537.02827	-3.91554	-0.00086	-5.1308	0.02304	-4.69637	0.04388	-5.32389	0.03774	-5.39112	0.04133				
J09161+018	58540.99461	-3.76587	-0.00061	-4.76163	0.04943	-4.65465	0.0508	-5.3096	0.04088	-5.26242	0.04369				
J09161+018	58546.004	-3.93034	-0.00089	-5.13028	0.02318	-4.76276	0.04192	-5.48269	0.03168	-5.40858	0.03801				
J11476+002	57487.97179	-3.96311	-0.001	-5.01692	0.13988	-4.91432	0.14126	-5.45958	0.12791	-5.38388	0.11536				
J11476+002	57503.89927	-3.93806	-0.00096	-5.00191	0.1396	-4.85839	0.14204	-5.29728	0.13115	-5.30405	0.11954				
J11476+002	57571.86728	-3.98169	-0.00106	-5.05762	0.13815	-4.81822	0.14265	-5.51737	0.12012						
J11476+002	58121.16082	-3.81857	-0.00072	-4.92266	0.14093	-4.71249	0.1441	-5.28327	0.13495	-5.24006	0.13311				
J11476+002	58122.13173	-3.73188	-0.0006	-4.66478	0.14447	-4.57093	0.14538	-4.99716	0.14043	-5.10885	0.13685				
J11476+002	58138.13785	-3.93625	-0.00096	-4.98181	0.14024	-4.75843	0.14364	-5.19805	0.13683	-5.2901	0.13227				
J12428+418	57489.02351	-4.12222	-0.00155	-5.32125	0.00481	-4.85116	0.0407	-5.46896	0.00392	-5.44126	0.02474				
J12428+418	57512.01461	-4.24155	-0.00195	-5.63629	-0.04305	-5.03724	0.02636	-5.55189	0.00783						
J12428+418	57533.92958	-4.1872	-0.0018	-5.64389	-0.04004	-5.04109	0.02626	-5.5036	0.00837	-5.30491	0.00741				
J12428+418	57564.88743	-4.08456	-0.00142	-5.08805	0.03613	-4.80692	0.04141	-5.3769	0.01699	-5.27198	0.01963				
J12428+418	57754.25142	-3.89865	-0.00094	-4.80174	0.04147	-4.61392	0.04332	-5.05414	0.03676	-5.18594	0.03489				
J13536+776	57488.03626	-4.03222	-0.00104	-5.17739	0.09159	-4.91267	0.10628	-5.55449	0.09032	-5.47535	0.10561				
J13536+776	57528.9591	-4.07674	-0.00117	-5.21773	0.08923	-4.81096	0.10684	-5.61341	0.08757	-5.58313	0.0952				
J13536+776	57557.9528	-3.9513	-0.00088	-5.08067	0.09675	-4.86951	0.10699	-5.49169	0.09521	-5.58666	0.09617				
J13536+776	57584.96169	-4.07766	-0.00102	-5.18251	0.09129	-4.88142	0.10511	-5.61864	0.09245	-5.55414	0.09661				
J13536+776	57910.9459	-4.03587	-0.00097	-5.18558	0.09111	-4.82201	0.10654	-5.53887	0.09768	-5.53865	0.09894				
J13536+776	57917.05656	-4.18155	-0.00151	-5.48606	0.06528	-4.97295	0.10225	-5.68938	0.08265	-5.66428	0.09447				
J13536+776	58142.21852	-4.11117	-0.00118	-5.27072	0.08563	-4.92447	0.10375	-5.67211	0.09044	-5.58593	0.09776				
J13536+776	58645.92144	-4.05462	-0.00112	-5.27876	0.08491	-4.82585	0.10649	-5.59609	0.09046	-5.53135	0.09572				
J13536+776	58665.90636	-4.06823	-0.00113	-5.30866	0.08277	-4.91356	0.10414	-5.58066	0.09169	-5.59871	0.09272				
J13536+776	58669.01055	-4.17118	-0.00147	-5.58183	0.05252	-4.94054	0.10325	-5.73562	0.07189	-5.63636	0.09299				
J13536+776	58677.90931	-3.46217	-0.00033	-4.04644	0.11582	-3.97839	0.11602	-4.42732	0.11519	-4.98156	0.11216	-3.2661	0.11352	-3.88904	0.11322
J13536+776	58678.90775	-3.9878	-0.00096	-5.05893	0.09774	-4.763	0.10839	-5.46079	0.09833	-5.6164	0.08992				
J13536+776	58679.85652	-4.13387	-0.00127	-5.36249	0.07809	-4.89232	0.10475	-5.70501	0.08391	-5.69662	0.08762				
J13536+776	58857.0921	-4.04239	-0.00109	-5.06574	0.09743	-4.78297	0.10786	-5.52954	0.09657	-5.55506	0.09977				
J13536+776	58877.21649	-3.90678	-0.0008	-4.83089	0.10998	-4.64866	0.11263	-5.30602	0.10427	-5.4095	0.10276	-3.92763	0.10574		
J13536+776	58880.08777	-4.11902	-0.00131	-5.25442	0.08666	-4.84735	0.10596	-5.61369	0.08959	-5.56681	0.09551	-3.99069	0.10398		
J13536+776	58883.19162	-4.08603	-0.00123	-5.23318	0.08811	-4.92662	0.10369	-5.47952	0.09421	-5.59331	0.0899				
J13536+776	58884.19854	-4.03161	-0.00097	-5.21185	0.08949	-4.85355	0.1058	-5.61149	0.09501	-5.59092	0.09772	-3.94982	0.10525		
J13536+776	58885.19101	-4.08673	-0.00125	-5.24569	0.08727	-4.84237	0.10608	-5.50034	0.09442	-5.52666	0.10072				
J13536+776	58891.05464	-4.10551	-0.00126	-5.3018	0.08316	-4.89746	0.10455	-5.77031	0.07646	-5.56248	0.0973				
J13536+776	58893.11666	-4.08535	-0.00119	-5.21372	0.08938	-4.8929	0.10473	-5.64119	0.08861	-5.59923	0.10016	-4.06606	0.10138		
J13536+776	58895.09426	-4.01903	-0.00104	-5.09804	0.09584	-4.82475	0.10647	-5.54713	0.09329	-5.56523	0.09921	-4.03176	0.10256		
J13536+776	58897.17476	-4.05586	-0.00113	-5.15655	0.09288	-4.81689	0.10666	-5.54467	0.0928	-5.41879	0.10993				
J13536+776	58904.21149	-4.15874	-0.00142	-5.57441	0.05361	-4.9776	0.10209	-5.72983	0.06546	-5.37815	0.11133				
J13536+776	58923.08859	-4.09992	-0.00123	-5.36137	0.07835	-4.93922	0.10329	-5.56699	0.08984	-5.59909	0.09468	-4.15273	0.09793		
J13591-198	57488.06308	-4.00786	-0.00107	-5.0315	0.08174	-4.84482	0.08498	-5.41797	0.06521	-5.33941	0.07278				
J13591-198	57534.93348	-4.05575	-0.00119	-5.33455	0.05801	-4.98484	0.08268	-5.84291	0.02894	-5.30586	0.08304				
J13591-198	58134.23566	-4.10821	-0.00135	-5.13264	0.07872	-4.96828	0.083	-5.74706	0.03904						
J13591-198	58172.14728	-4.06708	-0.00123	-5.10785	0.07931	-4.87026	0.0844	-5.67376	0.05765						
J13591-198	58186.1245	-4.03437	-0.00114	-5.07065	0.08019	-4.89974	0.08405	-5.38223	0.06074	-5.45658	0.0817				
J13591-198	58570.0845	-4.06789	-0.00122	-5.14124	0.07748	-4.97641	0.08291	-5.56652	0.04895	-5.45868	0.0655				
J13591-198	58587.02302	-4.05515	-0.00119	-5.0876	0.07949	-4.94684	0.083	-5.4139	0.07061	-5.25353	0.07764				

Continued on next page

// Star	MJD	Hα		Ca II IRT-a		Ca II IRT-b		He I D_3		Na I D_2		Paβ		Paδ	
		$log\left(\frac{L_{line}}{L_{Bol}}\right)$	δ	$log\left(\frac{L_{line}}{L_{Bol}}\right)$	δ	$log\left(\frac{L_{line}}{L_{Bol}}\right)$	δ	$log\left(\frac{L_{line}}{L_{Bol}}\right)$	δ	$log\left(\frac{L_{line}}{L_{Bol}}\right)$	δ	$log\left(\frac{L_{line}}{L_{Bol}}\right)$	δ	$log\left(\frac{L_{line}}{L_{Bol}}\right)$	δ
J13591-198	58590.03788	-4.0175	-0.00109	-5.15113	0.0785	-4.89768	0.0842	-5.57865	0.06537	-5.15227	0.08639				
J13591-198	58600.02089	-3.9928	-0.00105	-5.0897	0.07979	-4.86497	0.08448	-5.60911	0.05658	-5.42986	0.07007				
J13591-198	58615.97726	-4.14573	-0.00148	-5.23122	0.07412	-4.99949	0.08225	-5.63271	0.05484						
J13591-198	58629.92666	-4.03848	-0.00117	-5.07039	0.07994	-4.91063	0.08399	-5.4542	0.06775	-5.25175	0.08063				
J13591-198	58637.91278	-4.11818	-0.00139	-5.23251	0.07431	-4.91264	0.0836	-5.405	0.06088	-5.34749	0.08078				
J13591-198	58643.8907	-4.00149	-0.00107	-5.10476	0.07893	-4.76285	0.08584	-5.50189	0.06293	-5.35044	0.07957				
J13591-198	58649.88299	-4.10281	-0.00135	-5.15757	0.07758	-5.00395	0.08187	-5.50678	0.05024						
J13591-198	58895.18678	-4.03432	-0.00114	-5.08298	0.07926	-4.94747	0.08292	-5.43	0.07032						
J13591-198	58904.12746	-3.86126	-0.00079	-4.96909	0.08136	-4.84325	0.0849	-5.50023	0.06699						
J18131+260	57691.8322	-3.8263	-0.00028	-4.55993	0.1216	-4.32538	0.1224	-5.10008	0.11486	-5.13147	0.11614				
J18131+260	57692.81109	-3.82875	-0.00029	-4.582	0.12142	-4.33105	0.12223	-5.16824	0.112	-5.24688	0.11828				
J18131+260	57912.04549	-3.79056	-0.00026	-4.59875	0.12131	-4.30235	0.12261	-5.26943	0.10949	-5.28115	0.10839				
J18131+260	57913.9883	-3.78143	-0.00026	-4.68328	0.11911	-4.29328	0.12237	-5.2092	0.11259	-5.29609	0.10672				
J18131+260	57915.99561	-3.71067	-0.00022	-4.55174	0.12169	-4.34257	0.12225	-5.13497	0.1146	-5.30648	0.10686				
J18131+260	58666.02578	-3.77191	-0.00025	-4.75107	0.11816	-4.28129	0.12126	-5.12947	0.11364	-5.24283	0.10896				
J18131+260	58668.11842	-3.73113	-0.00023	-4.5411	0.12182	-4.27023	0.12285	-5.06332	0.11504	-5.22274	0.11253				
J18131+260	58669.03441	-3.77451	-0.00025	-4.67784	0.12071	-4.25998	0.12304	-5.14913	0.11371	-5.29753	0.10882				
J18131+260	58677.95866	-3.81331	-0.00027	-4.66907	0.11916	-4.39993	0.12009			-5.24822	0.11439				
J18131+260	58678.95762	-3.80851	-0.00027	-4.58719	0.12146	-4.29635	0.12267	-5.18436	0.11313	-5.2558	0.11031				
J18131+260	58679.94592	-3.80297	-0.00027	-4.61785	0.12111	-4.33935	0.12076	-5.28282	0.10972	-5.27714	0.10871				
J19511+464	57530.11572	-4.00611	-0.00095	-5.21087	0.10859	-4.87702	0.12643	-5.54656	0.10955	-5.27201	0.12109				
J19511+464	57557.08476	-3.94533	-0.00084	-5.11662	0.11481	-4.77249	0.12933	-5.45076	0.11736	-5.37735	0.11637				
J19511+464	57574.0602	-3.96236	-0.00085	-5.41524	0.0899	-4.95858	0.12369	-5.48741	0.11998	-5.38358	0.12385				
J19511+464	57586.02294	-3.98663	-0.00076	-5.06214	0.1177	-4.84136	0.12755	-5.67777	0.11368	-5.46499	0.12364				
J19511+464	57595.99602	-3.98313	-0.00093	-5.14108	0.11335	-4.82524	0.12796	-5.45596	0.1189	-5.44178	0.10886				
J19511+464	57606.98286	-3.9823	-0.00079	-5.53814	0.07327	-5.03074	0.12074	-5.53185	0.11971	-5.43311	0.12375				
J19511+464	57815.16678	-3.93787	-0.00084	-5.16109	0.11199	-4.89959	0.12576	-5.41598	0.1196	-5.32141	0.11552				
J19511+464	57818.1731	-3.98632	-0.00096	-5.43249	0.08787	-4.81933	0.12812	-5.40368	0.11997	-5.5537	0.12947				
J19511+464	57821.20838	-3.9157	-0.00074	-5.12099	0.11456	-4.79557	0.12875	-5.47429	0.12083	-5.26785	0.13016				
J19511+464	57848.16166	-3.99458	-0.00096	-5.15105	0.11273	-4.846	0.12737	-5.63609	0.10698	-5.29356	0.12593				
J19511+464	57850.11508	-4.01529	-0.00098	-5.33544	0.09816	-4.95429	0.12379	-5.60549	0.10838	-5.21586	0.13609				
J19511+464	57852.08142	-3.97894	-0.00091	-5.23933	0.10647	-4.88283	0.1263	-5.478	0.11139	-5.38335	0.12447				
J19511+464	57855.08186	-3.90854	-0.00078	-5.63039	0.05778	-4.82178	0.1281	-5.55653	0.11107	-5.25717	0.13583				
J22012+283	57554.12142	-3.79673	-0.00068	-4.89134	0.03954	-4.77968	0.04546	-5.57485	0.02301	-5.25129	0.04232				
J22012+283	57558.12459	-3.8024	-0.00068	-5.02824	0.03158	-4.77884	0.04549			-5.29044	0.03765				
J22012+283	57585.1439	-3.90801	-0.00072	-5.02791	0.0316	-4.80226	0.04463	-5.53627	0.03876	-5.30391	0.04782				
J22012+283	57586.09845	-3.9254	-0.00066	-5.32954	0.01423	-4.68895	0.05098			-5.26815	0.04635				
J22012+283	57588.07373	-3.83355	-0.00068	-4.84686	0.04251	-4.67474	0.04935	-5.60739	0.02409	-5.24574	0.04333				
J22012+283	57617.01479	-3.88495	-0.0008	-4.98178	0.03457	-4.75953	0.04616	-5.41373	0.03413	-5.28537	0.04087				
J22012+283	57752.82545	-3.75586	-0.00062	-4.88048	0.04007			-5.52565	0.02628	-5.2231	0.04317				
J22012+283	57753.82377	-3.59561	-0.00043	-4.41315	0.05758	-4.49918	0.05703	-5.16273	0.05097	-4.97462	0.05511				
J22012+283	57754.81351	-3.76519	-0.0006	-4.95298	0.03626			-5.4821	0.03308	-5.16148	0.03963				
J22012+283	57761.80277	-3.79669	-0.00064	-4.93495	0.03727	-5.2378	0.01636	-5.63358	0.01829	-5.33617	0.0435				
J22012+283	57762.77275	-3.80495	-0.00065	-4.83673	0.04207			-5.42051	0.03727	-5.18117	0.04924				
J23548+385	57592.15507	-3.82809	-0.00073	-5.04307	0.05388	-4.67318	0.06215	-5.12144	0.0561	-5.30598	0.04858				
J23548+385	57603.1576	-3.87436	-0.00082	-5.1772	0.03705	-4.71063	0.05673	-5.18844	0.05302						
J23548+385	57622.01743	-3.91749	-0.00089	-5.24661	0.03173	-4.69526	0.05709	-5.26434	0.05048	-5.30315	0.04823				
J23548+385	57643.06351	-3.64507	-0.00048	-4.81145	0.06081	-4.57077	0.06339	-5.11279	0.05683	-5.07557	0.05864				
J23548+385	57649.08109	-3.89317	-0.00084	-5.14925	0.03881	-4.77389	0.05542	-5.30595	0.04932	-5.31651	0.05163				
J23548+385	57659.10191	-3.82345	-0.00072	-5.09953	0.04787	-4.61716	0.06292	-5.05919	0.05273	-5.12716	0.05845				
J23548+385	57672.92681	-3.85242	-0.00077	-5.02694	0.05267	-4.72195	0.06165	-5.07775	0.05791	-5.17428	0.05766				
J23548+385	57690.94225	-3.84995	-0.00076	-5.07127	0.04711	-4.69837	0.06194	-5.16014	0.0555						
J23548+385	57705.84572	-3.7533	-0.00062	-4.83169	0.06012	-4.57874	0.06324	-5.04908	0.0573	-5.27403	0.04973				
J23548+385	57737.81024	-3.84815	-0.00077	-5.06629	0.05122	-4.75374	0.06121	-5.08283	0.05637						
J23548+385	57753.89008	-3.82488	-0.00073	-4.93015	0.0588	-4.68543	0.06219	-5.06667	0.05661	-5.28391	0.04683				
J23548+385	57761.85214	-3.92998	-0.00091	-5.23482	0.03479	-4.79371	0.05709	-5.07987	0.05199	-5.14762	0.05342				
J04153-076	57395	-4.05918	-0.00189	-5.47884	-0.05225	-5.14781	-0.01168			-5.32122	0.01723				
J04153-076	57436	-4.10157	-0.00206	-5.45764	-0.04771					-5.39278	0.01739				
J04153-076	57623.14696	-4.05448	-0.00162	-5.28738	-0.00767	-5.01548	0.01016	-5.52778	0.00937	-5.64287	-0.00054				
J04153-076	57629.15863	-4.0595	-0.00186	-5.43445	-0.04016	-5.11522	-0.00574	-5.57792	0.0012	-5.72699	-0.01055				
J04153-076	57630.16201	-4.13088	-0.00222	-5.39838	-0.03596	-5.24425	-0.02016	-5.65223	-0.01024	-5.75306	-0.03052				
J04153-076	57634.12438	-3.94868	-0.00122	-5.22819	0.02013	-4.97699	0.03031	-5.39197	0.01431	-5.65686	-0.00257				
J04153-076	57636.16488	-3.98654	-0.00159	-5.39536	-0.01249	-5.08197	0.00623	-5.53485	-0.01068	-5.47913	0.01099				
J04153-076	57647.10712	-4.16432	-0.00184	-5.52991	-0.03805			-5.64999	0.00504	-5.525	0.01237				

Continued on next page

// Star	MJD	Hα		Ca II IRT-a		Ca II IRT-b		He I D_3		Na I D_2		Paβ		Paδ	
		$log\left(\frac{L_{line}}{L_{Bol}}\right)$	δ	$log\left(\frac{L_{line}}{L_{Bol}}\right)$	δ	$log\left(\frac{L_{line}}{L_{Bol}}\right)$	δ	$log\left(\frac{L_{line}}{L_{Bol}}\right)$	δ	$log\left(\frac{L_{line}}{L_{Bol}}\right)$	δ	$log\left(\frac{L_{line}}{L_{Bol}}\right)$	δ	$log\left(\frac{L_{line}}{L_{Bol}}\right)$	δ
J04153-076	57649.19882	-4.03451	-0.00135	-5.23189	-0.00077	-5.02009	0.00981	-5.5886	0.00928	-5.50741	0.01914				
J04153-076	57655.20508	-4.04967	-0.00184	-5.325	-0.02369	-5.1265	-0.00906	-5.6908	-0.02167	-5.76219	-0.01916				
J04153-076	57657.09539	-4.05043	-0.00185	-5.15218	-0.00012			-5.48059	-0.01084						
J04153-076	57678.11244	-4.1242	-0.00196	-5.44241	-0.04305	-5.4179	-0.05539	-5.64297	-0.02443	-5.56015	0.00693				
J04153-076	57691.02087	-4.06051	-0.00136	-5.34342	-0.00869	-4.94495	0.0163	-5.60998	0.00668	-5.66793	0.00758				
J04153-076	57703.99878	-4.06821	-0.00137	-5.30704	-0.0058	-4.94951	0.01664								
J04153-076	57705.01126	-4.02596	-0.00116	-5.26987	0.00802	-5.07212	0.01156	-5.55309	0.01424						
J04153-076	57712.01331	-3.99656	-0.0012	-5.16073	0.01368	-4.91816	0.01796	-5.41313	0.02157	-5.76661	-0.02305				
J04153-076	57734.94726	-3.94862	-0.00101	-5.38052	-0.00264	-4.98022	0.01643	-5.41156	0.01994	-5.70788	0.00462				
J04153-076	57752.90752	-4.07086	-0.00135	-5.45716	-0.02575	-5.12718	0.00331			-5.71123	0.00444				
J04153-076	57753.81631	-4.02918	-0.00123	-5.39225	-0.00354	-4.92669	0.02144	-5.51874	0.01087	-5.61788	0.00918				
J04153-076	57754.85377	-3.9321	-0.00099	-5.2568	0.02621	-5.09736	0.01315	-5.62627	0.00638	-5.62334	0.01298				
J04153-076	57759.89292	-4.13083	-0.0016	-5.51402	-0.03741	-5.22691	-0.0081	-5.74407	-0.01111	-5.78563	-0.01399				
J04153-076	57760.9231	-4.09477	-0.00142	-5.52014	-0.03487	-5.02137	0.01262	-5.71745	-0.00337	-5.72988	-0.00014				
J04153-076	57787.79541	-4.0779	-0.00163	-5.49662	-0.04491	-5.21561	-0.01362	-5.69896	-0.00607	-5.80955	-0.02342				
J04153-076	57798.80986	-4.02142	-0.00099	-5.13247	0.03246	-4.89099	0.02843	-5.62088	0.01589	-5.61217	0.02226				
J04153-076	57798.85397	-3.9994	-0.00094	-5.15053	0.02917	-4.90362	0.02684	-5.56849	0.01649	-5.59267	0.02125				
J04153-076	57799.81443	-3.99877	-0.00147	-5.18521	0.00869	-4.92319	0.01592	-5.61625	-0.00579	-5.71518	-0.01678				
J04153-076	57799.85559	-4.06286	-0.00187	-5.43567	-0.04002	-5.12347	-0.0087	-5.61427	-0.01969	-5.51962	0.00528				
J04153-076	57805.85527	-3.94185	-0.00143	-5.15419	0.01323	-5.0748	0.00255	-5.47647	0.00799	-5.19561	0.02585				
J04153-076	57814.81182	-4.03038	-0.00068	-5.24083	0.0273	-4.97713	0.02846	-5.61248	0.02625	-5.68043	0.02645				
J04153-076	57818.80738	-4.06851	-0.00176	-5.40981	-0.03558	-5.04136	0.00173	-5.59704	-0.00731	-5.55035	0.00251				
J04153-076	57830.80061	-4.07831	-0.00085	-5.44295	0.00896	-4.94213	0.02698	-5.63813	0.02064	-5.66784	0.01874				
J04153-076	57831.80275	-4.05793	-0.00077	-5.25464	0.02144	-4.99168	0.02715	-5.68328	0.02024	-5.62067	0.02339				
J04153-076	58006.18862	-4.00195	-0.00122	-5.42722	-0.01153	-5.03986	0.01404	-5.52009	0.01583	-5.6483	0.01206				
J04153-076	58028.16412	-4.07458	-0.0008	-5.29748	0.02003	-4.96951	0.02833	-5.5797	0.02728	-5.50027	0.03165				
J04153-076	58060.03273	-4.13353	-0.00227	-5.42734	-0.04159	-4.89106	0.01267	-5.72273	-0.02898						
J04153-076	58117.93833	-4.12282	-0.00096	-5.39175	0.00489	-5.11829	0.01796	-5.74181	0.01769	-5.67719	0.02367				
J04153-076	58119.91066	-4.07925	-0.00143	-5.50906	-0.03515	-5.1136	0.00426	-5.66592	-0.00636	-5.81338	-0.01837				
J04173+088	58464.80567	-3.75484	-0.00086	-4.79454	0.02878			-5.38963	0.00604	-4.79094	0.02938				
J04173+088	58464.81712	-3.74649	-0.00089	-4.53217	0.03351			-5.17569	0.01852	-4.97452	0.02432				
J04173+088	58464.82833	-3.8053	-0.00097	-4.90929	0.00407	-4.71903	0.0113			-5.14339	0.01734				
J04173+088	58464.85271	-3.80323	-0.001	-4.97163	-0.00133	-4.86527	0.00021	-5.63272	-0.01918	-5.21471	0.01322				
J04173+088	58467.81649	-3.82157	-0.001	-5.04621	-0.00881	-4.85664	0.00102	-5.71721	-0.03318	-5.11937	0.02525				
J04173+088	58467.82787	-3.72045	-0.00082	-4.81887	0.01068	-4.75256	0.00911	-5.48228	0.00324	-5.16712	0.02532				
J04173+088	58467.83992	-3.76814	-0.00092	-4.685	0.01819	-4.59401	0.01825	-5.43116	0.00686	-5.09861	0.01872				
J04173+088	58467.87412	-3.84621	-0.00108	-5.27638	-0.04222	-4.52744	0.0212	-5.44134	0.00603	-5.64225	-0.04299				
J04173+088	58467.88495	-3.78886	-0.00096	-5.00366	-0.00435	-4.75173	0.00917	-5.34486	0.00927	-5.14914	0.00831				
J04173+088	58467.89639	-3.83528	-0.00107	-5.06434	-0.01085	-4.69365	0.0129	-5.46991	0.00643	-5.35137	0.00018				
J04173+088	58467.94215	-3.84181	-0.0011	-4.98413	-0.00244	-4.83819	0.0026	-5.63905	-0.02043	-5.25679	0.00561				
J04173+088	58467.96493	-3.83422	-0.00109	-5.0407	-0.00821	-4.78455	0.00683	-5.49093	0.0005	-5.17738	0.02101				
J04173+088	58467.97576	-3.84123	-0.0011	-5.14417	-0.02091	-4.73355	0.01039	-5.40683	0.00346						
J04173+088	58467.98741	-3.66831	-0.00077	-4.55933	0.03222	-4.37116	0.02924	-5.18532	0.02632	-5.02408	0.03164				
J04173+088	58467.99824	-3.61345	-0.00067	-4.45689	0.03391	-4.25823	0.03526	-5.29594	0.02264	-4.93092	0.03306				
J04173+088	58468.01676	-3.58095	-0.00061	-4.41052	0.0341	-4.36942	0.03403	-5.29777	0.02118	-5.0192	0.03154				
J04173+088	58468.02759	-3.65112	-0.0007	-4.70701	0.02859	-4.46996	0.03088	-5.2676	0.02194	-5.04706	0.02813				
J04173+088	58468.03916	-3.67851	-0.00074	-4.69937	0.01967	-4.49234	0.02283	-5.36006	0.01493	-5.16402	0.0272				
J04173+088	58468.04999	-3.69821	-0.00075	-4.90391	0.00455	-4.65697	0.01502			-5.64008	-0.00137				
J04173+088	58468.0619	-3.71256	-0.00077	-4.803	0.01169			-5.43646	0.00626	-5.50309	-0.01372				
J04173+088	58468.07336	-3.67872	-0.00071	-5.02697	-0.00674	-4.60642	0.01765	-5.39092	0.00801	-5.02666	0.02893				
J04173+088	58468.08482	-3.71648	-0.00078	-5.02825	-0.00588	-4.6732	0.0141	-5.4697	0.00471	-5.33941	0.00536				
J04173+088	58468.0962	-3.76803	-0.00088	-4.87949	0.00703	-4.51705	0.02162	-5.25612	0.01468	-5.26973	0.03285				
J04173+088	58468.10778	-3.86341	-0.00113	-4.74476	0.02974	-4.55111	0.02021	-5.59979	-0.01266	-4.96188	0.02493				
J04173+088	58468.11987	-3.75555	-0.00088	-4.79617	0.02883	-4.77132	0.00779	-5.48515	-0.00159	-4.95619	0.02475				
J07446+035	57395	-3.95864	-0.00052	-4.81058	0.26243	-4.66651	0.26437	-5.81923	0.26	-5.92586	0.25681				
J07446+035	57397	-3.95217	-0.00052	-4.78408	0.26283	-4.63576	0.2646	-5.82195	0.26	-5.83636	0.25897				
J07446+035	57398	-4.01002	-0.00088	-4.88852	0.25798	-4.74545	0.26149	-5.89664	0.25296	-6.03381	0.24504				
J07446+035	57400	-3.95763	-0.0005	-4.75603	0.26345	-4.61525	0.26492	-5.79587	0.2607	-5.98743	0.25709				
J07446+035	57401	-4.04042	-0.00041	-4.89196	0.26346	-4.7116	0.26515	-6.03898	0.25999	-6.01017	0.26089				
J07446+035	57414	-3.9748	-0.00048	-4.83212	0.26312	-4.69305	0.26437	-5.82247	0.26049	-6.00862	0.25719				
J07446+035	57415	-3.97672	-0.00042	-4.80737	0.26386	-4.66013	0.26508	-5.85497	0.26168	-6.04195	0.25906				
J07446+035	57418	-4.07429	-0.00064	-4.93519	0.26107	-4.74764	0.26373	-5.93301	0.25826	-5.99512	0.25714				
J07446+035	57421	-3.98159	-0.00035	-4.75272	0.26468	-4.62298	0.26568	-5.80227	0.26332	-5.95397	0.26205				
J07446+035	57441	-3.98353	-0.00048	-4.82833	0.26289	-4.68722	0.26453	-5.85173	0.26076	-6.10746	0.25586				

Continued on next page

// Star	MJD	Hα		Ca II IRT-a		Ca II IRT-b		He I D_3		Na I D_2		Paβ		Paδ	
		$log\left(\frac{L_{line}}{L_{Bol}}\right)$	δ	$log\left(\frac{L_{line}}{L_{Bol}}\right)$	δ	$log\left(\frac{L_{line}}{L_{Bol}}\right)$	δ	$log\left(\frac{L_{line}}{L_{Bol}}\right)$	δ	$log\left(\frac{L_{line}}{L_{Bol}}\right)$	δ	$log\left(\frac{L_{line}}{L_{Bol}}\right)$	δ	$log\left(\frac{L_{line}}{L_{Bol}}\right)$	δ
J07446+035	57443	-4.02132	-0.00074	-4.86296	0.26072	-4.70421	0.26315	-5.8875	0.2565	-6.13414	0.23994				
J07446+035	57444	-3.98471	-0.00043	-4.86383	0.263	-4.67091	0.26495	-5.84161	0.26158	-6.0884	0.25691	-4.18617	0.2551		
J07446+035	57465.9353	-4.00881	-0.0006	-4.81293	0.26251	-4.64025	0.26446	-5.79444	0.26082			-3.96866	0.25771		
J07446+035	57474.89281	-3.9295	-0.00033	-4.79784	0.26428	-4.64918	0.26548	-5.84867	0.26267						
J07446+035	57489.84222	-4.02433	-0.00084	-4.91679	0.259	-4.7821	0.26168	-6.0949	0.23671	-5.78812	0.23752				
J07446+035	57493.84697	-3.99041	-0.00057	-4.82334	0.26249	-4.65427	0.26442	-5.87402	0.25915						
J07446+035	57509.83309	-3.99232	-0.00064	-4.86556	0.26122	-4.72767	0.26334	-5.88686	0.25732						
J07446+035	57655.21126	-3.90258	-0.00077	-4.70714	0.26131	-4.57673	0.26346	-5.82879	0.25323	-5.72134	0.25724	-3.94962	0.24937		
J07446+035	57673.16323	-3.96303	-0.00068	-4.8525	0.26016	-4.67569	0.26303	-5.941	0.25381	-6.156	0.24586				
J07446+035	57689.22808	-3.97138	-0.0006	-4.84066	0.26128	-4.67782	0.26363	-5.97559	0.25554	-5.99429	0.25569	-4.14357	0.25079		
J07446+035	57692.22124	-3.92806	-0.00058	-4.69915	0.26286	-4.58612	0.26437	-5.83952	0.25838	-5.87423	0.25752				
J07446+035	57699.14675	-3.96617	-0.00088	-4.78439	0.26032	-4.65911	0.26264	-5.93419	0.24814	-5.77194	0.2575				
J07446+035	57704.09947	-3.94387	-0.00061	-4.75535	0.26251	-4.60225	0.26439	-5.9168	0.2541	-5.96091	0.25493				
J07446+035	57735.10166	-4.04711	-0.00075	-4.86908	0.2604	-4.68925	0.26351	-5.93273	0.2547	-5.98215	0.25392	-4.1797	0.24834		
J07446+035	57755.17775	-3.90187	-0.00055	-4.7355	0.26254	-4.59738	0.26443	-5.75525	0.25693	-6.01872	0.2476	-4.18226	0.24687		
J07446+035	57756.04622	-4.01609	-0.00064	-4.8698	0.26128	-4.67884	0.26389	-5.96962	0.25562	-5.98564	0.2539	-4.1716	0.2503		
J07446+035	57759.98826	-3.91695	-0.00058	-4.80758	0.26137	-4.65528	0.26364	-5.98317	0.2533	-5.92538	0.25506	-3.95886	0.25629		
J07446+035	57760.90053	-3.9214	-0.00058	-4.79226	0.26167	-4.62104	0.26412	-5.75277	0.25712	-5.98741	0.2502	-4.01051	0.25443		
J07446+035	57762.11015	-3.90811	-0.00054	-4.62929	0.26387	-4.50797	0.26514	-5.82769	0.25823	-5.82035	0.25917	-3.94499	0.2563		
J07446+035	57763.02057	-3.98678	-0.00068	-4.85069	0.26064	-4.69757	0.26334	-5.87195	0.25642	-5.93261	0.25446	-4.12387	0.25358		
J07446+035	57771.09105	-4.00602	-0.00098	-4.72967	0.26117	-4.6496	0.26286	-5.8454	0.2502	-5.80284	0.24897				
J07446+035	57778.95241	-4.0458	-0.0008	-4.89764	0.25989	-4.7234	0.26266	-5.91086	0.25491	-6.13587	0.24634	-4.07998	0.25291		
J07446+035	57785.98015	-3.85262	-0.00048	-4.62903	0.26378	-4.50384	0.26504	-5.70679	0.26051	-5.78707	0.25941	-4.00243	0.2555		
J07446+035	57787.97542	-3.77905	-0.00039	-4.47019	0.2649	-4.38925	0.26567	-5.42548	0.26438	-5.62914	0.2629	-3.96164	0.25811		
J07446+035	57789.97063	-4.08132	-0.00109	-4.89578	0.25786	-4.70943	0.26198	-5.92285	0.24916	-6.06013	0.23408				
J07446+035	57797.96882	-3.86794	-0.00044	-4.68841	0.26371	-4.56697	0.26501	-5.73843	0.26131	-5.79719	0.26071	-3.97667	0.25731		
J07446+035	57799.89458	-3.96307	-0.0005	-4.81301	0.26247	-4.66265	0.26441	-5.79244	0.26081	-5.9378	0.25833	-4.04156	0.25638		
J07446+035	57814.85076	-4.06707	-0.00045	-4.85347	0.26373	-4.70391	0.26512	-5.94494	0.26139	-6.02924	0.26033	-4.03559	0.25912		
J07446+035	57821.8556	-3.97242	-0.00037	-4.81428	0.26398	-4.64951	0.26543	-5.84128	0.26314			-4.00353	0.25995		
J07446+035	57829.90808	-3.88483	-0.00035	-4.73106	0.26441	-4.61139	0.26551	-5.81815	0.26155						
J07446+035	57848.85507	-3.95281	-0.00055	-4.76628	0.2628	-4.62709	0.26433	-5.76057	0.26034						
J07446+035	57851.91581	-3.99928	-0.00051	-4.83839	0.26289	-4.6716	0.26473	-6.03148	0.25563						
J07446+035	57855.83501	-3.98857	-0.00036	-4.79153	0.26458	-4.62633	0.26576	-5.85118	0.26312						
J07446+035	57862.87108	-3.98788	-0.00051	-4.81956	0.26299	-4.66038	0.26466	-5.86514	0.26006						
J07446+035	57874.85654	-4.0075	-0.00046	-4.84622	0.26352	-4.6652	0.26518	-5.89114	0.25996						
J07446+035	58041.12997	-3.92505	-0.00034	-4.80629	0.26409	-4.64646	0.26553	-5.90917	0.26007	-5.90651	0.26054	-4.04718	0.25917		
J07446+035	58056.22123	-3.93759	-0.00036	-4.72603	0.2646	-4.60526	0.26561	-5.84446	0.26249	-5.87752	0.26286	-4.11078	0.25716		
J07446+035	58064.13629	-3.97776	-0.00046	-4.83967	0.26295	-4.66789	0.26482	-5.93528	0.25945	-5.88929	0.26218				
J07446+035	58089.13423	-3.98323	-0.00093	-4.84036	0.25907	-4.69126	0.26234	-5.99504	0.24448	-5.95335	0.25306				
J07446+035	58117.07139	-3.92959	-0.00036	-4.77908	0.26409	-4.646	0.2654	-5.84531	0.26215	-5.94666	0.26081	-4.04761	0.25888		
J07446+035	58120.05191	-3.88893	-0.00032	-4.59984	0.2655	-4.4896	0.26619	-5.6543	0.26463	-5.75269	0.26397	-4.00685	0.25963		
J07558+833	57690.0066	-3.83086	-0.00083	-4.8512	0.04081	-4.62895	0.0511	-5.17333	0.04151			-4.23767	0.02902		
J07558+833	57704.00678	-3.8791	-0.00113	-4.89172	0.03414	-4.71116	0.04337	-5.30632	0.03172	-4.99274	0.05283	-4.25218	0.02028		
J07558+833	58001.15469	-3.76541	-0.00072	-4.61006	0.05178	-4.47631	0.05345	-5.19611	0.04089	-4.96845	0.05011	-4.20807	0.02993		
J07558+833	58024.08655	-3.88473	-0.0011	-5.00814	0.02864	-4.69204	0.04481	-5.28801	0.03067	-5.1649	0.0448				
J07558+833	58032.13585	-3.8776	-0.00103	-4.86839	0.03581	-4.67526	0.04378	-5.43633	0.025	-5.18807	0.04713				
J07558+833	58041.0806	-3.77548	-0.00065	-4.6885	0.05072	-4.51775	0.05318	-4.97627	0.05054	-4.95636	0.05183	-4.1844	0.03183		
J07558+833	58043.17578	-3.89062	-0.0008	-4.95322	0.03685	-4.71081	0.04589	-5.35784	0.03933	-5.08754	0.05404				
J07558+833	58049.00962	-3.88307	-0.00095	-4.88053	0.03797	-4.66982	0.04574	-5.32506	0.0347	-5.06579	0.05681				
J07558+833	58054.01611	-3.93653	-0.00117	-4.97494	0.03087	-4.78926	0.04031	-5.28191	0.03445	-5.08609	0.05277	-4.24203	0.02426		
J07558+833	58058.20828	-3.94428	-0.00113	-5.08461	0.02395	-4.79549	0.0405	-5.33181	0.03652	-5.01645	0.03933				
J07558+833	58084.08342	-3.94075	-0.0016	-5.05709	0.02053	-4.7264	0.0405	-5.20167	0.01542	-4.8693	0.05313				
J07558+833	58117.01844	-3.95794	-0.00138	-5.13728	0.01432	-4.79539	0.03807	-5.3792	0.02438	-5.1266	0.04496				
J07558+833	58124.00278	-3.95577	-0.00166	-5.08175	0.01843	-4.76796	0.03883	-5.35767	0.01605	-5.10747	0.05008				
J07558+833	58134.95025	-3.88344	-0.00121	-4.86461	0.03395	-4.67439	0.04248	-5.25308	0.03574	-4.92008	0.04875				
J13005+056	57422	-3.9352	-0.0011	-4.89427	0.06664	-4.77388	0.07548	-5.49653	0.057	-5.06096	0.07278				
J13005+056	57487.99573	-3.96665	-0.00103	-4.92707	0.07043	-4.91507	0.0724	-5.52049	0.05973	-5.1697	0.07497				
J13005+056	57509.99035	-3.95553	-0.00142	-4.95249	0.05899	-4.73999	0.07149	-5.39242	0.05336	-5.00979	0.07695				
J13005+056	57936.87002	-3.91469	-0.00125	-4.88262	0.06394	-4.74537	0.07179	-5.48516	0.03239						
J13005+056	57942.88017	-3.88359	-0.00117	-4.82475	0.07007	-4.68906	0.07615	-5.51475	0.04725	-4.87814	0.08524				
J13005+056	58139.16169	-3.88477	-0.00084	-4.89656	0.06994	-4.84275	0.07483	-5.39615	0.06837	-4.93798	0.07806				
J13005+056	58276.93065	-4.04733	-0.00132	-4.99991	0.06234	-4.86951	0.06873			-5.19664	0.07471				
J13005+056	58283.85782	-3.90049	-0.00083	-4.80621	0.07507	-4.7313	0.07785	-5.35997	0.06675	-5.02505	0.08019				
J13005+056	58288.94898	-4.06118	-0.00159	-4.8531	0.06741	-4.87992	0.06933			-5.05227	0.07689				

Continued on next page

// Star	MJD	Hα		Ca II IRT-a		Ca II IRT-b		He I D_3		Na I D_2		Paβ		Paδ	
		$log\left(\frac{L_{line}}{L_{Bol}}\right)$	δ	$log\left(\frac{L_{line}}{L_{Bol}}\right)$	δ	$log\left(\frac{L_{line}}{L_{Bol}}\right)$	δ	$log\left(\frac{L_{line}}{L_{Bol}}\right)$	δ	$log\left(\frac{L_{line}}{L_{Bol}}\right)$	δ	$log\left(\frac{L_{line}}{L_{Bol}}\right)$	δ	$log\left(\frac{L_{line}}{L_{Bol}}\right)$	δ
J13005+056	58297.8835	-3.91963	-0.00129	-4.69351	0.07868	-4.51444	0.08023								
J13005+056	58299.88042	-3.92574	-0.0011	-4.83094	0.06959	-4.69867	0.07649	-5.30082	0.06752	-5.10432	0.07652				
J13005+056	58305.86892	-3.92322	-0.0013	-4.75342	0.07364	-4.75533	0.07401	-5.45562	0.0558	-5.17274	0.07366				
J18075-159	57525.13422	-4.00272	-0.00176	-5.20432	0.00838										
J18075-159	57540.0925	-3.94692	-0.00154	-4.9904	0.04145	-4.75216	0.04667	-5.37504	0.02257						
J18075-159	57557.03699	-4.02478	-0.00183	-5.36545	-0.00685	-5.00343	0.03056	-5.4144	0.01383	-5.09471	0.02545			-5.45041	-0.03693
J18075-159	57570.01029	-3.99267	-0.00169	-5.07474	0.04086	-5.2792	0.03135	-5.22593	0.03087	-5.19781	0.02629				
J18075-159	57602.9025	-3.95324	-0.00155	-5.12512	0.0366	-4.96639	0.04101	-5.28552	0.02615	-5.14744	0.03459			-5.39944	-0.00901
J18075-159	57607.91116	-3.95524	-0.00158	-5.10536	0.03647	-4.95367	0.04075	-5.29053	0.02595	-5.07741	0.03897			-5.53045	-0.03375
J18075-159	57617.87422	-4.02822	-0.00185	-5.26498	0.02894	-4.85139	0.04423	-5.46738	0.0147	-5.26379	0.03076			-5.47797	-0.0225
J18075-159	58637.02468	-3.88312	-0.00135	-5.07887	0.03649	-4.72854	0.04577	-5.23398	0.03154					-5.04534	0.01785
J18075-159	58699.88388	-3.54205	-0.00058	-4.4666	0.05028	-4.35912	0.051	-4.75702	0.0479	-4.8543	0.04599			-5.03266	0.02313
J18189+661	57529.05472	-4.17812	-0.00169	-5.57364	-0.03106	-5.11419	0.02773	-5.63405	0.01043	-5.16816	0.04749				
J18189+661	57693.82657	-4.12423	-0.00189	-5.16622	0.01484	-5.0007	0.02883			-5.03151	0.05379				
J18189+661	57814.20491	-4.204	-0.0017	-5.47442	-0.00937	-5.19149	0.02336	-5.66781	0.0213	-5.00944	0.05297				
J18189+661	57823.12422	-4.11063	-0.00141	-5.35868	0.00504	-5.03035	0.03367	-5.49262	0.03107	-4.90909	0.05338				
J22231-176	57571.15635	-4.02588	-0.00181	-4.9459	0.07713	-4.80928	0.07938	-5.56271	0.00831	-4.8285	0.07474				
J22231-176	57586.11692	-3.58699	-0.0007	-4.65876	0.08184	-4.49289	0.08308	-5.05439	0.07223	-4.97902	0.07357				
J22231-176	57596.09288	-4.01857	-0.00178	-4.96687	0.07282	-4.74228	0.0719	-5.48932	0.04194	-5.24506	0.06313				
J22231-176	57604.08358	-3.94809	-0.00152	-4.96667	0.07329	-4.71274	0.0791	-5.41096	0.04829	-5.1302	0.07007				
J22231-176	57607.07906	-3.78675	-0.00087	-4.71046	0.08232	-4.56208	0.08347	-5.1643	0.07114	-5.0161	0.07524				
J22231-176	57641.99181	-4.07232	-0.00161	-4.97161	0.07746	-4.83758	0.07446	-5.38869	0.05434	-5.33301	0.06319				
J22231-176	57649.9437	-4.03326	-0.00182	-4.94193	0.07349	-4.76415	0.07095	-5.44242	0.04261	-5.19584	0.06865				
J22231-176	57651.97258	-3.9908	-0.00168	-4.90669	0.07632	-4.76193	0.07815	-5.48021	0.0481	-5.16596	0.07285				
J22231-176	57675.84395	-4.07151	-0.00202	-5.00681	0.06784	-4.90309	0.07464	-5.51446	0.01752	-5.11978	0.06921				
J22231-176	59096.03074	-3.92879	-0.00147	-4.77603	0.07846	-4.6409	0.08024	-5.10099	0.07025	-5.12677	0.07544				
J22231-176	59772.10312	-3.98626	-0.00167	-4.9777	0.07253	-5.04848	0.06965	-5.41926	0.04846	-5.1554	0.06512				
J22231-176	59832.9965	-4.14825	-0.00237	-5.04667	0.06964	-4.53627	0.07601	-5.46848	0.02626						
J01019+541	57748.87648	-4.10767	-0.00152	-5.60482	-0.02894	-5.11525	0.03863	-5.62935	0.01991	-5.18631	0.0633				
J01019+541	57760.81123	-3.68771	-0.0006	-4.36503	0.06712	-4.34075	0.06725	-4.88955	0.06638	-4.73658	0.07058				
J01019+541	57945.15145	-4.00084	-0.00121	-5.41949	0.0056	-5.12506	0.0378	-5.58165	0.02623	-5.06807	0.05808				
J01019+541	57956.06389	-4.15378	-0.00171	-5.47169	-0.00275			-5.66175	0.01823	-5.05845	0.06346				
J01019+541	58021.0434	-4.1494	-0.00166	-5.45198	0.00071			-5.48028	0.03476	-5.12381	0.05644				
J01019+541	58035.02671	-4.12588	-0.00159	-5.38207	0.011					-5.21623	0.06718				
J01019+541	58092.92516	-4.009	-0.00124	-5.12275	0.03806	-5.00258	0.04602	-5.68331	0.01405	-5.18985	0.06223				
J01019+541	58328.13043	-4.05961	-0.00136	-5.40233	0.00814			-5.3262	0.05367	-5.03431	0.0626				
J01019+541	58332.95234	-3.99162	-0.00115	-5.2861	0.0229	-5.24613	0.02713	-5.60028	0.02546	-5.00502	0.06144				
J01019+541	58342.14925	-4.09295	-0.00144	-5.488	-0.00537	-5.34781	0.0157			-5.03699	0.06311				
J01033+623	57621.1276	-3.83548	-0.00073	-4.8408	0.01875	-4.75413	0.02264	-5.4551	0.01906	-5.1938	0.02454				
J01033+623	57649.13178	-3.78331	-0.00063	-4.76488	0.02317	-4.68257	0.0249	-5.47541	0.01855	-5.23685	0.02408				
J01033+623	57659.06458	-3.78271	-0.00065	-4.73379	0.02419	-4.64471	0.026	-5.36098	0.022	-5.20723	0.02462			-5.31025	-0.02649
J01033+623	57672.97102	-3.78907	-0.00076	-4.71602	0.02428	-4.67641	0.02522	-5.29753	0.02204	-5.08611	0.02609				
J01033+623	57677.98065	-3.74706	-0.0007	-4.62634	0.02574	-4.60701	0.0259	-5.43993	0.018	-5.12008	0.02571				
J01033+623	57693.95801	-3.7656	-0.00059	-4.69654	0.02485	-4.55438	0.02754	-5.40984	0.02093	-5.10006	0.02763				
J01033+623	57737.86061	-3.72754	-0.00072	-4.63256	0.02578	-4.64249	0.02575	-5.39377	0.01296	-5.12351	0.02426				
J01033+623	57748.90201	-3.61845	-0.00038	-4.45073	0.02941	-4.41297	0.02962	-5.18148	0.02718	-4.99944	0.02923			-5.32095	-0.02031
J01033+623	57754.90457	-3.78419	-0.00061	-4.75269	0.02446	-4.64912	0.0265	-5.36394	0.02229	-5.1332	0.02688				
J01033+623	57760.78997	-3.77526	-0.00061	-4.79074	0.02304	-4.66447	0.02585	-5.41875	0.02062	-5.17218	0.02577				
J01033+623	57785.80787	-3.65932	-0.00061	-4.61077	0.02608	-4.57632	0.02678	-5.30851	0.01717	-5.11008	0.02324				
J01033+623	57813.81559	-3.61577	-0.00038	-4.47576	0.02902	-4.45494	0.02943	-5.34381	0.02114	-5.08906	0.02717				
J01033+623	57821.81177	-3.80345	-0.00068	-4.80004	0.02234	-4.6845	0.02548	-5.47376	0.01415	-5.23521	0.02484				
J04472+206	57633.17731	-3.80555	-0.00068	-4.69265	0.07717	-4.78452	0.07466	-5.8664	0.06514	-5.6525	0.08102				
J04472+206	57641.1369	-3.8713	-0.00083	-5.26046	0.03436										
J04472+206	57676.14123	-3.81676	-0.00072	-4.94876	0.06445	-4.92094	0.06789	-6.1002	0.04005						
J04472+206	57677.13919	-3.90059	-0.00095	-5.03583	0.05804	-5.08123	0.05668			-5.55559	0.08941				
J04472+206	57678.13553	-3.93714	-0.00103	-5.14443	0.04819	-5.21379	0.04371			-5.88057	0.08567				
J04472+206	57689.09469	-3.82439	-0.00078	-4.96894	0.06303	-4.838	0.07225			-5.7025	0.08781				
J04472+206	57692.08647	-3.77489	-0.00067	-4.98845	0.06171	-5.44331	0.00938	-6.08486	0.04588	-5.86911	0.08491				
J04472+206	57693.08166	-3.7725	-0.00065	-4.75314	0.07477	-4.82653	0.07279	-6.07741	0.04487	-5.64453	0.08804				
J04472+206	57813.84075	-3.92233	-0.001	-5.05458	0.0565			-6.00248	0.05411	-5.6921	0.05855				
J04472+206	57832.84289	-3.87219	-0.00084	-5.46124	-0.0001										
J04472+206	57849.82909	-3.80306	-0.00072	-5.00292	0.0606					-5.69066	0.08795				
J07051-101	59250.00679	-3.80464	-0.00098	-4.80646	0.01355	-4.92519	0.00272	-5.40748	-0.00147	-5.43748	-0.00424				
J07051-101	59294.86767	-3.89312	-0.00116	-4.95232	0.00659	-4.89426	0.00467	-5.44779	-0.00777	-5.35095	0.00213				

Continued on next page

// Star	MJD	Hα		Ca II IRT-a		Ca II IRT-b		He I D_3		Na I D_2		Paβ		Paδ	
		$log\left(\frac{L_{line}}{L_{Bol}}\right)$	δ	$log\left(\frac{L_{line}}{L_{Bol}}\right)$	δ	$log\left(\frac{L_{line}}{L_{Bol}}\right)$	δ	$log\left(\frac{L_{line}}{L_{Bol}}\right)$	δ	$log\left(\frac{L_{line}}{L_{Bol}}\right)$	δ	$log\left(\frac{L_{line}}{L_{Bol}}\right)$	δ	$log\left(\frac{L_{line}}{L_{Bol}}\right)$	δ
J07051-101	59560.12694	-3.96255	-0.00142	-5.26737	-0.01955	-5.26473	-0.0308			-5.63444	-0.02446				
J07051-101	59613.92422	-3.89947	-0.00129	-5.1259	-0.00549	-4.76863	0.01128	-5.29176	0.01143	-5.39158	0.00867				
J09449-123	57712.19742	-3.95496	-0.00069	-5.08786	0.09289	-4.92454	0.10404			-5.73026	0.12133				
J09449-123	57762.09083	-3.75562	-0.00043	-4.78794	0.1091	-4.70475	0.11213	-5.90936	0.10958	-5.93859	0.1155				
J09449-123	57763.08384	-3.81784	-0.0005	-5.00381	0.09831	-4.82059	0.10832			-5.80057	0.10755				
J09449-123	57820.90648	-3.8478	-0.00053	-5.06655	0.09438	-4.74368	0.11084			-5.79773	0.11435				
J09449-123	57822.97465	-3.76659	-0.00042	-4.92757	0.10299	-4.69076	0.11264			-5.93845	0.11061				
J09449-123	57847.87381	-3.72971	-0.00041	-4.71741	0.11083	-4.65937	0.11316	-5.8763	0.11103	-5.98844	0.10643				
J09449-123	57860.83045	-3.79424	-0.00049	-4.85141	0.10664	-4.70113	0.11244	-5.8864	0.10949	-5.94761	0.10595				
J09449-123	57875.83715	-3.70062	-0.00038	-4.66651	0.11554	-4.74629	0.11186	-5.92639	0.11032	-5.93642	0.10659				
J09449-123	57877.84054	-3.9967	-0.00076	-4.94308	0.10185	-4.84776	0.10727			-5.96723	0.10916				
J09449-123	57879.84179	-3.72374	-0.00043	-4.65093	0.11517	-4.62524	0.114	-5.99376	0.10695	-5.83604	0.10993				
J10584-107	57762.14493	-3.91742	-0.00126	-5.09871	0.00251	-4.89856	0.01597	-5.46255	-0.07485						
J10584-107	57815.00172	-3.91251	-0.00121	-5.08342	0.00183	-4.84774	0.01722	-5.18496	-0.05766	-5.37873	-0.01731				
J10584-107	57822.00502	-3.93358	-0.00127	-5.19085	-0.00479	-4.87973	0.01179	-5.28516	-0.05135	-5.26401	-0.0015				
J10584-107	58109.18027	-3.90262	-0.00121	-5.06964	0.00421	-4.94546	0.01519	-5.23323	-0.02105	-5.03233	-0.02563				
J10584-107	58228.90088	-3.95458	-0.00132	-5.16712	-0.0032	-4.92539	0.01319	-5.20344	-0.06144	-5.00503	-0.00497				
J10584-107	58261.85164	-3.96744	-0.00138	-5.13128	-0.00087	-4.98976	0.00881			-5.1329	-0.01423				
J10584-107	58458.22323	-3.90142	-0.0012	-4.98218	0.00855	-4.84438	0.01728	-5.07755	-0.01811	-5.06317	-0.00094				
J10584-107	58470.21565	-3.85171	-0.00107	-5.02444	0.01204	-4.86402	0.01713			-5.50242	-0.04849				
J10584-107	58475.14208	-3.91584	-0.00126	-5.10162	0.00289	-4.9001	0.01605	-5.3426	-0.06359	-5.72948	-0.02816				
J10584-107	58480.13361	-3.84725	-0.00107	-5.11339	0.00909	-4.85947	0.01685	-5.24355	-0.0404	-4.9526	-0.01743				
J10584-107	58486.1828	-3.9328	-0.0013	-5.1764	-0.0037	-4.91494	0.01574	-5.30711	-0.06404	-4.99513	0.00378				
J10584-107	58491.12035	-3.85036	-0.00108	-5.04079	0.00563	-4.84838	0.01666	-4.99482	4e-05	-5.05485	0.01375				
J10584-107	58496.1594	-3.9058	-0.00122	-5.10997	0.00192	-4.87095	0.01663			-5.1217	-0.03729				
J10584-107	58509.13567	-3.90395	-0.00118	-5.15069	-0.00215	-4.92619	0.01024	-5.12641	-0.04593	-5.17914	0.00785				
J10584-107	58529.08585	-3.87346	-0.00111	-4.97723	0.01378	-4.80732	0.01768	-5.16183	-0.02616	-4.92436	0.00852				
J10584-107	58546.08177	-3.86769	-0.00109	-4.98309	0.00797	-4.86414	0.01692	-4.96446	-0.02444	-5.36637	0.00057				
J10584-107	58553.01359	-3.89854	-0.00117	-4.97917	0.01035	-4.82949	0.01749	-5.04988	-0.03211	-5.57577	-0.06446				
J10584-107	58558.99217	-3.93582	-0.00128	-5.22371	-0.00511	-4.9384	0.01535	-5.27295	-0.07302						
J10584-107	58569.99146	-3.91151	-0.00119	-5.08373	0.00173	-4.88738	0.01675			-5.06912	-0.00114				
J10584-107	58589.96342	-4.0596	-0.0017	-5.25731	-0.00753	-4.91517	0.01026								
J10584-107	58599.8958	-3.93802	-0.00128	-5.01042	0.00744	-4.88609	0.0165								
J10584-107	58604.93443	-3.99195	-0.00145	-5.169	-0.00249	-4.85885	0.01267			-5.22818	0.00626				
J10584-107	58609.92354	-3.94249	-0.00129	-5.24352	-0.0085	-4.93369	0.00992	-5.20704	-0.06096	-4.855	-0.01132				
J10584-107	58613.90447	-3.93353	-0.00128	-5.24543	-0.00765	-4.91744	0.01018								
J10584-107	58616.89649	-3.95888	-0.00134	-5.15813	-0.00232	-4.94807	0.01501			-5.12485	-0.04047				
J10584-107	58624.86713	-3.87604	-0.0011	-5.11886	0.00209	-4.90186	0.01619	-4.86725	-0.01494						
J10584-107	58816.21727	-3.93964	-0.00132	-5.15159	-0.00221	-4.93091	0.01552	-5.53565	-0.06214	-5.05634	0.01408				
J10584-107	58846.22784	-3.95067	-0.00134	-5.18399	-0.00237	-4.85395	0.01554	-5.08024	-0.00885	-5.00553	0.00371				
J10584-107	58849.17595	-3.76431	-0.00088	-4.96663	0.01326	-4.7503	0.01866	-5.32359	-0.02602	-4.88452	-0.00886				
J10584-107	58852.16888	-3.95091	-0.00136	-5.28571	-0.01192	-4.91412	0.01035	-5.1153	-0.02234						
J10584-107	58858.17087	-3.62886	-0.00065	-4.61621	0.01988	-4.54661	0.02099	-4.84841	0.00851	-4.79878	0.01821				
J10584-107	58861.13764	-4.03037	-0.00161	-5.26969	-0.01058	-4.98786	0.00764	-5.12944	-0.0425	-5.26382	-0.06141				
J10584-107	58864.13195	-3.93568	-0.00129	-5.17597	-0.00368	-4.9555	0.00927	-5.31772	-0.06536	-5.17214	0.00085				
J10584-107	58878.08448	-3.97502	-0.00138	-5.20345	-0.00566	-4.93692	0.01067								
J10584-107	58881.09802	-3.90435	-0.00119	-5.07372	0.00393	-4.84105	0.01439	-5.27749	-0.0183	-5.4731	-0.00796				
J10584-107	58884.08133	-4.00882	-0.00149	-5.15439	-0.00239	-4.94852	0.00915			-5.62371	-0.01863				
J10584-107	58887.07593	-3.95417	-0.00131	-5.15113	-0.00208	-4.98589	0.01191			-5.07235	0.01329				
J10584-107	58890.0704	-3.85619	-0.00108	-4.83892	0.01601	-4.71939	0.01888	-5.08061	-0.00532	-5.10793	0.01029				
J10584-107	58893.06261	-3.94306	-0.00129	-5.16046	-0.00226	-4.90933	0.01598			-5.51418	-0.0112				
J10584-107	58896.05431	-3.86781	-0.00108	-5.00881	0.0104	-4.81983	0.01756	-5.08195	-0.01498	-5.33955	-0.01141				
J10584-107	58903.03475	-3.87569	-0.00111	-4.98952	0.01138	-4.81137	0.01761	-5.03561	-0.02079	-5.18092	0.00072				
J10584-107	58916.03464	-3.97345	-0.00138	-5.24636	-0.00872	-4.90786	0.01062	-5.09354	-0.04204	-5.51505	-0.05066				
J10584-107	58919.0016	-4.10571	-0.00185	-5.21642	-0.00648	-5.04266	0.00523			-5.31927	0.00638				
J10584-107	58920.97961	-3.88984	-0.00113	-5.11432	0.00012	-4.89391	0.01324	-5.14099	-0.04978	-4.92497	0.01911				
J10584-107	58922.99297	-3.89999	-0.00117	-5.11087	0.00077	-4.91411	0.01309	-5.16003	-0.03905	-5.16688	-0.00754				
J11474+667	57759.10382	-3.69415	-0.00068	-4.95957	0.10987	-4.77445	0.11348	-5.20413	0.10884	-5.15854	0.10157			-5.36996	0.03113
J11474+667	57762.04635	-3.14353	-0.00021	-4.06994	0.11949	-3.98893	0.11969	-4.40939	0.12026	-4.55894	0.11831	-3.71968	0.11293	-4.48946	0.10917
J11474+667	57831.90081	-3.76056	-0.00081	-4.88238	0.11073	-4.88069	0.11151	-5.30541	0.10251	-5.0961	0.10241				
J11474+667	57851.043	-3.75906	-0.00077	-5.09523	0.1063	-4.71588	0.11041			-5.12016	0.10109				
J11474+667	57857.96583	-3.86545	-0.00101	-5.24842	0.09274	-5.01701	0.09429			-5.15265	0.11144				
J11474+667	57891.90949	-3.72059	-0.00071	-5.02311	0.10753	-4.84783	0.11195	-5.31793	0.09072	-5.02743	0.1137				
J11474+667	57964.85744	-3.78103	-0.00084	-5.04203	0.10708	-4.94336	0.10906	-5.2069	0.09576	-5.18873	0.11023				

Continued on next page

// Star	MJD	Hα		Ca II IRT-a		Ca II IRT-b		He I D_3		Na I D_2		Paβ		Paδ	
		$log\left(\frac{L_{line}}{L_{Bol}}\right)$	δ	$log\left(\frac{L_{line}}{L_{Bol}}\right)$	δ	$log\left(\frac{L_{line}}{L_{Bol}}\right)$	δ	$log\left(\frac{L_{line}}{L_{Bol}}\right)$	δ	$log\left(\frac{L_{line}}{L_{Bol}}\right)$	δ	$log\left(\frac{L_{line}}{L_{Bol}}\right)$	δ	$log\left(\frac{L_{line}}{L_{Bol}}\right)$	δ
J11474+667	58175.04228	-3.64091	-0.00061	-4.89929	0.11109	-4.7601	0.11337	-5.16503	0.10754	-5.21352	0.11119				
J11474+667	58236.01454	-3.7761	-0.00082	-4.9625	0.11055	-4.90505	0.11096	-5.18963	0.10866	-5.15629	0.1111	-4.03038	0.10449		
J11474+667	58245.96768	-3.66706	-0.00065	-4.87481	0.11184	-4.72329	0.11439	-4.97137	0.11373	-5.11423	0.1117				
J11474+667	58260.91805	-3.72105	-0.00073	-4.93084	0.11005	-4.84316	0.1121	-5.12064	0.11075	-5.33168	0.10398				
J11474+667	58284.00553	-3.84063	-0.00096	-5.10104	0.1048	-4.98561	0.10931	-5.06197	0.11008					-5.63204	0.03902
J11474+667	58304.90644	-3.72354	-0.00072	-4.91972	0.11096	-4.83882	0.11247	-5.39435	0.10008	-5.38045	0.10314				
J11474+667	58327.85542	-3.68716	-0.00068	-4.99881	0.10826	-4.79453	0.11339	-5.31298	0.08912	-5.0791	0.11315				
J11474+667	58405.20041	-3.87673	-0.00101	-4.89623	0.11361	-4.82554	0.10395								
J11474+667	58426.20739	-3.95206	-0.00122	-5.26376	0.08691	-4.94004	0.10356			-5.12384	0.10444				
J11474+667	58449.15362	-3.79915	-0.00087	-4.99994	0.10326	-4.84151	0.10696			-4.98865	0.10917				
J11474+667	58470.24001	-3.78969	-0.00085	-5.01539	0.10541	-4.84956	0.11197	-5.16463	0.09521	-5.34128	0.10072				
J11474+667	58490.20004	-3.60138	-0.00056	-4.9038	0.1111	-4.66294	0.11531	-4.91894	0.11341	-5.24476	0.10492			-5.49206	0.06187
J11474+667	58510.2022	-3.78386	-0.00081	-5.00951	0.10421	-4.97591	0.10206	-5.35023	0.10266	-5.05141	0.11309				
J11474+667	58530.09195	-3.80653	-0.00088	-4.87297	0.11209	-4.7614	0.11395	-5.14483	0.10791	-5.05654	0.11272			-5.68036	0.02978
J11474+667	58553.04695	-3.87482	-0.00103	-5.0802	0.10539	-4.95975	0.10936	-5.12729	0.10825	-5.32759	0.10506			-5.55423	0.05247
J11474+667	58575.13484	-3.79223	-0.00083	-5.1057	0.09863	-4.87256	0.10597								
J11474+667	58616.94411	-3.64714	-0.00061	-4.82875	0.11295	-4.6929	0.11511	-5.17276	0.10724	-5.38794	0.10412				
J11474+667	58636.90598	-3.59683	-0.00056	-4.85274	0.1122	-4.78517	0.11317	-5.28622	0.10537						
J11474+667	58658.88759	-3.68466	-0.00067	-4.98318	0.10825	-4.69798	0.11091	-5.13077	0.1082	-5.04813	0.11214				
J11474+667	58678.88474	-3.76965	-0.00081	-5.00792	0.10778	-5.00698	0.10051			-5.29249	0.10844			-5.63788	0.03828
J11474+667	58698.85315	-3.8075	-0.00089	-5.03787	0.10639	-4.8575	0.10643	-5.31084	0.09916	-5.1577	0.11188				
J11474+667	58771.19173	-3.88441	-0.00105	-5.09778	0.10803	-5.00799	0.09456	-5.21909	0.08859						
J11474+667	58804.16692	-3.695	-0.00067	-4.90101	0.10693	-4.95478	0.10059	-5.40414	0.08208						
J11474+667	58831.11797	-3.67782	-0.00065	-4.95795	0.10978	-4.73222	0.11377			-5.16929	0.10169			-5.58715	0.0474
J11474+667	58852.21784	-2.94557	-0.00014	-3.96709	0.1198	-3.81231	0.12013	-4.27971	0.11916	-4.56902	0.11769	-3.25511	0.11767	-3.98097	0.11579
J11474+667	58877.19328	-3.787	-0.00083	-5.08892	0.106	-4.81808	0.10765			-5.30615	0.10433			-5.67129	0.03127
J11474+667	58897.10116	-3.68294	-0.00066	-4.82243	0.11334	-4.74916	0.11414	-5.15156	0.09909	-5.07226	0.10377				
J11474+667	58917.06314	-3.73429	-0.00073	-5.0172	0.1075	-4.77131	0.11325	-5.43325	0.09937	-5.11087	0.11642				
J11474+667	58975.93301	-3.89588	-0.00107	-5.02239	0.10334	-4.77235	0.10588	-5.5702	0.06467						
J11474+667	58996.96631	-3.83308	-0.0009	-5.21839	0.09018	-5.12641	0.0872	-5.12326	0.10884			-4.14668	0.11528		
J11474+667	59016.95946	-3.825	-0.0009	-5.02345	0.1065	-5.2001	0.08062	-4.97149	0.10237						
J11474+667	59036.89368	-3.77405	-0.00081	-4.90143	0.11137										
J11474+667	59058.87507	-3.85041	-0.00096	-5.10491	0.09744										
J11474+667	59146.18481	-3.79447	-0.00085	-5.27492	0.0859										
J11474+667	59171.16946	-3.86849	-0.00101	-5.05894	0.104										
J11474+667	59209.23834	-3.58505	-0.00052	-4.73186	0.11393										
J11474+667	59263.85814	-3.27032	-0.00028	-4.01922	0.11963										
J11474+667	59295.09798	-3.76008	-0.00078	-5.13889	0.10551									-5.67984	0.02988
J11474+667	59335.93949	-3.87726	-0.00103	-5.08164	0.10659										
J11474+667	59413.89576	-3.80835	-0.00087	-5.09331	0.10551									-5.66101	0.03375
J11474+667	59597.21076	-3.72266	-0.00073	-5.1552	0.10067							-4.10506	0.10144	-5.62921	0.03955
J11474+667	59632.09177	-3.87476	-0.00101	-5.28972	0.08495							-3.94696	0.10741		
J11474+667	59687.15121	-3.7318	-0.00073	-4.90905	0.11075										
J11474+667	59724.00152	-3.83525	-0.0009	-5.00564	0.10268										
J11474+667	59767.91189	-3.66109	-0.00061	-4.82764	0.11297									-5.461	0.06571
J11474+667	59958.24611	-3.70814	-0.00069	-5.08641	0.10516									-5.62064	0.0415
J12189+111	57466.03845	-3.89589	-0.0009	-4.98677	0.04076	-4.66838	0.05534	-5.32899	0.05672	-5.10041	0.06229				
J12189+111	57489.98631	-4.07551	-0.00133	-5.4795	-0.02311	-4.97047	0.04047			-5.38898	0.05761				
J12189+111	57503.94513	-3.96509	-0.00103	-5.30419	0.00748	-4.908	0.04435	-5.71517	0.02905	-5.02479	0.06251				
J12189+111	57534.90848	-4.15656	-0.00161	-5.21136	0.01932	-4.86636	0.04655			-5.14289	0.05923				
J12189+111	57747.24593	-4.00779	-0.00114	-5.24782	0.01508	-4.91555	0.04397	-5.67535	0.03868	-5.17065	0.05991				
J12189+111	57760.15632	-3.90435	-0.00091	-4.74918	0.05204	-5.03895	0.03694	-5.56323	0.04803	-5.04954	0.06233				
J12189+111	57814.10255	-3.84138	-0.00066	-4.88372	0.05685	-4.68299	0.05945	-5.41999	0.05573	-5.12597	0.0632				
J12189+111	57819.10785	-4.03758	-0.00123	-5.41329	-0.01009	-4.83258	0.04823	-5.73598	0.02204	-5.17704	0.06402				
J12189+111	57821.09444	-3.95934	-0.00087	-5.20739	0.0282	-4.96752	0.04552	-5.57782	0.04788	-5.08435	0.06443				
J13102+477	57747.18856	-4.02957	-0.00156	-5.59872	-0.03902	-5.18367	0.00603	-5.28706	-0.00046	-4.9247	0.02644				
J13102+477	57794.15571	-4.05926	-0.00169	-5.3248	-0.00286	-4.95723	0.01701	-5.13125	0.02066	-5.12895	0.02246				
J13102+477	57800.14361	-4.15842	-0.00213	-5.69532	-0.05831	-5.12995	0.00715			-4.93156	0.02726				
J13102+477	57815.08284	-4.07433	-0.00173	-5.53922	-0.02929	-5.16068	0.00506			-5.39068	0.01638				
J13102+477	57821.0698	-3.96462	-0.00135	-5.19608	0.01583	-4.8862	0.02843	-5.15307	0.02358	-4.97012	0.02732				
J13102+477	57830.06025	-4.06922	-0.0017	-5.66652	-0.0522	-5.33941	-0.01027			-5.14927	0.03051				
J13102+477	57880.92698	-4.08541	-0.0018	-5.63426	-0.04581	-5.29212	-0.00636								
J13102+477	58304.95196	-4.11408	-0.00191	-5.60106	-0.03972	-5.29222	-0.00623	-5.22173	-0.00175	-5.07409	0.02625				
J13102+477	58322.85957	-3.83176	-0.00104	-4.88217	0.02656	-4.65368	0.0315	-4.88915	0.02773	-5.04493	0.02779				

Continued on next page

// Star	MJD	Hα		Ca II IRT-a		Ca II IRT-b		He I D_3		Na I D_2		Paβ		Paδ	
		$log\left(\frac{L_{line}}{L_{Bol}}\right)$	δ	$log\left(\frac{L_{line}}{L_{Bol}}\right)$	δ	$log\left(\frac{L_{line}}{L_{Bol}}\right)$	δ	$log\left(\frac{L_{line}}{L_{Bol}}\right)$	δ	$log\left(\frac{L_{line}}{L_{Bol}}\right)$	δ	$log\left(\frac{L_{line}}{L_{Bol}}\right)$	δ	$log\left(\frac{L_{line}}{L_{Bol}}\right)$	δ
J13102+477	58327.91348	-4.05119	-0.00169	-5.46349	-0.01889	-5.08797	0.01077	-5.19747	0.0086	-5.12977	0.02603				
J13102+477	58480.15728	-3.97563	-0.00142	-5.2645	0.01183	-5.03817	0.01849	-5.40214	-0.01146	-4.85278	0.02057				
J13102+477	58496.20075	-4.05299	-0.00166	-5.53328	-0.02839	-5.17704	0.01183			-5.29457	0.01454				
J13102+477	58536.14934	-4.05776	-0.00169	-5.53867	-0.02921	-5.16796	0.01246	-5.46027	0.00344	-5.22207	0.0178				
J13102+477	58542.13268	-4.04666	-0.00165	-5.54691	-0.03047	-5.14324	0.01204	-5.34331	0.01099						
J13102+477	58554.12772	-4.05268	-0.00171	-5.36764	-0.00765	-5.20992	0.00801	-5.30536	0.01194	-5.12311	0.02476				
J13102+477	58570.10919	-4.20047	-0.00231	-5.55433	-0.03189	-5.30631	0.00081	-5.38688	-0.0212	-5.31003	0.02194				
J13102+477	58585.10426	-4.0729	-0.00175	-5.4075	-0.01213	-5.28131	0.0027	-5.32943	-0.0166	-4.58762	0.02799				
J13102+477	58590.01023	-3.93656	-0.00127	-5.17875	0.01302	-5.04412	0.0253			-4.97912	0.03209				
J13102+477	58601.03231	-4.0704	-0.0017	-5.68581	-0.0559	-5.16034	0.01104	-5.43672	-0.01913	-5.11306	0.02791				
J13102+477	58628.96743	-4.09545	-0.00185	-5.61206	-0.04168	-5.26771	0.00389			-5.1463	0.02493				
J13102+477	58695.93365	-3.85238	-0.00105	-5.01645	0.02514	-4.90453	0.02806	-4.9522	0.01792						
J13102+477	58893.19254	-3.99343	-0.00145	-5.41715	-0.01101	-5.07137	0.02438	-5.43919	0.0063	-5.19516	0.01904				
J14173+454	57526.93668	-3.98329	-0.00152	-5.28235	-0.06551	-5.05253	-0.01189	-5.62341	-0.05562	-4.92233	0.01313				
J14173+454	57815.1158	-3.96639	-0.00146	-4.88852	-0.0109	-5.37004	-0.05253	-5.37806	-0.02341	-4.68316	0.02377				
J14173+454	57851.0126	-4.02912	-0.00167	-4.65545	0.0044			-5.43233	-0.02795	-4.9118	0.02109				
J14173+454	57866.99706	-3.98113	-0.00152	-5.24039	-0.05708			-5.62966	-0.05319	-5.02357	0.01273				
J15499+796	57752.22311	-3.94131	-0.0011	-4.91338	0.05546	-4.89745	0.05638	-5.8267	0.00729	-5.25522	0.07622				
J15499+796	57762.11878	-4.00143	-0.00126	-5.30588	0.01808	-4.98627	0.05086			-5.16402	0.06273				
J15499+796	57802.03981	-4.02438	-0.00131	-5.31086	0.01722			-5.57221	0.03945	-5.1432	0.06359				
J15499+796	57832.10278	-3.96486	-0.00115	-5.05634	0.0455	-4.92446	0.0548	-5.65435	0.04375	-5.30982	0.0558				
J15499+796	57895.95664	-4.04332	-0.00137	-5.1996	0.03163	-4.93488	0.05416	-5.72429	0.02459	-5.20999	0.07404				
J15499+796	57916.96682	-4.04045	-0.00138	-5.27966	0.02176	-4.9456	0.05355	-5.73064	0.02387	-5.33952	0.06608				
J15499+796	57918.9642	-4.12461	-0.00164	-5.19373	0.0323	-4.99475	0.05124	-5.77079	0.01505	-5.3972	0.06626				
J15499+796	57928.00763	-3.91405	-0.00102	-4.98662	0.05077	-4.90062	0.05625	-5.49099	0.05004	-5.12346	0.0717				
J15499+796	57937.93965	-3.93575	-0.00107	-5.17321	0.03454	-5.02185	0.04821	-5.6155	0.04616	-5.02093	0.07325				
J15499+796	57943.98932	-3.99488	-0.00124	-5.17007	0.03488	-5.12689	0.03924	-5.61345	0.04749	-5.15721	0.07029				
J16313+408	57472.18787	-3.8245	-0.00091	-4.81961	0.09298	-4.88145	0.09171	-5.33432	0.08382	-4.8658	0.09465				
J16313+408	57494.16277	-3.6966	-0.00068	-4.6713	0.0962	-4.62751	0.09688	-5.24487	0.08598	-4.67598	0.09772				
J16313+408	57503.10174	-3.75975	-0.00078	-4.68293	0.09622	-4.68716	0.09605	-5.27852	0.08519	-4.81255	0.0961				
J16313+408	57505.0677	-3.84283	-0.00095	-4.82249	0.08934	-4.73533	0.09467			-4.69107	0.09822				
J16313+408	57527.98861	-3.79232	-0.00084	-4.75402	0.09427	-4.80193	0.09338	-5.2138	0.08795	-4.84879	0.09604				
J16313+408	57562.97411	-3.74089	-0.00076	-4.70144	0.09453	-4.73168	0.09452	-5.12329	0.09084						
J16313+408	57587.85781	-3.84983	-0.00095	-4.68368	0.09028			-5.04111	0.08645						
J16313+408	57621.91795	-3.78222	-0.00082	-4.7751	0.09429	-4.67434	0.09576	-5.36629	0.07389	-4.92125	0.0954				
J16313+408	57759.21392	-3.7862	-0.00084	-4.68139	0.09598	-4.68571	0.09544			-4.44268	0.09795				
J16313+408	57801.19313	-3.72446	-0.00073	-4.669	0.09598	-4.72675	0.09469	-5.18808	0.0896	-4.8273	0.0956				
J16313+408	57814.16023	-3.7641	-0.00079	-4.7635	0.09411	-4.83788	0.09226	-5.27769	0.08505	-4.89925	0.09369				
J16313+408	57817.07273	-3.78527	-0.00083	-4.79827	0.09008	-4.69227	0.0959			-4.83407	0.09056				
J16313+408	57819.0841	-3.65285	-0.00062	-4.7209	0.09538	-4.77384	0.09452	-5.21029	0.0877	-4.79836	0.0958				
J16313+408	57822.08111	-3.62846	-0.00059	-4.61726	0.09663	-4.64848	0.09618	-5.07641	0.09219	-4.7383	0.09671				
J18022+642	57538.13807	-3.86539	-0.00111	-5.01262	0.14624	-4.72253	0.15872	-5.25407	0.15008	-4.93102	0.16535				
J18022+642	57554.03921	-3.91455	-0.00125	-5.2467	0.12525	-4.98676	0.14676	-5.31107	0.14738	-5.05545	0.16076				
J18022+642	57556.00856	-3.97093	-0.00141	-5.31875	0.11649	-5.20451	0.12967	-5.36168	0.14308	-4.9534	0.16396				
J18022+642	57568.00539	-3.96883	-0.00137	-5.31302	0.11723	-4.945	0.14916	-5.41435	0.14505	-5.02346	0.1624				
J18022+642	57602.92716	-3.95585	-0.00123	-5.23455	0.12742	-4.94198	0.14939	-5.52517	0.13211	-5.04603	0.16252				
J18022+642	57671.8956	-3.786	-0.00092	-4.97938	0.1472	-4.74299	0.16409	-5.29214	0.14914	-4.86749	0.16757				
J18022+642	57692.87802	-3.94177	-0.00129	-5.27702	0.12501	-4.93175	0.15103			-4.99145	0.16813				
J18022+642	57759.23916	-3.94419	-0.00131	-5.34511	0.11295	-4.98342	0.14689	-5.31982	0.13558	-4.75798	0.16019				
J18022+642	57762.2151	-3.84796	-0.00107	-5.17304	0.1326	-4.97115	0.14768	-5.26448	0.14891	-4.9133	0.15466				
J18022+642	57787.16491	-3.9535	-0.00135	-5.15441	0.13429	-5.08328	0.14014	-5.37565	0.12586	-4.83865	0.15767				
J18022+642	57798.19542	-3.92378	-0.00126	-5.23424	0.12648	-4.97553	0.14736	-5.3742	0.14278	-5.02725	0.16488				
J18022+642	57801.22663	-3.96928	-0.00121	-5.54638	0.09197	-5.06225	0.14601	-5.57135	0.10994	-5.02776	0.16571				
J18022+642	57819.06072	-3.89542	-0.00117	-5.33173	0.11493	-4.92034	0.15042	-5.41363	0.13126	-4.93057	0.16782				
J18022+642	57821.15441	-3.75176	-0.00072	-4.71989	0.16637	-4.64587	0.16719	-5.11455	0.16149	-4.80026	0.169				
J18022+642	57823.15363	-3.97402	-0.00119	-5.46837	0.10675	-5.10547	0.144	-5.41364	0.13278	-5.05581	0.16439				
J18022+642	58374.92416	-3.90016	-0.00106	-5.29366	0.12244										
J18022+642	58380.98802	-3.90882	-0.00123	-5.19809	0.13031							-4.26623	0.14945		
J18022+642	58381.80857	-3.97344	-0.00104	-5.45944	0.11257										
J18022+642	58382.79447	-3.98676	-0.00105	-5.19539	0.1401										
J18022+642	58391.78782	-3.94386	-0.00102	-5.3224	0.12655										
J18022+642	58392.86321	-3.7311	-0.00082	-5.00707	0.14543										
J18022+642	58394.86668	-3.97082	-0.00126	-5.36219	0.11298										
J18022+642	58395.86296	-3.84492	-0.00086	-5.04991	0.1459										

Continued on next page

// Star	MJD	Hα		Ca II IRT-a		Ca II IRT-b		He I D_3		Na I D_2		Paβ		Paδ	
		$log\left(\frac{L_{line}}{L_{Bol}}\right)$	δ	$log\left(\frac{L_{line}}{L_{Bol}}\right)$	δ	$log\left(\frac{L_{line}}{L_{Bol}}\right)$	δ	$log\left(\frac{L_{line}}{L_{Bol}}\right)$	δ	$log\left(\frac{L_{line}}{L_{Bol}}\right)$	δ	$log\left(\frac{L_{line}}{L_{Bol}}\right)$	δ	$log\left(\frac{L_{line}}{L_{Bol}}\right)$	δ
J18022+642	58396.96331	-3.7478	-0.00076	-4.81007	0.15786										
J18022+642	58397.85379	-3.92104	-0.00096	-5.21718	0.13608										
J18022+642	58398.86736	-3.94574	-0.00132	-5.17381	0.13263										
J18482+076	57563.10019	-4.07976	-0.00161	-5.23841	0.00525	-5.19899	0.0196					-4.2629	0.01075		
J18482+076	57571.01708	-4.04235	-0.00146	-5.11366	0.02091	-5.16378	0.01985								
J18482+076	57573.0061	-4.11327	-0.00172	-5.24902	0.00754	-5.41633	-0.01732								
J18482+076	57583.03693	-3.94834	-0.00119	-5.0318	0.02442	-4.9122	0.0279								
J18482+076	57594.94694	-4.19697	-0.00208	-5.28193	0.00628	-5.16967	0.01021								
J18482+076	57607.93417	-4.10856	-0.00171	-5.18783	0.01439										
J18482+076	57611.87889	-4.09672	-0.00166	-5.18748	0.01793										
J18482+076	57613.89214	-4.07875	-0.0016	-5.08426	0.0228										
J18482+076	57614.92317	-4.1688	-0.00197	-5.16356	0.01008										
J18482+076	57616.91789	-3.97666	-0.00125	-5.05508	0.02475										
J18482+076	57617.89721	-4.10633	-0.00169	-5.22752	0.00896										
J18482+076	57618.88034	-3.98851	-0.00129	-5.12131	0.02245										
J18482+076	57619.85735	-4.1761	-0.00199	-5.2547	0.00478										
J18482+076	57620.94608	-4.04312	-0.00147	-5.16053	0.01797										
J18482+076	57630.95538	-3.63132	-0.00061	-4.55947	0.03276										
J18482+076	57633.96075	-4.04525	-0.00148	-5.1303	0.02										
J18482+076	57634.8916	-4.09881	-0.00168	-5.21229	0.00959										
J18482+076	57881.12414	-4.09696	-0.00167	-5.17609	0.01199	-5.04997	0.02442								
J18482+076	57888.07848	-4.02769	-0.00142	-5.13849	0.01968	-5.0221	0.02528								
J18482+076	57893.03917	-4.14443	-0.00185	-5.22226	0.01484	-5.06089	0.0249								
J18482+076	57935.99089	-4.06512	-0.00155	-5.13065	0.02017	-5.07926	0.02313					-4.21507	0.01651		
J18482+076	57943.00032	-4.1853	-0.00205	-5.19361	0.00869	-5.12579	0.0125								
J18482+076	57954.98449	-3.89879	-0.00105	-4.93963	0.02797	-4.83661	0.02969								
J18482+076	57959.927	-4.04476	-0.00146	-5.175	0.02054	-5.06727	0.02399								
J18482+076	57968.91784	-4.15178	-0.00188	-5.19511	0.01184	-5.11225	0.01415								
J18482+076	57974.87652	-4.13712	-0.00183	-5.1605	0.01327										
J18482+076	57985.90516	-4.00649	-0.00135	-5.12326	0.02055										
J18482+076	57996.82191	-3.97702	-0.00127	-5.11863	0.02009										
J18482+076	57998.82374	-4.1289	-0.00179	-5.14854	0.01849										
J18482+076	58000.86564	-4.10622	-0.00171	-5.23766	0.00878										
J18482+076	58020.81178	-4.10678	-0.0017	-5.16972	0.01869										
J18482+076	58303.9984	-3.98461	-0.00128	-5.09949	0.01855										
J18482+076	58314.95603	-3.99414	-0.00131	-5.01568	0.0243										
J18482+076	58326.94847	-4.12193	-0.00179	-5.17725	0.01171										
J18482+076	58332.85782	-4.07899	-0.00162	-5.08377	0.02106	-5.0352	0.01884								
J18482+076	58351.89995	-4.13795	-0.00185	-5.19743	0.01694										
J18482+076	58385.90219	-4.12264	-0.00174	-5.18757	0.01739										
J18482+076	58617.09742	-4.01348	-0.00136	-5.10552	0.02262										
J18482+076	58629.06552	-4.14219	-0.00184	-5.19535	0.01563										
J18482+076	58637.04792	-4.14356	-0.00185	-5.16105	0.01775							-4.2973	0.00866		
J18482+076	58644.99934	-4.14451	-0.00186	-5.28084	0.01058										
J18482+076	58657.98525	-4.11144	-0.00172	-5.16443	0.01912										
J18482+076	58682.9429	-4.00939	-0.00135	-5.05741	0.02397										
J18482+076	58692.86874	-4.26698	-0.00244	-5.27325	0.00416										
J18482+076	58697.92573	-4.17154	-0.00198	-5.18883	0.01017							-4.29185	0.01226		
J18482+076	58703.91639	-4.08902	-0.00164	-5.06083	0.02259										
J18482+076	58710.86205	-4.04113	-0.00149	-5.06632	0.02217										
J18482+076	58990.11705	-4.14174	-0.00185	-5.19343	0.01594										
J18482+076	59090.92304	-4.03924	-0.00145	-5.15328	0.02164										
J18482+076	59092.92426	-3.94129	-0.00117	-5.01013	0.02517										
J18482+076	59443.99418	-4.20043	-0.00211	-5.20521	0.00803										
J18482+076	59484.91008	-4.19185	-0.00205	-5.25625	0.00479										
J18482+076	59485.86297	-4.00275	-0.00133	-5.06958	0.02376										
J18482+076	59486.88339	-4.12797	-0.00178	-5.14154	0.01716										
J19422-207	57906.11003	-3.86971	-0.00115	-5.14028	0.01904	-4.87926	0.04207	-5.22786	0.02759	-5.24924	0.02807				
J19422-207	57912.1164	-3.68342	-0.00076	-4.8119	0.04173	-4.66351	0.04622	-4.88628	0.04106	-4.89053	0.04125				
J19422-207	57914.09876	-3.72228	-0.00083	-4.94962	0.03598	-4.76018	0.04445	-5.28032	0.025	-5.03244	0.03558				
J19422-207	57919.08499	-3.75096	-0.00088	-5.06296	0.03063	-4.82063	0.0438	-5.11257	0.03539	-4.89701	0.04109				
J19422-207	57921.08731	-3.70066	-0.0008	-4.90432	0.04021	-4.66672	0.04611	-5.11401	0.03833	-5.1625	0.03345				
J19422-207	57981.9292	-3.799	-0.00098	-5.17785	0.01595	-4.88777	0.03955			-5.24863	0.03158				
J19422-207	58001.89043	-3.79679	-0.00098	-5.28983	0.00549	-4.8374	0.04328			-5.05163	0.04634				

Continued on next page

// Star	MJD	Hα		Ca II IRT-a		Ca II IRT-b		He I D_3		Na I D_2		Paβ		Paδ	
		$log\left(\frac{L_{line}}{L_{Bol}}\right)$	δ	$log\left(\frac{L_{line}}{L_{Bol}}\right)$	δ	$log\left(\frac{L_{line}}{L_{Bol}}\right)$	δ	$log\left(\frac{L_{line}}{L_{Bol}}\right)$	δ	$log\left(\frac{L_{line}}{L_{Bol}}\right)$	δ	$log\left(\frac{L_{line}}{L_{Bol}}\right)$	δ	$log\left(\frac{L_{line}}{L_{Bol}}\right)$	δ
J19422-207	58296.04039	-3.85943	-0.00113	-5.15125	0.01809	-4.92864	0.03674			-5.20053	0.03669				
J19422-207	58301.03723	-3.78938	-0.00097	-5.11461	0.02084	-4.77951	0.04385			-4.99894	0.04388				
J19422-207	58304.04557	-3.76308	-0.0009	-5.01185	0.02799	-4.77152	0.04408			-5.02967	0.02471				
J20093-012	57575.05825	-3.76121	-0.00097	-5.01127	0.00595	-4.88293	0.02115	-4.78696	0.0208						
J20093-012	57591.99954	-3.77644	-0.001	-5.11879	-0.00192	-4.8755	0.02488	-5.20983	0.00995	-4.81419	0.01932				
J20093-012	57603.99531	-3.7048	-0.00085	-4.84304	0.02591	-4.80914	0.02679	-4.99315	0.01844	-4.64731	0.02919				
J20093-012	57641.85913	-3.74397	-0.00094	-5.07132	0.00364	-4.85704	0.02551	-5.40314	-0.00368	-4.69646	0.02849				
J20093-012	57676.77289	-3.88952	-0.00131	-5.3446	-0.02758	-4.99357	0.00849	-5.18999	0.01041	-4.71987	0.02518				
J20093-012	57702.8081	-3.84688	-0.00118	-5.28887	-0.02004	-5.07856	0.00303	-5.27225	0.00671	-4.83624	0.03072				
J20093-012	57876.14948	-3.8256	-0.00113	-5.16398	-0.00618	-4.86453	0.01989	-5.10661	0.01461	-4.78788	0.01748				
J20093-012	57880.11559	-3.70454	-0.00085	-4.9107	0.01298	-4.8049	0.02639	-4.99807	0.01825	-4.63571	0.02286				
J20093-012	57888.12822	-3.98461	-0.00163	-5.48708	-0.05165	-5.09442	0.0001	-5.12176	-0.01055						
J20093-012	57896.11486	-3.82533	-0.00114	-5.19995	-0.00985	-4.92112	0.01251	-5.02824	0.01697	-4.71701	0.02043				
J20093-012	57910.05436	-3.84798	-0.00119	-4.97859	0.00806	-4.76138	0.02219								
J15305+094	57822.17037	-4.11981	-0.00199	-5.36431	-0.02752	-5.18429	-0.00343			-4.97371	0.0227				
J15305+094	57856.03582	-4.05569	-0.00172	-5.12855	-0.00124	-5.01327	0.00908	-5.53601	-0.03879	-5.16433	6e-05				
J15305+094	57942.9687	-4.03097	-0.00167	-5.41461	-0.0352	-5.16581	-0.00183	-5.55218	-0.03889	-4.95309	0.01306				
J15305+094	57953.90595	-3.9194	-0.00128	-4.92756	0.01213	-4.85275	0.01857	-5.22555	0.01399	-4.96328	0.02234				
J15305+094	57955.89228	-4.1967	-0.0024	-5.33197	-0.0229	-5.16614	-0.00195			-5.02131	0.01971				
J15305+094	57958.90507	-4.10362	-0.00192	-5.48742	-0.04801	-5.10075	0.0033			-4.95248	0.02515				
J22114+409	57906.13479	-4.01809	-0.00167	-5.3212	-0.03166	-5.12873	-0.0034	-5.35906	-0.04192	-5.36521	-0.0397				
J22114+409	57909.13209	-4.03399	-0.00177	-5.37499	-0.03748					-5.62822	-0.05383				
J22114+409	57911.13073	-3.99083	-0.0016	-5.25183	-0.00445	-5.23641	-0.00916	-5.36817	-0.00516	-5.71942	-0.04054				
J22114+409	57915.12461	-3.82202	-0.00111	-4.91624	0.01515	-4.83755	0.01823	-5.27766	-0.00446	-5.34169	-0.01723				
J22114+409	57917.10603	-3.71137	-0.00084	-4.841	0.01746	-4.74472	0.02085			-5.04036	0.00512				
J22114+409	57955.08073	-3.96313	-0.00151	-5.18027	-0.00182	-4.87016	0.01164	-5.53342	-0.05217	-5.57236	-0.04772				
J22114+409	58284.03617	-3.7509	-0.00092	-4.8872	0.01701	-4.64627	0.02189	-5.16117	0.0195	-5.06875	0.00333				
J22114+409	58291.09679	-3.79395	-0.00103	-4.79632	0.01847	-4.60095	0.02207	-4.88363	0.0156	-5.02887	0.0049				
J22114+409	58303.12292	-4.0738	-0.00198	-5.30518	-0.02967	-5.60435	-0.07067	-5.20784	-0.0202	-5.03045	0.00659				
J22114+409	58309.12154	-3.72342	-0.00088	-4.87471	0.01648	-4.69293	0.02081	-5.27423	-0.00234	-5.11826	0.00119				
J22114+409	58313.92924	-3.65779	-0.00078	-4.53243	0.02197	-4.50358	0.02306	-4.90166	0.01351	-5.13878	-0.001	-4.16346	0.00291		
J22114+409	58320.04812	-3.87796	-0.00124	-5.38875	-0.01874	-4.88458	0.0165			-4.8901	0.00564				
J22114+409	58326.06244	-3.77287	-0.00097	-4.78098	0.01824	-4.73426	0.01976	-5.31398	-0.01083	-4.98111	0.00792				
J22114+409	58331.08027	-3.69899	-0.00082	-4.72288	0.01966	-4.56424	0.02282	-5.22451	0.00489	-5.31317	-0.01301				
J22114+409	58336.02183	-3.80011	-0.00106	-4.73843	0.01762	-4.55184	0.02198	-5.23714	-0.0008	-5.17332	0.00585				
J22114+409	58341.06823	-3.81526	-0.00107	-5.0617	0.0074	-4.74316	0.01901	-4.67746	0.01844	-4.58425	0.01748				
J22114+409	58346.00661	-3.75285	-0.00095	-4.68545	0.01886	-4.5554	0.02198	-5.03799	0.01207	-5.07033	0.00497				
J22114+409	58350.99709	-3.73903	-0.00094	-4.70875	0.0201	-4.55785	0.0222	-4.77981	0.01781	-5.08172	0.01183				
J22114+409	58359.0048	-3.95082	-0.00145	-5.2098	-0.01008	-5.01783	0.00324			-5.34285	-0.01213				
J22114+409	58364.98293	-3.84653	-0.00115	-5.04329	0.00643	-4.8013	0.01829	-5.07985	0.00648	-5.1932	0.00285				
J22114+409	58382.93784	-3.98116	-0.00156	-5.1439	-0.01191	-4.77865	0.01752	-5.44152	-0.01819	-5.50512	-0.02392				
J22114+409	58389.91283	-3.73782	-0.00091	-4.76084	0.01906	-4.60663	0.02185	-5.16128	0.00464	-4.82991	0.02022				
J22114+409	58395.88766	-3.99702	-0.0016	-5.39035	-0.0393	-5.00449	0.00178	-5.33781	-0.02397	-5.20004	0.01591				
J22114+409	58404.88469	-4.04508	-0.00181	-5.40978	-0.04493	-4.87712	0.00839			-5.16444	0.01358				
J22114+409	58414.87773	-3.89452	-0.00129	-4.96541	0.01304	-4.74072	0.0198	-5.22835	-0.00122	-4.95261	0.00408				
J22114+409	58426.007	-3.7083	-0.00086	-4.68343	0.02023	-4.52597	0.02274	-4.99848	0.01095	-4.79373	0.01107	-4.16485	0.00283		
J22114+409	58432.95321	-4.03829	-0.00176	-5.18117	-0.0156	-4.90984	0.00968			-5.09699	-0.00496				
J22114+409	58446.91864	-3.91938	-0.00138	-5.1654	-0.0126	-4.62677	0.02083	-4.86236	0.00728	-4.85278	0.00875				
J22114+409	58473.8429	-4.07263	-0.00191	-5.30756	-0.02807	-5.01614	0.00165	-5.24714	-0.011	-5.76438	-0.03365				
J22114+409	58475.79549	-3.96863	-0.00152	-5.07605	-0.00363	-4.93304	0.01376			-5.53325	0.02137				
J22114+409	58480.77258	-3.90141	-0.00132	-4.9185	0.01307	-4.74023	0.01747	-4.83007	0.01125	-4.94342	0.00451				
J22114+409	58485.77799	-3.97053	-0.0015	-5.26876	-0.00682	-4.90667	0.01628	-5.31958	-0.02235	-5.14763	0.01565				
J22114+409	58488.81161	-3.63042	-0.0007	-4.55498	0.02281	-4.47104	0.02363	-5.05633	0.0127	-4.7868	0.01132				
J22114+409	58489.80038	-3.92485	-0.00138	-5.15105	0.00493	-4.74551	0.01968	-5.2038	0.00125	-5.38918	-0.00244				
J22114+409	58490.80992	-4.04705	-0.00179	-5.2873	-0.02739	-4.95149	0.00449	-5.36361	-0.0394	-5.10131	-0.0046				
J22114+409	58492.78003	-4.00267	-0.00163	-5.04612	0.00224	-4.90674	0.01557	-5.24332	-0.02301	-4.99591	0.00211				
J22114+409	58495.80473	-3.99396	-0.00161	-5.22423	-0.00206	-4.86976	0.01635	-5.30296	-0.00049	-5.09409	-0.00401				
J22114+409	58496.81637	-3.97785	-0.00159	-5.0483	0.00475	-4.92835	0.01487	-5.41409	-0.0181	-4.85034	0.00885				
J22114+409	58498.79551	-4.09892	-0.00201	-5.41321	-0.04551	-5.04337	-0.00096	-5.40083	-0.04592	-5.12309	-0.00694				
J22114+409	58508.78261	-4.01158	-0.00165	-5.1065	-0.00447	-4.93211	0.01448			-5.11605	-0.00526				
J22114+409	58588.15779	-3.93464	-0.0014	-4.88877	0.00689	-4.78047	0.01906	-5.24028	-0.02184	-4.9459	0.0084				
J22114+409	58599.13611	-3.40417	-0.00048	-4.66877	0.0209	-4.63061	0.02132	-4.86933	0.01183	-5.03417	0.016	-3.86115	0.01483		
J22114+409	58600.14671	-3.98107	-0.00157	-5.06451	0.00727	-4.83475	0.01759	-5.41177	-0.01646	-5.29225	0.01533	-4.14702	0.0038		
J22114+409	58604.14312	-4.07315	-0.00193	-5.12066	-0.00934	-5.07659	-0.00286			-5.45507	-0.02144				

Continued on next page

// Star	MJD	Hα		Ca II IRT-a		Ca II IRT-b		He I D_3		Na I D_2		Paβ		Paδ	
		$log\left(\frac{L_{line}}{L_{Bol}}\right)$	δ	$log\left(\frac{L_{line}}{L_{Bol}}\right)$	δ	$log\left(\frac{L_{line}}{L_{Bol}}\right)$	δ	$log\left(\frac{L_{line}}{L_{Bol}}\right)$	δ	$log\left(\frac{L_{line}}{L_{Bol}}\right)$	δ	$log\left(\frac{L_{line}}{L_{Bol}}\right)$	δ	$log\left(\frac{L_{line}}{L_{Bol}}\right)$	δ
J22114+409	58606.15429	-4.02181	-0.00172	-5.29334	-0.02484	-4.96026	0.00785			-5.09527	0.00167				
J22114+409	58609.15129	-4.00674	-0.0017	-5.23474	-0.02107	-5.02643	0.0004	-5.34293	-0.03284	-4.97264	0.00759				
J22114+409	58610.14085	-3.91835	-0.00135	-5.2162	-0.01906	-4.89992	0.01151	-5.34428	-0.00949	-5.24383	-0.00416				
J22114+409	58615.13822	-4.11442	-0.00212	-5.31467	-0.03079	-5.10658	-0.00482			-5.32702	-0.01386				
J22114+409	58618.14277	-3.74139	-0.00094	-4.8992	0.01694	-4.63043	0.02179	-4.94324	0.01258	-5.1529	-0.00086	-4.16451	0.00259		
J10564+070	57397	-3.77257	-0.00088	-4.84295	0.08342	-4.63915	0.08666	-5.08212	0.07887						
J10564+070	57401	-3.79862	-0.0008	-4.79095	0.08559	-4.70961	0.08681	-5.30797	0.07729						
J10564+070	57419	-3.66477	-0.0007	-4.60696	0.08851	-4.56228	0.08885	-5.02353	0.08616	-4.84347	0.08461				
J10564+070	57444	-3.66528	-0.00069	-4.74464	0.08494	-4.59339	0.08735	-5.14318	0.07972	-5.05013	0.08249			-5.32269	0.05391
J10564+070	57475.95697	-3.8036	-0.00073	-4.77885	0.08487	-4.74292	0.08378	-5.19907	0.08241	-5.06803	0.07729				
J10564+070	57489.93726	-3.84843	-0.00104	-4.81044	0.08361	-4.69655	0.08219	-5.39156	0.07102	-5.03345	0.08263			-5.31144	0.05558
J10564+070	57509.86806	-3.83281	-0.001	-4.72245	0.08033	-4.71468	0.08198	-5.48172	0.06113	-5.02821	0.08242				
J10564+070	57509.8835	-3.82276	-0.00098	-4.80154	0.08387	-4.70447	0.08221	-5.31486	0.07142	-5.03374	0.07254				
J10564+070	57511.88486	-3.78035	-0.00071	-4.82031	0.08574	-4.70879	0.08742	-5.28293	0.07881	-4.86998	0.08756			-5.29184	0.06201
J10564+070	57537.8564	-3.79315	-0.00092	-4.78208	0.08438	-4.66014	0.08322	-5.23355	0.05761	-5.3228	0.05713			-5.24578	0.046
J10564+070	57543.85066	-3.83678	-0.001	-4.80438	0.08381	-4.69703	0.08554	-5.4595	0.06684	-5.21329	0.07719			-5.20031	0.05058
J10564+070	57689.2399	-3.81446	-0.00096	-4.79132	0.08454	-4.6652	0.08693	-5.39947	0.04246	-4.76673	0.08166			-5.26738	0.05342
J10564+070	57690.2449	-3.95078	-0.00132	-4.82745	0.08328	-4.74835	0.08459	-5.48725	0.04413	-4.83051	0.08452			-5.34076	0.04763
J10564+070	57691.21411	-3.75936	-0.00085	-4.75823	0.08494	-4.63672	0.08691	-5.02913	0.08149	-4.74246	0.08172			-5.27482	0.05436
J10564+070	57692.23661	-3.81321	-0.00096	-4.77653	0.0844	-4.71118	0.08573	-5.29548	0.0712	-4.99315	0.08382			-5.27346	0.05352
J10564+070	57693.23832	-3.80643	-0.00094	-4.76137	0.08474	-4.7057	0.08587	-5.45419	0.0458	-4.88331	0.08673			-5.22519	0.05785
J10564+070	57694.21647	-3.49887	-0.00063	-4.69169	0.08588	-4.56518	0.08771	-5.05852	0.08011	-4.79051	0.07963			-5.31369	0.05276
J10564+070	57695.21501	-3.65699	-0.00068	-4.56122	0.08761	-4.5147	0.08822	-5.23305	0.06334	-4.70526	0.08257	-4.10727	0.07212	-5.11568	0.05791
J10564+070	57699.18449	-3.50518	-0.00077	-4.54821	0.08803	-4.46199	0.08888	-5.11114	0.07903	-4.65975	0.08876			-5.2359	0.04704
J10564+070	57703.16927	-3.80182	-0.00093	-4.80005	0.08414	-4.68585	0.08605	-5.14828	0.07787	-4.86963	0.085			-5.21737	0.06028
J10564+070	57704.17799	-3.76589	-0.00085	-4.79088	0.08398	-4.60836	0.08689	-5.23229	0.07151	-4.76311	0.08028			-5.17851	0.05735
J10564+070	57706.1635	-3.71788	-0.00077	-4.75267	0.08495	-4.61673	0.08701	-5.10052	0.07621	-4.79269	0.07952			-5.25485	0.05467
J10564+070	57709.20593	-3.69527	-0.00073	-4.68538	0.08628	-4.88081	0.08367	-5.26092	0.07577	-4.98374	0.08268			-5.26782	0.05449
J10564+070	57712.18439	-3.79731	-0.00092	-4.80177	0.08345	-4.81005	0.08362			-4.84679	0.08908			-5.25479	0.04535
J10564+070	57735.09243	-3.49892	-0.00072	-4.61979	0.08751	-4.50003	0.08864	-5.15317	0.07911	-4.75671	0.08167	-4.26281	0.0664	-5.28757	0.05307
J10564+070	57746.26339	-3.70027	-0.00073	-4.7536	0.08479	-4.58386	0.08757	-5.05445	0.08173	-4.8925	0.08505			-5.26695	0.05535
J10564+070	57747.21322	-3.7557	-0.00083	-4.79415	0.08392	-4.63839	0.08667	-5.27499	0.0757	-4.8204	0.07935			-5.22739	0.05739
J10564+070	57752.16081	-3.74248	-0.00081	-4.76481	0.08506	-4.69313	0.08646	-5.27031	0.07556	-4.87355	0.079			-5.2482	0.05494
J10564+070	57754.12306	-3.71796	-0.00077	-4.79192	0.08461	-4.75065	0.08575	-4.93856	0.08449	-4.93919	0.0758			-5.22267	0.0572
J10564+070	57756.18919	-3.76982	-0.00087	-4.75593	0.08468	-4.59769	0.08686	-5.08193	0.08059	-4.87183	0.08525			-5.20183	0.06208
J10564+070	57759.15995	-3.68068	-5.00E-05	-4.61248	0.08674	-4.57516	0.08741	-5.32594	0.07104	-4.86572	0.07726			-5.20772	0.05933
J10564+070	57761.11631	-3.74717	-0.00082	-4.76194	0.08465	-4.64968	0.0863	-5.23509	0.07589	-4.99016	0.07226			-5.24863	0.05626
J10564+070	57763.15715	-3.76846	-0.00085	-4.8584	0.08273	-4.75533	0.08107	-5.44656	0.0428	-4.97697	0.08395			-5.28328	0.05378
J10564+070	57766.01343	-3.71044	-0.00075	-4.76946	0.08437	-4.653	0.08675	-5.47885	0.06175	-5.1082	0.06656			-5.28716	0.05064
J10564+070	57778.96051	-3.85779	-0.00106	-4.83651	0.08136	-4.70133	0.08466	-5.59723	0.02673	-4.89662	0.08559			-5.20784	0.05534
J10564+070	57786.93929	-3.90533	-0.00118	-4.83096	0.08119	-4.61062	0.08597	-5.08526	0.06007	-4.78983	0.08054			-5.2989	0.04036
J10564+070	57790.0941	-3.74066	-0.0008	-4.81556	0.08402	-4.66121	0.08332	-5.29476	0.0722	-4.68608	0.08296			-5.17225	0.05342
J10564+070	57794.12013	-3.70659	-0.00075	-4.67113	0.0861	-4.55915	0.08786	-5.04057	0.08154	-4.83785	0.0856			-5.16813	0.06281
J10564+070	57798.91186	-3.78385	-0.00088	-4.81522	0.08208	-4.88793	0.07722	-5.413	0.06421	-4.93385	0.08363			-5.24445	0.05899
J10564+070	57800.98197	-3.73709	-0.00079	-4.73847	0.08546	-4.63432	0.08683	-5.14011	0.08074	-4.92466	0.08545			-5.1815	0.0668
J10564+070	57806.01522	-3.8121	-0.00095	-4.79678	0.08396	-4.64438	0.08705	-5.26488	0.07461	-4.89854	0.08775			-5.26107	0.05088
J10564+070	57808.07684	-3.9505	-0.00133	-4.83922	0.08143	-4.71895	0.08123	-5.30167	0.04089	-5.4	0.07089				
J10564+070	57814.01941	-3.79677	-0.00066	-4.80909	0.08607	-4.76436	0.08382	-5.452	0.07684	-5.08163	0.08612			-5.18186	0.07273
J10564+070	57817.04697	-3.71611	-0.00076	-4.77948	0.08435	-4.61465	0.08412	-5.2163	0.07596	-4.93613	0.0818			-5.35764	0.04199
J10564+070	57818.08206	-3.8235	-0.00079	-4.82374	0.08448	-4.71535	0.08708	-5.16921	0.08321	-5.12764	0.08415			-5.27173	0.06719
J10564+070	57818.0992	-3.81377	-0.00074	-4.78788	0.08631	-4.65144	0.0856	-5.13616	0.08281	-5.021	0.08604			-5.24574	0.06938
J10564+070	57819.02144	-3.79227	-0.00065	-4.79321	0.08668	-4.65716	0.08596	-5.18367	0.08188	-5.05613	0.08674			-5.23253	0.07122
J10564+070	57819.15623	-3.84285	-0.00086	-4.79457	0.08602	-4.73196	0.08395	-5.19891	0.07896	-4.99275	0.08279				
J10564+070	57820.93014	-3.89437	-0.00083	-4.83743	0.08571	-4.74316	0.08414	-5.45972	0.0763	-5.14914	0.08504			-5.24261	0.07118
J10564+070	57821.86575	-3.72843	-0.00062	-4.76732	0.08669	-4.68157	0.08776	-5.05956	0.08386	-5.03993	0.085				
J10564+070	57822.15133	-3.87822	-0.0008	-4.79787	0.08675	-4.69016	0.08561	-5.57601	0.06552	-5.22222	0.07832			-5.39694	0.05656
J10564+070	57827.99185	-3.72981	-0.0008	-4.75508	0.08539	-4.62113	0.08728	-5.297	0.06706	-4.92315	0.08141			-5.38358	0.03665
J10564+070	57828.83821	-3.86966	-0.00109	-4.84506	0.08292	-4.64502	0.08344	-5.36973	0.03619	-5.05177	0.07744			-5.33443	0.03559
J10564+070	57829.85307	-3.74761	-0.00083	-4.74466	0.08494	-4.64848	0.08683	-5.09761	0.07806	-4.93948	0.08426			-5.40057	0.04856
J10564+070	57829.9903	-3.82861	-0.00072	-4.77414	0.08676	-4.69562	0.08772	-5.476	0.07706	-5.11773	0.08539			-5.31869	0.06648
J10564+070	57830.85536	-3.79554	-0.0007	-4.79192	0.0865	-4.6981	0.08504	-5.25639	0.08019	-4.91603	0.0816			-5.30296	0.06671
J10564+070	57831.9244	-3.70889	-0.00053	-4.65274	0.08812	-4.57189	0.0889	-5.09959	0.08566	-4.90874	0.08824			-5.28058	0.06863
J10564+070	57833.06976	-3.63693	-0.00042	-4.56953	0.08938	-4.56295	0.08946	-5.05342	0.08674	-4.79318	0.0859			-5.29731	0.06855
J10564+070	57847.83162	-3.69635	-0.00056	-4.6914	0.08782	-4.72446	0.08749	-5.17278	0.08286	-4.98846	0.0815			-5.27458	0.06895

Continued on next page

// Star	MJD	Hα		Ca II IRT-a		Ca II IRT-b		He I D_3		Na I D_2		Paβ		Paδ	
		$log\left(\frac{L_{line}}{L_{Bol}}\right)$	δ	$log\left(\frac{L_{line}}{L_{Bol}}\right)$	δ	$log\left(\frac{L_{line}}{L_{Bol}}\right)$	δ	$log\left(\frac{L_{line}}{L_{Bol}}\right)$	δ	$log\left(\frac{L_{line}}{L_{Bol}}\right)$	δ	$log\left(\frac{L_{line}}{L_{Bol}}\right)$	δ	$log\left(\frac{L_{line}}{L_{Bol}}\right)$	δ
J10564+070	57848.82541	-3.77715	-0.00087	-4.77817	0.08429	-4.72872	0.08575	-5.22663	0.07421	-5.01869	0.08303			-5.27043	0.05791
J10564+070	57849.85453	-3.86756	-0.00096	-4.84289	0.08473	-4.84044	0.08077			-5.13233	0.08387			-5.33987	0.05944
J10564+070	57852.83152	-3.90403	-0.0009	-4.80776	0.08592	-4.74225	0.08412			-5.22349	0.08313			-5.31415	0.06622
J10564+070	57856.83378	-3.53779	-0.00034	-4.53612	0.0893	-4.43261	0.08994	-5.01281	0.08757	-4.75979	0.08953				
J10564+070	57862.89447	-3.86743	-0.00108	-4.84276	0.08306	-4.66395	0.08237	-5.51438	0.01533	-5.02418	0.07876			-5.22626	0.05089
J10564+070	57890.84744	-3.90995	-0.00087	-4.77549	0.08658	-4.79357	0.08337	-5.3089	0.07271	-5.11018	0.08535			-5.30578	0.06775
J10564+070	57893.84534	-3.77615	-0.00064	-4.81174	0.0862	-4.70267	0.08755	-5.26026	0.08237	-4.94643	0.08758			-5.3001	0.06738
J10564+070	57909.88138	-3.77998	-0.00062	-4.80374	0.08659	-4.76367	0.08458	-5.35131	0.07706	-4.96168	0.0874			-5.2734	0.06789
J10564+070	57913.85628	-3.8153	-0.0009	-4.73717	0.08545	-4.64656	0.08651	-5.29472	0.07718	-5.00303	0.08535			-5.24195	0.06245
J10564+070	58052.21825	-3.79065	-0.00069	-4.77083	0.0866	-4.7706	0.08634	-5.20194	0.08165	-4.9612	0.07971				
J10564+070	58055.21248	-3.75264	-0.00065	-4.73414	0.08732	-4.58376	0.08879	-5.3918	0.07293	-4.85163	0.08214				
J10564+070	58056.20309	-3.74541	-0.00068	-4.68486	0.08754	-4.6008	0.0882	-4.94922	0.08312	-4.81989	0.08144				
J10564+070	58094.16551	-3.76821	-0.00068	-4.78388	0.08628	-4.66824	0.08792	-5.17401	0.08231	-4.99231	0.08606				
J10564+070	58166.94446	-3.75596	-0.00067	-4.81086	0.08587	-4.60937	0.08791	-5.17421	0.08208	-4.97256	0.08585				
J10564+070	58172.02207	-3.83488	-0.00082	-4.85102	0.08482	-4.70059	0.08445	-5.58138	0.07013	-5.11334	0.08456				
J10564+070	58174.99127	-3.68648	-0.00055	-4.66717	0.08769	-4.59466	0.08853	-5.17588	0.08369	-4.91386	0.08768				
J10564+070	58212.9323	-3.88454	-0.00095	-4.77105	0.08622	-4.76965	0.0833	-5.29703	0.07808	-5.12804	0.08405				
J14321+081	57787.14051	-3.60705	-0.00072	-4.69351	0.05373	-4.53197	0.05726	-4.76891	0.05061	-4.41967	0.05199				
J14321+081	57823.10042	-3.87306	-0.00129	-4.92455	0.04856	-4.83383	0.05175	-5.19175	0.02893	-4.9891	0.0389				
J14321+081	57851.07293	-3.79296	-0.0011	-4.68219	0.05454	-4.68776	0.05478			-4.72318	0.05954				
J14321+081	57895.93228	-3.8409	-0.00121	-4.87572	0.04947	-4.74976	0.0539	-5.17377	0.03183	-4.75179	0.05916				
J14321+081	57930.96076	-3.95472	-0.00153	-4.88531	0.04751	-4.9117	0.04917			-4.68879	0.04242				
J14321+081	57954.87505	-3.7603	-0.00099	-4.84532	0.04792	-4.74232	0.05347			-4.659	0.04264				
J14321+081	57958.88196	-3.96323	-0.00158	-4.89496	0.04362	-4.81522	0.05195			-4.96463	0.02395				
J14321+081	58625.9958	-3.93555	-0.00151	-4.89037	0.04872	-4.76254	0.05354			-5.01988	0.0443				
J14321+081	58630.97472	-3.88863	-0.00136	-5.03455	0.0342	-4.72493	0.05435	-5.2227	0.01618						
J14321+081	58635.94354	-3.88418	-0.00133	-4.86889	0.04875	-4.80721	0.05293								
J14321+081	58640.93525	-3.94125	-0.00151	-5.00285	0.04342	-4.82737	0.05185	-5.17794	0.01396	-4.90328	0.05102				
J14321+081	58645.88142	-3.97126	-0.00162	-4.94965	0.04354	-5.23722	0.02218								
J14321+081	58655.03316	-3.85232	-0.00125	-4.76062	0.05235	-4.67981	0.05465			-4.60629	0.05856				
J14321+081	58659.86636	-3.92863	-0.00148	-5.0124	0.04484	-4.78642	0.05306								
J14321+081	58665.88193	-3.8161	-0.00114	-4.78724	0.05145	-4.81308	0.0529			-4.78196	0.05411				
J14321+081	58677.88423	-3.78354	-0.00106	-4.97875	0.0471	-4.65475	0.05562								
J14321+081	58682.86248	-3.95945	-0.00158	-4.84637	0.04273	-4.86695	0.05068								
J14321+081	58687.86325	-3.84327	-0.0012	-4.90785	0.04846	-5.00375	0.04788	-5.18063	0.01436	-4.98235	0.04975				
J14321+081	58689.87923	-3.81365	-0.00113	-4.75779	0.05273	-4.75022	0.05416	-5.21673	0.03005						
J14321+081	58694.87011	-3.85994	-0.00126	-4.88554	0.0475	-4.85271	0.05154	-5.15588	0.02188	-4.89979	0.06049				
J14321+081	58699.85573	-3.83896	-0.00118	-4.89214	0.04936	-4.74404	0.05363	-5.17097	0.01219						
J14321+081	58705.8542	-3.96787	-0.00159	-4.85403	0.04175	-4.92617	0.04428			-4.80166	0.03493				
J08298+267	57415	-4.17563	-0.00191	-5.00412	-0.00128					-4.88554	0.01577				
J08298+267	57421	-4.18879	-0.00197	-4.99716	0.00115	-5.13428	-0.00371			-5.17986	0.00904				
J08298+267	57709.12343	-4.15494	-0.00182	-5.02602	-0.00237	-5.25449	-0.016			-5.06412	0.00279				
J08298+267	57752.14058	-4.05688	-0.00144	-4.98172	-0.00016	-5.20494	-0.01192			-4.89338	0.00813				
J08298+267	57754.21913	-4.13234	-0.0017	-5.04389	-0.00342	-5.13433	-0.00673			-4.98179	0.01667				
J08298+267	57761.99334	-4.02262	-0.00136	-4.90412	0.00503	-5.10239	-0.00336	-5.38942	0.00173	-5.00381	0.01598				
J08298+267	57813.88641	-4.12359	-0.00169	-4.96983	0.00311	-5.21084	-0.00837			-5.12925	0.01177				
J08298+267	57859.85519	-4.02807	-0.00135	-4.85207	0.00639	-5.07952	-0.00078			-5.12243	0.01221				
J08298+267	57876.91013	-4.10561	-0.00164	-4.95673	0.00102	-5.19334	-0.01114								
J08298+267	57880.90053	-4.30966	-0.00252	-5.0295	-0.00262	-5.38328	-0.02878								
J08298+267	57882.84583	-4.32633	-0.00266	-5.03439	-0.00282	-5.37655	-0.02787								
J08298+267	57885.85122	-3.90475	-0.00105	-4.82118	0.00976	-4.94666	0.00442	-5.49005	-0.01405						
J08298+267	57887.84655	-4.06902	-0.00145	-4.92039	0.00406	-5.12369	-0.00409								
J08298+267	58399.19129	-4.01608	-0.00134	-4.93443	0.00208	-4.9251	0.00532	-5.37222	-0.00265	-4.81015	0.01697				
J08298+267	58474.14099	-3.87522	-0.00097	-4.83176	0.01153	-4.9109	0.01109	-5.3852	0.00436	-4.92663	0.00824				
J08298+267	58484.98383	-3.94113	-0.00111	-4.87048	0.00927	-4.95181	0.00868	-5.34569	0.0034	-4.97323	0.01547				
J08298+267	58487.10962	-4.18879	-0.00193	-5.04079	-0.00318	-5.35555	-0.0257			-4.98042	0.00617				
J08298+267	58489.22273	-4.0355	-0.0014	-4.95943	0.0009	-5.05956	-0.001			-5.07791	0.01422				
J08298+267	58491.06784	-3.93343	-0.00112	-4.87563	0.00563	-4.84713	0.00807	-5.30881	0.00368	-5.06146	0.0035				
J08298+267	58496.0196	-4.06798	-0.00146	-4.98934	0.00036	-5.01371	0.00082			-5.02327	0.01401				
J08298+267	58498.16255	-3.84184	-0.00087	-4.94533	0.00295	-4.97576	0.00402	-5.48638	-0.01515	-4.91119	0.01647				
J08298+267	58528.84575	-4.18688	-0.00194	-4.99066	0.00229	-5.32385	-0.01658			-5.07895	0.01152				
J08298+267	58536.98132	-4.21327	-0.00205	-5.01163	-0.00015	-5.32606	-0.01964			-5.19198	0.01026				
J08298+267	58539.09507	-4.10268	-0.00159	-4.94658	0.00148	-5.0683	-0.00217			-5.17937	0.01078				
J08298+267	58542.98623	-3.82222	-0.00085	-4.79944	0.01174	-4.85293	0.01206	-5.33447	0.00402	-4.86497	0.01621				

Continued on next page

// Star	MJD	Hα		Ca II IRT-a		Ca II IRT-b		He I D_3		Na I D_2		Paβ		Paδ	
		$log\left(\frac{L_{line}}{L_{Bol}}\right)$	δ	$log\left(\frac{L_{line}}{L_{Bol}}\right)$	δ	$log\left(\frac{L_{line}}{L_{Bol}}\right)$	δ	$log\left(\frac{L_{line}}{L_{Bol}}\right)$	δ	$log\left(\frac{L_{line}}{L_{Bol}}\right)$	δ	$log\left(\frac{L_{line}}{L_{Bol}}\right)$	δ	$log\left(\frac{L_{line}}{L_{Bol}}\right)$	δ
J09003+218	57759.07858	-3.80965	-0.00093	-5.14992	-0.01039	-4.94846	0.00999	-5.09893	0.00063	-4.59409	0.02111				
J09003+218	57763.05314	-3.54544	-0.00051	-4.72545	0.02102	-4.62404	0.02281	-5.16961	0.01165	-4.63185	0.02038				
J09003+218	57829.87826	-3.84908	-0.00103	-5.05952	-0.00297	-5.15718	-0.00828			-4.93166	0.01174				
J09003+218	57832.86712	-3.72292	-0.00076	-4.9342	0.00507	-5.13084	-0.00538			-5.07535	0.00286				
J09003+218	58135.10591	-3.88023	-0.00111	-5.0293	-0.00081	-5.03612	0.00074	-5.5199	-0.04287	-4.68791	0.01919				
J09003+218	58397.18402	-3.81385	-0.00093	-5.02085	-0.00017	-4.97642	0.00445	-5.45879	-0.02002	-4.56949	0.02161				
J09003+218	58434.19478	-3.88723	-0.00117	-5.2411	-0.0195	-4.92807	0.00705			-4.71087	0.01866				
J09003+218	58454.18095	-3.84139	-0.00101	-5.13447	-0.00901	-5.05283	-0.00037	-5.3534	-0.00384	-4.61104	0.02079				
J09003+218	58480.04331	-3.77654	-0.00085	-5.04853	-0.00209	-4.89879	0.00853			-4.59457	0.02123				
J09003+218	58485.16364	-3.90653	-0.00117	-5.10161	-0.00623	-5.08523	-0.00257			-4.64174	0.02677				
J09003+218	58490.14059	-3.85553	-0.00105	-5.21744	-0.01703	-5.03225	0.001	-5.27939	-0.01209	-4.93695	0.01698				
J09003+218	58495.1271	-3.77111	-0.00085	-5.04719	-0.002	-4.86321	0.01156			-4.36659	0.02437				
J09003+218	58527.15134	-3.88502	-0.00109	-5.23305	-0.01861	-4.95967	0.00532			-5.1422	0.00086				
J09003+218	58537.07583	-3.80406	-0.00091	-5.27586	-0.02355	-5.00545	0.00274	-5.31488	-0.01492	-4.99093	0.0092				
J09003+218	58542.06733	-3.8352	-0.00098	-5.09225	-0.0054	-5.21238	-0.01345	-5.34691	-0.01657	-4.96237	0.01704				
J09003+218	58845.06373	-3.86843	-0.00107	-5.1429	-0.00967	-5.0264	0.00144	-5.22685	-0.00858	-4.81116	0.01572				
J09003+218	58904.00956	-3.86451	-0.00105	-5.28671	-0.02501	-5.07043	-0.00151	-5.43988	-0.02435	-5.19317	0.01334				
J09033+056	57735.1497	-4.08593	-0.00238	-5.51839	-0.04938	-5.491	-0.03998	-5.30063	-0.0122	-4.79706	0.02326				
J09033+056	58127.02204	-4.03281	-0.00259	-5.50569	-0.04715										
J09033+056	58166.0516	-4.25866	-0.0035	-5.25827	-0.01451	-5.55171	-0.04995	-5.31184	-0.01225	-4.76663	0.01949				
J09033+056	58486.08305	-4.21089	-0.00299	-5.49973	-0.04633										
J09033+056	58496.09512	-4.08202	-0.00228	-5.26953	-0.01563			-5.47269	-0.03278	-5.19867	0.01311				
J09033+056	58524.06496	-4.17732	-0.00288	-5.33121	-0.02229					-5.00245	0.01338				
J09033+056	58527.04645	-4.22867	-0.00313	-5.52139	-0.04992	-5.20554	-0.00672	-5.36538	-0.01754	-5.24578	0.02043				
J09033+056	58535.98869	-4.29069	-0.00368	-5.59074	-0.06341					-5.24396	0.00556				
J09033+056	58541.94824	-4.18067	-0.00286	-5.21015	-0.01016	-5.64579	-0.06909			-5.37479	0.0061				
J09033+056	58567.93657	-4.15887	-0.00273	-5.33762	-0.02317			-5.2595	-0.00598						
J09033+056	58607.89425	-4.20987	-0.00305	-5.30386	-0.01922			-5.14884	-0.00016	-4.94008	0.01531				
J09033+056	58772.18747	-4.21804	-0.00375	-5.61495	-0.06891					-4.96125	0.022				
J09033+056	58783.15551	-4.27627	-0.00357	-5.24719	-0.01344	-5.53798	-0.04774			-4.43998	0.02579				
J09033+056	58828.17899	-4.11621	-0.00242	-5.4405	-0.03668			-5.58119	-0.05011	-5.07555	0.019				
J16555-083	57488.14753	-4.01006	-0.00184	-5.13309	-0.00947	-5.26732	-0.01284								
J16555-083	57510.11385	-4.39532	-0.00462	-5.28022	-0.02406										
J16555-083	57510.13639	-4.25314	-0.00309	-5.0651	-0.00419										
J16555-083	57511.07303	-4.24234	-0.00321	-5.41527	-0.04285										
J16555-083	57540.0222	-3.68114	-0.00085	-5.12322	-0.00857	-4.92414	0.01578								
J16555-083	57556.97054	-4.07836	-0.00215	-5.18371	-0.01389										
J16555-083	57562.95024	-4.06056	-0.00213	-5.11375	-0.0078	-5.33483	-0.01954								
J16555-083	57567.9426	-4.49856	-0.00597	-5.40051	-0.04036										
J16555-083	57569.93615	-4.14563	-0.00256	-5.14017	-0.01007	-5.22837	-0.00942								
J16555-083	57570.94325	-4.24554	-0.00325	-5.22978	-0.01846	-5.22276	-0.00895								
J16555-083	57571.94486	-4.07601	-0.00223	-5.41069	-0.04195	-5.27604	-0.01365								
J16555-083	57572.92459	-4.26008	-0.00354	-4.94958	0.0031	-5.22702	-0.00931								
J16555-083	57573.9151	-4.02107	-0.00201	-5.40993	-0.04199										
J16555-083	57583.91384	-3.67291	-0.00087	-4.93434	0.00392	-4.97212	0.00861								
J16555-083	57584.91352	-3.88078	-0.00134	-5.02326	-0.00132	-5.04945	0.00281					-4.14465	0.00616		
J16555-083	57586.93307	-4.23645	-0.00311	-5.15225	-0.01112										
J16555-083	57591.93056	-3.62786	-0.00083	-4.69195	0.01951	-4.72129	0.01935								
J16555-083	57592.925	-3.55084	-0.00092	-4.97007	0.01257	-4.80286	0.01926								
J16555-083	57594.87118	-4.12891	-0.00245	-5.30949	-0.02775	-5.36645	-0.02305								
J16555-083	57596.86597	-4.17527	-0.00269	-5.11177	-0.00773	-5.31911	-0.01788								
J16555-083	57602.85067	-3.85652	-0.00128	-5.38213	-0.03772										
J16555-083	57603.86948	-3.54042	-0.00064	-4.79686	0.01844										
J16555-083	57604.86176	-4.06104	-0.00209	-5.30015	-0.02658										
J16555-083	57605.86106	-4.22056	-0.00301	-5.41835	-0.04334										
J16555-083	57606.87095	-3.96218	-0.00168	-5.12786	-0.00904	-5.26912	-0.013								
J16555-083	57611.85052	-4.18799	-0.00268	-5.215	-0.01704										
J16555-083	57613.86828	-4.20871	-0.00297	-5.1271	-0.00897										
J16555-083	57614.85289	-4.47074	-0.00517	-5.23215	-0.01882	-5.19332	-0.0066								
J16555-083	57616.85442	-3.95399	-0.00161	-5.22358	-0.01782	-5.18629	-0.00606								
J16555-083	57617.85028	-4.10308	-0.00227	-5.17372	-0.01296										
J16555-083	57618.85603	-4.02607	-0.00191	-5.28873	-0.02519	-5.3893	-0.02576								
J16555-083	57619.83331	-4.24447	-0.00332	-5.22153	-0.01771										
J16555-083	57620.85743	-4.00408	-0.00221	-5.28683	-0.02484	-5.39882	-0.02692								

Continued on next page

// Star	MJD	Hα		Ca II IRT-a		Ca II IRT-b		He I D_3		Na I D_2		Paβ		Paδ	
		$log\left(\frac{L_{line}}{L_{Bol}}\right)$	δ	$log\left(\frac{L_{line}}{L_{Bol}}\right)$	δ	$log\left(\frac{L_{line}}{L_{Bol}}\right)$	δ	$log\left(\frac{L_{line}}{L_{Bol}}\right)$	δ	$log\left(\frac{L_{line}}{L_{Bol}}\right)$	δ	$log\left(\frac{L_{line}}{L_{Bol}}\right)$	δ	$log\left(\frac{L_{line}}{L_{Bol}}\right)$	δ
J16555-083	57621.8373	-4.25252	-0.00313	-5.3741	-0.03653										
J16555-083	57624.82961	-4.0951	-0.00224	-5.29943	-0.02637	-5.23065	-0.00961								
J16555-083	57626.82882	-4.16655	-0.0026	-5.05426	-0.00342										
J16555-083	57627.85038	-3.93742	-0.00156	-5.24508	-0.0202	-5.26133	-0.01229								
J16555-083	57629.82966	-4.04116	-0.002	-5.00521	-0.00011	-5.20749	-0.00781								
J16555-083	57633.83921	-4.06257	-0.00209	-5.44445	-0.0477										
J16555-083	57634.82711	-3.90133	-0.00142	-5.14543	-0.01052	-5.45562	-0.03446								
J16555-083	57635.84341	-4.00905	-0.00179	-5.2075	-0.01619	-5.47832	-0.03776								
J16555-083	57641.8109	-3.54872	-0.00064	-5.25728	0.0034	-4.99615	0.0148								
J16555-083	57643.81659	-4.02563	-0.00194	-5.07225	-0.00463	-5.33961	-0.02019								
J16555-083	57649.80699	-3.84706	-0.00128	-4.86851	0.00721										
J16555-083	57651.82214	-3.99465	-0.00182	-5.23323	-0.01893										
J16555-083	57653.80681	-3.88434	-0.00144	-5.09029	-0.00597	-5.07642	0.00384								
J16555-083	57655.7984	-4.20779	-0.00294	-5.1522	-0.01111										
J16555-083	57861.07116	-4.02864	-0.00188	-5.12919	-0.00915	-5.16896	-0.00485								
J16555-083	57863.15455	-4.04108	-0.00196	-5.24242	-0.01981	-5.21924	-0.00866								
J16555-083	57864.04383	-3.9357	-0.00163	-4.98802	0.00094	-5.11516	-0.00114					-4.10084	0.00837		
J16555-083	57864.11586	-4.18788	-0.00056	-5.35313	-0.03339							-4.18051	0.00437		
J16555-083	57866.05001	-4.17815	-0.00269	-5.42667	-0.04454										
J16555-083	57867.08701	-3.98464	-0.00171	-5.34216	-0.03189	-5.53023	-0.04598								
J16555-083	57875.05778	-3.96085	-0.00163	-5.39135	-0.0391	-5.32054	-0.01816								
J16555-083	57877.09029	-3.63725	-0.00082	-4.57393	0.01793	-5.04427	0.01453								
J16555-083	57881.00855	-4.34526	-0.00377	-5.17966	-0.0136	-5.45628	-0.03473								
J16555-083	57882.02219	-3.90885	-0.00146	-5.21829	-0.01738	-5.29311	-0.01527								
J16555-083	57887.95534	-3.85593	-0.00129	-5.17545	-0.01312	-5.44125	-0.03263								
J16555-083	57889.06174	-4.20389	-0.00296	-5.29155	-0.02553										
J16555-083	57889.98965	-4.10116	-0.00224	-5.23216	-0.01871										
J16555-083	57890.13311	-4.09852	-0.00223	-5.35901	-0.03422										
J16555-083	57891.0005	-4.15438	-0.0025	-5.02216	-0.00125	-5.01964	0.00441								
J16555-083	57892.00052	-3.92955	-0.00144	-5.11458	-0.00787	-5.44604	-0.03329								
J16555-083	57892.0777	-4.20959	-0.00289	-5.30921	-0.02759										
J16555-083	57892.96036	-3.85105	-0.00125	-5.37469	-0.03647	-5.35388	-0.02176								
J16555-083	57893.98067	-3.97883	-0.00168	-5.17878	-0.01352	-5.32814	-0.01883								
J16555-083	57895.98706	-3.88525	-0.00132	-5.29904	-0.02645	-5.27009	-0.01309								
J16555-083	57898.02848	-4.04452	-0.002	-5.3887	-0.03855										
J16555-083	57898.12486	-4.11017	-0.00232	-5.44433	-0.04751	-5.17203	-0.00499								
J16555-083	57901.05773	-4.38818	-0.00457	-5.13748	-0.00976	-5.31019	-0.01697								
J16555-083	57905.01006	-4.01306	-0.00181	-5.36257	-0.03486	-5.36487	-0.02301								
J16555-083	57915.94843	-4.14198	-0.00252	-5.39791	-0.04011	-5.26404	-0.01254								
J16555-083	57916.99204	-3.94279	-0.00155	-5.32913	-0.03028	-5.23889	-0.01031								
J16555-083	57944.93265	-4.15129	-0.00265	-5.35626	-0.03383										
J16555-083	57945.96051	-4.42807	-0.00506	-5.24483	-0.02007										
J16555-083	57947.93038	-4.17442	-0.0026	-5.12461	-0.00877	-5.3426	-0.02051								
J16555-083	57953.92921	-4.07944	-0.00218	-5.24425	-0.02	-5.3041	-0.01648								
J16555-083	57954.9325	-4.02864	-0.00192	-5.18195	-0.01382										
J16555-083	57957.9205	-4.18825	-0.00287	-5.31912	-0.02885										
J16555-083	57958.92817	-3.66332	-0.00081	-5.05938	-0.00378	-5.19087	0.00262								
J16555-083	57975.872	-4.12265	-0.00235	-5.17485	-0.01315	-5.45469	-0.03433								
J16555-083	58175.1905	-4.02723	-0.00184	-5.17087	-0.0127										
J16555-083	58205.09579	-3.94264	-0.00162	-5.24088	-0.01975	-5.2555	-0.01177								
J16555-083	58225.14762	-4.07892	-0.00215	-5.18731	-0.01432	-5.33137	-0.01917								
J16555-083	58246.06653	-4.03719	-0.00193	-5.34901	-0.03296										
J16555-083	58260.07046	-4.04029	-0.00193	-5.08194	-0.00542	-5.24674	-0.01099								
J16555-083	58288.97299	-4.05471	-0.002	-5.35911	-0.03437	-5.32244	-0.01836								
J16555-083	58300.91412	-4.06541	-0.0021	-5.31996	-0.02908										
J16555-083	58309.94741	-4.14802	-0.00257	-5.43268	-0.04554	-5.52882	-0.04574								
J16555-083	58316.92024	-4.06764	-0.0021	-5.17616	-0.01328										
J16555-083	58327.93707	-4.35914	-0.00453	-5.26929	-0.02291	-5.50675	-0.04234								
J16555-083	58345.86575	-3.87115	-0.00134	-5.3621	-0.03466	-5.35522	-0.02177								
J16555-083	58355.8535	-4.00448	-0.0018	-5.03814	-0.00224	-5.42482	-0.03042								
J16555-083	58365.83144	-3.96721	-0.00168	-5.13715	-0.00973	-5.24967	-0.01125								
J02002+130	57596.12587	-4.24244	-0.0012	-5.19778	0.05591	-5.14375	0.06097			-4.98265	0.07335				
J02002+130	57597.07377	-4.19949	-0.00107	-5.0471	0.06608	-5.0678	0.06354	-5.09609	0.06676	-5.02347	0.07302				
J02002+130	57617.11532	-4.24871	-0.00123	-5.03446	0.06159	-5.02688	0.06452	-5.37643	0.05714	-5.10542	0.07178				

Continued on next page

// Star	MJD	Hα		Ca II IRT-a		Ca II IRT-b		He I D_3		Na I D_2		Paβ		Paδ	
		$log\left(\frac{L_{line}}{L_{Bol}}\right)$	δ	$log\left(\frac{L_{line}}{L_{Bol}}\right)$	δ	$log\left(\frac{L_{line}}{L_{Bol}}\right)$	δ	$log\left(\frac{L_{line}}{L_{Bol}}\right)$	δ	$log\left(\frac{L_{line}}{L_{Bol}}\right)$	δ	$log\left(\frac{L_{line}}{L_{Bol}}\right)$	δ	$log\left(\frac{L_{line}}{L_{Bol}}\right)$	δ
J02002+130	57622.07917	-4.27731	-0.00129	-5.12653	0.05757	-5.16074	0.05991	-5.26819	0.06171	-5.17331	0.07109				
J02002+130	57630.08446	-4.18213	-0.00105	-5.06352	0.05978	-5.06202	0.06413	-5.31708	0.05997	-5.15955	0.07186				
J02002+130	57632.14459	-4.17136	-0.00103	-4.98541	0.0687	-5.05316	0.06851	-5.29919	0.06285	-5.32152	0.06891				
J02002+130	57653.11675	-4.35406	-0.00154	-5.0671	0.06006	-5.08897	0.05918	-5.11832	0.06614	-5.23753	0.0702				
J02002+130	57751.78704	-4.2359	-0.00119	-5.16222	0.05778	-5.06016	0.06295			-5.25372	0.0704			-5.41774	0.02718
J02002+130	57753.83559	-4.20654	-0.00111	-4.96811	0.06956	-5.01082	0.0682	-5.15974	0.06573	-5.2376	0.07106				
J02002+130	57761.87591	-4.24237	-0.0012	-5.02405	0.06657	-5.00764	0.06441			-5.03225	0.0733			-5.39926	0.03114
J02002+130	57765.78983	-4.09228	-0.00086	-5.01468	0.0662	-5.05201	0.06402	-5.15449	0.06515	-5.14304	0.07197			-5.47902	0.02189
J02002+130	57974.06301	-4.29138	-0.00133	-5.10147	0.06327	-5.16457	0.05611	-5.3166	0.05985	-5.08399	0.06852			-5.45043	0.03718
J02002+130	57989.1236	-4.33429	-0.00149	-5.17514	0.0542	-5.21795	0.05586			-5.09992	0.07218			-5.46788	0.04364
J02002+130	57990.01925	-4.27402	-0.00133	-5.13306	0.0567	-5.27269	0.04993	-5.36486	0.05806	-5.15045	0.07162			-5.42888	0.04673
J02002+130	58021.02364	-4.22953	-0.00116	-5.00867	0.06883	-4.99195	0.06528	-5.18305	0.06438	-5.18687	0.07148				
J02002+130	58026.00961	-4.33997	-0.00151	-5.10939	0.06329	-5.09966	0.06009	-5.38939	0.05705	-5.1979	0.06751			-5.46935	0.04378
J02002+130	58031.16596	-4.31016	-0.0014	-5.12204	0.06251	-5.17886	0.05746	-5.19584	0.06406	-5.18291	0.0679				
J02002+130	58041.06194	-4.27614	-0.0013	-5.11795	0.06002	-5.21406	0.05651	-5.18896	0.06422	-5.1661	0.07138			-5.40975	0.04868
J02002+130	58046.99043	-4.28152	-0.00131	-5.08335	0.06444	-5.10732	0.0618	-5.21145	0.0636	-5.15943	0.07169			-5.49127	0.04128
J02002+130	58051.11113	-4.35858	-0.00156	-5.10086	0.06094	-5.23261	0.0533	-5.25768	0.06213	-5.23415	0.0678			-5.42785	0.04681
J02002+130	58051.97152	-4.36703	-0.0016	-5.13439	0.05537	-5.07679	0.05942							-5.49864	-0.00382
J02002+130	58057.00056	-4.29698	-0.00137	-5.05425	0.06557	-5.1275	0.06069	-5.13288	0.06579	-5.07931	0.07093			-5.48145	0.04132
J02002+130	58059.02244	-4.32031	-0.00144	-5.09123	0.06359	-5.12935	0.05966			-5.17919	0.06939			-5.37348	0.0474
J02002+130	58064.98276	-4.34512	-0.00151	-5.11111	0.05779	-5.15925	0.05595			-5.18615	0.06954				
J02002+130	58137.8554	-4.12378	-0.0009	-4.94238	0.07024	-5.01495	0.06901	-5.12253	0.06607	-5.10731	0.07265				
J02002+130	58320.12043	-4.36538	-0.0016	-5.14696	0.05613	-5.20739	0.0536	-5.25193	0.06238	-5.1923	0.06589			-5.45216	0.02662
J02002+130	58350.15022	-4.33475	-0.00149	-5.23974	0.05005	-5.40549	0.03989	-5.40538	0.05606	-5.13184	0.07137			-5.42255	0.04651
J02002+130	58355.1616	-4.22054	-0.00112	-5.07447	0.05943	-5.09469	0.06259	-5.24922	0.0623	-5.04743	0.07283			-5.43682	0.04526
J02002+130	58361.14149	-4.35342	-0.00155	-5.05837	0.0617	-5.16904	0.05568	-5.2815	0.06122	-5.18963	0.07069			-5.4074	0.04734
J02002+130	58366.11186	-4.19817	-0.00108	-5.03189	0.06853	-5.01049	0.06542	-5.20188	0.06383	-5.05299	0.07285			-5.46162	0.04146
J02002+130	58384.0884	-3.97064	-0.00063	-4.84902	0.07225	-4.78376	0.07274	-5.11459	0.07073	-4.99216	0.07359			-5.44548	0.04462
J02002+130	58390.0595	-4.30428	-0.00139	-5.09523	0.05857	-5.14535	0.05661	-5.1972	0.06397	-5.17354	0.07069			-5.40689	0.0461
J02002+130	58395.2016	-4.22157	-0.00114	-5.08983	0.06724	-4.95958	0.07088	-5.15811	0.06509	-5.0068	0.0709			-5.46422	0.04271
J02002+130	58413.10588	-4.26134	-0.00127	-5.06468	0.0643	-5.05412	0.06299	-5.22614	0.06333	-5.06613	0.0707			-5.41706	0.04689
J02002+130	58421.07105	-4.08542	-0.00085	-4.9822	0.06966	-4.97771	0.06926			-4.86278	0.07014			-5.30795	0.02524
J02002+130	58426.0585	-4.24811	-0.00122	-5.0716	0.06427	-5.12968	0.05753	-5.32488	0.05964	-5.244	0.06799				
J02002+130	58433.05182	-4.27691	-0.00129	-4.99364	0.06121	-5.20945	0.05337	-5.19465	0.06408	-5.1988	0.06944			-5.42859	0.03846
J02002+130	58449.90402	-4.18462	-0.00107	-4.93193	0.0707	-4.9163	0.07087	-5.2603	0.06213	-5.07191	0.07219				
J02002+130	58469.86798	-4.28212	-0.00131	-5.07535	0.06152	-5.11022	0.06041			-5.15203	0.0715				
J02002+130	58474.8925	-4.11619	-0.00089	-4.90191	0.07129	-4.8771	0.07183	-5.18837	0.0645	-4.98876	0.07369			-5.41342	0.04606
J02002+130	58480.82489	-4.11469	-0.0009	-4.91777	0.07043	-4.84145	0.07159	-4.99456	0.069	-4.94835	0.07404			-5.46357	0.03475
J02002+130	58486.82336	-4.1426	-0.00094	-4.99855	0.06845	-4.96414	0.06949	-5.25555	0.06208	-5.04413	0.07306			-5.39802	0.04651
J02002+130	58491.82514	-4.3202	-0.00143	-5.0003	0.06591	-5.06121	0.06218	-5.14531	0.06557	-5.04244	0.07291				
J02002+130	58496.88685	-4.17438	-0.00102	-4.95842	0.06816	-4.94261	0.06973			-4.99423	0.07367			-5.42661	0.03797
J02002+130	58509.79202	-4.32356	-0.00143	-5.12997	0.06186	-5.16982	0.05564			-5.14054	0.07167				
J02002+130	58517.85958	-4.12956	-0.00092	-5.00528	0.06361	-4.89111	0.07054			-4.98476	0.07636			-5.4882	-0.0019
J02002+130	58526.78718	-4.00198	-0.00069	-4.7288	0.0734	-4.73764	0.07336	-5.04928	0.06909	-4.95852	0.07391			-5.40581	0.04362
J02002+130	58533.83765	-4.3449	-0.00152	-5.09535	0.06132	-5.0963	0.06102			-5.08105	0.07286				
J02002+130	58536.78502	-4.22221	-0.00112	-5.04522	0.06549	-5.01525	0.06485	-5.14804	0.06545	-5.15292	0.0724				
J02002+130	58538.82466	-4.29729	-0.00135	-5.07584	0.05954	-5.12302	0.0602	-5.32368	0.05977	-5.13193	0.0727			-5.45276	0.03152
J02002+130	58541.82956	-4.13595	-0.00093	-4.99529	0.06901	-4.95769	0.07084			-5.0719	0.07318				
J02002+130	58684.14751	-4.13674	-0.00096	-4.9916	0.06893	-5.02716	0.06923	-5.16342	0.06492	-5.13919	0.07176			-5.46068	0.03985
J02002+130	58686.15567	-4.18783	-0.00106	-4.9945	0.06895	-5.08712	0.06765	-5.28908	0.06189	-5.07126	0.0726			-5.47784	0.04136
J02002+130	58688.15757	-4.27539	-0.00129	-5.11748	0.0606	-5.19206	0.05819	-5.43429	0.05496	-5.04711	0.06916			-5.45495	0.03724
J02002+130	58690.15565	-4.16673	-0.001	-5.02177	0.06783	-5.01846	0.06954	-5.16612	0.0648	-5.03504	0.07304			-5.41818	0.04616
J02002+130	58693.14054	-4.28022	-0.00131	-5.1115	0.05805	-5.11597	0.06131	-5.42046	0.05539	-5.14037	0.07175			-5.47575	0.04154
J02002+130	58697.14598	-4.26634	-0.00125	-5.12606	0.05759	-5.13124	0.06123	-5.40309	0.05614	-5.09048	0.07222			-5.39167	0.0484
J02002+130	58699.16098	-4.3061	-0.00139	-5.09951	0.06315	-5.13239	0.06099	-5.22478	0.06326	-5.16071	0.07118			-5.38219	0.04881
J01339-176	57625.16084	-4.33457	-0.00271	-5.45261	0.00519	-5.20761	0.01966			-5.17437	0.01315				
J01339-176	57642.1011	-4.2297	-0.00213	-5.68149	-0.02419	-5.23421	0.01793			-5.36077	-0.01782				
J01339-176	57676.00156	-4.27195	-0.0024	-5.5849	-0.0097	-5.19806	0.02001			-4.97976	0.042				
J01339-176	57676.99834	-4.30742	-0.00261	-5.79338	-0.04464	-5.14627	0.02305			-4.9078	0.04276				
J01339-176	57705.91428	-4.39585	-0.00319	-5.68802	-0.0249					-5.34902	0.03326				
J01339-176	57748.8484	-4.31727	-0.0026	-5.50715	-0.00041	-5.22663	0.01831			-5.27512	-0.01995				
J01339-176	57752.80102	-4.32765	-0.00268	-5.64169	-0.01763					-5.33131	-0.01225				
J01339-176	57754.78571	-4.27078	-0.00235	-5.6784	-0.02333	-5.17257	0.02155			-5.28874	-0.02408				
J01339-176	57762.79167	-4.18574	-0.00192	-5.37848	0.01175	-5.01628	0.03114	-5.01333	0.02321	-5.51375	-0.00098				

Continued on next page

// Star	MJD	Hα		Ca II IRT-a		Ca II IRT-b		He I D_3		Na I D_2		Paβ		Paδ	
		$log\left(\frac{L_{line}}{L_{Bol}}\right)$	δ	$log\left(\frac{L_{line}}{L_{Bol}}\right)$	δ	$log\left(\frac{L_{line}}{L_{Bol}}\right)$	δ	$log\left(\frac{L_{line}}{L_{Bol}}\right)$	δ	$log\left(\frac{L_{line}}{L_{Bol}}\right)$	δ	$log\left(\frac{L_{line}}{L_{Bol}}\right)$	δ	$log\left(\frac{L_{line}}{L_{Bol}}\right)$	δ
J01339-176	57981.10713	-4.27867	-0.00243	-5.80892	-0.04847	-5.02627	0.02891			-5.29096	-0.00354				
J01339-176	57986.09575	-4.24195	-0.00227	-5.82092	-0.05114	-5.06237	0.02734			-5.4604	-0.02699				
J01339-176	57987.12125	-4.32189	-0.00269	-5.62628	-0.01569	-5.14833	0.02293	-5.08667	0.01898						
J01339-176	57988.15338	-4.27497	-0.00243	-5.55261	-0.00591	-5.18892	0.02069			-5.17028	0.01078				
J01339-176	57990.10089	-4.03655	-0.00138	-5.05289	0.03747	-4.83192	0.04106	-5.13987	0.01642	-5.04386	0.03784				
J01339-176	58029.08193	-4.28955	-0.00244	-5.67749	-0.02318	-5.25249	0.01655			-5.03814	0.04128				
J01339-176	58031.05318	-3.81709	-0.00084	-4.65345	0.04341	-4.52066	0.04423	-5.01465	0.02672	-4.89974	0.0405				
J01339-176	58032.97595	-4.21452	-0.00214	-5.27212	0.01926	-5.09319	0.0274			-4.93287	0.02476				
J01339-176	58041.01465	-4.34122	-0.00257	-5.47901	0.00257	-5.14796	0.02306	-5.19274	0.01473	-5.42672	0.02341				
J01339-176	58048.01696	-4.24674	-0.00233	-5.37809	0.01178	-5.10432	0.03289	-5.02455	0.02256	-4.93923	0.04289				
J01339-176	58050.02231	-4.25576	-0.00229	-5.36587	0.01276	-5.07491	0.02686	-4.98727	0.02428	-5.07305	0.04121				
J01339-176	58053.00113	-4.37282	-0.00297	-5.80573	-0.04777			-5.16516	0.01326	-5.09657	0.04089				
J01339-176	58054.97957	-4.1946	-0.002	-5.3594	0.01326	-4.972	0.03895			-5.10234	0.04057				
J01339-176	58056.97732	-4.32438	-0.00271	-5.40926	0.00896	-5.20257	0.01973	-5.06255	0.02042	-5.45463	0.03254				
J01339-176	58058.90485	-4.21777	-0.00209	-5.32429	0.01588	-5.07983	0.02781	-5.01987	0.02285	-5.0754	0.04137				
J01339-176	58064.91925	-4.14861	-0.00173	-5.27034	0.01938	-5.01512	0.03787	-4.96601	0.02778	-5.1638	0.0313				
J01339-176	59488.06265	-4.31238	-0.00257	-5.56934	-0.00771										
J01339-176	60181.12813	-4.42401	-0.00334	-5.56561	-0.00752										
J23431+365	57596.07892	-4.1714	-0.00167	-5.29735	0.00545	-5.06057	0.02583	-5.33654	0.0063						
J23431+365	57597.01278	-4.4171	-0.00294	-5.62928	-0.03965	-5.29749	0.00325								
J23431+365	57613.07127	-4.41902	-0.00296	-5.39275	-0.00788	-5.27666	0.00576	-5.27421	0.00301						
J23431+365	57692.98546	-4.35167	-0.00383	-5.54029	-0.02538	-5.44736	-0.01025	-5.22517	0.00634						
J23431+365	58356.09678	-4.43949	-0.00256	-5.58954	-0.02588	-5.22459	0.01202								
J23431+365	58487.88335	-4.91197	-0.01627	-5.66061	-0.04531	-5.59853	-0.0298								
J23431+365	58759.045	-4.40613	-0.00287	-5.41673	-0.02942	-5.20396	0.01961	-5.1959	0.00885						
J01125-169	57622.07185	-4.04429	-0.0019	-5.11617	0.02551	-4.99244	0.03034								
J01125-169	57632.11911	-4.19691	-0.0024	-5.4372	-0.01681	-5.20687	0.01228								
J01125-169	57646.03093	-4.25056	-0.00233	-5.36436	-0.00477	-5.228	0.01087								
J01125-169	57959.17391	-4.08692	-0.00137	-5.06978	0.03347	-4.91603	0.03578								
J01125-169	57961.1642	-3.96027	-0.00079	-5.03557	0.03589	-4.93172	0.03765								
J01125-169	57974.17008	-4.16106	-0.00137	-5.58236	-0.01986	-5.24488	0.01835								
J01125-169	57990.12681	-4.08382	-0.00206	-5.35832	0.01457	-5.15675	0.01318								
J09005+465	57690.14369	-4.5031	-0.00448	-5.60173	-0.04506	-5.28668	0.01261			-5.32973	0.01801				
J09005+465	57759.13069	-4.56109	-0.00612	-5.42826	-0.02564	-5.3967	-0.0159			-5.37111	0.02556				
J09005+465	58882.98723	-4.6011	-0.00524	-5.53286	-0.02465	-5.38159	0.00026	-5.48461	-0.03562						
J10238+438	59305.89	-4.51757	-0.00258	-5.45643	-0.02498	-5.2452	-0.002								
J10238+438	59614.02116	-4.50191	-0.00249	-5.6699	-0.05925										
J10238+438	59687.07327	-4.53366	-0.00265	-5.70267	-0.06645										
J10238+438	59719.97912	-4.50542	-0.00251	-5.69004	-0.06372										
J02164+135	59231.82667	-4.35788	-0.00193	-5.14341	0.05135										
J02164+135	59420.14898	-4.30153	-0.00166	-5.1973	0.04805	-5.16982	0.05164								
J02164+135	59452.1397	-4.40117	-0.00207	-5.29597	0.04056	-5.23177	0.04776								
J02164+135	59483.00884	-4.30382	-0.00171	-5.24406	0.04476	-5.52713	0.01927								
J08413+594	57814.95197	-4.29524	-0.00325	-5.42086	-0.03201	-5.37664	-0.02193								
J08413+594	57847.84992	-4.4632	-0.0048	-5.31902	-0.01877										
J08413+594	57904.89245	-4.08974	-0.00206	-5.09125	0.00589	-5.09154	0.01198								
J08413+594	58031.1946	-4.13515	-0.00223	-5.20368	-0.00617	-5.09405	0.00622								
J08413+594	58084.17814	-3.85355	-0.00117	-4.87308	0.02339	-4.8127	0.02477								
J08413+594	58088.1726	-4.13711	-0.00224	-5.20791	-0.0072	-5.04496	0.0068								
J08413+594	58111.23149	-4.42699	-0.00431	-5.37094	-0.02521										
J08413+594	58117.08393	-4.21248	-0.0027	-5.17391	-0.00435	-5.01352	0.00919								
J08413+594	58118.08391	-4.1871	-0.00251	-5.15334	-0.00267	-5.11791	0.00405								
J08413+594	58123.08499	-4.31986	-0.00342	-5.47301	-0.04017										
J08413+594	58131.07023	-4.21852	-0.00261	-5.42864	-0.03316	-5.23815	-0.00509								
J08413+594	58132.21104	-3.90241	-0.00129	-5.05781	0.00813	-5.20199	0.01321								
J08413+594	58135.06243	-4.16874	-0.00239	-5.18829	-0.00557	-5.27874	-0.0077								
J08413+594	58135.972	-4.35771	-0.00373	-5.36418	-0.02433	-5.46106	-0.03351								
J08413+594	58138.00849	-4.35385	-0.00366	-5.30411	-0.01692	-5.27258	-0.01044								
J08413+594	58139.01443	-3.94985	-0.00146	-4.95977	0.02075	-4.8665	0.02347								
J08413+594	58142.10315	-3.92253	-0.00149	-5.14367	-0.00181	-5.20897	-0.00455								
J08413+594	58142.89576	-4.31063	-0.0033	-5.48758	-0.04284										
J08413+594	58149.02199	-4.34525	-0.00372	-5.45997	-0.03804	-5.51235	-0.04172								
J08413+594	58170.16137	-4.15402	-0.00232	-5.39683	-0.02873										
J08413+594	58170.94015	-4.4592	-0.00476	-5.25745	-0.01193										

Continued on next page

// Star	MJD	Hα		Ca II IRT-a		Ca II IRT-b		He I D_3		Na I D_2		Paβ		Paδ	
		$log\left(\frac{L_{line}}{L_{Bol}}\right)$	δ	$log\left(\frac{L_{line}}{L_{Bol}}\right)$	δ	$log\left(\frac{L_{line}}{L_{Bol}}\right)$	δ	$log\left(\frac{L_{line}}{L_{Bol}}\right)$	δ	$log\left(\frac{L_{line}}{L_{Bol}}\right)$	δ	$log\left(\frac{L_{line}}{L_{Bol}}\right)$	δ	$log\left(\frac{L_{line}}{L_{Bol}}\right)$	δ
J08413+594	58174.92384	-4.56185	-0.00585	-5.31443	-0.01809										
J08413+594	58186.06152	-3.9443	-0.00142	-5.03431	0.01915	-4.78662	0.02482								
J08413+594	58204.85883	-4.54758	-0.00598	-5.38646	-0.0273										
J08413+594	58206.84389	-4.01663	-0.00168	-5.07752	0.01675	-5.10172	0.01794								
J08413+594	58214.84877	-4.25831	-0.00293	-5.42008	-0.03207	-5.4192	-0.02731								
J08413+594	58217.82469	-4.10035	-0.00221	-4.93497	0.01214	-4.83627	0.01711								
J08413+594	58224.87628	-4.41969	-0.00425	-5.44057	-0.03516	-5.50805	-0.04099								
J08413+594	58236.8406	-4.23479	-0.00302	-5.20604	-0.00714										
J08413+594	58237.86202	-4.27977	-0.00329	-5.2396	-0.01017										
J08413+594	58259.89848	-4.18093	-0.0026	-5.08237	0.00617	-5.09097	0.01452								
J08413+594	58262.90651	-4.38689	-0.00405	-5.34706	-0.022	-5.30689	-0.01393								
J08413+594	58269.8588	-4.21052	-0.00266	-5.33697	-0.02091	-5.24559	-0.00681								
J08413+594	58276.88283	-4.12824	-0.00218	-5.24531	-0.01084	-5.19542	-0.00247								
J08413+594	58367.17396	-4.4702	-0.00489	-5.3352	-0.02069										
J08413+594	58375.19275	-4.30231	-0.00335	-5.45622	-0.03743	-5.02093	0.00815								
J08413+594	58381.18859	-4.29613	-0.00321	-5.36821	-0.0247	-5.50532	-0.04053								
J08413+594	58382.17576	-4.26357	-0.00298	-5.38794	-0.02733	-5.20751	-0.00344								
J08413+594	58390.18508	-3.83111	-0.0011	-5.00808	0.02025	-4.86993	0.0236								
J08413+594	58426.17326	-4.47647	-0.0049	-5.38512	-0.02695	-5.20215	-0.00409								
J08413+594	58429.17762	-4.34778	-0.00366	-5.27196	-0.01343	-5.33071	-0.01608								
J08413+594	58474.11691	-4.30671	-0.00324	-5.41089	-0.03055	-5.43217	-0.02782								
J08413+594	58485.09251	-4.47077	-0.00484	-5.29364	-0.01589										
J08413+594	58524.09139	-4.36021	-0.00381	-5.30283	-0.01677	-5.0804	0.00531								
J08413+594	58557.85801	-4.18593	-0.00264	-5.3481	-0.02228	-5.38785	-0.02053								
J08413+594	58559.85046	-4.10934	-0.00212	-5.27851	-0.01412	-5.00536	0.00975								
J08413+594	58570.01853	-4.35398	-0.00363	-5.38933	-0.02769	-5.46396	-0.03394								
J08413+594	58632.8781	-4.56373	-0.0061	-5.31178	-0.01779	-5.48629	-0.03763								
J08413+594	58640.88633	-4.41875	-0.00429	-5.18645	-0.00531										
J08413+594	58756.15671	-4.0069	-0.00165	-5.03443	0.01012	-4.99922	0.0194								
J08413+594	58763.16921	-4.35858	-0.00373	-5.27896	-0.01416	-5.21826	-0.00545								
J08413+594	58782.13692	-4.48832	-0.00493	-5.3102	-0.01761	-5.44357	-0.03111								
J08413+594	58791.21184	-4.40634	-0.00401	-5.39901	-0.02903										
J08413+594	58827.20532	-3.88041	-0.00121	-5.12305	0.01732	-5.00174	0.02144								
J08413+594	58835.16806	-3.87472	-0.00124	-4.73861	0.0255	-4.75949	0.02498								
J08413+594	58892.95959	-4.4291	-0.00448	-5.36081	-0.0239	-5.49056	-0.03811								
J08413+594	58902.93618	-4.056	-0.00199	-5.06432	0.00997	-5.14363	0.0065								
J08413+594	58917.91235	-4.57992	-0.00633	-5.17547	-0.00438										
J08413+594	58975.88573	-4.41489	-0.00434	-5.48309	-0.04187	-5.47455	-0.03577								
J14578+566	59306.08076	-4.34694	-0.00287	-5.42245	0.03065	-5.29519	0.04839								
J14578+566	59735.93779	-4.31385	-0.0027	-5.62421	-0.00412	-5.24912	0.05248								
J23351-023	58079.85835	-4.34872	-0.00388	-5.17169	-0.00478	-5.0435	0.00807								
J23351-023	58366.0179	-4.69944	-0.00773	-5.37038	-0.02901	-5.19454	-0.00407								
J23351-023	58756.97424	-4.9758	-0.01634	-5.4067	-0.03477										
J23351-023	58759.95214	-5.10031	-0.02516	-5.33549	-0.02392										
J23351-023	58791.91533	-4.45003	-0.00455	-5.19595	-0.00718	-5.04897	0.0077								
J23351-023	58793.8324	-4.37827	-0.0038	-5.40341	-0.03423	-5.34168	-0.02063								
J10482-113	57419	-4.44955	-0.00363	-5.14768	0.06424	-5.29405	0.0546								
J10482-113	57471.95672	-4.51761	-0.00417	-5.06379	0.06982	-5.3289	0.05114								
J10482-113	57511.85605	-4.48776	-0.00398	-5.01358	0.07267										
J10482-113	57709.21618	-4.20362	-0.00205	-5.04397	0.07105										
J10482-113	57735.22071	-4.4902	-0.00401	-4.94734	0.07603										
J10482-113	57821.95777	-4.51885	-0.00424	-5.13362	0.06525	-5.34925	0.04899								
J10482-113	57852.902	-4.26343	-0.00234	-5.01069	0.07283										
J10482-113	57860.8813	-3.98207	-0.00123	-4.98012	0.07615	-5.23482	0.06345								
J10482-113	57865.95363	-4.2694	-0.00237	-5.10949	0.06691	-5.21702	0.06133								
J10482-113	57879.9134	-4.40124	-0.00336	-5.00727	0.07307										
J10482-113	57881.90003	-4.43464	-0.00351	-5.10918	0.06693										
J10482-113	57889.88538	-4.30242	-0.00269	-5.0345	0.07159										
J10482-113	58074.21525	-4.53238	-0.00442	-4.99431	0.07369										
J10482-113	58078.22429	-4.39605	-0.00325	-5.12642	0.06634										
J10482-113	58092.16288	-4.37038	-0.00305	-5.0122	0.07281										
J10482-113	58094.20217	-4.60458	-0.00526	-5.08623	0.0685										
J10482-113	58109.15663	-4.42361	-0.00345	-5.11927	0.06625	-5.26597	0.0572								
J10482-113	58121.1376	-4.50433	-0.00401	-5.14287	0.0652										

Continued on next page

// Star	MJD	Hα		Ca II IRT-a		Ca II IRT-b		He I D_3		Na I D_2		Paβ		Paδ	
		$log\left(\frac{L_{line}}{L_{Bol}}\right)$	δ	$log\left(\frac{L_{line}}{L_{Bol}}\right)$	δ	$log\left(\frac{L_{line}}{L_{Bol}}\right)$	δ	$log\left(\frac{L_{line}}{L_{Bol}}\right)$	δ	$log\left(\frac{L_{line}}{L_{Bol}}\right)$	δ	$log\left(\frac{L_{line}}{L_{Bol}}\right)$	δ	$log\left(\frac{L_{line}}{L_{Bol}}\right)$	δ
J10482-113	58123.15553	-4.48287	-0.00397	-5.11073	0.06805	-5.27826	0.05608								
J10482-113	58134.12513	-4.24754	-0.00225	-5.04945	0.07194	-5.23221	0.06063								
J10482-113	58136.12622	-4.41902	-0.00343	-5.04124	0.07114	-5.37425	0.04621								
J10482-113	58139.0868	-4.37795	-0.00308	-5.18622	0.06138	-5.22775	0.06217								
J10482-113	58141.09357	-4.27719	-0.00245	-5.02798	0.07283	-5.23424	0.06241								
J10482-113	58172.03979	-4.3746	-0.00307	-5.1081	0.067	-5.23718	0.06262								
J10482-113	58175.00606	-4.22441	-0.00217	-5.18905	0.06155	-5.30407	0.05617								
J10482-113	58199.03204	-4.21023	-0.00213	-5.13708	0.06828	-5.30392	0.05365								
J10482-113	58204.90155	-4.2092	-0.00206	-5.10738	0.06802	-5.37373	0.04716								
J10482-113	58451.18526	-4.51291	-0.00419	-4.99793	0.0735	-5.15547	0.06582								
J10482-113	58458.20055	-4.19167	-0.00201	-5.12227	0.06846										
J10482-113	58462.19503	-4.39206	-0.00318	-5.18367	0.06168	-5.21254	0.06169								
J10482-113	58468.20505	-4.37709	-0.00301	-5.03747	0.07142	-5.35273	0.04918								
J10482-113	58470.19244	-4.42722	-0.00346	-5.14008	0.06479	-5.24915	0.05867								
J10482-113	58474.18936	-4.44205	-0.00354	-5.08004	0.06995										
J10482-113	58479.20907	-4.30812	-0.00262	-5.02196	0.07341	-5.39794	0.04782								
J10482-113	58485.11711	-3.88765	-0.00105	-4.8021	0.08857	-4.96792	0.08337								
J10482-113	58487.14161	-4.19583	-0.00203	-5.00753	0.07377										
J10482-113	58489.15845	-4.38502	-0.00315	-5.2259	0.0586	-5.29597	0.05504								
J10482-113	58491.14294	-4.21798	-0.00214	-5.05543	0.07146	-5.31613	0.05727								
J10482-113	58493.14122	-4.44097	-0.00356	-4.99155	0.07383										
J10482-113	58495.16271	-4.24824	-0.00223	-5.16188	0.06327	-5.21377	0.0618								
J10482-113	58497.14319	-4.52026	-0.00425	-5.09108	0.0692	-5.31713	0.05234								
J10482-113	58510.15441	-4.34395	-0.00283	-5.11712	0.06648	-5.17548	0.06647								
J10482-113	58518.15748	-4.34206	-0.00284	-5.01771	0.07245										
J10482-113	58525.10796	-4.4232	-0.0034	-5.14505	0.06443										
J10482-113	58528.13234	-4.1767	-0.00198	-5.05308	0.07145										
J10482-113	58529.02542	-4.28041	-0.00249	-5.01873	0.07358	-5.35684	0.05146								
J10482-113	58530.06313	-4.24536	-0.00231	-5.04281	0.07147	-5.27975	0.0587								
J10482-113	58532.082	-4.15088	-0.00197	-4.91557	0.07744										
J10482-113	58536.10664	-4.44382	-0.00352	-5.01496	0.07266										
J10482-113	58537.11254	-4.44225	-0.00357	-4.99135	0.0739										
J10482-113	58538.07484	-4.49753	-0.00411	-5.05782	0.07017										
J10482-113	58540.09608	-4.09771	-0.00163	-4.94892	0.07596	-5.22571	0.06338								
J10482-113	58541.04794	-4.40895	-0.00344	-5.12631	0.06584										
J10482-113	58543.0665	-4.29829	-0.00254	-5.18089	0.06181	-5.32086	0.05276								
J10482-113	58567.95992	-4.29786	-0.00262	-4.9892	0.07395	-5.23507	0.06019								
J10482-113	58569.95998	-4.08084	-0.00159	-5.00272	0.07388	-5.39366	0.05079								
J10482-113	58570.98041	-4.50367	-0.00414	-5.09792	0.06775	-5.13603	0.06714								
J10482-113	58572.00859	-4.03899	-0.00146	-4.98521	0.0775	-5.0954	0.07686								
J10482-113	58586.89733	-4.17984	-0.00209	-4.99792	0.07469	-5.40313	0.04788								
J10482-113	58588.95006	-4.50194	-0.0041	-5.04724	0.07964										
J10482-113	58589.91765	-4.36528	-0.00298	-5.19248	0.06235	-5.23439	0.06035								
J10482-113	58597.94201	-4.28686	-0.00248	-5.25979	0.05488	-5.16922	0.06485								
J10482-113	58599.873	-4.55282	-0.00478	-5.03198	0.07166										
J10482-113	58600.91182	-4.39294	-0.00321	-5.04959	0.07235										
J10482-113	58601.91139	-4.47319	-0.00385	-5.14497	0.06443										
J10482-113	58602.91363	-4.23933	-0.00222	-5.04573	0.07095										
J10482-113	58603.93046	-4.10082	-0.00168	-5.01515	0.07259	-5.36275	0.05143								
J10482-113	58607.91731	-4.37498	-0.0031	-4.98025	0.07446										
J10482-113	58608.88117	-4.31377	-0.00264	-5.15247	0.06397										
J10482-113	58613.85479	-4.25426	-0.00234	-5.15469	0.06444										
J10482-113	58614.86265	-4.46979	-0.00382	-5.15267	0.06396	-5.33453	0.05083								
J10482-113	58615.88407	-4.07383	-0.00157	-4.93487	0.07811	-5.28941	0.05909								
J10482-113	58616.8733	-4.38925	-0.00332	-5.33295	0.05615	-5.06304	0.07175								
J10482-113	58617.84741	-4.37194	-0.00309	-5.1314	0.0654	-5.33015	0.05102								
J10482-113	58807.23586	-4.50086	-0.00427	-5.04482	0.07261	-5.17781	0.06432								
J05394+406	57760.93362	-4.14292	-0.00101	-5.0174	0.02248	-5.1199	0.02583								
J05394+406	58047.03186	-4.36089	-0.00171	-5.17328	0.01572										
J05394+406	58121.9512	-4.3976	-0.00174	-5.20684	0.01393										
J05394+406	58382.15179	-4.57491	-0.00282	-5.51067	-0.01031										
J05394+406	58396.1236	-4.51656	-0.00235	-5.46757	-0.00575										
J05394+406	58745.1532	-4.45508	-0.00214	-5.37645	0.00244	-5.3705	0.00526								
J05394+406	58773.07848	-4.52333	-0.00242	-5.48461	-0.00762										

Continued on next page

// Star	MJD	Hα		Ca II IRT-a		Ca II IRT-b		He I D_3		Na I D_2		Paβ		Paδ	
		$log\left(\frac{L_{line}}{L_{Bol}}\right)$	δ	$log\left(\frac{L_{line}}{L_{Bol}}\right)$	δ	$log\left(\frac{L_{line}}{L_{Bol}}\right)$	δ	$log\left(\frac{L_{line}}{L_{Bol}}\right)$	δ	$log\left(\frac{L_{line}}{L_{Bol}}\right)$	δ	$log\left(\frac{L_{line}}{L_{Bol}}\right)$	δ	$log\left(\frac{L_{line}}{L_{Bol}}\right)$	δ
J05394+406	58881.85726	-4.38613	-0.00174	-5.32363	0.00794										
J19169+051S	57568.03593	-4.13041	-0.00096	-5.12467	0.01567	-4.95047	0.02148								
J19169+051S	57575.03515	-4.26088	-0.00128	-5.19373	0.00671	-5.43248	-0.00646								
J19169+051S	57584.99222	-4.55895	-0.00252	-5.26866	0.00225	-5.46147	-0.00909								
J19169+051S	57592.95718	-4.58585	-0.00263	-5.41008	-0.00771	-5.39838	-0.00481								
J19169+051S	57594.98479	-4.57644	-0.00258	-5.63693	-0.03461	-5.11754	0.0146								
J19169+051S	57596.98089	-4.32838	-0.00147	-5.2509	0.00436	-5.11511	0.01432								
J19169+051S	57605.93024	-4.5467	-0.00224	-5.51089	-0.01847	-5.3388	0.00105								
J19169+051S	57611.90784	-4.58933	-0.00268	-5.2753	0.00183	-5.44407	-0.00833								
J19169+051S	57612.94609	-4.2706	-0.00132	-5.11133	0.01079	-5.08297	0.01718								
J19169+051S	57613.91558	-4.60638	-0.00279	-5.35052	-0.0035	-5.43955	-0.00376								
J19169+051S	57619.94668	-4.60696	-0.00289	-5.36279	-0.00446	-5.48286	-0.01058								
J19169+051S	57620.88679	-4.65284	-0.003	-5.55274	-0.02294	-5.24829	0.00692								
J19169+051S	57621.94332	-4.26744	-0.00128	-5.42856	-0.00838	-5.40782	0.00445								
J19169+051S	57624.90787	-4.55661	-0.00242	-5.62619	-0.03304	-5.39605	0.00165								
J19169+051S	57628.91363	-4.39607	-0.00173	-5.2223	0.006	-5.18508	0.01084								
J19169+051S	57629.86134	-4.47192	-0.00199	-5.60273	-0.02972	-5.31446	0.00749								
J19169+051S	57630.88749	-4.13811	-0.00095	-5.23141	0.01468	-5.13708	0.01553								
J19169+051S	57633.89537	-4.46554	-0.00201	-5.23356	0.00454	-5.69125	-0.03478								
J19169+051S	57671.86992	-4.50471	-0.00225	-5.22514	0.00497	-5.36519	0.00424								
J19169+051S	57690.79606	-4.51078	-0.00223	-5.41074	-0.00838	-5.46466	-0.01066								
J19169+051S	57833.18215	-4.2625	-0.0001	-5.21879	0.01208	-5.39656	-0.00247								
J19169+051S	57916.05568	-4.23316	-0.00123	-5.1239	0.01799	-5.11607	0.01825								
J19169+051S	57936.01479	-4.40626	-0.00173	-5.33093	0.0008	-5.44696	-0.00479								
J19169+051S	57938.97617	-4.39533	-0.00171	-5.30265	7e-05	-5.13053	0.01494								
J19169+051S	57950.01201	-4.3159	-0.00143	-5.31339	0.00064	-5.16885	0.01367								
J19169+051S	57957.95872	-4.35196	-0.0015	-5.3241	-0.00144	-5.10945	0.01627								
J19169+051S	57959.98361	-3.93195	-0.00078	-5.31104	0.00342	-5.30302	0.01041								
J19169+051S	57962.91801	-4.20632	-0.00111	-5.39266	-0.00652	-5.04629	0.01479								
J19169+051S	57968.94527	-4.42519	-0.00183	-5.24247	0.00465	-5.47157	-0.00161								
J19169+051S	57970.88848	-4.48593	-0.00208	-5.63421	-0.03387	-5.42972	0.00162								
J19169+051S	57996.90219	-4.38548	-0.00178	-5.20741	0.01389	-5.19878	0.0144								
J19169+051S	58009.91126	-4.39614	-0.00169	-5.33037	-0.00164	-5.49175	-0.01117								
J19169+051S	58329.97261	-4.533	-0.00229	-5.2507	0.00338	-5.25137	0.00868								
J19169+051S	58334.92824	-4.46689	-0.00192	-5.36032	-0.00353	-5.22979	0.01073								
J19169+051S	58348.93587	-4.0404	-0.00078	-5.07425	0.01981	-4.92904	0.02318								
J19169+051S	58366.85864	-4.43467	-0.00188	-5.31252	-0.0007	-5.36457	-0.00164								
J19169+051S	58382.84037	-4.42819	-0.00182	-5.31529	-0.00089	-5.35346	0.0015								
J19169+051S	58392.81598	-4.43396	-0.00189	-5.35046	-0.0035	-5.38082	-0.00323								
J19169+051S	58630.0556	-4.44391	-0.00193	-5.2871	0.00391	-5.25354	0.00679								
J19169+051S	58637.07162	-4.6119	-0.00279	-5.4578	-0.01277	-5.47444	-0.01159								
J04198+425	57760.87625	-4.22443	-0.00068	-5.18281	0.02155	-5.12664	0.02777							-5.20282	-0.0138
J04198+425	57851.83089	-4.45156	-0.00119	-5.34221	0.01364	-5.10494	0.02489								
J04198+425	57969.10623	-4.02397	-0.00083	-5.50198	0.01248	-5.03361	0.02928								
J04198+425	58020.07664	-4.35718	-0.00091	-5.62391	-0.00768	-5.33268	0.01819								
J04198+425	58035.11819	-4.23066	-0.00149	-5.67782	-0.01183	-5.64633	-0.00248							-5.28556	-0.02282
J04198+425	58040.06925	-4.24349	-0.00146	-5.61353	-0.00534	-5.16879	0.02679							-5.19195	-0.00683
J04198+425	58117.87103	-4.2611	-0.00073	-5.27582	0.0169	-5.44767	0.01217								
J04198+425	58142.83568	-4.22979	-0.00152	-5.22776	0.02213	-5.31962	0.01786								
J04198+425	58359.1166	-4.56277	-0.00147	-5.42701	0.01134	-5.19271	0.02271								
J04198+425	58384.10918	-4.59792	-0.0016	-5.58231	0.00587	-5.24171	0.0204								
J04198+425	58394.10506	-4.47424	-0.00121	-5.78722	-0.02686	-5.10456	0.02689					-4.64855	-0.00506		
J04198+425	58399.11094	-4.44489	-0.00111	-5.46341	0.00662	-5.13278	0.02699					-4.53921	0.00384		
J04198+425	58413.02792	-4.23823	-0.00148	-5.28064	0.0189	-4.97649	0.02858								
J04198+425	58469.93935	-4.50619	-0.0013	-5.29201	0.01641	-5.38643	0.0144							-5.25797	-0.01671
J04198+425	58479.94276	-4.1526	-0.00108	-5.33727	0.01589	-5.06835	0.02863							-5.2242	-0.01601
J04198+425	58485.9275	-4.3862	-0.00215	-5.41199	0.0095	-5.34627	0.01721							-5.24536	-0.01778
J04198+425	58492.03272	-4.47984	-0.0012	-5.3252	0.01454	-5.15061	0.02572								
J04198+425	58496.94483	-4.06016	-0.00086	-5.58145	0.0031	-5.26584	0.02534								
J04198+425	58697.12265	-2.97625	-8.00E-05	-4.05334	0.03637	-3.99432	0.03648					-3.76632	0.02902	-4.77144	0.00163
J04198+425	58745.17771	-4.44229	-0.00111	-5.45033	0.00696	-5.28732	0.01967					-4.46953	0.0086	-5.34692	-0.03378
J04198+425	58760.08244	-4.42231	-0.00109	-5.11022	0.02371	-5.25079	0.0199					-4.51104	0.00601		
J04198+425	58765.01528	-4.10002	-0.00105	-5.66388	-0.01002	-5.15354	0.02471								
J04198+425	58773.04761	-4.57012	-0.0015	-5.44879	0.00706	-5.28988	0.02434								

Continued on next page

// Star	MJD	Hα		Ca II IRT-a		Ca II IRT-b		He I D_3		Na I D_2		Paβ		Paδ	
		$log\left(\frac{L_{line}}{L_{Bol}}\right)$	δ	$log\left(\frac{L_{line}}{L_{Bol}}\right)$	δ	$log\left(\frac{L_{line}}{L_{Bol}}\right)$	δ	$log\left(\frac{L_{line}}{L_{Bol}}\right)$	δ	$log\left(\frac{L_{line}}{L_{Bol}}\right)$	δ	$log\left(\frac{L_{line}}{L_{Bol}}\right)$	δ	$log\left(\frac{L_{line}}{L_{Bol}}\right)$	δ
J04198+425	58818.03897	-4.20753	-0.00122	-5.27953	0.01721	-4.99329	0.02777								
J04198+425	58844.881	-4.42401	-8.00E-05	-5.39996	0.01032	-5.23525	0.02368								
J04198+425	58846.93471	-4.39358	-0.00193	-5.34109	0.0137	-5.61267	0.00711								
J04198+425	58848.9456	-3.6897	-0.00041	-4.59866	0.0351	-4.5911	0.03514							-5.12223	-0.00519
J04198+425	58851.92816	-4.50578	-0.00131	-5.30018	0.01619	-5.51513	0.00604								
J04198+425	58856.93626	-4.3868	-0.00098	-5.39851	0.01041	-5.07251	0.02812								
J04167-120	58534.82215	-5.21389	-0.02011	-5.44209	0.02165	-5.69463	-0.00668								
J04167-120	58536.81402	-5.18406	-0.01868	-5.63095	-0.00106	-5.71603	-0.01025								
J04167-120	58538.85077	-5.00692	-0.01242	-5.51129	0.01433	-5.07942	0.04686								
J04167-120	58542.79551	-5.09923	-0.01545	-5.65392	-0.00459										
J04167-120	58554.80278	-5.16611	-0.01792	-5.4726	0.01882	-5.5587	0.01232								
J04167-120	58756.12337	-5.06178	-0.01409	-5.45856	0.02026	-5.33493	0.03313								
J04167-120	58758.14152	-4.99137	-0.01199	-5.55892	0.00858										
J04167-120	58761.12853	-5.40943	-0.03155	-5.65167	-0.00424										
J04167-120	58769.12457	-5.19324	-0.01908	-5.4338	0.02268										
J04167-120	58770.1253	-5.14519	-0.01708	-5.44141	0.02195										
J04167-120	58771.1179	-5.16222	-0.01786	-5.32553	0.03162										
J04167-120	58772.11601	-5.08764	-0.01504	-5.49538	0.01612	-5.69603	-0.00691								
J04167-120	58775.10689	-5.49705	-0.0384	-5.66759	-0.00679										
J04167-120	58784.12074	-5.11462	-0.016	-5.59204	0.00452	-5.2543	0.03836								
J04167-120	58796.03713	-5.29814	-0.02442	-5.61972	0.00025										
J05365+113	57395	-4.43347	-0.00323	-4.85808	0.14867	-4.67647	0.15012								
J05365+113	57397	-4.5078	-0.00374	-4.83577	0.14894	-4.70874	0.14987								
J05365+113	57398	-4.53562	-0.00397	-4.81935	0.1489	-4.70624	0.14994								
J05365+113	57401	-4.47719	-0.00253	-4.83786	0.15027	-4.67247	0.15121								
J05365+113	57411	-4.4522	-0.00275	-4.81097	0.14961	-4.66574	0.15054								
J05365+113	57412	-4.47971	-0.00293	-4.82827	0.14954	-4.67872	0.15056								
J05365+113	57414	-4.38244	-0.00277	-4.80397	0.1494	-4.62387	0.15067								
J05365+113	57415	-4.45858	-0.00334	-4.87739	0.14856	-4.67599	0.15017								
J05365+113	57418	-4.54764	-0.00473	-4.89558	0.14812	-4.72272	0.14964								
J05365+113	57419	-4.59588	-0.00484	-4.91212	0.14838	-4.73428	0.14985								
J05365+113	57421	-4.51974	-0.00286	-4.87636	0.14973	-4.71662	0.15082								
J05365+113	57427	-4.38455	-0.00278	-4.79717	0.14947	-4.61932	0.15075								
J05365+113	57443	-4.59001	-0.00541	-4.89176	0.14804	-4.77329	0.14911								
J05365+113	57476.81902	-4.50115	-0.00369	-4.84786	0.14885	-4.70313	0.14988								
J05365+113	57658.16772	-4.47955	-0.00519	-4.82995	0.14912	-4.64716	0.15045								
J05365+113	57691.13274	-4.642	-0.00807	-4.93015	0.14712	-4.81377	0.14846								
J05365+113	57692.13066	-4.6171	-0.00783	-4.98927	0.14654	-4.7804	0.14861								
J05365+113	57698.0219	-4.53903	-0.00632	-4.87469	0.14846	-4.70059	0.14999								
J05365+113	57699.06093	-4.61665	-0.00747	-4.96287	0.14722	-4.74368	0.14924								
J05365+113	57703.09957	-4.6856	-0.00924	-4.94243	0.147	-4.80917	0.14824								
J05365+113	57703.94488	-4.63043	-0.0081	-4.97605	0.14684	-4.76677	0.14878								
J05365+113	57704.99751	-4.58509	-0.00722	-4.91101	0.14784	-4.75538	0.14921								
J05365+113	57711.99907	-4.60595	-0.00668	-4.94942	0.14696	-4.77177	0.14907								
J05365+113	57759.87839	-4.56576	-0.00599	-4.92954	0.14764	-4.73984	0.14933								
J05365+113	57778.94117	-4.55886	-0.00483	-4.86176	0.14856	-4.75537	0.1493								
J05365+113	57792.89418	-4.59573	-0.00667	-4.93695	0.14746	-4.76224	0.14918								
J05365+113	57799.87868	-4.62562	-0.00729	-4.89538	0.14812	-4.77913	0.14899								
J05365+113	57979.19086	-4.62647	-0.00806	-4.89548	0.14819	-4.71914	0.14963								
J05365+113	58001.19443	-4.62525	-0.00804	-4.90249	0.14796	-4.74379	0.14938								
J05365+113	58018.17831	-4.64564	-0.00842	-4.96894	0.14696	-4.76026	0.1491								
J05365+113	58020.21317	-4.61163	-0.0077	-4.90014	0.14799	-4.75221	0.14929								
J05365+113	58022.18542	-4.60452	-0.00695	-4.93942	0.1472	-4.76808	0.14911								
J05365+113	58027.15597	-4.43707	-0.00474	-4.80484	0.1495	-4.64156	0.15065								
J05365+113	58028.15588	-4.67529	-0.00902	-4.96798	0.14698	-4.74851	0.14928								
J05365+113	58035.111	-4.64484	-0.00841	-4.9556	0.14678	-4.76061	0.14925								
J05365+113	58041.18933	-4.69132	-0.00915	-4.93488	0.14764	-4.76309	0.14922								
J05365+113	58048.10958	-4.55647	-0.00619	-4.89843	0.14808	-4.74434	0.14933								
J05365+113	58050.07987	-4.56585	-0.00696	-4.93303	0.14759	-4.73641	0.14946								
J05365+113	58050.21349	-4.52946	-0.00575	-4.88456	0.1484	-4.7093	0.14982								
J05365+113	58051.13039	-4.53199	-0.00566	-4.87331	0.14822	-4.71856	0.14964								
J05365+113	58053.10252	-4.52192	-0.00465	-4.863	0.14861	-4.73665	0.14945								
J05365+113	58055.1815	-4.59764	-0.00687	-4.94639	0.14701	-4.76083	0.14905								
J05365+113	58060.0466	-4.56451	-0.00537	-4.90881	0.14794	-4.71932	0.14968								

Continued on next page

// Star	MJD	Hα		Ca II IRT-a		Ca II IRT-b		He I D_3		Na I D_2		Paβ		Paδ	
		$log\left(\frac{L_{line}}{L_{Bol}}\right)$	δ	$log\left(\frac{L_{line}}{L_{Bol}}\right)$	δ	$log\left(\frac{L_{line}}{L_{Bol}}\right)$	δ	$log\left(\frac{L_{line}}{L_{Bol}}\right)$	δ	$log\left(\frac{L_{line}}{L_{Bol}}\right)$	δ	$log\left(\frac{L_{line}}{L_{Bol}}\right)$	δ	$log\left(\frac{L_{line}}{L_{Bol}}\right)$	δ
J05365+113	58060.14042	-4.53299	-0.0065	-4.83885	0.14866	-4.77025	0.14625								
J05365+113	58073.93343	-4.15804	-0.00163	-4.62616	0.15109	-4.49487	0.15166								
J05365+113	58074.09278	-4.37958	-0.0027	-4.73634	0.15011	-4.61315	0.15086								
J05365+113	58078.91588	-4.65105	-0.00764	-4.91238	0.14796	-4.74616	0.14945								
J05365+113	58080.21372	-4.66131	-0.00873	-4.92433	0.14765	-4.77622	0.14892								
J05365+113	58080.92103	-4.56815	-0.00705	-4.90242	0.14741	-4.80405	0.14612								
J05365+113	58083.91324	-4.51939	-0.00432	-4.88069	0.14838	-4.73134	0.14956								
J05365+113	58084.07289	-4.57086	-0.00627	-4.88388	0.14801	-4.74103	0.14955								
J05365+113	58093.00647	-4.57052	-0.00515	-4.88603	0.14838	-4.74918	0.14932								
J05365+113	58093.86798	-4.57117	-0.00476	-4.90875	0.14801	-4.72617	0.14952								
J05365+113	58094.03423	-4.59678	-0.00595	-4.94089	0.14755	-4.74193	0.14945								
J05365+113	58094.90318	-4.57782	-0.0048	-4.94896	0.14735	-4.77979	0.14893								
J05365+113	58095.04017	-4.53693	-0.00405	-4.83615	0.14899	-4.72212	0.14969								
J05365+113	58098.9257	-4.62507	-0.005	-4.87577	0.14813	-4.7201	0.14944								
J05365+113	58104.90408	-4.64175	-0.00669	-4.92254	0.14774	-4.76814	0.14911								
J05365+113	58105.05674	-4.64162	-0.00606	-4.91226	0.14754	-4.76746	0.14912								
J05365+113	58109.84086	-4.54387	-0.00492	-4.83636	0.14899	-4.71799	0.14974								
J05365+113	58113.88526	-4.56494	-0.00639	-4.86954	0.14834	-4.77281	0.14916								
J05365+113	58116.96843	-4.51452	-0.00408	-4.83583	0.14899	-4.70681	0.14984								
J05365+113	58117.92701	-4.5654	-0.00483	-4.86656	0.14856	-4.75287	0.14928								
J05365+113	58122.88349	-4.48122	-0.00341	-4.78547	0.1496	-4.64356	0.15052								
J05365+113	58131.93347	-4.47297	-0.0039	-4.88264	0.1481	-4.72943	0.14967								
J05365+113	58133.88516	-4.48746	-0.00362	-4.84394	0.1489	-4.70947	0.14977								
J05365+113	58140.86868	-4.5817	-0.00485	-4.90109	0.14811	-4.71012	0.14986								
J05365+113	58140.92506	-4.59686	-0.00505	-4.9021	0.14817	-4.7445	0.14947								
J05365+113	58142.91987	-4.48932	-0.00343	-4.84058	0.14912	-4.69302	0.15019								
J05365+113	58143.79366	-4.53584	-0.00448	-4.90652	0.14804	-4.71532	0.14972								
J05365+113	58148.92316	-4.62341	-0.00752	-4.95424	0.14735	-4.77459	0.14909								
J05365+113	58159.83418	-4.58128	-0.00506	-4.95796	0.14721	-4.76389	0.14921								
J05365+113	58160.84637	-4.62143	-0.00728	-4.91288	0.14795	-4.74369	0.14948								
J05365+113	58165.87929	-4.58386	-0.00446	-4.88735	0.14836	-4.76012	0.1494								
J05365+113	58166.77741	-4.5407	-0.00456	-4.88408	0.14834	-4.71609	0.14971								
J05365+113	58170.93134	-4.57153	-0.00476	-4.9152	0.14785	-4.74211	0.1494								
J05365+113	58172.92627	-4.64414	-0.00811	-4.93554	0.14718	-4.7825	0.14884								
J05365+113	58181.89079	-4.46901	-0.00334	-4.7704	0.14975	-4.63776	0.15053								
J05365+113	58186.93988	-4.54297	-0.0062	-4.8267	0.14385	-4.95449	0.14626								
J05365+113	58187.92508	-4.60475	-0.00574	-4.93448	0.1475	-4.8193	0.14833								
J05365+113	58190.82693	-4.6011	-0.00621	-4.93781	0.1476	-4.76106	0.14914								
J05365+113	58345.18054	-4.5778	-0.00721	-4.85699	0.14899	-4.69252	0.15015								
J05365+113	58347.19399	-4.59487	-0.0075	-4.84439	0.14896	-4.68593	0.15008								
J05365+113	58348.1745	-4.62696	-0.00807	-4.90036	0.14806	-4.66437	0.15015								
J05365+113	58355.17774	-4.5801	-0.00724	-4.88895	0.14841	-4.69984	0.14991								
J05365+113	58361.15773	-4.65209	-0.00855	-4.8872	0.1483	-4.71933	0.14972								
J05365+113	58381.18232	-4.55925	-0.0069	-4.88919	0.14821	-4.70327	0.14992								
J05365+113	58383.08951	-4.474	-0.00553	-4.85913	0.14878	-4.70424	0.15004								
J05365+113	58384.19891	-4.67054	-0.00892	-4.87815	0.14809	-4.74976	0.14936								
J05365+113	58385.15248	-4.69084	-0.00935	-4.94921	0.14735	-4.73742	0.1494								
J05365+113	58390.07647	-4.46259	-0.00348	-4.82946	0.14913	-4.66871	0.15031								
J05365+113	58391.20541	-4.5121	-0.00554	-4.84465	0.14889	-4.67699	0.15012								
J05365+113	58393.11894	-4.48604	-0.00367	-4.83506	0.149	-4.6826	0.15015								
J05365+113	58394.04543	-4.57502	-0.00676	-4.87216	0.14881	-4.72219	0.14997								
J05365+113	58396.07701	-4.5959	-0.00751	-4.95226	0.1473	-4.73552	0.14947								
J05365+113	58397.21321	-4.70627	-0.00969	-4.9484	0.14736	-4.7654	0.14909								
J05365+113	58398.15692	-4.60524	-0.00768	-4.93431	0.14765	-4.77047	0.14914								
J05365+113	58399.05165	-4.68584	-0.00924	-4.935	0.14756	-4.77182	0.14907								
J05365+113	58413.12816	-4.62704	-0.00798	-4.90923	0.14793	-4.75875	0.14927								
J05365+113	58417.02807	-4.55134	-0.00556	-4.83155	0.14904	-4.71229	0.14979								
J05365+113	58427.03149	-4.61986	-0.00764	-4.92294	0.14795	-4.7342	0.14748								
J05365+113	58429.11308	-4.51051	-0.0043	-4.88535	0.14839	-4.70701	0.14984								
J05365+113	58433.08053	-4.6232	-0.008	-4.9314	0.14762	-4.72477	0.14949								
J05365+113	58434.13048	-4.71798	-0.00995	-4.99615	0.1465	-4.81415	0.14834								
J05365+113	58451.01219	-4.47467	-0.00353	-4.80087	0.14938	-4.69927	0.14996								
J05365+113	58451.98709	-4.66411	-0.00872	-4.86638	0.14812	-4.74048	0.14946								
J05365+113	58453.90635	-4.49799	-0.006	-4.89445	0.1482	-4.75294	0.14938								

Continued on next page

// Star	MJD	Hα		Ca II IRT-a		Ca II IRT-b		He I D_3		Na I D_2		Paβ		Paδ	
		$log\left(\frac{L_{line}}{L_{Bol}}\right)$	δ	$log\left(\frac{L_{line}}{L_{Bol}}\right)$	δ	$log\left(\frac{L_{line}}{L_{Bol}}\right)$	δ	$log\left(\frac{L_{line}}{L_{Bol}}\right)$	δ	$log\left(\frac{L_{line}}{L_{Bol}}\right)$	δ	$log\left(\frac{L_{line}}{L_{Bol}}\right)$	δ	$log\left(\frac{L_{line}}{L_{Bol}}\right)$	δ
J05365+113	58458.18787	-4.60101	-0.00421	-4.90695	0.14866	-4.74263	0.14991								
J05365+113	58470.14499	-4.52551	-0.00392	-4.84741	0.14886	-4.71447	0.1499								
J05365+113	58470.91845	-4.57799	-0.00483	-4.89842	0.14808	-4.73428	0.14939								
J05365+113	58471.97545	-4.49761	-0.00361	-4.83509	0.149	-4.66819	0.1502								
J05365+113	58472.88869	-4.55437	-0.00417	-4.84042	0.149	-4.69084	0.14999								
J05365+113	58475.8929	-4.44489	-0.00318	-4.79816	0.14946	-4.65323	0.15036								
J05365+113	58476.9348	-4.5294	-0.00391	-4.85338	0.14873	-4.73035	0.14966								
J05365+113	58477.912	-4.51632	-0.00415	-4.89363	0.14821	-4.73718	0.14954								
J05365+113	58483.88277	-4.49522	-0.00362	-4.8494	0.14884	-4.69951	0.15								
J05365+113	58484.90776	-4.50411	-0.00405	-4.87839	0.14841	-4.70186	0.14989								
J05365+113	58487.10029	-4.44864	-0.00315	-4.78517	0.14965	-4.65881	0.15044								
J05365+113	58490.79272	-4.64249	-0.00702	-4.95502	0.1471	-4.77248	0.14886								
J05365+113	58492.02374	-4.63454	-0.0079	-4.92218	0.14725	-4.7777	0.14895								
J05365+113	58493.03431	-4.60051	-0.00537	-4.88949	0.14814	-4.75447	0.14922								
J05365+113	58493.82148	-4.58864	-0.0052	-4.89636	0.14804	-4.73594	0.14946								
J05365+113	58494.92072	-4.52131	-0.00386	-4.84818	0.14879	-4.73077	0.14956								
J05365+113	58495.95492	-4.38441	-0.00277	-4.72949	0.15013	-4.62708	0.15065								
J05365+113	58497.07442	-4.53715	-0.00361	-4.84858	0.14885	-4.71882	0.14982								
J05365+113	58499.8248	-4.49212	-0.00357	-4.84362	0.1489	-4.68057	0.15017								
J09143+526	58210.91121	-5.47029	-0.06027	-5.54603	0.13533	-5.34205	0.15752								
J09143+526	58385.18315	-5.26795	-0.03782	-5.57864	0.13115	-5.13816	0.16931								
J09143+526	58472.91257	-5.39542	-0.05072	-5.49604	0.1409	-5.20976	0.16579								
J09143+526	58474.93858	-5.28604	-0.03943	-5.61105	0.12666	-5.1446	0.16902								
J09143+526	58486.92274	-5.5111	-0.06621	-5.55516	0.13419	-5.38832	0.15398								
J09144+526	57653.17378	-5.45825	-0.05698	-5.2119	0.1826	-4.91912	0.1849								
J09144+526	57695.24019	-4.9343	-0.01705	-5.55205	0.15298										
J09144+526	57771.13444	-5.46977	-0.05851	-5.44745	0.16454										
J09144+526	58166.81389	-5.00573	-0.0201	-5.4389	0.16537	-4.97759	0.18171								
J11423+230	59244.18505	-5.11184	-0.02224	-5.19311	-0.00116	-5.19421	0.00098								
J11423+230	59247.11953	-5.08565	-0.02094	-5.32485	-0.0122	-5.00123	0.01167								
J11423+230	59248.11834	-5.23616	-0.02962	-5.31256	-0.01134	-5.03441	0.01013								
J11423+230	59249.18485	-5.15962	-0.02475	-5.41323	-0.02239	-4.97148	0.01295								
J11423+230	59250.05385	-5.10224	-0.02176	-5.39071	-0.01969	-5.20845	-0.00016								
J11423+230	59264.18266	-5.24783	-0.03032	-5.2625	-0.00673	-5.15794	0.00339								
J11423+230	59265.081	-5.24086	-0.02994	-5.22328	-0.00348	-5.21799	-0.00071								
J11423+230	59266.04561	-5.05297	-0.01943	-5.16934	0.00055	-5.07146	0.00837								
J11423+230	59272.09905	-5.13405	-0.02341	-5.15293	0.00168	-4.98192	0.01267								
J11423+230	59278.08596	-5.55816	-0.06217	-5.37554	-0.01795	-5.12906	0.00516								
J11423+230	59295.04923	-5.29483	-0.0339	-5.33574	-0.01367	-5.01657	0.01097								
J11423+230	59296.13188	-5.19468	-0.02692	-5.33596	-0.01369	-5.00516	0.01149								
J11423+230	59299.00201	-5.26509	-0.03155	-5.24704	-0.00541	-5.07589	0.00814								
J11423+230	59300.10446	-5.15574	-0.02461	-5.33594	-0.01369	-5.07192	0.00825								
J11423+230	59300.96712	-5.16623	-0.02513	-5.25524	-0.00611	-5.10631	0.00637								
J11423+230	59301.95397	-5.08031	-0.02069	-5.16692	0.00072	-5.13609	0.00462								
J11423+230	59307.06387	-5.33919	-0.03742	-5.24231	-0.00502	-5.12346	0.00538								
J11423+230	59308.05787	-5.42247	-0.04533	-5.21071	-0.00249	-5.22398	-0.00129								
J11423+230	59335.89268	-5.2084	-0.02778	-5.35383	-0.01556	-5.12362	0.00537								
J11423+230	59337.92889	-5.23241	-0.02926	-5.31693	-0.01177	-5.04619	0.00965								
J11423+230	59338.90159	-5.53767	-0.05848	-5.28287	-0.00855	-5.19166	0.00102								
J11423+230	59339.86291	-5.12628	-0.02196	-5.27818	-0.00812	-5.09548	0.00708								
J11423+230	59340.94451	-5.12527	-0.02286	-5.11681	0.00691	-5.0993	0.00709								
J11423+230	59341.97511	-5.25491	-0.03082	-5.28443	-0.00869	-5.15828	0.00324								
J11423+230	59345.89657	-4.93143	-0.01468	-5.07686	0.01854	-4.92202	0.02071								
J11423+230	59349.912	-5.42094	-0.04532	-5.17668	3e-05	-5.17841	0.00193								
J11423+230	59353.89191	-5.30989	-0.03425	-5.29691	-0.00984	-5.11978	0.00571								
J11423+230	59354.86647	-5.08623	-0.02097	-5.17998	-0.0002	-5.12532	0.00538								
J11423+230	59355.94003	-5.27495	-0.03238	-5.34623	-0.01476	-5.10796	0.00639								
J11423+230	59358.88562	-5.16761	-0.02529	-5.15823	0.00132	-5.08242	0.00779								
J11423+230	59359.87844	-5.08505	-0.02091	-5.21059	-0.00248	-4.95823	0.01357								
J11423+230	59362.92846	-4.89827	-0.0136	-5.06436	0.01801	-4.96874	0.02033								
J11423+230	59363.87732	-5.13085	-0.02324	-5.31944	-0.01202	-5.08888	0.00745								
J11423+230	59366.93877	-5.15151	-0.02437	-5.14726	0.00206	-5.13873	0.00458								
J11423+230	59367.88613	-5.18553	-0.02636	-5.25602	-0.00617	-5.10628	0.00637								
J11423+230	59371.89234	-5.2344	-0.02848	-5.18397	-0.00049	-5.16344	0.00291								

Continued on next page

// Star	MJD	Hα		Ca II IRT-a		Ca II IRT-b		He I D_3		Na I D_2		Paβ		Paδ	
		$log\left(\frac{L_{line}}{L_{Bol}}\right)$	δ	$log\left(\frac{L_{line}}{L_{Bol}}\right)$	δ	$log\left(\frac{L_{line}}{L_{Bol}}\right)$	δ	$log\left(\frac{L_{line}}{L_{Bol}}\right)$	δ	$log\left(\frac{L_{line}}{L_{Bol}}\right)$	δ	$log\left(\frac{L_{line}}{L_{Bol}}\right)$	δ	$log\left(\frac{L_{line}}{L_{Bol}}\right)$	δ
J11423+230	59385.89867	-5.44946	-0.0484	-5.15341	0.00165	-5.23922	-0.0023								
J11423+230	59386.9055	-5.55173	-0.06104	-5.24698	-0.00541	-5.29351	-0.0069								
J11423+230	59387.89494	-5.32367	-0.0361	-5.31987	-0.01206	-5.2385	-0.00224								
J11423+230	59389.89027	-5.12719	-0.02305	-5.19518	-0.00132	-5.1233	0.0055								
J11423+230	59390.89346	-5.15731	-0.02461	-5.10661	0.00465	-5.14189	0.00439								
J11423+230	59391.87459	-5.03911	-0.01875	-4.99598	0.01293	-5.06029	0.00963								
J11423+230	59392.89244	-4.94842	-0.01527	-5.0666	0.00697	-4.9863	0.01232								
J11423+230	59597.15976	-5.3407	-0.03755	-5.15264	0.01532	-5.02815	0.01333								
J11423+230	59608.13241	-5.27696	-0.03254	-5.27838	-0.00814	-5.06029	0.00895								
J11423+230	59612.16504	-5.10655	-0.0219	-5.20142	0.00226	-5.01319	0.01139								
J11423+230	59616.23521	-5.27455	-0.03224	-5.26524	-0.00697	-4.95881	0.01346								
J11423+230	59618.1072	-5.32725	-0.0364	-5.32613	-0.01269	-5.0567	0.00903								
J11423+230	59620.10465	-5.16374	-0.02507	-5.31282	-0.01137	-5.0399	0.00986								
J11423+230	59632.12366	-5.36207	-0.03944	-5.3168	-0.01176	-5.05142	0.00939								
J11423+230	59634.05977	-5.52174	-0.05717	-5.40757	-0.0217	-5.16022	0.00324								
J11423+230	59640.044	-5.35998	-0.03939	-5.38527	-0.01906	-5.16085	0.0032								
J11423+230	59648.0236	-5.47053	-0.05063	-5.33143	-0.01322	-5.06597	0.00856								
J11423+230	59671.99253	-5.05526	-0.01946	-5.52584	-0.03819	-5.1751	0.00227								
J11423+230	59679.95335	-5.07037	-0.02022	-5.05782	0.00745	-5.02199	0.01081								
J11423+230	59684.96022	-5.02569	-0.01818	-5.42618	-0.02401	-5.06966	0.00837								
J11423+230	59686.95238	-5.05201	-0.01931	-5.17645	5e-05	-5.03768	0.01007								
J11423+230	59694.90806	-5.3093	-0.03505	-5.27165	-0.00754	-5.20218	0.00042								
J11423+230	59699.04883	-5.34553	-0.0381	-5.35207	-0.01538	-5.12091	0.00553								
J11423+230	59705.00586	-5.36656	-0.03985	-5.35484	-0.01567	-5.11512	0.00587								
J11423+230	59706.92229	-5.13732	-0.02359	-5.2129	-0.00266	-5.1428	0.00421								
J11423+230	59711.85037	-5.46124	-0.04956	-5.34265	-0.01438	-5.14812	0.004								
J11423+230	59714.88819	-5.46155	-0.04959	-5.3141	-0.01149	-5.04613	0.00965								
J11423+230	59717.89814	-5.40773	-0.04381	-5.25669	-0.00623	-5.1399	0.00451								
J11423+230	59719.9092	-5.58099	-0.0653	-5.28281	-0.00854	-5.13738	0.00455								
J11423+230	59721.91098	-5.26713	-0.03181	-5.17799	-6.00E-05	-5.02425	0.0107								
J11423+230	59723.96726	-4.79381	-0.01066	-5.18255	-0.00026	-5.09578	0.0077								
J11423+230	59725.8855	-5.45038	-0.04834	-5.2829	-0.00855	-5.06928	0.00839								
J11423+230	59733.96274	-5.08355	-0.02077	-5.43592	-0.02525	-5.26025	-0.0041								
J11423+230	59735.89028	-5.39839	-0.04303	-5.27989	-0.00827	-5.13911	0.00456								
J11423+230	59737.88435	-4.87975	-0.01299	-5.18402	-0.0005	-5.15091	0.00371								
J11423+230	59739.87982	-4.76961	-0.01005	-5.05946	0.00736	-5.10797	0.00639								
J11423+230	59741.87601	-5.06679	-0.02005	-5.23651	-0.00454	-5.22087	-0.00106								
J15598-082	57476.14948	-5.17826	-0.01556	-5.46036	0.01242	-5.28829	0.0291								
J15598-082	57493.13709	-5.36028	-0.02366	-5.38951	0.01933	-5.29299	0.02879								
J15598-082	57504.09081	-5.42622	-0.02754	-5.47231	0.01142	-5.56667	0.00403								
J15598-082	57539.99051	-5.29744	-0.02048	-5.30572	0.02594	-5.33505	0.02593								
J15598-082	57553.94641	-5.3901	-0.02535	-5.42333	0.01628	-5.34078	0.02551								
J15598-082	58141.25028	-5.045	-0.01145	-5.26735	0.02857	-5.26005	0.03085								
J15598-082	58659.90965	-5.18455	-0.01579	-5.46847	0.01158	-5.33972	0.02559								
J15598-082	58662.92364	-5.43844	-0.02833	-5.35237	0.02242	-5.24869	0.03153								
J15598-082	58697.90603	-5.3593	-0.02155	-5.45733	0.0182	-5.37111	0.02733								
J15598-082	58717.86003	-5.24511	-0.01815	-5.48157	0.01044	-5.55278	0.0057								
J15598-082	58914.22944	-5.25106	-0.0184	-5.37022	0.02097	-5.33742	0.02576								
J15598-082	58988.08298	-5.53515	-0.0354	-5.52507	0.00887	-5.30153	0.03006								
J15598-082	58999.9964	-5.18566	-0.01583	-5.3618	0.02147	-5.37323	0.02307								
J15598-082	59003.04998	-5.70382	-0.05219	-5.5827	-0.00209	-5.31536	0.0273								
J15598-082	59007.98223	-5.5384	-0.03566	-5.48266	0.01032	-5.44693	0.0168								
J00403+612	59010.14091	-4.85919	-0.01772	-5.4976	-0.01835	-5.11701	0.01862								
J00403+612	59013.08003	-4.99042	-0.02398	-4.98911	0.02329	-4.99049	0.02445								
J00403+612	59018.12351	-5.03387	-0.0265	-5.38439	-0.00349	-5.00598	0.02389								
J00403+612	59034.08171	-5.18966	-0.03793	-5.30074	0.00365	-5.02652	0.02302								
J00403+612	59055.09568	-5.38834	-0.05994	-5.25766	0.00727	-4.89603	0.02794								
J00403+612	59056.08971	-5.25913	-0.04451	-5.28845	0.00472	-5.01811	0.02338								
J00403+612	59059.12155	-5.19543	-0.03844	-5.31501	0.00237	-5.17355	0.01537								
J00403+612	59061.13091	-5.02856	-0.02618	-5.51222	-0.02041	-5.06184	0.02131								
J00403+612	59063.10066	-5.22755	-0.04139	-5.18116	0.01288	-5.20075	0.01351								
J01026+623	57397	-5.20689	-0.03054	-4.96754	0.07495	-4.86366	0.0762								
J01026+623	57592.18667	-5.30776	-0.02445	-5.06222	0.07614	-4.89388	0.07425								
J01026+623	57646.97713	-5.50189	-0.06023	-5.08795	0.06649	-4.99541	0.06611								

Continued on next page

// Star	MJD	Hα		Ca II IRT-a		Ca II IRT-b		He I D_3		Na I D_2		Paβ		Paδ	
		$log\left(\frac{L_{line}}{L_{Bol}}\right)$	δ	$log\left(\frac{L_{line}}{L_{Bol}}\right)$	δ	$log\left(\frac{L_{line}}{L_{Bol}}\right)$	δ	$log\left(\frac{L_{line}}{L_{Bol}}\right)$	δ	$log\left(\frac{L_{line}}{L_{Bol}}\right)$	δ	$log\left(\frac{L_{line}}{L_{Bol}}\right)$	δ	$log\left(\frac{L_{line}}{L_{Bol}}\right)$	δ
J01026+623	57656.96289	-5.47694	-0.05687	-5.22204	0.05694	-4.93012	0.06853								
J01026+623	57677.88933	-5.45065	-0.05259	-5.10647	0.07207	-4.93216	0.07494								
J01026+623	57684.86082	-5.37883	-0.04537	-5.00866	0.07422	-4.96674	0.07161								
J01026+623	57697.95611	-5.14943	-0.02675	-5.03446	0.07389	-4.93491	0.06981								
J01026+623	57704.83046	-5.37024	-0.04448	-5.05334	0.06299	-4.93618	0.0689								
J01026+623	57737.90523	-5.5737	-0.07106	-5.01577	0.0738	-4.90944	0.06925								
J01026+623	57765.78433	-5.57681	-0.06783	-5.09823	0.06196	-5.01116	0.06562								
J01026+623	57896.16635	-5.51618	-0.03879	-5.11282	0.07615	-4.95265	0.07344								
J01026+623	57917.15309	-5.67948	-0.05781	-5.08832	0.07627	-4.94091	0.07527								
J01026+623	57938.14638	-5.57985	-0.05076	-5.07522	0.0754	-4.93592	0.07254								
J01026+623	57944.169	-5.68665	-0.06278	-5.10954	0.0722	-4.87923	0.07413								
J01026+623	57945.11361	-5.52143	-0.04145	-5.07193	0.07626	-4.91504	0.07577								
J01026+623	57960.01458	-5.38479	-0.03346	-5.07138	0.07538	-4.90011	0.07571								
J01026+623	57962.15416	-5.20097	-0.0206	-5.04546	0.07625	-4.81905	0.07884								
J01026+623	57963.17248	-5.23463	-0.02123	-5.12307	0.07507	-4.91828	0.07362								
J01026+623	57964.13969	-5.49178	-0.04093	-5.07368	0.07553	-4.87975	0.07558								
J01026+623	57997.08023	-5.56871	-0.04541	-5.06994	0.0759	-4.91416	0.07372								
J01026+623	58094.88764	-5.69746	-0.05587	-5.20482	0.06405										
J01026+623	58095.78322	-5.26082	-0.03457	-5.15142	0.05647										
J01026+623	58113.79457	-5.53227	-0.06459	-5.14112	0.05793										
J01026+623	58140.93244	-5.73088	-0.05797	-5.12035	0.07213										
J01026+623	58148.87898	-5.64269	-0.06084	-5.12701	0.06485										
J01026+623	58171.78286	-5.43437	-0.05156	-5.18742	0.055										
J01026+623	58173.78979	-5.47454	-0.05606	-5.13917	0.05724										
J01026+623	58174.80337	-5.61084	-0.05631	-5.24355	0.05763										
J09163-186	57400	-5.16696	-0.04715	-5.11154	0.08185										
J09163-186	57401	-4.61249	-0.00623	-4.94966	0.10858	-4.85664	0.10919								
J09163-186	57760.1425	-5.01115	-0.03289	-5.0712	0.08496	-5.08432	0.08428								
J09163-186	58091.18127	-4.71842	-0.00513	-5.00129	0.11018	-4.99281	0.1095								
J09163-186	58135.03918	-5.00814	-0.02928	-5.2603	0.085	-5.12692	0.08358								
J02489-145W	58803.93875	-4.97411	-0.01351	-5.44454	0.01038										
J02489-145W	58816.92278	-5.15366	-0.02043	-5.39247	0.01556	-5.51671	0.00556								
J02489-145W	58844.8321	-5.05675	-0.01634	-5.47218	0.00725	-5.47208	0.01044								
J02489-145W	58845.85965	-4.96338	-0.01318	-5.46637	0.00769	-5.27104	0.02821								
J02489-145W	58846.86562	-4.93055	-0.01222	-5.58132	-0.00724	-5.33904	0.02317								
J02489-145W	58847.83632	-4.89027	-0.01114	-5.48476	0.00551	-5.39068	0.01877								
J02489-145W	58848.84123	-5.21281	-0.02341	-5.44485	0.01012										
J02489-145W	58851.83236	-5.37029	-0.03364	-5.547	-0.00229	-5.32185	0.02452								
J02489-145W	58855.83804	-5.34163	-0.03149	-5.4211	0.01288	-5.51483	0.00552								
J02489-145W	58859.86234	-4.874	-0.01073	-5.60893	-0.01153										
J02489-145W	58880.80824	-5.05206	-0.01617	-5.55361	-0.00351	-5.34895	0.02218								
J02489-145W	58881.80532	-5.0386	-0.01567	-5.57407	-0.00647										
J02489-145W	58889.79224	-4.942	-0.01255	-5.52766	6e-05	-5.2012	0.03264								
J02489-145W	58890.78736	-4.85541	-0.01028	-5.43681	0.011	-5.61589	-0.00824								
J03217-066	57629.18152	-4.9189	-0.01458	-5.31911	0.02329	-5.23141	0.03164								
J03217-066	57643.18573	-4.87214	-0.01288	-5.33033	0.02217	-5.10065	0.03886								
J03217-066	57656.05385	-4.81396	-0.01111	-5.24529	0.02872	-5.07953	0.03971								
J03217-066	57678.07527	-4.90238	-0.01404	-5.32191	0.02305	-5.22069	0.03244								
J03217-066	57693.03343	-4.87698	-0.00952	-5.28967	0.02563	-5.06812	0.04031								
J03217-066	57701.0456	-4.77888	-0.00851	-5.30495	0.02443	-5.15234	0.03619								
J03217-066	57705.99306	-4.79631	-0.00779	-5.22826	0.03003	-5.099	0.03893								
J03217-066	58173.83411	-4.67729	-0.00685	-5.26767	0.02727	-5.17414	0.03502								
J03217-066	58528.81592	-4.7612	-0.00707	-5.21074	0.03104	-5.13623	0.03702								
J03217-066	58528.82095	-4.74439	-0.00559	-5.27327	0.03258	-5.07552	0.04332								
J03217-066	58764.07482	-4.92038	-0.01175	-5.30187	0.0321										
J09425+700	57397	-4.63287	-0.00464	-5.08819	0.10455	-5.09388	0.10597								
J09425+700	57414	-4.72852	-0.00574	-5.18355	0.10136	-4.98754	0.1119	-5.63277	0.06708	-5.58077	0.09681				
J09425+700	57415	-4.67862	-0.00506	-5.18217	0.10132	-5.02794	0.10917								
J09425+700	57418	-4.73793	-0.00575	-5.30284	0.09131	-5.12418	0.10428								
J09425+700	57442	-4.63566	-0.00446	-5.08139	0.11406	-4.96992	0.11302								
J09425+700	57444	-4.60363	-0.00419	-5.08179	0.11027	-5.08651	0.11119								
J09425+700	57449	-4.70885	-0.0042	-5.18016	0.1058	-5.09437	0.11024			-5.52856	0.05781				
J09425+700	57473.90677	-4.71165	-0.00643	-5.14416	0.10319	-5.05428	0.10727								
J09425+700	57493.89938	-4.72633	-0.00543	-5.10002	0.11025	-5.01873	0.11109								

Continued on next page

// Star	MJD	Hα		Ca II IRT-a		Ca II IRT-b		He I D_3		Na I D_2		Paβ		Paδ	
		$log\left(\frac{L_{line}}{L_{Bol}}\right)$	δ	$log\left(\frac{L_{line}}{L_{Bol}}\right)$	δ	$log\left(\frac{L_{line}}{L_{Bol}}\right)$	δ	$log\left(\frac{L_{line}}{L_{Bol}}\right)$	δ	$log\left(\frac{L_{line}}{L_{Bol}}\right)$	δ	$log\left(\frac{L_{line}}{L_{Bol}}\right)$	δ	$log\left(\frac{L_{line}}{L_{Bol}}\right)$	δ
J09425+700	57699.23045	-4.91542	-0.01219	-5.08197	0.10513	-4.9672	0.11056								
J09425+700	57704.14638	-4.87445	-0.0127	-5.23192	0.09639	-5.19416	0.10053								
J09425+700	57760.03584	-4.70979	-0.00539	-5.08986	0.10565	-5.03575	0.10984								
J09425+700	57779.04993	-4.41071	-0.00267	-4.9844	0.11672	-4.90913	0.11732			-5.45306	0.06004				
J09425+700	57798.0845	-4.57114	-0.00386	-5.12375	0.11198	-5.01174	0.11428								
J09425+700	57799.96924	-4.58884	-0.00405	-5.07903	0.11325	-4.96024	0.11577								
J09425+700	57818.91397	-4.53554	-0.00358	-5.02789	0.1143	-4.96341	0.116								
J09425+700	58216.86738	-4.66505	-0.00481	-5.14585	0.10265	-5.10486	0.10906								
J09425+700	58417.17994	-4.47737	-0.00291	-5.04336	0.11613	-4.93916	0.1174								
J09425+700	58451.12677	-4.63924	-0.00415	-5.13395	0.11353	-5.02668	0.1151								
J09425+700	58475.0753	-4.56693	-0.00358	-5.12449	0.11121	-4.9711	0.11599								
J09425+700	58534.01973	-4.75162	-0.00496	-5.16856	0.10524	-5.10108	0.1092								
J09425+700	58560.00821	-4.57227	-0.00391	-5.03879	0.11491	-4.91421	0.1165								
J09425+700	58560.11581	-4.59142	-0.00406	-5.03952	0.11436	-5.02095	0.11388	-5.57162	0.07447						
J09425+700	58817.07427	-4.71505	-0.00908	-5.22987	0.09652	-4.99635	0.10956			-5.77694	0.09383				
J09425+700	58831.14117	-4.65073	-0.00712	-5.20859	0.09801	-5.10089	0.10526								
J09425+700	58860.10184	-4.7057	-0.00788	-5.16462	0.10307	-5.05937	0.1089								
J09425+700	58881.05789	-4.61375	-0.0038	-5.05003	0.11158	-4.97609	0.11642								
J09425+700	58889.00807	-4.7819	-0.00954	-5.247	0.09679	-5.11848	0.10549								
J09425+700	58894.25829	-4.50487	-0.00266	-5.01462	0.11803	-4.92769	0.11868	-5.42922	0.09158	-5.23346	0.11949				
J09425+700	58912.9262	-4.79428	-0.00981	-5.18273	0.10006	-5.10057	0.10578								
J09425+700	58915.92666	-4.69313	-0.00828	-5.05739	0.10595	-5.0871	0.10666								
J09425+700	58921.13856	-4.67073	-0.00423	-5.17148	0.10427	-5.0348	0.11204								
J09425+700	58976.85552	-4.70408	-0.00482	-5.18669	0.10353	-5.08195	0.1092								
J09425+700	58980.86365	-4.65191	-0.00477	-5.16228	0.10179	-5.07471	0.10708								
J11026+219	57397	-4.64193	-0.01102	-4.86594	0.02582										
J11026+219	57411	-4.70357	-0.0082	-4.88408	0.02834	-4.68512	0.0312								
J11026+219	57412	-4.71821	-0.00788	-4.84684	0.03259	-4.64198	0.0324								
J11026+219	57415	-4.693	-0.00683	-4.85434	0.03292	-4.67656	0.03105								
J11026+219	57418	-4.50386	-0.0047	-4.81005	0.03254	-4.62304	0.03196								
J11026+219	57421	-4.58749	-0.00873	-4.79168	0.03156	-4.6112	0.03071								
J11026+219	57426	-4.59885	-0.00707	-4.8278	0.03088	-4.66557	0.02793								
J11026+219	57449	-4.58973	-0.0043	-4.80737	0.03425	-4.59419	0.03411								
J11026+219	57474.9655	-4.65921	-0.00927	-4.82082	0.03173	-4.64149	0.03085								
J11026+219	57489.92531	-4.62645	-0.00775	-4.80094	0.03142	-4.60972	0.03087								
J11026+219	57503.87688	-4.57633	-0.0061	-4.77416	0.03216	-4.58426	0.03368								
J11026+219	57508.88596	-4.71149	-0.00922	-4.82025	0.03235	-4.63274	0.03146								
J11026+219	57534.8631	-4.59364	-0.00925	-4.8492	0.03076	-4.63844	0.02839								
J11026+219	57538.84959	-4.76097	-0.01151	-4.84709	0.03104	-4.70062	0.02751								
J11026+219	57540.87868	-4.70072	-0.00879	-4.84082	0.03108	-4.64395	0.03051								
J11026+219	57542.86344	-4.50654	-0.00538	-4.74002	0.03247	-4.55649	0.03364								
J11026+219	57557.85853	-4.79759	-0.01369	-4.87296	0.03023	-4.68278	0.02711								
J11026+219	57756.1491	-4.5717	-0.00866	-4.8478	0.03031	-4.61729	0.03078								
J11026+219	57760.12484	-4.61162	-0.00956	-4.83776	0.03049	-4.62879	0.03051								
J11026+219	57761.1534	-4.584	-0.00826	-4.82136	0.03099	-4.64021	0.03046								
J11026+219	57779.07536	-4.77205	-0.01487	-4.87642	0.02832	-4.67585	0.02777								
J11026+219	57792.99291	-4.66215	-0.01155	-4.90094	0.02607	-4.68112	0.02764								
J11026+219	57798.02946	-4.6174	-0.00972	-4.85397	0.03038	-4.66849	0.02956								
J11026+219	57799.0658	-4.65425	-0.00934	-4.83794	0.03101	-4.6514	0.03011								
J11026+219	57799.99986	-4.52082	-0.00591	-4.76036	0.03201	-4.58259	0.03136								
J11026+219	57818.96544	-4.55633	-0.008	-4.78662	0.03184	-4.56674	0.03138								
J11026+219	57828.92557	-4.5405	-0.00685	-4.76642	0.03182	-4.61738	0.03071								
J11026+219	57858.89005	-4.62319	-0.0053	-4.84882	0.0328	-4.63555	0.03127								
J11026+219	58050.22287	-4.58584	-0.00637	-4.83362	0.03235	-4.64628	0.032								
J11026+219	58055.18898	-4.74581	-0.00852	-4.95377	0.02506	-4.72151	0.0294								
J11026+219	58074.15568	-4.80275	-0.01142	-4.91977	0.02435	-4.69873	0.02895								
J11026+219	58089.18562	-4.65944	-0.01161	-4.86437	0.02611	-4.68653	0.02747								
J11026+219	58093.12189	-4.5762	-0.00528	-4.83756	0.03195	-4.63541	0.03164								
J11026+219	58095.10135	-4.58424	-0.0065	-4.86377	0.02916	-4.67463	0.03132								
J11026+219	58097.22223	-4.67426	-0.00976	-4.90749	0.02446	-4.68822	0.0285								
J11026+219	58105.07228	-4.66318	-0.00954	-4.91211	0.02569	-4.66087	0.02854								
J11026+219	58118.13276	-4.74365	-0.01151	-4.87177	0.02742	-4.69992	0.02973								
J11026+219	58119.13472	-4.69133	-0.01132	-4.86371	0.03021	-4.68363	0.0293								
J11026+219	58120.17838	-4.58279	-0.00712	-4.79507	0.0313	-4.60468	0.03085								

Continued on next page

// Star	MJD	Hα		Ca II IRT-a		Ca II IRT-b		He I D_3		Na I D_2		Paβ		Paδ	
		$log\left(\frac{L_{line}}{L_{Bol}}\right)$	δ	$log\left(\frac{L_{line}}{L_{Bol}}\right)$	δ	$log\left(\frac{L_{line}}{L_{Bol}}\right)$	δ	$log\left(\frac{L_{line}}{L_{Bol}}\right)$	δ	$log\left(\frac{L_{line}}{L_{Bol}}\right)$	δ	$log\left(\frac{L_{line}}{L_{Bol}}\right)$	δ	$log\left(\frac{L_{line}}{L_{Bol}}\right)$	δ
J11026+219	58122.15468	-4.68165	-0.00805	-4.8856	0.02948	-4.66009	0.03189								
J11026+219	58131.21026	-4.83308	-0.01731	-4.93186	0.01868	-4.75413	0.02517								
J11026+219	58135.16321	-4.63528	-0.00708	-4.86347	0.03176	-4.63178	0.03202								
J11026+219	58148.95137	-4.64469	-0.00888	-4.8439	0.02796	-4.67234	0.02984								
J11026+219	58172.11095	-4.79733	-0.00992	-4.97953	0.02298	-4.72171	0.02971								
J11026+219	58200.03252	-4.81789	-0.01672	-4.90561	0.01988	-4.72273	0.02611								
J11026+219	58214.88415	-4.6748	-0.00815	-4.83543	0.03261	-4.67796	0.03026								
J11026+219	58216.89822	-4.61067	-0.00914	-4.83057	0.03107	-4.63879	0.02842								
J11026+219	58240.92621	-4.90749	-0.02055	-4.92582	0.01909	-4.70943	0.02643								
J11026+219	58244.81953	-4.67492	-0.0109	-4.7678	0.0318	-4.62586	0.03285								
J11026+219	58244.82185	-4.57648	-0.00487	-4.79677	0.03312	-4.58988	0.03445								
J18174+483	57499.15403	-4.16039	-0.00082	-4.72026	0.06625	-4.59458	0.06717	-5.40363	0.01199	-5.32491	0.02272				
J18174+483	57532.10213	-4.15825	-0.00082	-4.68386	0.06663	-4.59162	0.0672	-5.27487	0.02712	-5.30054	0.02445				
J18174+483	57556.05517	-4.15426	-0.00078	-4.72662	0.06614	-4.60002	0.06709	-5.29686	0.02476	-5.16082	0.03718				
J18174+483	57584.01227	-4.14442	-0.00056	-4.74269	0.066	-4.58102	0.06722	-5.44737	0.01184	-5.24728	0.03366				
J18174+483	57595.92274	-4.15227	-0.00078	-4.7724	0.06555	-4.56191	0.06609			-5.48418	-2.00E-05				
J18174+483	57604.90953	-4.15633	-0.00081	-4.71225	0.06638	-4.5769	0.06723	-5.32129	0.02716	-5.26582	0.02802				
J18174+483	57632.91117	-4.14699	-0.00079	-4.75194	0.06571	-4.59625	0.06709	-5.50886	-0.00417	-5.21366	0.03288				
J18174+483	57766.25516	-4.16744	-0.00086	-4.73754	0.06611	-4.61722	0.06697	-5.25703	0.02888	-5.28691	0.0266				
J18174+483	57823.21524	-4.13287	-0.0007	-4.70426	0.06646	-4.59856	0.06723	-5.20746	0.03335	-5.22382	0.03198				
J18174+483	57833.20545	-4.18782	-0.00068	-4.76937	0.06661	-4.65132	0.06742	-5.48036	0.00718	-5.31735	0.02713				
J18174+483	57848.19187	-4.23453	-0.00108	-4.8077	0.06563	-4.68055	0.0667	-5.603	-0.02252	-5.36644	0.01674				
J18174+483	57850.13834	-4.13987	-0.00073	-4.73576	0.06608	-4.60543	0.06711	-5.40452	0.01177	-5.23533	0.03086				
J18174+483	57853.13563	-4.14459	-0.00055	-4.69345	0.06731	-4.58711	0.06791	-5.21758	0.03565	-5.19039	0.03779				
J18174+483	57855.05834	-4.14445	-0.00055	-4.73137	0.06689	-4.6232	0.06761	-5.39378	0.01555	-5.21793	0.034				
J18174+483	57860.97131	-4.12184	-0.00041	-4.708	0.06719	-4.61572	0.0677	-5.44295	0.00652	-5.26571	0.02811				
J18174+483	57863.12906	-4.15659	-0.0008	-4.69575	0.06655	-4.599	0.06717	-5.13111	0.03947	-5.30845	0.02376				
J18174+483	57880.95898	-4.17851	-0.00046	-4.73443	0.0674	-4.63108	0.06794	-5.57139	-0.00234	-5.40362	0.02114				
J18174+483	57883.11039	-4.16375	-0.00084	-4.71902	0.06626	-4.65166	0.0666								
J18174+483	57888.02887	-4.01897	-0.0001	-4.59797	0.06819	-4.50619	0.06856	-5.16368	0.04205	-5.09879	0.05858				
J18174+483	57890.10873	-4.02859	-4.00E-05	-4.58367	0.06838	-4.51042	0.06864	-5.24656	0.03865	-5.12068	0.05897				
J18174+483	57891.94377	-4.15066	-0.00077	-4.73043	0.0661	-4.62813	0.06673	-5.44518	0.00596	-5.4495	0.00531				
J18174+483	57920.97883	-3.96672	7e-05	-4.6163	0.06818	-4.52957	0.06851	-5.1523	0.04751	-5.09875	0.05461				
J18174+483	57927.98623	-4.20843	-0.00061	-4.78146	0.06684	-4.65719	0.06753	-5.5257	0.0087	-5.31287	0.03281				
J18174+483	57950.95815	-4.07584	-0.00019	-4.65221	0.0679	-4.53108	0.06839	-5.36522	0.02888	-5.25842	0.0382				
J18174+483	57953.99067	-4.07481	-0.00027	-4.65169	0.06753	-4.51286	0.06828	-5.11363	0.04711	-5.18996	0.04081				
J18174+483	57981.90072	-4.10139	-0.00033	-4.61965	0.06791	-4.48924	0.06852	-5.26311	0.04033	-5.13611	0.05792				
J18174+483	57985.88502	-4.07745	-0.00026	-4.72075	0.06712	-4.58489	0.06789	-5.4081	0.01989	-5.24853	0.03559				
J18174+483	58032.82393	-4.09815	-0.00034	-4.68951	0.0673	-4.58108	0.06785	-5.41243	0.01843	-5.18917	0.03954				
J18174+483	58047.78615	-4.10703	-0.00034	-4.70368	0.06714	-4.58846	0.06783	-5.35947	0.02633	-5.20942	0.03937				
J18174+483	58123.25217	-4.13928	-0.00059	-4.71155	0.06664	-4.60861	0.06725	-5.33897	0.02006	-5.22859	0.03148				
J18174+483	58135.23519	-4.13542	-0.00066	-4.74567	0.06624	-4.6197	0.06715	-5.48726	-0.00053	-5.15004	0.03807				
J18174+483	58161.16856	-4.06003	-0.00044	-4.68407	0.06655	-4.56211	0.06741	-5.46546	0.00369	-5.22785	0.04466				
J18174+483	58166.18371	-4.05988	-0.00045	-4.66997	0.0668	-4.56429	0.06749	-5.24858	0.03093	-5.09942	0.04199				
J18174+483	58172.12358	-4.14099	-0.00074	-4.71543	0.06622	-4.61802	0.06693	-5.25044	0.03134	-5.17339	0.03619				
J18174+483	58175.14308	-4.08952	-0.00055	-4.68841	0.06654	-4.57181	0.06739	-5.30908	0.02445	-5.1101	0.0409				
J18174+483	58200.07074	-4.11365	-0.00063	-4.77308	0.06555	-4.57164	0.0674			-5.18662	0.04742				
J18174+483	58206.07738	-4.14211	-0.00073	-4.72347	0.06613	-4.61041	0.067	-5.38371	0.01464	-5.28904	0.02575				
J18174+483	58209.11337	-4.04193	-0.0003	-4.66506	0.06723	-4.57704	0.06776	-5.15834	0.03791	-5.22824	0.04144				
J18174+483	58213.01456	-4.0912	-0.00055	-4.67231	0.06674	-4.59785	0.06711	-5.29051	0.02551	-5.21961	0.03236				
J18174+483	58305.96717	-4.07769	-0.00052	-4.70619	0.06636	-4.58333	0.06714	-5.40697	0.01154	-5.32014	0.0223				
J18174+483	58354.87775	-4.12904	-0.00066	-4.70224	0.06678	-4.57954	0.06752	-5.35175	0.02057	-5.25235	0.02926				
J18174+483	58358.86228	-4.13268	-0.00057	-4.72156	0.06667	-4.60323	0.06743	-5.3022	0.02666	-5.19304	0.0365				
J18174+483	58360.83884	-4.13558	-0.0005	-4.72873	0.06687	-4.60656	0.0676	-5.44158	0.01398	-5.21907	0.03682				
J18174+483	58364.84577	-3.99211	-0.00026	-4.57602	0.06758	-4.48429	0.06804	-5.11155	0.05312	-5.01805	0.05828				
J18174+483	58366.80807	-4.10894	-0.00051	-4.69528	0.06701	-4.57925	0.06771	-5.26671	0.02801	-5.11603	0.0406				
J18174+483	58374.94709	-4.06067	-0.00048	-4.6724	0.0667	-4.56653	0.06738	-5.17725	0.036	-5.20205	0.03382				
J18174+483	58381.86137	-3.98806	-1.00E-05	-4.56739	0.06826	-4.45477	0.06878	-5.11774	0.05404	-5.0281	0.06066				
J18174+483	58383.81667	-4.07689	-0.00027	-4.66833	0.0674	-4.56292	0.06801	-5.25476	0.03766	-5.18868	0.04008				
J18174+483	58389.84211	-4.02971	-0.00035	-4.66541	0.06681	-4.53196	0.06771	-5.15246	0.0457	-5.06737	0.04372				
J18174+483	58391.81101	-4.14024	-0.00044	-4.73503	0.06699	-4.59047	0.06785	-5.29668	0.03218	-5.3746	0.02456				
J18174+483	58393.79152	-4.1024	-0.00061	-4.73359	0.06619	-4.60195	0.06717	-5.16562	0.04107	-5.16466	0.03688				
J18174+483	58394.78914	-4.13846	-0.00066	-4.72638	0.06649	-4.60025	0.06735	-5.15618	0.03772	-5.18223	0.03566				
J18174+483	58397.80895	-4.07293	-0.00026	-4.66779	0.0674	-4.56234	0.06799	-5.2871	0.03255	-5.18707	0.04038				

Continued on next page

// Star	MJD	Hα		Ca II IRT-a		Ca II IRT-b		He I D_3		Na I D_2		Paβ		Paδ	
		$log\left(\frac{L_{line}}{L_{Bol}}\right)$	δ	$log\left(\frac{L_{line}}{L_{Bol}}\right)$	δ	$log\left(\frac{L_{line}}{L_{Bol}}\right)$	δ	$log\left(\frac{L_{line}}{L_{Bol}}\right)$	δ	$log\left(\frac{L_{line}}{L_{Bol}}\right)$	δ	$log\left(\frac{L_{line}}{L_{Bol}}\right)$	δ	$log\left(\frac{L_{line}}{L_{Bol}}\right)$	δ
J18174+483	58398.77138	-4.09911	-0.00043	-4.73532	0.06658	-4.58998	0.06763	-5.36409	0.02102	-5.21539	0.03543				
J18174+483	58404.80698	-4.06965	-0.00029	-4.66971	0.06731	-4.57335	0.06785	-5.2005	0.04301	-5.16473	0.04198				
J18174+483	58412.87614	-4.1108	-0.00063	-4.72799	0.06612	-4.58666	0.06718	-5.29859	0.02539	-5.18539	0.03522				
J18174+483	58413.85821	-4.09421	-0.00057	-4.67791	0.06665	-4.57091	0.06734	-5.41468	0.01901	-5.12049	0.05665				
J18174+483	58414.83023	-4.08999	-0.00055	-4.6832	0.06656	-4.58159	0.06728	-5.23118	0.03131	-5.22156	0.03232				
J18174+483	58416.89441	-4.07497	-0.0005	-4.68595	0.06657	-4.56189	0.06741	-5.50405	-0.00348	-5.14532	0.03854				
J18174+483	58426.81082	-3.9625	-0.00019	-4.52125	0.06795	-4.42815	0.0684	-5.02514	0.05646	-4.89066	0.06233				
J18174+483	58450.78713	-4.08884	-0.00054	-4.73622	0.06598	-4.58886	0.06719			-5.21706	0.03258				
J18174+483	58451.7489	-4.01095	-0.00028	-4.64064	0.06704	-4.50906	0.06787			-4.92745	0.06567				
J18174+483	58452.78582	-4.02351	-0.00034	-4.66598	0.06684	-4.53199	0.06771	-5.17378	0.04075	-4.99939	0.04869				
J18174+483	58486.25951	-3.89528	-1.00E-05	-4.48608	0.06823	-4.41643	0.06846	-4.98649	0.05837	-4.87444	0.06037				
J18174+483	58490.25161	-4.13756	-0.00074	-4.76502	0.0655	-4.66647	0.0663	-5.20772	0.0334	-5.32769	0.02145				
J18174+483	58496.24881	-4.07153	-0.00038	-4.69874	0.06685	-4.58332	0.06762	-5.20963	0.03396	-5.06527	0.0459				
J18174+483	58500.22001	-4.16857	-0.00085	-4.72148	0.06602	-4.59719	0.06702	-5.3338	0.02075						
J09133+688	57444	-4.70904	-0.01738	-5.05396	0.06946	-4.8689	0.08208								
J09133+688	57487.87543	-4.41357	-0.00614	-5.04849	0.08083	-4.89761	0.08355								
J09133+688	57650.17345	-4.62571	-0.01071	-5.02112	0.08024	-4.87412	0.08255								
J09133+688	57756.08517	-4.48737	-0.01256	-5.05374	0.06023	-4.94893	0.07615								
J09133+688	58074.17364	-4.4614	-0.00325	-5.01106	0.08846	-4.87393	0.08911								
J09133+688	58078.05408	-4.54851	-0.00457	-5.02773	0.08725	-4.84662	0.08876								
J09133+688	58092.09366	-4.45881	-0.00359	-4.98631	0.0883	-4.85981	0.08897								
J09133+688	58124.02622	-4.5952	-0.01216	-5.06959	0.06349	-4.92786	0.07825								
J09133+688	58845.92448	-4.70274	-0.00918	-5.05814	0.08555	-4.89803	0.0865								
J09133+688	58864.18191	-4.58208	-0.00865	-5.06186	0.07868	-4.88087	0.08603								
J09133+688	58882.08342	-4.43103	-0.00485	-5.08184	0.08588	-4.92575	0.08709								
J09133+688	58889.14895	-4.52329	-0.0065	-5.03903	0.08255	-4.87814	0.0877								
J09133+688	58896.21458	-4.5272	-0.00685	-5.00264	0.08681	-4.85003	0.08816								
J09133+688	58904.16752	-4.45201	-0.00777	-5.04062	0.08213	-4.78754	0.08656								
J09133+688	58918.09839	-4.33948	-0.00663	-4.97171	0.08266	-4.88982	0.08271								
J09133+688	58921.08916	-4.4887	-0.00587	-5.03081	0.08683	-4.87848	0.0884								
J20305+654	57922.08884	-4.96543	-0.01463	-5.71767	0.00856	-5.72107	0.01223								
J20305+654	58260.04989	-5.0984	-0.02121	-5.4706	0.03433	-5.76602	0.00027								
J20305+654	58269.12114	-4.72045	-0.00807	-5.54373	0.02604	-5.52477	0.03106								
J20305+654	58295.01265	-4.59677	-0.00595	-5.5419	0.02652	-5.42646	0.04017								
J20305+654	58344.88057	-5.18561	-0.02641	-5.54847	0.02522										
J20305+654	58603.06658	-4.92342	-0.01374	-5.7252	0.00444										
J09428+700	57397	-4.56129	-0.00429	-5.26761	0.10391	-5.06783	0.11771	-5.65831	0.05338	-5.52812	0.10807				
J09428+700	57401	-4.57461	-0.00432	-5.18873	0.116	-5.07753	0.1189			-5.51092	0.08692				
J09428+700	57426	-4.48726	-0.00363	-5.21988	0.11326	-5.0791	0.11791			-5.63069	0.0597				
J09428+700	57442	-4.49448	-0.00332	-5.1843	0.11636	-5.01194	0.12009	-5.51261	0.08201	-5.64963	0.06607				
J09428+700	57449	-4.51742	-0.00327	-5.21427	0.11553	-5.03946	0.12001	-5.45696	0.0897	-5.5733	0.07841				
J09428+700	57466.91778	-4.65193	-0.0054	-5.20182	0.10351	-4.92642	0.11514	-5.49395	0.07681	-5.46158	0.09329				
J09428+700	57493.91417	-4.66503	-0.00858	-5.38709	0.08874	-5.13158	0.11597								
J09428+700	57709.10963	-4.62481	-0.00753	-5.31311	0.09342	-5.11014	0.11052			-5.55872	0.07595				
J09428+700	57766.00113	-4.6075	-0.00486	-5.21127	0.10065	-5.13646	0.11616			-5.62686	0.05849				
J09428+700	57805.96976	-4.64774	-0.00542	-5.29413	0.10411	-5.10731	0.11642			-5.51128	0.07587				
J09428+700	57829.94354	-4.45348	-0.00261	-5.13118	0.11952	-4.99276	0.12145	-5.43298	0.09775	-5.55911	0.09457				
J09428+700	58476.14906	-4.61484	-0.00496	-5.36178	0.08987	-5.11326	0.11637			-5.65206	0.09438				
J09428+700	58497.19938	-4.62268	-0.00412	-5.2578	0.11579	-5.0686	0.11973	-5.74628	0.05582	-5.41473	0.09462				
J09428+700	58528.15661	-4.67392	-0.00484	-5.40049	0.09449	-5.14936	0.11704			-5.67589	0.06293				
J09428+700	58557.12351	-4.4778	-0.003	-5.08179	0.1189	-4.95559	0.1212	-5.42878	0.09231	-5.63249	0.07095				
J09428+700	58616.96738	-4.46555	-0.00323	-5.23626	0.11515	-5.04435	0.11922								
J16102-193	57568.99865	-4.06381	-0.00109	-4.36611	0.04094	-4.51022	0.03906								
J16102-193	57569.89109	-4.23964	-0.0016	-4.75832	0.03749	-4.66246	0.0373								
J16102-193	57570.90722	-4.09831	-0.0012	-4.70743	0.03829	-4.58165	0.03709								
J16102-193	57573.89204	-4.21323	-0.00143	-4.60877	0.03756	-4.78588	0.03442								
J16102-193	57574.91928	-4.14458	-0.00131	-4.72027	0.03823	-4.71388	0.03703								
J16102-193	57583.88985	-4.26737	-0.00169	-4.70503	0.0382	-4.6567	0.03788								
J16102-193	57585.87009	-4.24075	-0.00162	-4.60283	0.03915	-4.69702	0.03722								
J16102-193	57590.8634	-4.254	-0.00162	-4.7832	0.03749	-4.62947	0.03816								
J16102-193	57591.87916	-4.23636	-0.00157	-4.73902	0.03678	-4.81301	0.03595								
J16102-193	57592.90142	-4.15394	-0.00127	-4.70695	0.03799	-4.63817	0.03789								
J16102-193	57593.86159	-4.19393	-0.00141	-4.78063	0.0372	-4.68438	0.03739								
J16102-193	57594.84679	-4.26996	-0.00174	-4.83707	0.03639	-4.53925	0.03859								

Continued on next page

// Star	MJD	Hα		Ca II IRT-a		Ca II IRT-b		He I D_3		Na I D_2		Paβ		Paδ	
		$log\left(\frac{L_{line}}{L_{Bol}}\right)$	δ	$log\left(\frac{L_{line}}{L_{Bol}}\right)$	δ	$log\left(\frac{L_{line}}{L_{Bol}}\right)$	δ	$log\left(\frac{L_{line}}{L_{Bol}}\right)$	δ	$log\left(\frac{L_{line}}{L_{Bol}}\right)$	δ	$log\left(\frac{L_{line}}{L_{Bol}}\right)$	δ	$log\left(\frac{L_{line}}{L_{Bol}}\right)$	δ
J16102-193	57596.89141	-4.18946	-0.00141	-4.81081	0.03698	-4.61818	0.03817								
J16102-193	57603.84635	-4.25995	-0.00176	-4.67976	0.03815	-4.74198	0.03703								
J16102-193	57604.83874	-4.35954	-0.00209	-4.76439	0.03706	-4.57671	0.03854								
J16102-193	57607.83686	-4.28326	-0.00176	-4.75204	0.03753	-4.67668	0.03758								
J16102-193	57613.83998	-4.38419	-0.00217	-4.82331	0.03247	-4.58812	0.03807								
J16102-193	57614.82877	-4.43005	-0.00249	-4.86012	0.03428	-4.63387	0.03799								
J16102-193	57616.8303	-4.3389	-0.00202	-4.69326	0.03684	-4.54705	0.03744								
J16102-193	57617.82425	-4.38336	-0.0023	-4.79558	0.03676	-4.62513	0.03814								
J16102-193	57618.83272	-4.24698	-0.00161	-4.72312	0.03772	-4.65039	0.03763								
J13300-087	59334.03674	-4.99776	-0.00469	-5.21325	0.01366	-4.72307	0.0272								
J13300-087	59612.18973	-5.10896	-0.00612	-4.96531	0.02213	-4.67923	0.02772								
J13300-087	59707.02896	-4.79246	-0.00295	-4.9481	0.0225	-4.6185	0.02841								
J13300-087	59747.94492	-4.79217	-0.00296	-4.83805	0.02489										
J13300-087	59747.9663	-4.96115	-0.00437	-4.89238	0.02381	-4.60806	0.02852								
J06594+193	57690.20705	-5.03316	-0.01935	-5.16727	-0.0223										
J06594+193	57692.17679	-4.98049	-0.01722	-4.99842	-0.00557										
J06594+193	57703.03426	-5.11432	-0.02803	-5.33341	-0.04611										
J06594+193	57761.00156	-5.02074	-0.02276	-5.0473	-0.01468	-5.37403	-0.03312								
J06594+193	57814.87999	-5.33495	-0.05255	-5.11359	-0.01893										
J06594+193	58052.19398	-4.825	-0.01073	-5.11367	-0.01283										
J06594+193	58095.07513	-5.24867	-0.04444	-5.20992	-0.03039	-5.33928	-0.0285								
J06594+193	58112.06673	-5.19557	-0.03129	-5.00533	-0.00641										
J06594+193	58385.15876	-5.32019	-0.05385	-5.0426	-0.01155										
J06594+193	58390.16118	-5.36637	-0.06412	-5.18716	-0.02934										
J06594+193	58398.16404	-5.20654	-0.05059	-5.21294	-0.04033										
J06594+193	58416.08887	-5.15471	-0.04124	-5.01165	-0.01561										
J06594+193	58474.09335	-5.33884	-0.05572	-5.0213	-0.01152										
J06594+193	58484.92806	-5.2342	-0.04672	-5.13094	-0.02366										
J06594+193	58528.8997	-5.01869	-0.02007	-5.08988	-0.01534										
J06594+193	58536.88526	-4.94397	-0.02557	-5.0637	-0.02621										
J06594+193	58542.96297	-5.01866	-0.02206	-5.05707	-0.0145										
J06594+193	58828.03395	-5.08775	-0.03142	-5.07824	-0.01908	-5.33193	-0.0276								
J06594+193	58849.02174	-5.12546	-0.03358	-5.22457	-0.03445										
J06594+193	58892.90174	-5.21157	-0.05019	-5.04922	-0.02133										
J23419+441	57557.1484	-5.05418	-0.0219	-5.35801	-0.0082	-5.60118	-0.0312								
J23419+441	57575.15123	-5.16805	-0.03165	-5.55792	-0.0364										
J23419+441	57620.05664	-5.14833	-0.03475	-5.42331	-0.03326	-5.5146	-0.04235								
J23419+441	57625.03088	-4.70727	-0.01138	-5.4321	-0.03414	-5.31292	-0.01622								
J23419+441	57642.20372	-4.58993	-0.00821	-5.13155	-0.00263	-5.26069	-0.01057								
J23419+441	57642.998	-4.98263	-0.01966	-5.48829	-0.02772	-5.62135	-0.04274								
J23419+441	57646.99475	-5.1887	-0.03813	-5.32384	-0.02087										
J23419+441	57648.13141	-4.98707	-0.02397	-5.3465	-0.02348										
J23419+441	57649.87419	-4.7967	-0.01405	-5.21119	-0.00585	-5.1843	-0.00095								
J23419+441	57652.21125	-5.09521	-0.03075	-5.4847	-0.04299										
J23419+441	57655.82731	-4.98684	-0.02398	-5.3605	-0.02517	-5.44503	-0.03233								
J23419+441	57658.82778	-5.10161	-0.0312	-5.45541	-0.03836	-5.47006	-0.03611								
J23419+441	57672.08264	-4.54431	-0.00657	-5.10112	-0.00135	-5.33931	-0.01929								
J23419+441	57673.0053	-4.79235	-0.01319	-5.247	-0.01294	-5.39393	-0.0258								
J23419+441	57690.82118	-4.55136	-0.00461	-5.39754	-0.03008	-5.3078	-0.01598								
J23419+441	57702.85944	-4.76993	-0.01248	-5.48853	-0.04362										
J23419+441	57704.82313	-4.64694	-0.00944	-5.36849	-0.02616	-5.51673	-0.04316								
J23419+441	57752.85141	-4.71631	-0.01108	-5.37792	-0.02751										
J23419+441	58029.97591	-5.1178	-0.01784	-5.65634	-0.03984										
J23419+441	58142.78847	-5.26469	-0.0263	-5.65956	-0.04003	-5.65052	-0.03396								
J23419+441	58334.04719	-5.07024	-0.01791	-5.64522	-0.0409	-5.43916	-0.012								
J23419+441	58338.99549	-4.70649	-0.0082	-5.3397	-0.00762	-5.24537	0.00117								
J22468+443	57918.1663					-4.44999	0.03319								
J06000+027	57694.14054					-5.23396	0.03779								
J13591-198	57552.88631	-4.11847	-0.00138			-4.88919	0.08377	-5.56411	0.05012	-5.28403	0.08031				
J04173+088	58464.90119					-4.93659	-0.00174								
J04173+088	58464.91341	-3.82036	-0.00121			-4.09652	0.03245			-4.79025	0.02939				
J04173+088	58464.92423	-3.90764	-0.00267			-4.40162	0.0258	-5.39901	0.02439						
J10182-204	57735.19747	-3.98634	-0.00112			-4.59188	0.06799			-5.55369	0.06705				
J10182-204	57799.02624	-3.88872	-0.0009			-4.63248	0.06761	-5.73841	0.0478	-5.57505	0.05178				

Continued on next page

// Star	MJD	Hα		Ca II IRT-a		Ca II IRT-b		He I D_3		Na I D_2		Paβ		Paδ	
		$log\left(\frac{L_{line}}{L_{Bol}}\right)$	δ	$log\left(\frac{L_{line}}{L_{Bol}}\right)$	δ	$log\left(\frac{L_{line}}{L_{Bol}}\right)$	δ	$log\left(\frac{L_{line}}{L_{Bol}}\right)$	δ	$log\left(\frac{L_{line}}{L_{Bol}}\right)$	δ	$log\left(\frac{L_{line}}{L_{Bol}}\right)$	δ	$log\left(\frac{L_{line}}{L_{Bol}}\right)$	δ
J10182-204	57813.96419	-3.85163	-0.00076			-4.52627	0.06911	-5.5282	0.05965	-5.62967	0.05625				
J10182-204	57820.94596	-3.81937	-0.00077			-4.61316	0.06766	-5.4312	0.06029	-5.66119	0.05618				
J10182-204	57829.96715	-3.73115	-0.00063			-4.3721	0.07004	-5.34463	0.06398						
J10182-204	57831.96935	-3.89641	-0.00092			-4.68777	0.06703	-5.71128	0.05046	-5.60179	0.05993				
J10182-204	57847.90999	-3.81054	-0.00076			-4.58121	0.06821	-5.56048	0.05757						
J10182-204	57849.87299	-3.68932	-0.00058			-4.43017	0.06953	-5.46922	0.05931	-5.45845	0.06021				
J10182-204	57855.85013	-3.85757	-0.00085			-4.55766	0.06842	-5.63404	0.05384	-5.69698	0.0557				
J10182-204	57860.85818	-3.82572	-0.00079			-4.59568	0.06805	-5.65161	0.05572						
J10182-204	57865.87561	-3.89875	-0.00092			-4.65292	0.06729	-5.63683	0.05608	-5.79347	0.06095				
J10182-204	58080.22451	-3.82825	-0.00078			-4.71431	0.06643	-5.67752	0.0529	-5.29185	0.07177				
J10182-204	58092.19902	-3.9022	-0.0009			-4.66955	0.06762	-5.63658	0.05316	-5.69457	0.06315				
J10182-204	58094.23714	-3.84669	-0.00079			-4.69179	0.06724	-5.65714	0.0531						
J07001-190	57695.1723	-3.87664	-0.00098			-4.60996	0.04118			-5.01649	0.03836				
J07001-190	57759.03022	-3.89664	-0.00103			-4.74983	0.03938	-5.54504	0.03378	-5.33034	0.0305				
J07001-190	57787.95081	-3.9178	-0.00109			-4.81779	0.03814	-5.87816	0.01811	-5.37207	0.02868				
J07001-190	57798.8872	-3.90003	-0.00105			-4.67518	0.04022	-5.7364	0.02599	-5.68647	0.02678				
J07001-190	57823.85109	-3.93095	-0.00111			-4.65564	0.04059	-5.89393	0.01753	-5.49037	0.0328				
J07001-190	57831.84503	-3.90781	-0.00099			-4.71918	0.03935	-5.87669	0.01864	-5.60985	0.02831				
J07001-190	58034.19575	-3.88028	-0.001			-4.61768	0.04102	-5.62542	0.03303	-5.29526	0.03134				
J07001-190	58043.20112	-3.92615	-0.00098			-4.60358	0.04128	-5.57306	0.03254	-5.52963	0.0211				
J07001-190	58047.19832	-3.89319	-0.00077			-4.64219	0.04097	-5.66448	0.03122	-5.39732	0.02748				
J07001-190	58051.19548	-3.89907	-0.00086			-4.68644	0.0401	-5.58221	0.03225	-5.50274	0.04133				
J07001-190	58054.19343	-3.92507	-0.0011			-4.73061	0.03947	-5.73681	0.02668	-5.46535	0.02434				
J07001-190	58058.18328	-3.78072	-0.0008			-4.48103	0.04242	-5.49209	0.03524	-5.31343	0.03089				
J07001-190	58061.21882	-3.9646	-0.00122			-4.61617	0.04055	-5.69324	0.00643	-5.03088	0.0381				
J07001-190	58064.17577	-3.73315	-0.00071			-4.61039	0.0411	-5.63492	0.02026	-5.112	0.03648				
J07001-190	58074.13156	-3.86627	-0.00079			-4.68018	0.04007	-5.58109	0.03152	-5.41332	0.02681				
J07001-190	58078.12175	-3.73114	-0.00064			-4.45381	0.04269	-5.48104	0.03563	-5.2759	0.0414				
J07001-190	58084.12903	-3.92194	-0.0011			-4.72176	0.03957	-5.66888	0.03107	-5.73197	0.00637				
J07001-190	58123.01371	-3.9301	-0.00112			-4.73879	0.03955	-5.77446	0.0247	-5.62893	0.03575				
J07001-190	58166.90454	-3.93619	-0.00114			-4.71257	0.03983	-5.71566	0.02664	-5.43608	0.02613				
J07001-190	58171.86791	-3.88937	-0.00102			-4.60979	0.04103	-5.84387	0.01948	-5.51687	0.03267				
J07001-190	58172.8823	-3.92392	-0.0011			-4.69431	0.04	-5.67066	0.02804	-5.59386	0.02988				
J07001-190	58173.87101	-3.93412	-0.00114			-4.74037	0.03959	-5.73472	0.02546	-5.46453	0.03408				
J07001-190	58174.87228	-3.93795	-0.00114			-4.71669	0.03987	-5.7897	0.02478	-5.3426	0.02996				
J07001-190	58181.86755	-3.93083	-0.00111			-4.80805	0.03851	-5.58764	0.02291	-5.3874	0.02796				
J07001-190	58190.83304	-3.91021	-0.00107			-4.70626	0.04002	-5.64238	0.03158	-5.43836	0.03496				
J07001-190	58426.14682	-3.86387	-0.00096			-4.5638	0.04176	-5.54127	0.03342	-5.38986	0.0424				
J07001-190	58433.14668	-3.8978	-0.00105			-4.54246	0.04177	-5.41641	0.03604	-5.26702	0.03225				
J10584-107	58586.92081	-3.95289	-0.00134			-4.9521	0.0125	-4.80472	-0.00922	-4.99384	-0.02342				
J10584-107	58630.86843	-4.02215	-0.00155			-5.13639	0.00047	-5.25724	-0.07314	-4.93534	-0.01885				
J15499+796	57890.93639	-4.00714	-0.00127			-4.83816	0.05957			-5.34191	0.06658				
J15499+796	57935.96308	-3.93738	-0.0011			-5.07536	0.04392	-5.38811	0.06003	-5.20546	0.06972				
J19422-207	57910.10115	-3.81665	-0.00102			-4.88189	0.03824	-5.17215	0.01837	-4.80644	0.04337				
J19422-207	58297.05887					-4.87862	0.03835								
J19422-207	58314.00398					-4.91501	0.04139								
J19422-207	58319.95443					-4.73995	0.04523								
J09003+218	57814.97755					-5.36089	-0.03065								
J09003+218	58894.9299	-3.92217	-0.00119			-4.95423	0.00568	-5.60999	-0.05675	-4.85121	0.02317				
J02002+130	57958.1192					-5.38319	0.04088								
J10482-113	58434.21831					-5.08006	0.07071								
J10482-113	58621.85259					-5.22743	0.0607								
J05394+406	58362.13709					-5.43864	-0.0003								
J15598-082	59015.97296					-5.38497	0.02214								
J11026+219	58217.86725					-4.45723	0.03296								
J18174+483	57691.82115					-4.64316	0.06665								
J09140+196	57673.20851					-5.39348	0.00034								
J09140+196	58135.08814					-5.45711	-0.00592								
J09140+196	58264.84368					-5.4688	-0.00694								
J09140+196	58405.18647					-5.08802	0.02037								
J09140+196	58435.21772					-5.22101	0.01347								
J09140+196	58498.13659					-5.0822	0.02735								
J09140+196	58557.96374					-5.36501	0.00285								
J09428+700	58396.19971					-5.13922	0.11292								

Continued on next page

// Star	MJD	Hα		Ca II IRT-a		Ca II IRT-b		He I D_3		Na I D_2		Paβ		Paδ	
		$log\left(\frac{L_{line}}{L_{Bol}}\right)$	δ	$log\left(\frac{L_{line}}{L_{Bol}}\right)$	δ	$log\left(\frac{L_{line}}{L_{Bol}}\right)$	δ	$log\left(\frac{L_{line}}{L_{Bol}}\right)$	δ	$log\left(\frac{L_{line}}{L_{Bol}}\right)$	δ	$log\left(\frac{L_{line}}{L_{Bol}}\right)$	δ	$log\left(\frac{L_{line}}{L_{Bol}}\right)$	δ
J09428+700	58452.14953					-5.11184	0.10809								
J16102-193	57584.88975					-4.60885	0.03803								
J16102-193	57587.88075					-4.64938	0.03532								
J16102-193	57611.82552					-4.76864	0.03605								
J13300-087	59769.88247					-4.82032	0.0257								
J06594+193	57688.17567					-5.4257	-0.04046								
J06594+193	58772.16318					-5.15851	-0.01038								
J23419+441	57633.93377					-5.44218	-0.03193								
J23419+441	58135.84296					-5.6345	-0.03322								
J23419+441	58302.11271					-5.53529	-0.03958								
J12156+526	57788.09781	-3.56594	-0.0007					-5.05639	0.04927	-4.56256	0.08651				
J12156+526	57818.22074	-3.68728	-0.00081					-5.05813	0.05766	-4.74737	0.08332				
J05084-210	58103.9849	-3.55132	-0.00055					-5.45902	0.22468	-4.55534	0.29112				
J05337+019	58077.99027	-3.78619	-0.00048					-5.15119	0.07238	-4.99104	0.07684				
J05337+019	58094.06633	-3.74539	-0.00042					-4.99487	0.07657	-4.92898	0.07804				
J05337+019	58159.84539	-3.65847	-0.00076					-4.9683	0.07055	-4.91158	0.07309				
J05337+019	58205.8297	-3.76331	-0.0007					-4.99312	0.07163	-4.93926	0.07381				
J07319+362N	57401	-4.0878	-0.00106					-5.41377	0.01854	-5.54966	0.03636				
J18498-238	57992.91922	-4.2511	-0.00142					-5.30599	0.01867						
J22468+443	57555.12683	-3.8528	-0.00056					-4.97227	0.03173	-5.19064	0.03075			-5.47775	-0.00242
J05366+112	58137.93016	-3.99583	-0.00121					-5.48706	0.07613						
J05366+112	58509.8401	-4.10154	-0.00118					-5.46493	0.08873	-5.33412	0.08152				
J05366+112	58524.85693	-4.09084	-0.00152					-5.48545	0.07533	-5.33276	0.06635				
J06000+027	57678.18656	-4.20834	-0.00183					-5.23977	0.03302	-5.13347	0.05066				
J06000+027	57691.15071	-4.21154	-0.00187					-5.50108	0.0084	-5.17729	0.04725				
J06574+740	58035.14443	-3.96952	-0.00085					-5.51859	0.04726	-5.30027	0.05664				
J12428+418	57511.98571	-4.23955	-0.00188					-5.63207	-0.00041						
J12428+418	57584.86459	-4.20379	-0.00146					-5.56913	0.02236	-5.33205	0.02172				
J19511+464	57833.13061	-3.94594	-0.00085					-5.58626	0.10823	-5.19998	0.12982				
J04153-076	57421	-4.06913	-0.00069					-5.56137	0.03066	-5.63465	0.03042				
J04153-076	57612.17953	-4.01039	-0.00167					-5.52321	0.00401	-5.70823	-0.00589				
J04153-076	57635.14896	-4.2049	-0.00239					-5.76754	-0.02578	-5.65398	-0.0084				
J04153-076	57641.1267	-4.15405	-0.00191					-5.73638	-0.02883	-5.59458	0.00404				
J04153-076	57645.12708	-4.03654	-0.00178					-5.6891	-0.04384	-5.12998	0.02416				
J04153-076	57646.16277	-4.1599	-0.0021					-5.73433	-0.01785	-5.84205	-0.03196				
J04153-076	57656.09619	-4.17126	-0.00244					-5.66729	-0.0185	-5.72324	-0.01969				
J04153-076	57676.11439	-4.13332	-0.00206					-5.75851	-0.02373						
J04153-076	57785.79814	-4.13143	-0.00152					-5.75134	-0.00269	-5.81307	-0.00862				
J04153-076	57792.86098	-4.16654	-0.00239					-5.74278	-0.03185	-5.69423	-0.01702				
J04153-076	57792.90473	-4.05296	-0.00184					-5.74265	-0.02589	-5.50021	0.00674				
J04173+088	58464.79393	-3.84151	-0.00104					-5.25007	0.01462						
J04173+088	58464.84028	-3.84138	-0.00107					-5.48967	-0.00361	-4.81933	0.02873				
J04173+088	58464.86453	-3.83553	-0.00104					-5.84636	-0.05723	-5.24768	0.03349				
J04173+088	58464.87873	-3.88417	-0.00116					-5.63582	-0.01126	-4.98393	0.036				
J04173+088	58464.89037	-3.82834	-0.00104					-5.49853	-0.00358	-5.27413	0.01013				
J04173+088	58467.80477	-3.80297	-0.00096					-5.50826	0.00496	-5.43833	0.01722				
J04173+088	58467.85144	-3.76152	-0.00088					-5.38403	0.00614	-5.17669	0.01389				
J04173+088	58467.86227	-3.85122	-0.00108					-5.46368	0.00526	-5.09597	0.02022				
J04173+088	58467.90721	-3.81432	-0.00101					-5.62325	-0.01473	-5.3337	-0.00836				
J04173+088	58467.91894	-3.86875	-0.00113					-5.46003	0.00237	-5.31128	-0.00417				
J04173+088	58467.92977	-3.84057	-0.00108					-5.68911	-0.02467						
J04173+088	58467.95298	-3.86932	-0.00119					-5.63299	-0.01314	-5.20875	0.01465				
J18189+661	57559.07051	-4.23796	-0.00189					-5.55842	0.03006	-5.07691	0.04966				
J18189+661	57602.94987	-4.34288	-0.00283					-5.82859	-0.03374	-5.11634	0.04739				
J18189+661	57690.8358	-4.26806	-0.00221					-5.48035	0.01356	-5.12989	0.05384				
J18189+661	57801.15398	-4.24613	-0.00261					-5.73349	-0.02886	-5.05491	0.05334				
J18189+661	57818.11851	-4.2588	-0.00242					-5.74607	-0.04024	-5.10981	0.05114				
J18189+661	57821.13141	-4.22775	-0.00188					-5.81433	-0.0288	-5.03128	0.05496				
J01019+541	57961.09266	-3.96663	-0.00105					-5.56858	0.02867						
J01019+541	58039.95327	-4.04118	-0.00127					-5.69375	0.01478	-5.00129	0.06588				
J01019+541	58349.13515	-4.06426	-0.00139					-5.56091	0.02781	-5.24771	0.05804				
J01019+541	58351.98704	-4.07936	-0.00142					-5.74764	0.00787	-5.17229	0.0592				
J01019+541	58352.05994	-3.98313	-0.00109					-5.39876	0.04253	-5.27615	0.04474				
J01019+541	58352.1458	-4.11939	-0.00158					-5.461	0.03732	-5.163	0.05967				

Continued on next page

// Star	MJD	Hα		Ca II IRT-a		Ca II IRT-b		He I D_3		Na I D_2		Paβ		Paδ	
		$log\left(\frac{L_{line}}{L_{Bol}}\right)$	δ	$log\left(\frac{L_{line}}{L_{Bol}}\right)$	δ	$log\left(\frac{L_{line}}{L_{Bol}}\right)$	δ	$log\left(\frac{L_{line}}{L_{Bol}}\right)$	δ	$log\left(\frac{L_{line}}{L_{Bol}}\right)$	δ	$log\left(\frac{L_{line}}{L_{Bol}}\right)$	δ	$log\left(\frac{L_{line}}{L_{Bol}}\right)$	δ
J01019+541	58353.04839	-4.06271	-0.00139					-5.55195	0.02843	-5.07818	0.06245				
J01019+541	58353.17878	-4.11372	-0.00152					-5.52222	0.03108	-5.09279	0.06386				
J10584-107	58538.12246	-3.85734	-0.00107					-5.13659	-0.04261	-5.28502	-0.07122				
J10584-107	58564.03979	-3.98032	-0.0014					-5.26806	-0.07392	-5.15886	-0.04713				
J10584-107	58831.16489	-3.94831	-0.00135					-5.08826	-0.03897	-5.00791	-0.02186				
J10584-107	58855.16703	-3.95003	-0.00133					-5.45468	-0.04767						
J12189+111	57553.89791	-4.04613	-0.00123					-5.82232	0.00714	-5.33876	0.05241				
J12189+111	57755.15564	-4.07568	-0.00133					-5.80225	0.01277	-5.25018	0.05834				
J12189+111	57788.06214	-3.86007	-0.00083					-5.45475	0.04914	-5.03257	0.05756				
J12189+111	57801.12972	-3.94914	-0.0009					-5.57749	0.0497	-5.1731	0.06186				
J13102+477	58475.17288	-4.09969	-0.00185					-5.3771	-0.00932	-5.07603	0.0216				
J13102+477	58486.21658	-4.1916	-0.00232					-5.53566	-0.04826						
J13102+477	58491.24281	-4.05101	-0.00165					-5.46646	-0.00442	-4.70946	0.03087				
J13102+477	58524.19162	-4.21513	-0.00245					-5.44995	-0.02114	-4.89444	0.01876				
J13102+477	58529.10984	-4.09773	-0.00188					-5.44208	0.00282	-5.22304	0.01591				
J13102+477	58560.08436	-4.17177	-0.00222					-5.51349	-0.00599	-5.00285	0.0281				
J13102+477	58636.96005	-4.2082	-0.00241					-5.40661	0.00496	-5.40519	0.01432				
J14173+454	57472.07661	-4.06412	-0.00184					-5.43172	-0.02111	-4.97759	0.01905				
J14173+454	57494.06411	-4.0278	-0.00169					-5.50381	-0.0378	-5.30186	0.01537				
J14173+454	57832.07314	-4.01863	-0.00165					-5.29122	-0.0144	-5.06855	0.01534				
J14173+454	57855.99538	-3.99384	-0.00154					-5.46294	-0.02233	-5.04593	0.01663				
J14173+454	57857.98984	-4.01435	-0.00163					-5.39778	-0.01707	-5.09609	0.01093				
J14173+454	57880.04742	-4.04456	-0.00173					-5.42371	-0.0276	-5.18312	-0.00574				
J14173+454	57882.06499	-3.93913	-0.00138					-5.37028	-0.00577	-5.01537	0.01157				
J15499+796	57909.94786	-4.02483	-0.00135					-5.66408	0.0371	-5.34443	0.06302				
J18022+642	57815.14154	-3.9044	-0.00122					-5.58968	0.10362	-4.90041	0.16936				
J22114+409	58491.77942	-3.96079	-0.00147					-5.46126	-0.02524	-5.62148	0.01723				
J22114+409	58497.78978	-4.08274	-0.00196					-5.39713	-0.0452	-5.38123	-0.03359				
J22114+409	58598.1608	-3.99976	-0.00168					-5.55329	-0.06395	-5.11332	0.01899				
J10564+070	57449	-3.84803	-0.00072					-5.41976	0.08021	-5.13411	0.0856			-5.22035	0.07151
J09003+218	58470.12148	-3.88093	-0.00111					-5.13255	-0.0008	-4.92512	0.01126				
J09033+056	57830.93325	-4.24074	-0.00331					-5.4738	-0.03293	-4.88027	0.01697				
J09033+056	58553.98389	-4.08405	-0.00233					-5.54331	-0.03981	-4.95019	0.01504				
J09033+056	58597.91859	-4.29035	-0.00354					-5.6433	-0.02796						
J02002+130	57419	-4.24368	-0.00119					-4.94027	0.06977	-4.95753	0.07476				
J23431+365	58385.97435	-4.40606	-0.00237					-5.15901	0.01627						
J05084-210	58499.89598	-3.35449	-0.0004							-5.41454	0.22335				
J11055+435	57498.93757	-3.74219	-0.00119							-4.75708	0.06462				
J17338+169	57503.14913	-3.6169	0.00006							-4.86667	0.06577				
J17338+169	57540.06956	-3.57068	0.00018							-4.94548	0.06798				
J07319+362N	57397	-4.20334	-0.00137							-5.65765	0.03579				
J04153-076	57788.76958	-4.10532	-0.00208							-5.58894	0.02403				
J18189+661	57574.98368	-4.27734	-0.00239							-5.11543	0.04809				
J18189+661	57617.9281	-4.28938	-0.0025							-5.09379	0.04817				
J18189+661	57830.10047	-4.31462	-0.00339							-4.91287	0.04065				
J01019+541	58079.90661	-4.14749	-0.00166							-5.15754	0.0487				
J01019+541	58094.93768	-4.21223	-0.00196							-5.14954	0.06418				
J13102+477	57896.91734	-4.24388	-0.00261							-5.34637	0.01838				
J13102+477	58509.1864	-4.02475	-0.00155							-5.0896	0.02111				
J13102+477	58614.02452	-4.25689	-0.00271							-5.24259	0.02248				
J13102+477	58644.91494	-4.20364	-0.0024							-5.40258	-0.01563				
J13102+477	58655.91723	-4.0874	-0.00179							-5.28411	0.0177				
J14173+454	57504.95116	-3.91224	-0.0013							-4.77419	0.02029				
J15499+796	57914.95376	-4.06229	-0.00146							-5.06685	0.07341				
J20093-012	57568.07284	-3.6774	-0.00082							-4.85281	0.00274				
J22114+409	58410.04271	-3.92787	-0.00138							-4.56608	0.01759				
J22114+409	58486.79966	-4.048	-0.0018							-5.12931	-0.00692				
J22114+409	58494.80601	-4.13679	-0.00225							-4.98511	0.0023				
J22114+409	58616.0986	-4.11541	-0.0021							-5.34177	-0.01352				
J09033+056	57761.07278	-4.12167	-0.00254							-4.75923	0.01963				
J09033+056	58462.13656	-4.10793	-0.0024							-4.72814	0.02456				
J09033+056	58557.94102	-4.15715	-0.00275							-5.32796	-0.00293				
J01339-176	57678.00317	-4.34288	-0.00282							-4.90888	0.04275				
J01339-176	57989.14149	-4.31877	-0.00263							-5.3779	-0.04166				

Continued on next page

// Star	MJD	Hα		Ca II IRT-a		Ca II IRT-b		He I D_3		Na I D_2		Paβ		Paδ	
		$log\left(\frac{L_{line}}{L_{Bol}}\right)$	δ	$log\left(\frac{L_{line}}{L_{Bol}}\right)$	δ	$log\left(\frac{L_{line}}{L_{Bol}}\right)$	δ	$log\left(\frac{L_{line}}{L_{Bol}}\right)$	δ	$log\left(\frac{L_{line}}{L_{Bol}}\right)$	δ	$log\left(\frac{L_{line}}{L_{Bol}}\right)$	δ	$log\left(\frac{L_{line}}{L_{Bol}}\right)$	δ
J23431+365	58103.86745	-4.47098	-0.00554							-5.40885	-0.02505				
J09005+465	57655.16593	-4.48627	-0.00577							-5.34246	0.03244				
J09005+465	57709.1509	-4.59274	-0.00689							-5.62531	0.01882				
J09005+465	57712.07418	-4.58743	-0.00544							-5.4718	0.0318				
J16555-083	57866.13829	-4.19351	-0.00281									-4.15632	0.0056		

Mean Flux Data of Catalogue Stars

Table 10 lists the average chromospheric activity measurements for each star in the sample, computed from all available epochs, derived from the available spectral datasets. For every diagnostic, the first column represents the mean activity index and the second the corresponding mean uncertainty. The final column (n) gives the number of individual observations contributing to each mean value.

Table 10. Mean values per star across all datasets, with observation counts (n).

Star	Hα $\langle log\left(\frac{L_{line}}{L_{\mathbf{Bol}}}\right)\rangle$	Hα δ	Ca II IRT-a $\langle log\left(\frac{L_{line}}{L_{\mathbf{Bol}}}\right)\rangle$	Ca II IRT-a δ	Ca II IRT-b $\langle log\left(\frac{L_{line}}{L_{\mathbf{Bol}}}\right)\rangle$	Ca II IRT-b δ	He I D_3 $\langle log\left(\frac{L_{line}}{L_{\mathbf{Bol}}}\right)\rangle$	He I D_3 δ	Na I D_2 $\langle log\left(\frac{L_{line}}{L_{\mathbf{Bol}}}\right)\rangle$	Na I D_2 δ	Paβ $\langle log\left(\frac{L_{line}}{L_{\mathbf{Bol}}}\right)\rangle$	Paβ δ	Paδ $\langle log\left(\frac{L_{line}}{L_{\mathbf{Bol}}}\right)\rangle$	Paδ δ	n
J00403+612	-5.13	-0.035	-5.3029	0.0013	-5.054	0.021									9
J01019+541	-4.0584	-0.0014	-5.299	0.012	-5.03	0.039	-5.522	0.03	-5.105	0.061					20
J01026+623	-5.473	-0.048	-5.1	0.069	-4.921	0.073									28
J01033+623	-3.74517	-0.00062	-4.684	0.025	-4.616	0.026	-5.379	0.02	-5.139	0.026			-5.316	-0.023	13
J01125-169	-4.112	-0.0017	-5.2805	0.0097	-5.097	0.023									7
J01339-176	-4.2626	-0.0024	-5.4962	-0.0056	-5.087	0.027	-5.061	0.021	-5.178	0.018					29
J01352-072	-3.77372	-0.00072	-4.579	0.055	-4.446	0.057	-5.074	0.051	-5.268	0.055					11
J02002+130	-4.2389	-0.0012	-5.052	0.064	-5.079	0.062	-5.226	0.063	-5.108	0.072			-5.436	0.039	60
J02088+494	-3.74678	-0.00043	-4.663	0.045	-4.554	0.048	-5.162	0.046	-5.127	0.046					16
J02164+135	-4.3411	-0.0018	-5.22	0.046	-5.31	0.04									4
J02489-145W	-5.047	-0.017	-5.4968	0.0035	-5.399	0.016									14
J02519+224	-4.01616	-0.00074	-5.159	0.03	-4.784	0.049	-5.962	0.03	-5.998	0.029					13
J03217-066	-4.8239	-0.01	-5.281	0.027	-5.134	0.037									11
J03473-019	-3.83593	-0.00068	-4.56	0.11	-4.42	0.11	-5.057	0.099	-5.02	0.1					11
J04153-076	-4.0667	-0.0015	-5.349	-0.011	-5.0479	0.0085	-5.6219	-0.0014	-5.6233	0.004					49
J04167-120	-5.175	-0.019	-5.53	0.011	-5.476	0.015									15
J04173+088	-3.7836	-0.001	-4.8515	0.0086	-4.612	0.016	-5.4596	0.0012	-5.161	0.017					40
J04198+425	-4.2774	-0.0011	-5.344	0.01	-5.174	0.022					-4.3869	0.0085	-5.183	-0.015	29
J04472+206	-3.84552	-0.00081	-5.028	0.054	-5.015	0.057	-6.026	0.05	-5.711	0.083					11
J05019+011	-3.86487	-0.00058	-4.753	0.041	-4.599	0.039	-5.62	0.033	-5.696	0.03	-4.071	0.031			19
J05062+046	-3.91337	-0.00061	-4.825	0.068	-4.67	0.073	-5.791	0.06	-5.813	0.07					13
J05084-210	-3.50988	-0.00054	-5.05	0.26	-4.76	0.28	-5.42	0.24	-5.0	0.27			-4.4	0.29	26
J05337+019	-3.73834	-0.00059					-5.027	0.073	-4.943	0.075					4
J05365+113	-4.5595	-0.0057	-4.88	0.15	-4.73	0.15									126
J05366+112	-4.0299	-0.0012	-5.329	0.072	-5.061	0.087	-5.42	0.083	-5.406	0.082					14
J05394+406	-4.4197	-0.002	-5.3201	0.0049	-5.31	0.01									9
J06000+027	-4.1047	-0.0015	-5.363	0.021	-5.011	0.05	-5.364	0.025	-5.345	0.034					15
J06574+740	-3.95692	-0.00082	-4.891	0.052	-4.785	0.058	-5.513	0.049	-5.386	0.059					12
J06594+193	-5.139	-0.036	-5.108	-0.021	-5.326	-0.028									22
J07001-190	-3.8928	-0.001			-4.663	0.04	-5.668	0.027	-5.409	0.031					27
J07033+346	-4.0135	-0.0012	-5.26	0.1	-4.94	0.13	-5.4	0.11	-5.4	0.11	-4.17	0.12			14
J07051-101	-3.8899	-0.0012	-5.038	-0.0012	-4.9632	-0.003	-5.38234	0.00073	-5.4536	-0.0045					4
J07319+362N	-4.03937	-0.00095	-5.027	0.052	-4.857	0.055	-5.278	0.033	-5.537	0.023	-4.056	0.047	-5.393	0.031	37
J07446+035	-3.96731	-0.00056	-4.8	0.26	-4.65	0.26	-5.86	0.26	-5.94	0.26	-4.05	0.26			51
J07472+503	-4.0196	-0.0011	-5.243	0.028	-4.845	0.052	-5.503	0.037	-5.48	0.039					15
J07558+833	-3.8861	-0.0011	-4.925	0.033	-4.688	0.044	-5.276	0.033	-5.042	0.05	-4.225	0.027			14
J08298+267	-4.0729	-0.0016	-4.9495	0.0025	-5.1148	-0.0056	-5.389	-0.0018	-5.017	0.012					25
J08413+594	-4.2506	-0.0032	-5.256	-0.013	-5.1956	-0.0049									59
J09003+218	-3.82736	-0.00099	-5.1024	-0.0074	-5.017	0.001	-5.329	-0.016	-4.801	0.017					20
J09005+465	-4.5553	-0.0057	-5.521	-0.032	-5.355	-0.001	-5.485	-0.036	-5.428	0.025					6
J09033+056	-4.1764	-0.0029	-5.404	-0.034	-5.486	-0.043	-5.41	-0.023	-4.981	0.016					20
J09133+688	-4.5216	-0.0079	-5.035	0.081	-4.88	0.085									16
J09140+196					-5.2965	0.0074									7
J09143+526	-5.386	-0.051	-5.56	0.13	-5.24	0.16									5
J09144+526	-5.217	-0.038	-5.41	0.17	-4.95	0.18									4
J09161+018	-3.87296	-0.00078	-4.945	0.034	-4.699	0.045	-5.364	0.037	-5.387	0.037					9
J09163-186	-4.903	-0.024	-5.079	0.094	-5.015	0.097									5
J09425+700	-4.6624	-0.0056	-5.13	0.11	-5.03	0.11	-5.545	0.078	-5.515	0.086					34
J09428+700	-4.5713	-0.0046	-5.25	0.11	-5.07	0.12	-5.533	0.078	-5.57	0.08					18
J09449-123	-3.80878	-0.0005	-4.87	0.1	-4.75	0.11	-5.92	0.11	-5.89	0.11					10
J10182-204	-3.84519	-0.00082			-4.594	0.068	-5.591	0.056	-5.596	0.06					14
J10196+198	-3.85245	-0.00079	-4.634	0.065	-4.554	0.066	-5.02	0.06	-5.123	0.058					63
J10238+438	-4.5146	-0.0026	-5.63	-0.054	-5.2452	-0.002									4
J10360+051	-3.86539	-0.00054	-4.897	0.057	-4.746	0.062	-5.185	0.05	-5.248	0.058					7
J10482-113	-4.3392	-0.003	-5.071	0.07	-5.258	0.059									77
J10564+070	-3.7713	-0.0008	-4.762	0.085	-4.67	0.086	-5.253	0.072	-4.958	0.082	-4.185	0.069	-5.265	0.058	77
J10584-107	-3.9226	-0.0013	-5.1069	0.0014	-4.893	0.014	-5.168	-0.038	-5.175	-0.013					51
J11026+219	-4.6569	-0.0092	-4.848	0.029	-4.648	0.03									51
J11055+435	-3.61329	-0.00088	-5.236	0.034	-5.082	0.057	-4.637	0.061	-4.403	0.064					20
J11201-104	-4.0643	-0.0013	-4.529	0.09	-4.427	0.091	-5.27	0.046	-5.298	0.041			-5.689	0.035	27

Continued on next page

Star	Hα $\langle log\left(\frac{L_{line}}{L_{\mathbf{Bol}}}\right)\rangle$	δ	Ca II IRT-a $\langle log\left(\frac{L_{line}}{L_{\mathbf{Bol}}}\right)\rangle$	δ	Ca II IRT-b $\langle log\left(\frac{L_{line}}{L_{\mathbf{Bol}}}\right)\rangle$	δ	He I D_3 $\langle log\left(\frac{L_{line}}{L_{\mathbf{Bol}}}\right)\rangle$	δ	Na I D_2 $\langle log\left(\frac{L_{line}}{L_{\mathbf{Bol}}}\right)\rangle$	δ	Paβ $\langle log\left(\frac{L_{line}}{L_{\mathbf{Bol}}}\right)\rangle$	δ	Paδ $\langle log\left(\frac{L_{line}}{L_{\mathbf{Bol}}}\right)\rangle$	δ	n
J11423+230	-5.219	-0.031	-5.2531	-0.0063	-5.1028	0.0065									73
J11474+667	-3.72917	-0.00078	-4.96	0.11	-4.81	0.11	-5.15	0.1	-5.13	0.11	-3.87	0.11	-5.41	0.051	53
J11476+002	-3.89493	-0.00088	-4.94	0.14	-4.77	0.14	-5.29	0.13	-5.27	0.13					6
J12156+526	-3.62215	-0.00074	-4.863	0.069	-4.861	0.074	-4.931	0.063	-4.751	0.073					13
J12189+111	-3.9827	-0.0011	-5.165	0.021	-4.872	0.047	-5.607	0.038	-5.158	0.06					13
J12428+418	-4.1396	-0.0016	-5.29824	-0.00014	-4.87	0.036	-5.451	0.014	-5.307	0.022					7
J13005+056	-3.9432	-0.0012	-4.86	0.069	-4.763	0.074	-5.436	0.056	-5.061	0.077					12
J13102+477	-4.0793	-0.0018	-5.442	-0.02	-5.125	0.011	-5.32394	-0.00094	-5.108	0.022					34
J13300-087	-4.9305	-0.0042	-4.971	0.021	-4.69	0.028									6
J13536+776	-4.0457	-0.0011	-5.191	0.087	-4.83	0.11	-5.541	0.091	-5.537	0.098	-3.91	0.1	-3.89	0.11	25
J13591-198	-4.0487	-0.0012	-5.125	0.077	-4.913	0.084	-5.543	0.057	-5.33	0.078					17
J14173+454	-3.9979	-0.0016	-5.017	-0.032	-5.211	-0.032	-5.45	-0.028	-5.0	0.015					12
J14321+081	-3.8671	-0.0013	-4.874	0.047	-4.805	0.051	-5.14	0.024	-4.799	0.048					22
J14578+566	-4.3304	-0.0028	-5.523	0.013	-5.272	0.05									2
J15218+209	-3.847	0.00012	-4.39	0.045	-4.302	0.045	-5.089	0.017	-4.847	0.037	-3.862	0.036	-5.064	0.011	48
J15305+094	-4.071	-0.0018	-5.276	-0.02	-5.0805	0.004	-5.438	-0.021	-5.005	0.017					6
J15499+796	-4.0012	-0.0013	-5.159	0.034	-4.968	0.052	-5.641	0.036	-5.22	0.068					14
J15598-082	-5.343	-0.024	-5.427	0.016	-5.36	0.024									16
J16102-193	-4.2501	-0.0017	-4.725	0.037	-4.65	0.037									24
J16313+408	-3.75931	-0.00079	-4.726	0.094	-4.731	0.095	-5.214	0.086	-4.78	0.096					14
J16555-083	-4.0512	-0.0022	-5.206	-0.018	-5.26	-0.014					-4.1456	0.0061			95
J16570-043	-3.957	-0.00062	-4.969	0.07	-4.799	0.074	-5.421	0.063	-5.346	0.069					15
J17338+169	-3.5694	0.0002	-4.996	0.053	-4.851	0.07	-5.346	0.037	-4.969	0.069					12
J18022+642	-3.9053	-0.0011	-5.21	0.13	-4.95	0.15	-5.37	0.14	-4.95	0.16	-4.27	0.15			27
J18075-159	-3.9254	-0.0015	-5.075	0.03	-4.862	0.041	-5.256	0.027	-5.106	0.034			-5.323	-0.01	9
J18131+260	-3.78546	-0.00026	-4.62	0.12	-4.31	0.12	-5.17	0.11	-5.26	0.11					11
J18174+483	-4.10224	-0.00051	-4.694	0.067	-4.578	0.068	-5.303	0.026	-5.199	0.037					68
J18189+661	-4.2369	-0.0022	-5.3932	-0.0051	-5.084	0.028	-5.6617	-0.0028	-5.058	0.05					13
J18482+076	-4.0777	-0.0016	-5.143	0.017	-5.089	0.018					-4.267	0.012			54
J18498-238	-4.1862	-0.0012	-5.258	0.018	-5.006	0.035	-5.093	0.028	-4.97	0.037			-5.681	-0.017	36
J19169+051S	-4.4053	-0.0018	-5.3292	-0.0021	-5.3005	0.0038									40
J19422-207	-3.7774	-0.00095	-5.061	0.026	-4.815	0.042	-5.132	0.031	-5.052	0.037					14
J19511+464	-3.96779	-0.00087	-5.27	0.1	-4.87	0.13	-5.52	0.11	-5.35	0.12					14
J20093-012	-3.799	-0.0011	-5.1289	-0.0055	-4.904	0.017	-5.111	0.01	-4.745	0.022					12
J20305+654	-4.915	-0.015	-5.591	0.021	-5.61	0.021									6
J20451-313	-3.79296	-0.0006	-4.32	0.1	-4.26	0.1	-5.217	0.08	-5.032	0.076	-3.907	0.091	-5.673	0.045	98
J22012+283	-3.8063	-0.00065	-4.92	0.037	-4.778	0.044	-5.484	0.032	-5.229	0.044					11
J22114+409	-3.914	-0.0014	-5.0495	-0.0023	-4.828	0.012	-5.2023	-0.0092	-5.1532	-0.0015	-4.1002	0.0054			56
J22231-176	-3.9665	-0.0016	-4.906	0.075	-4.734	0.077	-5.375	0.046	-5.118	0.07					12
J22468+443	-3.78877	-0.00047	-4.826	0.033	-4.517	0.038	-4.988	0.032	-5.105	0.034	-4.036	0.027	-5.249	0.013	101
J22518+317	-3.93661	-0.00057	-4.497	0.074	-4.385	0.075	-5.447	0.068	-5.38	0.07	-3.904	0.067	-5.597	0.029	12
J23351-023	-4.659	-0.01	-5.314	-0.022	-5.1572	-0.0022									6
J23419+441	-4.908	-0.019	-5.402	-0.026	-5.44	-0.026									25
J23431+365	-4.4438	-0.0046	-5.504	-0.024	-5.3013	0.0038	-5.2382	0.0082	-5.409	-0.025					9
J23548+385	-3.83669	-0.00075	-5.057	0.048	-4.689	0.06	-5.131	0.055	-5.223	0.053					12

List of Publications

Publications directly related with the thesis

Labarga, F., & Montes, D. 2026, iSTARMOD: a Python Code to Quantify Chromospheric Activity by Using Spectral Subtraction Technique, AJ, 171, 14, doi: 10.3847/1538-3881/ae173e

Labarga, F., Montes, D., Duque-Arribas, C., et al. 2026, The CARMENES search for exoplanets around M dwarfs. Chromospheric activity and Flux-Flux relationships, to be submitted to A&A

Other publications

Alonso-Floriano, F. J., Snellen, I. A. G., Czesla, S., et al. 2019, He I λ 10 830 Å in the transmission spectrum of HD209458 b, A&A, 629, A110, doi: 10.1051/0004-6361/201935979

Morales, J. C., Mustill, A. J., Ribas, I., et al. 2019, A giant exoplanet orbiting a very-low-mass star challenges planet formation models, Science, 365, 1441, doi: 10.1126/science.aax3198

Quirrenbach, A., Amado, P. J., Ribas, I., et al. 2018, in Society of Photo-Optical Instrumentation Engineers (SPIE) Conference Series, Vol. 10702, Ground-based and Airborne Instrumentation for Astronomy VII, ed. C. J. Evans, L. Simard, & H. Takami, 107020W, doi: 10.1117/12.2313689

Quirrenbach, A., CARMENES Consortium, Amado, P. J., et al. 2020, in Society of Photo-Optical Instrumentation Engineers (SPIE) Conference Series, Vol. 11447, Ground-based and Airborne Instrumentation for Astronomy VIII, ed. C. J. Evans, J. J. Bryant, & K. Motohara, 114473C, doi: 10.1117/12.2561380

Reiners, A., Ribas, I., Zechmeister, M., et al. 2018, The CARMENES search for exoplanets around M dwarfs. HD147379 b: A nearby Neptune in the temperate zone of an early-M dwarf, A&A, 609, L5, doi: 10.1051/0004-6361/201732165

Ribas, I., Reiners, A., Zechmeister, M., et al. 2023, The CARMENES search for exoplanets around M dwarfs. Guaranteed time observations Data Release 1 (2016-2020), A&A, 670, A139, doi: 10.1051/0004-6361/202244879

Zechmeister, M., Dreizler, S., Ribas, I., et al. 2019, The CARMENES search for exoplanets around M dwarfs. Two temperate Earth-mass planet candidates around Teegarden's Star, A&A, 627, A49, doi: 10.1051/0004-6361/201935460

Congress and Conference contributions

Labarga, F., & Montes, D. 2020, in XIV.0 Scientific Meeting (virtual) of the Spanish Astronomical Society, 153. https://ui.adsabs.harvard.edu/abs/2020sea..confE.153L

Labarga, F., Montes, D., Cano, J., et al. 2020, in XIV.0 Scientific Meeting (virtual) of the Spanish Astronomical Society, 152. https://ui.adsabs.harvard.edu/abs/2020sea..confE.152L

Labarga, F., Montes, D., Lopez-Gallifa, A., et al. 2021, in The 20.5th Cambridge Workshop on Cool Stars, Stellar Systems, and the Sun (CS20.5), Cambridge Workshop on Cool Stars, Stellar Systems, and the Sun, 202, doi: 10.5281/zenodo.4566168

Labarga, F., Montes, D., Duque-Arribas, C., et al. 2022, in The 21st Cambridge Workshop on Cool Stars, Stellar Systems, and the Sun, Cambridge Workshop on Cool Stars, Stellar Systems, and the Sun, 219, doi: 10.5281/zenodo.7670149

Labarga, F., Montes, D., Duque-Arribas, C., et al. 2023, in Highlights on Spanish Astrophysics XI, ed. M. Manteiga, L. Bellot, P. Benavidez, A. de Lorenzo-Cáceres, M. A. Fuente, M. J. Martínez, M. Vázquez Acosta, & C. Dafonte, 272, doi: 10.5281/zenodo.7668217

López-Gallifa, Á., Montes, D., Labarga, F., et al. 2021, in The 20.5th Cambridge Workshop on Cool Stars, Stellar Systems, and the Sun (CS20.5), Cambridge Workshop on Cool Stars, Stellar Systems, and the Sun, 138, doi: 10.5281/zenodo.4564191

Montes, D., López-Gallifa, Á., & Labarga, F. 2023, in EAS2023, European Astronomical Society Annual Meeting, 2134

Montes, D., López-Gallifa, A., Labarga, F., et al. 2020, in XIV.0 Scientific Meeting (virtual) of the Spanish Astronomical Society, 168